MPHIL

Optimized Interlaminar Shear Strength Of Thick Laminates

Pestana, Jony

Award date:
2014

Awarding institution:
University of Bath

UNIVERSITY OF BATH

DEPARTMENT OF MECHANICAL ENGINEERING

OPTIMIZED INTERLAMINAR SHEAR STRENGTH OF THICK LAMINATES

by

Jony U. Azevedo Pestana

July 2014

A thesis submitted to the University of Bath for the degree of Master of Philosophy (MPhil)

COPYRIGHT

CHEATING AND PLAGIARISM

"I certify that I have read and understood the section in the Integrated/MPhil/PhD Student Handbook on Cheating and Plagiarism and that all material in this assignment is my own work, except where I have indicated with appropriate references."

Name: Jony Pestana
Student Number: 119326327

Signed: Date:

ABSTRACT

Static and fatigue properties are important factors when developing design rules to optimize the reduction of damage in the middle of a composite component loaded under a three point bending test.

The progressive damage which occurs in a composite laminate during fatigue will affect the mechanical properties of the component to an extent which depends on the material type and lay-up of the composite and on the mode of testing. By choosing an appropriate combination of ply materials and ply stacking sequence for the composite laminate, a better static condition, as well as better fatigue behavior of the component is expected under *in-service* conditions.

In order to minimize the through-thickness damage in the middle of a composite laminate under a short beam shear test, the present work focuses on determining the best stacking sequence, combining two different materials through-thickness of a composite component. The use of an algorithm that has been created to run all possible combinations of angles and materials was the key to finding the best stacking sequence for a composite component. Through the optimization method, two different hybrid laminate lay-ups were obtained for a maximum of 40% of glass plies within a composite laminate. The laminates developed through the algorithm, which are, the Hybrid Design 1 $\left(\left[(0_C)_2/(\pm45_C)_2/(\pm45_g)_2/(\pm45_C)\right]_s\right)$ and Hybrid Design 2 $\left(\left[(0_c)_2/(\pm45_g)/(90_C)_4/(\pm45_g)/(90_C)_2\right]_s\right)$, have shown that the best ply orientations to minimize the damage in the middle of a composite component occur when the value of the variable angle θ in $\pm\theta$ plies has a maximum value of 90 degrees. The algorithm used showed that best laminates were obtained when glass plies were not used as the central plies in a glass/carbon composite laminate, with a maximum 40% of glass plies.

Static and fatigue tests were performed on both hybrid designs and on a quasi-isotropic composite laminate ($[(0/45/90/-45)_3]_s$) made of carbon plies. The results of the static and fatigue tests have demonstrated that the best design, giving the best static and fatigue behavior is the Hybrid Design 1. Also, it has been demonstrated through experimental tests that 90 degree plies within a composite laminate subject to a three point bending condition will cause the component to be weaker in terms of fatigue and static properties due to the tendency to develop inclined cracks in the through-thickness direction on the 90 degree plies of the composite laminate, causing delamination and loss of stiffness of the component.

ACKNOWLEDGMENT

I would like to thank the patience and availability of my supervisor Richard Butler who has supported me and advised me during this project.

Also, I would also like to thank the following people who have helped me to answer some of the questions, that have arisen during this project:

Andy Stevenson, Dave Bowhay, Roberto Aguiar, Luis Cruz, James Mitchell, Robert Gover, Boyd Charlotte, and Marcelo Cardoso which are working in AgustaWestland, Yeovil, and also, a special thanks to Stuart Hanson and Peter Wood.

I would also like to thank, Phil Parkes, Andrew Rhead and Shi Hua (both from Bath University) for their patience and valuable support, Ji Han who did the experimental part of this work (excellent work) and Wenli Liu.

Also, in regards to the *Student Sponsorship Agreement* that was signed off by all of the parties involved, I would like to thank AgustaWestland for the financial support of my MPhil.

And finally, I would like to dedicate this work to all of my three brothers, parents and specially Maggie Manica for their comprehension, advise, etc.

TABLE OF CONTENTS

LIST OF TABLES

LIST OF FIGURES

ACRONYMS AND DEFINITIONS

LIST OF ABREVIATIONS:

3PB	Three point bending tests which uses a wider distance between the support rollers in regards to the SBS test, these tests also require a longer specimen than the one used in a SBS test.
ABD Matrix	ABD matrix given by the constitutive equation which represents the bending and stretching coupling terms, and the coupling between normal stress, shearing and twisting deformation.
CDS	Characteristic damage state.
CLPT	Classical laminate plate theory.
CT	Computerised tomography.
ILSS	Interlaminar shear strength.
$ILSS_{Apparent}$	Interlaminar shear strength based on the standard D2344/2344M (2006) and BS14130:1998 (2004)
$ILSS_{FE}$	Interlaminar shear strength based on the finite elements model.
$ILSS_{2\text{-}D}$	Interlaminar shear strength in accordance with the equation (99).
$ILSS_{Reddy}$	Interlaminar shear strength in accordance with the equation (80).
ISS	Interlaminar shear stress for any load applied below the ultimate load.
N.A.	Neutral Axis.
NLR	National aerospace laboratory of the Netherlands.
SBS	Short beam shear.
S-N curve	Fatigue curve. *S* means stress, and *N* means number of cycles
Static Fatigue ISS	Static fatigue interlaminar shear strength.
Static ISS	Static interlaminar shear strength.
TTSS	Through-thickness shear stress.
UD	Unidirectional.

LIST OF ALGORITHM VARIABLES:

$\boldsymbol{\theta_{min}}$	Minimum value for angle θ
$\boldsymbol{\theta_{min\_1}}$	Minimum value for angle θ_1
$\boldsymbol{\theta_{max}}$	Maximum limit for angle θ
$\boldsymbol{\theta_{max\_1}}$	Maximum limit for angle θ_1

$\boldsymbol{\theta_{increment}}$	Increment on the angle θ
$\boldsymbol{\theta_{increment\_1}}$	Increment on the angle θ_1
$\boldsymbol{\theta_{fix}}$	Ply angle chosen by the user to be fixed during the execution of the algorithm
$\boldsymbol{\tau_j}$	Interlaminar shear strength of ply *j* ($\tau_j = \tau_{j\,xz}$)
anglecomb	Instruction to be typed in the command window of Matlab to get the total amount of angle combinations for a determined input.
$\boldsymbol{angles_{\_n}}$	Number of angles chosen by the user to be run.
$\boldsymbol{angle_{min\,\%}}$	Minimum percentage required within the laminate for each angle chosen.
base number	Number of base $\mathrm{angles_{\_n}}$ (i.e. if $\mathrm{angles_{\_n}} = 2$, the number will be based in a binary format).
'C'	Carbon ply.
dtotal	Sum of all values equal to $\mathrm{D_{11}(j)}$ which belongs to the ply (j).
$\boldsymbol{e_{11} = E_x}$	Young modulus of each ply.
$\boldsymbol{e_{11f} = E_{x\,f}}$	Young modulus of the fibre without the resin (matrix) surrounding it.
$\boldsymbol{e_{11mm} = E_{x\,m}}$	Young modulus of the matrix.
$\boldsymbol{e_{11}(j)}$	Young modulus of each single ply (equal to $\mathrm{E_x(j)}$).
$\boldsymbol{e_{11f}(j)}$	Young modulus of the fibre without the resin (matrix) surrounding it (for each single ply will be equal to $\mathrm{E_{x\,f}(j)}$).
$\boldsymbol{e_{11mm}(j)}$	Young modulus of the matrix (equal to $\mathrm{E_{x\,m}(j)}$).
$\boldsymbol{e_{2222}(j)}$	Young modulus in the second direction of each single ply (equal to $\mathrm{E_y(j)}$).
$\boldsymbol{e_{11parcels}(j)}$	Young modulus in the *x* principal of the laminate for each single ply (in accordance with the Rule of Mixtures).
$\boldsymbol{e_{11total}}$	Young modulus in the *x* direction of the laminate in accordance with the Rule of Mixtures (equal to $\mathrm{E_{x\ of\ the\ Laminate}}$).
'G'	Glass ply.
$\boldsymbol{Glass_{ply\,\%}}$	Variable that defines the maximum percentage of glass plies within the laminate.
$\boldsymbol{k_j}$	Extensional stiffness component of *x* direction of the composite laminate ($k_j = \mathrm{A_{11}(j)}$).
$\boldsymbol{kia_{11}(j)}$	In the algorithm this variable represents: $\mathrm{A_{11}(j)}$

loadapplied	Load to be inputted by the user.
Matthick	Thickness of each ply.
$\mathbf{N_{solution}}$	Number of solutions given by the algorithm.
p	Load per unit width.
Plies_n	Number of plies that the laminate has.
Py=qq	Half of the total load input by the user in accordance with Young & Budynas (2002), section 8.17; table 8.1 - case 1c (for a right and left end simply supported).
$\mathbf{t_{carbon}}$	Thickness of the carbon ply (average).
$\mathbf{t_{glass}}$	Thickness of the glass ply (average).
totalthick	Sum of all the ply thicknesses along the thickness of the laminate.
$\mathbf{V_{f\ ration}(j)}$	Volume fraction of the fibre. Dimensionless parameter.
$\mathbf{V_{m\ ration}(j)}$	Volume fraction of the fibre. Dimensionless parameter.
$\mathbf{V_{m\_average}}$	Matrix volume fraction average.
width	Width of the composite laminate to be input by the user.
ydistance (j)	Dimension taken from the middle plane of the symmetric laminate up to the top of each ply.

LIST OF SYMBOLS:

Material Properties:

Subscriptions **1,2,3**	The subscriptions 1,2,3 denote the material principal axes.
α	Factor used in the Timoshenko's equation (166).
η_θ	reinforcing efficiency for each group of fibres (rule of Mixtures).
ε	Material strain.
ε_1	Strain in principal direction of the ply which is parallel to the fibre.
ε_{eff}	Effective strain of the material, which is given by the ratio between the initial length of the component and the final length just before the failure of the material due to the ultimate load ($\varepsilon_{eff} = \frac{\Delta L}{L}$) .
σ	One dimensional stress
$\sigma_{\text{Tensile strength}}$	Maximum stress that a material can withstand under tensile load before failing or breaking.

$\sigma_{\text{Flexural strength}}$	Maximum stress that a material or structural member can withstand under bending loading conditions.
$\sigma_{\text{Compressive strength}}$	Maximum stress that a material can withstand under compressive loading.
σ_{P_1}	Principal stress in direction *x* of the stress element which is within a ply.
σ_{P_3}	Principal stress in direction *z* of the stress element which is within a ply.
τ_{xy}	In plane (on the lamina) shear stress.
τ_{xz}	Through-thickness shear stress. τ_{xz} will be equal to ILSS when the variable P is equal to the ultimate load.
$\tau_{max_{z'x'}}$; $\tau_{max_{x'z'}}$	Maximum shear stress on the z-x plane of a stress element that is within a composite ply
a_n	Proportion of total fibre content
D	Sum of values $D_{11}(j)$ which belong to the ply (j) (equal to the variable dtotal, which was used in the algorithm).
E	Young's Modulus
E_c	Composite modulus
E_f	Longitudinal modulus of the fibre (without resin surrounding the fibres)
E_m	Resin (matrix) Young's Modulus
E_x	Longitudinal Young's Modulus
$E_{x\ 45\ \text{degree tensile test}}$ – Figure 32	Young's Modulus in the *x* system's axis direction an orthotropic composite ply subjected to an uniaxial loading at 45 degrees to the 1 direction (see Figure 32)
$E_{y\ 45\ \text{degree tensile test}}$ – Figure 32	Young's Modulus in the *y* system's axis direction of an orthotropic composite ply subjected to an uniaxial loading at 45 degrees to the 1 direction (see Figure 32)
E_y	Transverse Young's Modulus
E_z	Through-thickness Young's Modulus
F_x	Tensile load applied on a single orthotropic ply. The tensile load F_x does an angle of 45 degrees in regards to the fibre direction of the orthotropic ply.
G_{xy}	Longitudinal / transverse shear modulus
G_{yz}	Transverse / through-thickness shear modulus
G_{xz}	Longitudinal / through-thickness shear modulus

v_{xy}	Poisson's ratio for transverse stress from longitudinal stress
$\nu_{xy\ 45\ \text{degree tensile test}}$ – Figure 32	Poisson's ration in the x-y plane of an orthotropic composite ply subjected to an uniaxial loading at 45 degrees to the 1 direction of the (see Figure 32)
v_{yz}	Poisson's ratio for through-thickness stress from transverse stress
v_{yx}	Poisson's ratio for longitudinal stress from transverse stress
$\nu_{yx\ 45\ \text{degree tensile test}}$ – Figure 32	Poisson's ration in the y-x plane of an orthotropic composite ply subjected to an uniaxial loading at 45 degrees to the 1 direction of the (see Figure 32)
v_f	Poisson's ratio of the fibre
v_m	Poisson's ratio of the matrix (resin)
$\mathbf{V_f}$	Fibre volume fraction
$\mathbf{V_f(j)}$	Volume fraction of the fibre, which is used for calculating the Young's modulus of the principal direction of the laminate - *x* direction (in accordance with the rule of mixtures) -- expressed in percentage.
$\mathbf{V_m(j)}$	Volume fraction of the matrix (resin) -- expressed in percentage.
γ	Shear strain.

Miscellaneous:

$\boldsymbol{\theta}$	Ply orientation angle.
a	Span of the composite beam.
A'	Shape parameter of the S-N curve (equation (176)).
A	Cross section area of the composite laminate.
$\mathbf{b_{average}}$	Width of a single fatigue specimen which is obtained from the table D.1 and D.2 of the Appendix J.
$\mathbf{A_{mn}}$	General expression that represents the extensional stiffness couplings of the ABD matrix (for in plane stress on a lamina).
$\mathbf{A_{mn_{Each\ Ply}}}$	Extensional stiffness coupling for a single ply (lamina).
$\mathbf{A_{11}(j)}$	Extensional stiffness component of the principal direction 1, taken from the ABD matrix of the laminate for each ply (Campbell 2010, p.432).
B	Scale parameter of time which has the dimension of the cycle life *N* and is the rational unit of fatigue life.
$\mathbf{B_{mn}}$	General expression which represents the bending membrane couplings of the ABD Matrix (for in plane stress on a lamina).

$\mathbf{b}$	Width of the laminate that will be submitted to a SBS test according to standard D2344/2344M (2006) and BS14130:1998 (2004)
$\mathbf{D_{mn}}$	General expression which represent the bending stiffness couplings of the ABD Matrix (from in plane stresses on a lamina).
$\mathbf{D_{mn_{Each\ Ply}}}$	Bending couplings for a single ply (lamina)
$\mathbf{D_{11}(j)}$	Bending stiffness coupling of the principal direction 1. Taken from the ABD matrix of the laminate.
Endurance	Lower limit of the fatigue curve (S-N curve).
F	Apparent static ultimate load (*F*) of a single composite laminate that will be submitted to a fatigue test condition.
$\mathbf{F_0}$	Central point load
$\mathbf{f_{max}}$	Fatigue variable that refers to the maximum external load applied on the component.
$\mathbf{f_{min}}$	Fatigue variable that refers to the minimum external load applied on the component.
$\mathbf{f_{mean}}$	Fatigue variable that refers to the mean load applied on the component.
$\mathbf{h_{j-1}}$	Distance from the mid-plane up to the top of the jth-1 lamina
$\mathbf{h_j}$	Distance from the mid-plane to the bottom of the jth lamina
$\mathbf{I_y}$, $\mathbf{I_x}$, $\mathbf{I_{xy}}$	Moments of inertia in regards to the *x* axis, *y* axis and the rectangular plane *xy* respectively
$\mathbf{j^{th}\ ply}$	Subscript used to identify a single ply into a laminate.
$\mathbf{k_y}$	Radius of gyration of the cross section with respect to the *y* axis.
L	Span of a composite laminate subjected to a SBS test. Distance between the two support rollers.
$\mathbf{M_{y_{(x)}}}$	Moment around the *y* axis which is a function of the *x* coordinate of the composite laminate axis system.
$\mathbf{M_{x\ around\ y\ axis}}$	Resultant of the bending moment per unit width that acts around the *y* axis direction which is perpendicular to the plane x-z and its vector is located onto the plane y-z (Figure 35).
$\mathbf{M_{y\ around\ X\ axis}}$	Resultant of the bending moment per unit length that acts around the *x* axis direction which is perpendicular to the plane y-z and its vector is located onto the plane x-z (Figure 35).
$\mathbf{M_{xy\ around\ y\ axis}}$	Resultant of the bending moment per unit length that acts around the *y* axis direction and its vector is perpendicular to the plane x-z (Figure 35).

$\mathbf{M_{yx\ around\ X\ axis}}$	Resultant of the bending moment per unit width that acts around the *x* axis direction and its vector is perpendicular to the plane y-z (Figure 35).
$\mathbf{N}$	Total number of plies in the laminate (in Chapter 5 the variable *N* means the number of cycles).
$\mathbf{N_x}$	Resultant of the force per unit width that acts in the *x* axis direction and its vector is perpendicular to the plane y-z (Figure 35).
$\mathbf{N_y}$	Resultant of the force per unit length that acts in the *y* axis direction and its vector is perpendicular to the plane x-z (Figure 35).
$\mathbf{N_{xy}}$	Resultant of the force per unit width that acts in the *y* axis direction and its vector is onto the plane y-z (Figure 35).
$\mathbf{N_{yx}}$	Resultant of the force per unit length that acts in the *x* axis direction and its vector is onto the plane x-z (Figure 35).
$[\mathbf{Q_{mn}}]$	Stiffness matrix for a lamina in natural coordinate system
$\mathbf{q_{(x)}}$	Shear flow per unit area of the composite laminate (see Figure 37).
$\mathbf{Q_{(x)}}$	Resultant of the shear flow as a function of the x coordinate of the composite laminate system axis (see Figure 37).
$\mathbf{Q_{x_{(x)}}}$	Resultant shear flow per unit width of the composite laminate as a function of the *x* coordinate of the composite laminate system axis.
$\mathbf{Q_{11}}^*$; $\mathbf{Q_{22}}^*$; $\mathbf{Q_{12}}^*$ $\mathbf{Q_{66}}^*$; $\mathbf{Q_{16}}^*$; $\mathbf{Q_{26}}^*$	Components of the lamina (ply) stiffness matrix
$\mathbf{Q_{11}(j)}$; $\mathbf{Q_{12}(j)}$; $\mathbf{Q_{21}(j)}$; $\mathbf{Q_{22}(j)}$; $\mathbf{Q_{66}(j)}$	Components of the stiffness matrix for an orthotropic lamina (ply) in accordance with Hooke's law for a single ply.
$\mathbf{P}$	Load applied (in Newtons) on a SBS test according to standard D2344/2344M (2006) and BS14130:1998 (2004).
$\mathbf{P_{z\ for\ fatigue}}$	Apparent static ultimate load of a single composite laminate that will be submitted to a fatigue test condition.
$\mathbf{P_z}$	Same as the variable *P*.
$\mathbf{P_1}$	Tensile load applied on a orthotropic composite laminate.
$\mathbf{S}$	Shear force. In the Chapter 5 this variable is the maximum interlaminar shear stress (maximum ISS) of the S-N fatigue curve.

S_e	Median shear stress at infinite number of cycles (median of the fatigue life).
S_u	Median of the static strength.
S_x and S_z	Support shear loads
T	Torque applied on the ends of a thin composite tube.
t	Thickness of the laminate that will be submitted to a SBS test according to standard D2344/2344M (2006) and BS14130:1998 (2004)
$t_{average}$	Thickness of a single fatigue specimen which is obtained from the table D.1 and D.2 of the Appendix J.
w_o	Transverse deflection of the beam.

Chapter 1

INTRODUCTION AND LITERATURE REVIEW

1.1. INTRODUCTION

Due to the lighter, stronger, low density and stiffer properties of composites when compared with other materials like metals, composite materials are becoming increasingly used in industry. Composite materials have an enormous potential in the construction, transport and wind energy sectors. A composite material is a combined structure consisting of individual materials laid up in different sequences so as to have a dramatic effect on the overall mechanical behaviour. An accurate knowledge about the through-thickness fibre arrangements, material disposition, damage improvement, fatigue, modes of failure and crack behaviour are essential to achieve a reliable and lightweight composite structure. Composite materials are intended to be far more efficient than any structural materials known previously. The concept of fibre reinforced material was known and employed in ancient times. Straw was used by the Israelites in the manufacture of bricks in 800 BC (Ashton et al. 1969), plywood was used by the ancient Egyptians when they realized that wood could be arranged to achieve superior strength and resistance to thermal expansion as well as to swelling owing to the presence of moisture (Jones 1975). In the past few decades considerable progress in composite materials has been made in order to improve the strength of both the fibre material and resin, as well as in research to unlock the true strength of a composite component, improving its mechanical properties. Ideally, the properties of engineering materials should be reproducible and accurately known (Harris 1999), thus, research has been developed to understand how to achieve new designs that, under fatigue and static conditions, have the best in-service structural performance.

1.2. AN OVERVIEW ABOUT COMPOSITE LAMINATES

A composite material is defined as the combination of two or more micro or macro constituents which differ in form and chemical composition and which do not merge between them. The word composite is derived from the word compound, which of means that is something made of different materials. For instance, in the aerospace industry, one of the materials used on the construction of some components for airplanes consists of high performance fibres, which are extremely fine strands of glass or carbon material that makes small filaments (fibres). Those filaments, when combined with a compatible chemical material like resin (matrix) in an unidirectional orientation will form an individual orthotropic lamina (ply), which is used to form a composite component when multiple plies are stacked together through-thickness of the component.

Figure 1 shows the different types of composite material systems available, classified with the respective constituent reinforcing elements.

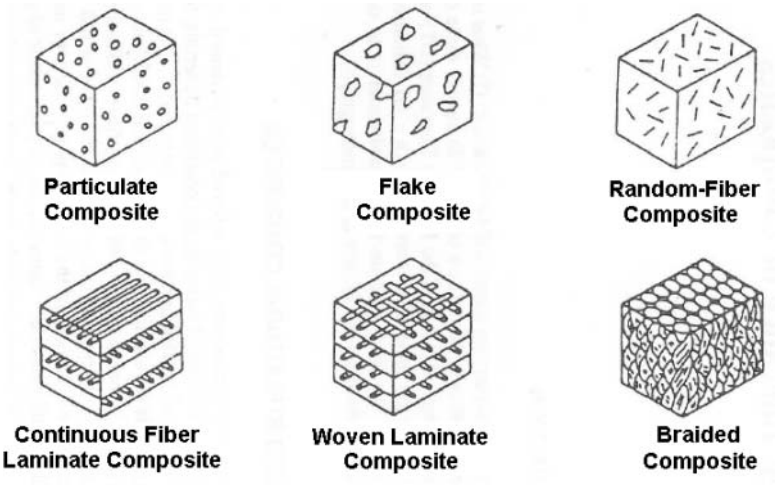

Figure 1 - Types of composite materials (Sierakowski 1995).

An overview scheme about composites laminates could be drawn as shown in Figure 2.

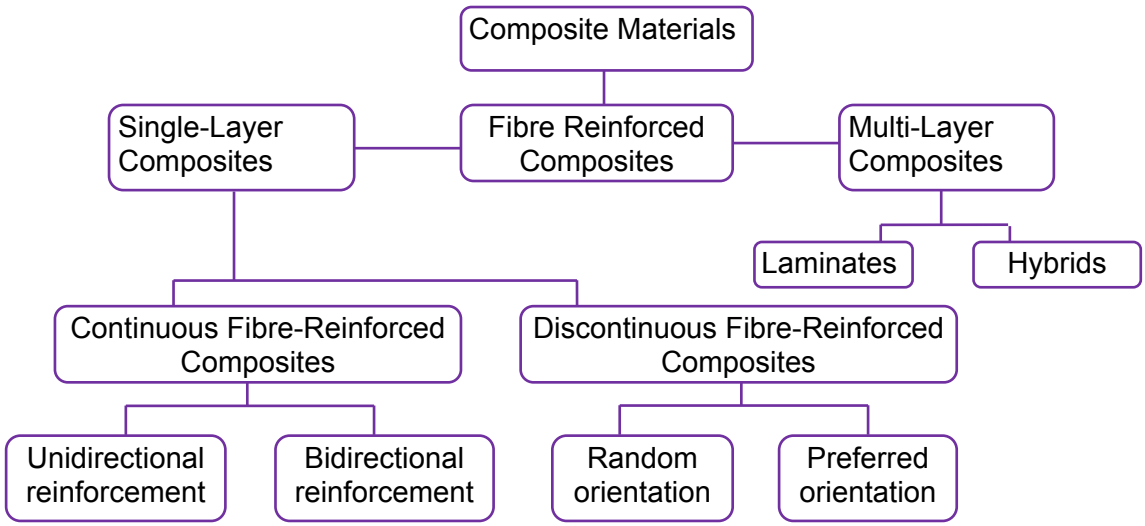

Figure 2 - Composite construction. Flow chart (Sierakowski 1995)

1.3. COMPOSITE LAMINATES - MANUFACTURE PROCESS

Composite laminates could be of quasi-isotropic, orthotropic or anisotropic layup as shown in Figure 3.

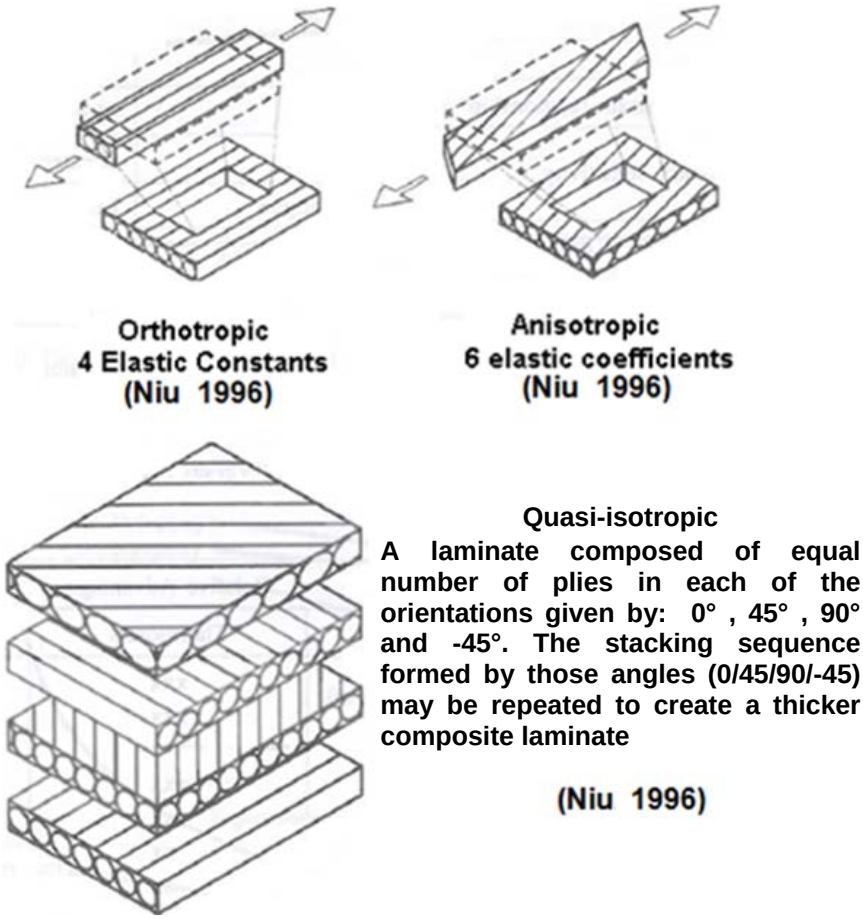

Figure 3 - Composite structures (Niu, 1996)

One of many manufacture process of a composite laminate involves a series of procedures in order to achieve the final product. First of all, the reinforcing fibre and matrix are combined by stacking each unidirectional ply at a determined orientation in order to provide the intended final design characteristics. After this, a bagging process will be required in order to place the stacked plies in the autoclave, and to hold the laminate in position during the curing process. During the bagging process a bagging film, bag sealant, breather plies, bleeder plies, dam separator film and a mold release ply are required. After sealing the part inside the vacuum bag, a vacuum is drawn and held on the laminate part during the cure cycle. Subsequently, the bagged part is put in an autoclave in order to apply pressure and heat simultaneously for a fixed period of time. The autoclave, which is a heated pressure chamber will treat the assembly (laminate) in order to achieve a high fibre volume fraction and low void content for a maximum structural efficiency.

Figure 4 shows a example of a cure that has been performed on a composite structure, which is in a vacuum bag in the Autoclave.

Figure 4 - Composite structure after the Autoclave cure cycle (Anon. 2011)

1.4. LAMINATE STACKING SEQUENCE

During the laminate stacking process, the plies are stacked with a determined orientation as shown in Figure 5.

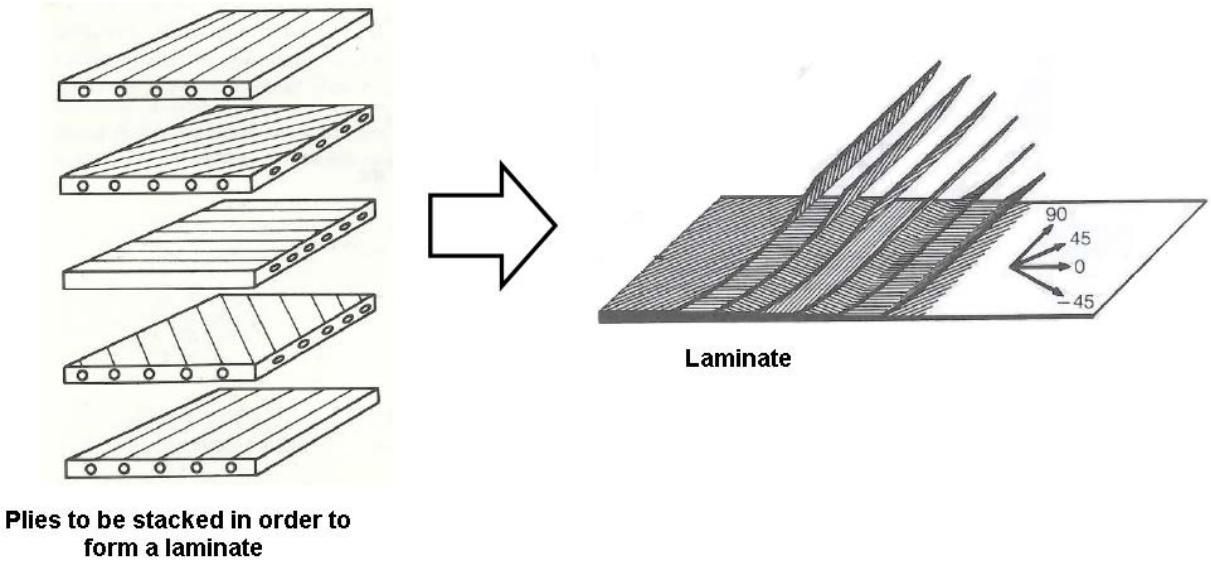

Figure 5 - Laminate with the stacked plies (Niu 1996)

In order to identify the arrangement of the ply orientations within a laminate adopted for a single composite structure (stacking sequence), there is a *code* commonly used in composite engineering analysis, which, according to Niu (1996) should respect the following procedures:

- Each lamina is labeled by its ply orientation.
- Lamina are listed in sequence with the first number representing the lamina to which arrow is pointing.
- Individual adjacent lamina are separated by a slash if their angles differ.
- Adjacent lamina of the same orientation are depicted by a numerical subscript indicating the total number of lamina which are laid up in sequence at that angle.
- Each complete laminate is enclosed by brackets.
- When the laminate is symmetrical and has an even number on each side of the plane of symmetry (know as the midplane) the code may be shortened by listing only the angles from the arrow side to the mid-plane. A subscript *s* is used to indicate that the code for only one half of the laminate is shown.
- When plies of fabric are used in a laminate, the direction of the fabric warp is used as the ply orientation angle. The ply angle is enclosed in parentheses to identify the ply as fabric ply.
- When the laminate is composed of both fabric and tape plies (a hybrid laminate), The parentheses around the fabric plies will distinguish the fabric plies from the tape plies.
- When the laminate is symmetrical and has an odd number of plies the center ply is overlined to indicate that it is the midplane.

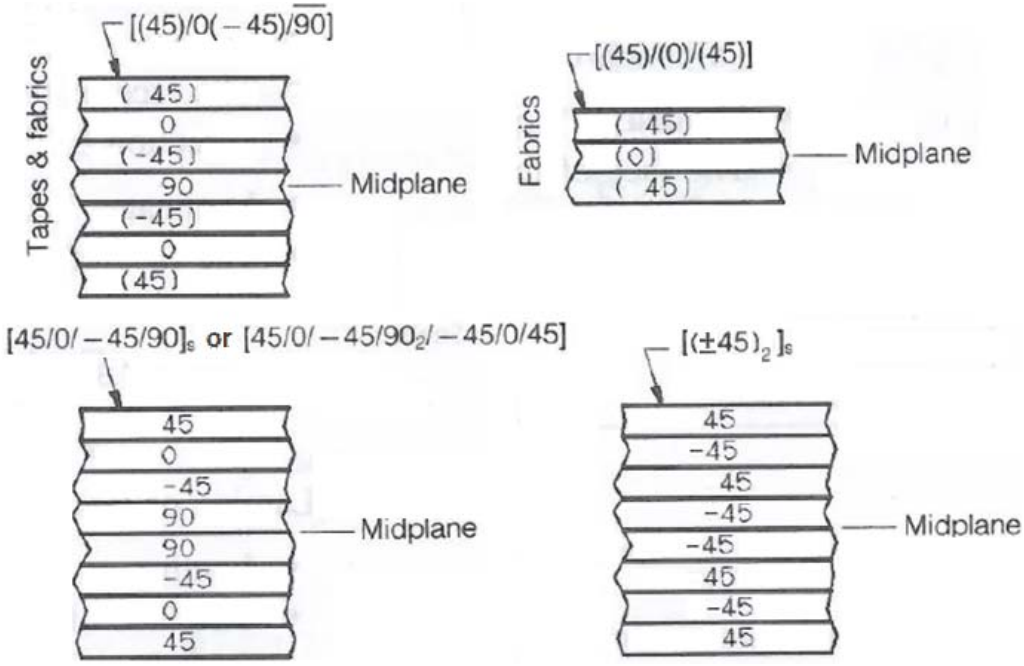

Figure 6 - Example of stacking sequence notations (Niu 1996)

Each of the plies within a laminate has a local coordinate axis system, in which the number *1* determines the longitudinal direction of the fibre, the number *2* determines the transverse direction of the fibre, and finally the number *3* determines the through-thickness direction of the ply which is constructed of unidirectional (UD) fibres.

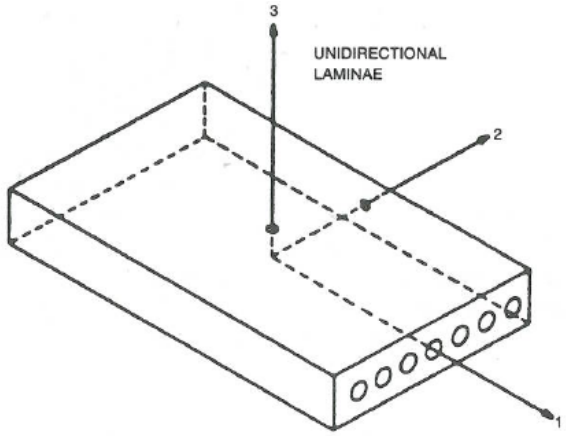

Figure 7 - Ply principal axis (Jones 1999)

1.5. COMPOSITE LAMINATES - DAMAGE MECHANISMS

Composite damage mechanisms are identified by two different types of failure, inter-laminar damage and intra-laminar damage. These types of damage are described below:

Inter-laminar damage:

Inter-laminar damage is a failure that occurs between two adjacent plies, due to the displacement of plies within a laminate. There are three different modes of inter-laminar damage that can cause delamination within a composite laminate. These modes are: Interlaminar tension (Mode I); Interlaminar sliding shear (Mode II) and Interlaminar scissoring shear (Mode III). The representation of each Mode is shown in Figure 8.

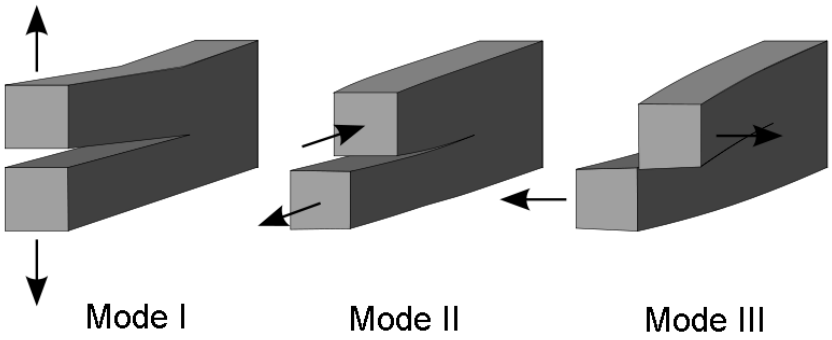

Figure 8 - Modes of interlaminar failure in a composite laminate.

Intra-laminar damage:

Intra-laminar damage refers to the failure within a single ply of the laminate. This type of damage is characterized by different modes of failure, such as: transverse matrix cracking, fibre breakage, interfacial debonding, interfacial shear failure. Figure 9 and Figure 10 shows some examples of this.

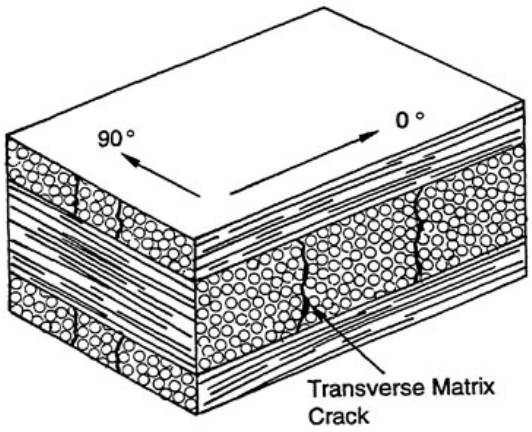

Figure 9 - Transverse matrix crack (Anon. 1996)

Figure 10 - Fibre breakage (Anon. 1994)

Intra-laminar combined with Inter-laminar damage:

An example of a combined damage mechanism within a composite laminate is shown in Figure 11.

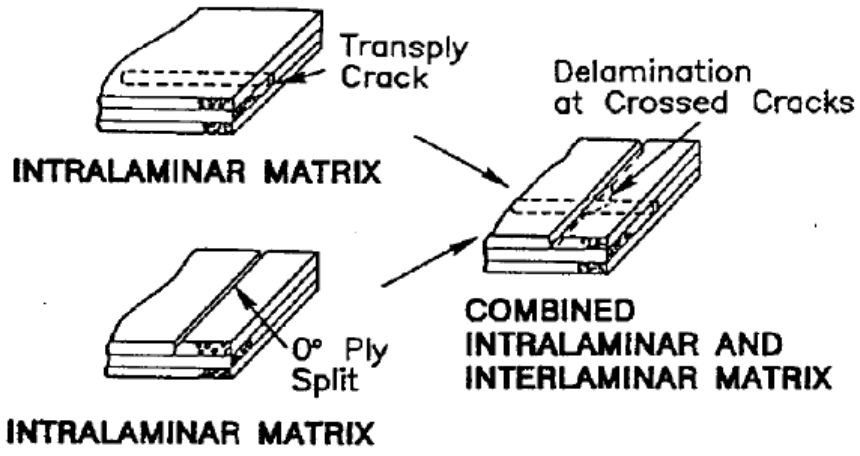

Figure 11 - Combined damage mechanism (Anon. 1994)

1.6. THROUGH-THICKNESS SHEAR STRESS

Laminate composite materials have excellent properties when loaded in the fibre direction, under in-plane loading, but, when out of plane loads act on the composite part this becomes a matrix dominated problem, in which the interlaminar shear stress (τ_{xz} or τ_{zx}) which are represented in Figure 13 could become significant, resulting in a static or fatigue failure on the composite component due to the in-plane stresses (σ_x , σ_y and τ_{xy}). Attachment of a composite lug can be exposed to large out-of-plane transverse loads. An example is shown in Figure 12.

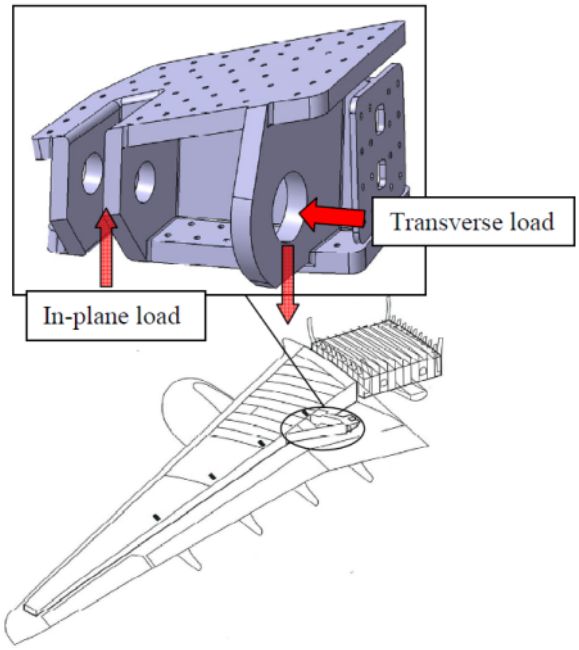

Figure 12 - "ALCAS main landing gear support beam and its primary load components" (Creemers 2010)

Most of the theories and assessments in composite laminates are based on the constitutive equations for composite laminates, in which relationships are for a plane state stress applied on each individual ply. A plane state stress considers only the stresses in the principal directions of the lamina (ply), except for direction *z*, in which the through-thickness shear stress τ_{xz} or τ_{zx} , as well as the principal stress σ_z , are ignored based on certain assumptions that are explained in Chapter 2.

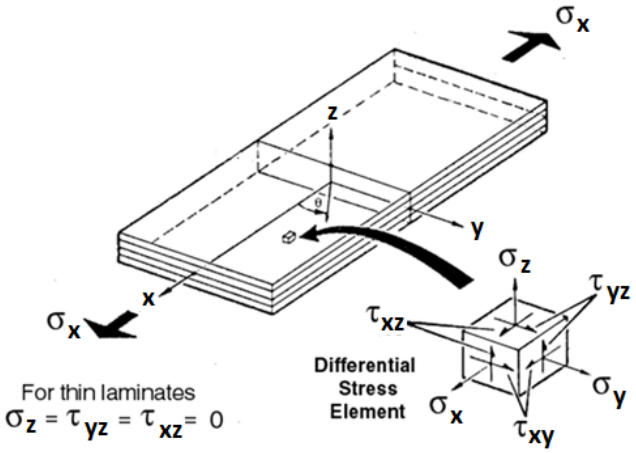

Figure 13 - Example of a plane state stress for a thin laminate (Anon. n.d.)

Despite considering the through-thickness shear stress and principal stress σ_z to be equal to zero, " these stresses do exist in reality, and they can be responsible for failures in composite laminate materials because of the relatively low shear and transverse normal strengths of materials used" (Reddy 2004). Materials such as the resin present a low shear and transverse normal strength.

"The influence of transverse loads on the failure behavior (statically and in fatigue) of thick composite structures was investigated in a 2007 Strategic Research Program "Transverse load introduction in thick composite aircraft structures". This program showed that composites are indeed sensitive to fatigue for stresses in the matrix-dominated transverse shear mode. Further, the research gave strong indications that in some cases traditional Interlaminar Shear (ILS) failure criteria are somewhat conservative" (Creemers 2010).

In 2009, NLR performed a research program to investigate the interlaminar shear stress failure criteria in more detail. During this research thin ILS coupons were manufactured and tested. It was concluded that "not all differences in strength can be explained by the traditional ILS criteria, such as Hashin (1980) and Kim & Soni (1984) " (Creemers 2010). In order to provide a better prediction and explanation of these differences, a newly formulated failure criterion which includes the interlaminar shear stress τ_{xz} has been derived by Creemers (2010). According to NLR, this failure criterion is able to explain such differences.

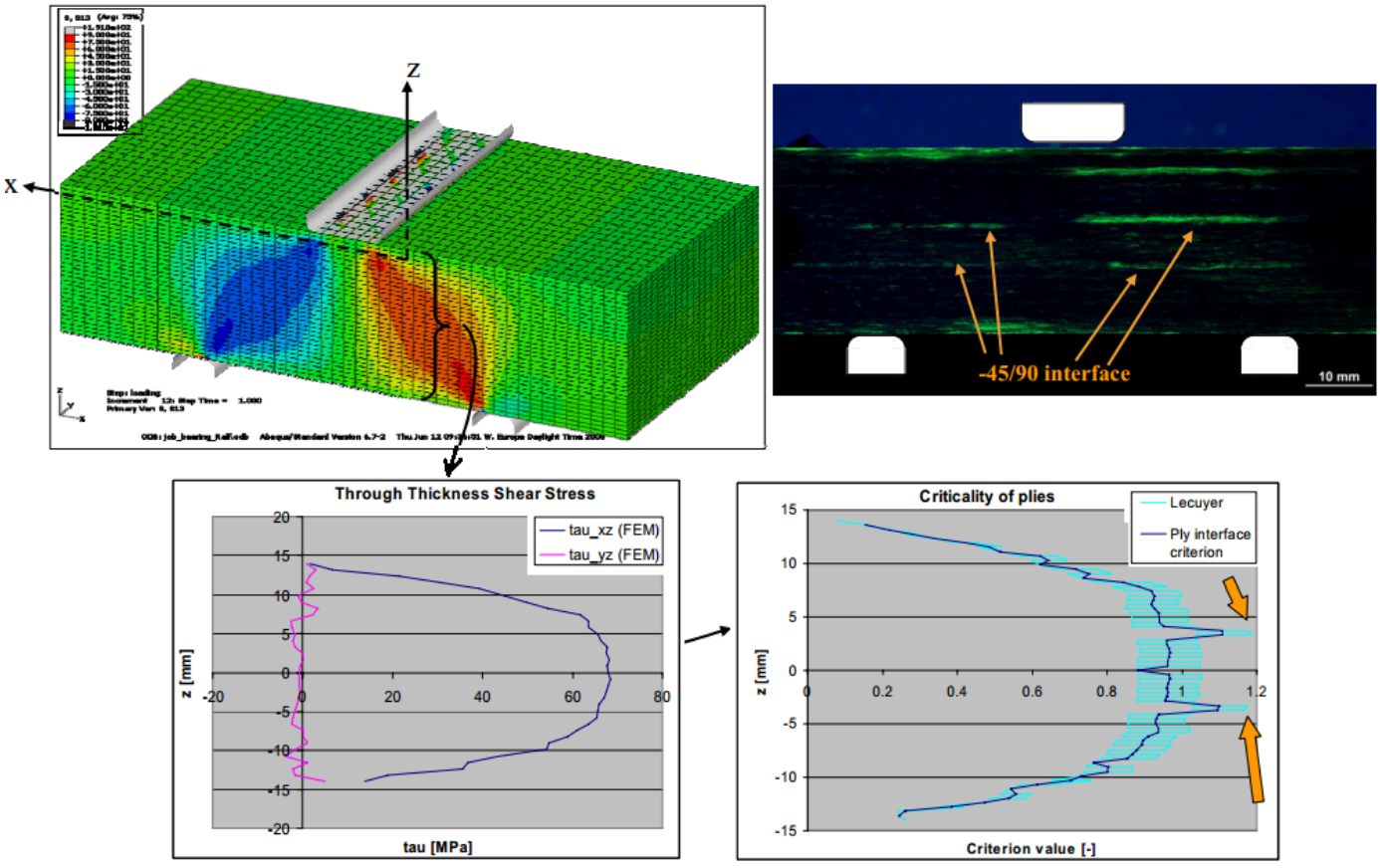

Figure 14 - "Transverse shear stresses in thick coupons and criticality of the different interfaces" (Creemers 2010)

Reddy (2004) has demonstrated how to obtain interlaminar shear stress (τ_{xz}) by combining the laminate constitutive equations for a composite laminate with the equilibrium equations for 3-D elasticity as will be explained in Chapter 2. Transverse deflections of laminated composite beams have been assessed by Reddy (2004) when subjected to a point load as shown in Figure 15, or to an uniformly distributed load under three point bending conditions.

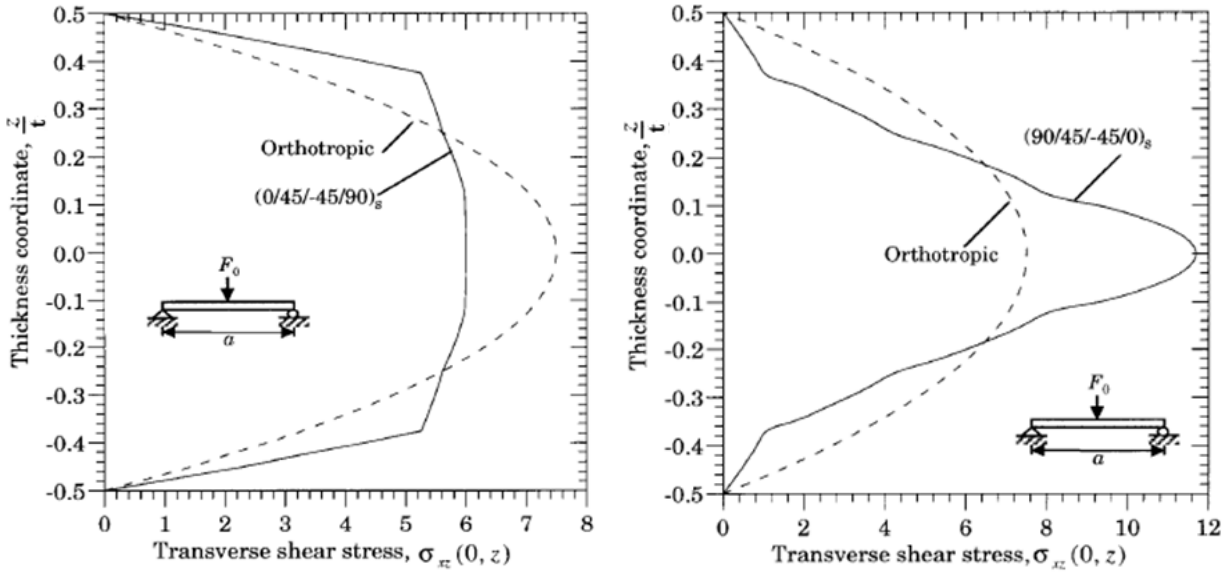

Figure 15 - through-thickness shear stress $\sigma_{xz} = \tau_{xz}$ of two different composite laminate under a transverse load according to Reddy (2004).

According to Reddy (2004) Figure 15 "shows the effect of the stacking sequence on the maximum transverse shear stress τ_{xz} for laminates $(0/45/-45/90)_s$ and $(90/45/-45/0)_s$ in which F_0=1.0, b=0.2, a=1.0 and t=0.1. The parabolic distribution of the transverse shear stress through the thickness (z coordinate) of an UD beam is shown in dashed lines for comparison. The maximum stress value is dependent on the stacking sequence."

Other studies have been performed on interlaminar stress. Choi & Thangjitham (1994) studied the interlaminar crack-tip response in a fibre-reinforced composite laminate, Makeev, et al. (2009) have studied the test method for assessment of shear properties for thick composites, Voyiadjis & Woelke (2008) have studied the determination of transverse shear stresses and delamination in composite laminates using finite elements.

1.7. COMPOSITE FATIGUE

In the past when composite laminates have started to be used in structures and experiments, it was believed that they did not suffer from fatigue. According to Harris (2003), in "the earliest days of composite development, their fatigue behavior was a subject of serious study. What was usually implied was that, because most of the carbon fibre reinforced plastics (CFRPs) were extremely stiff in the fibre direction, the working strains in practical components at conventional design stress levels were usually too low to initiate any of the local damage mechanisms that might

otherwise have caused deterioration under cyclic loading". Due to this assumption made on UD carbon composite laminates, it was believed that composites did not suffer from fatigue. Nowdays, composite fatigue is a concern during the development phase of a composite structural component.

Fatigue damage is characterised by the degradation of either a composite or a metal component under cycled loading as shown in Figure 16.

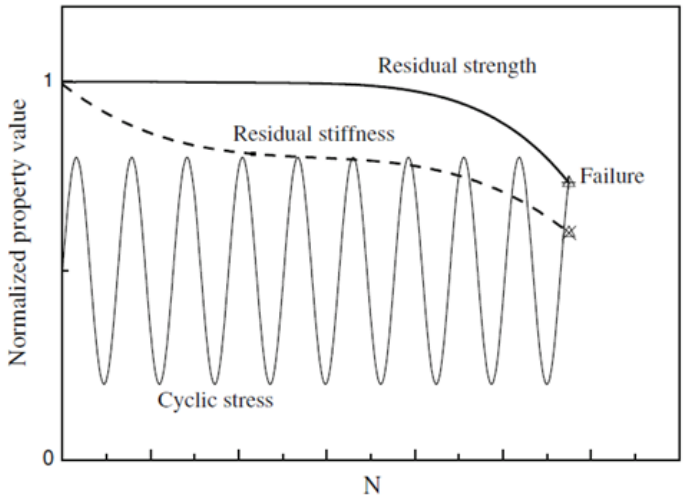

Figure 16 - Normalised property value (could represented by stress in MPa or load in Newtons) Vs Number of cycles (N). (Vassilopoulos & Keller 2011)

According to Harris (2003), many factors can affect the fatigue behavior of a composite laminate such as: fibre type, the matrix and environment, hybrid composites, short-fibre composites, interleaving and loading conditions.

Figure 17 show a few plots are shown that describe those fatigue behaviors:

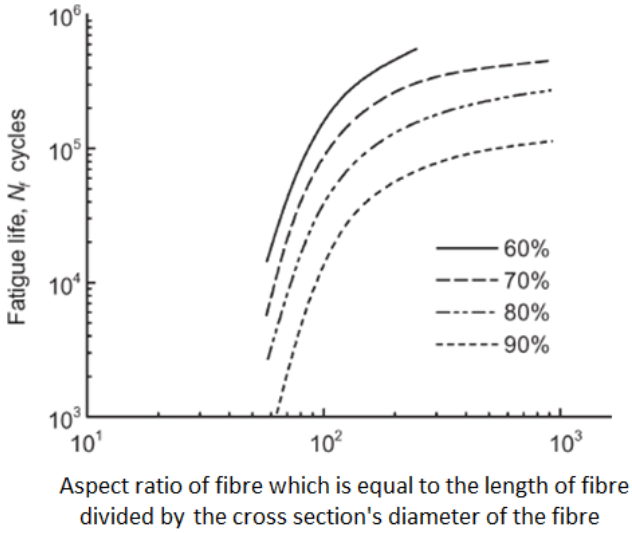

Figure 17 - Fatigue life versus aspect ratio for an applied stress of the indicated percentage of the composite tensile strength. The materials are short-fibre-reinforced boron/epoxy composites; in cyclic tension (Harris 2003)

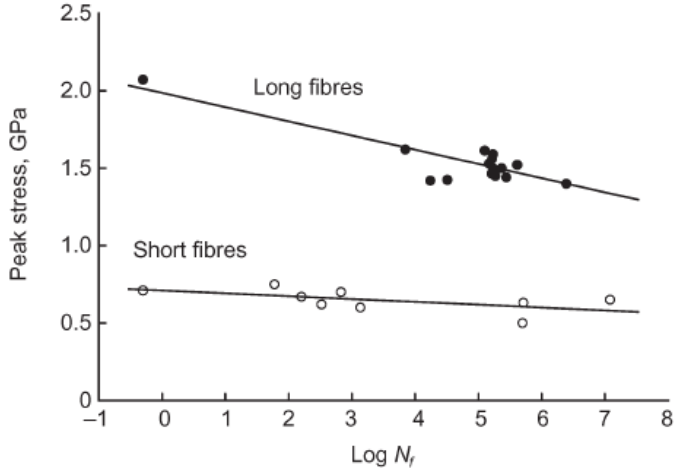

Figure 18 - Logarithmic life vs Stress curve, data for UD composites of XAS/914 carbon/epoxy laminates reinforced with continuous and discontinuous fibres (R=0.1) (Harris 2003)

Other studies have been done on this field. Shinji Ogihara et al. (1999) have studied the effects of stacking sequence on microscopic fatigue damage development in quasi-isotropic CFRP laminates with interlaminar-toughened layers as shown in Figure 19.

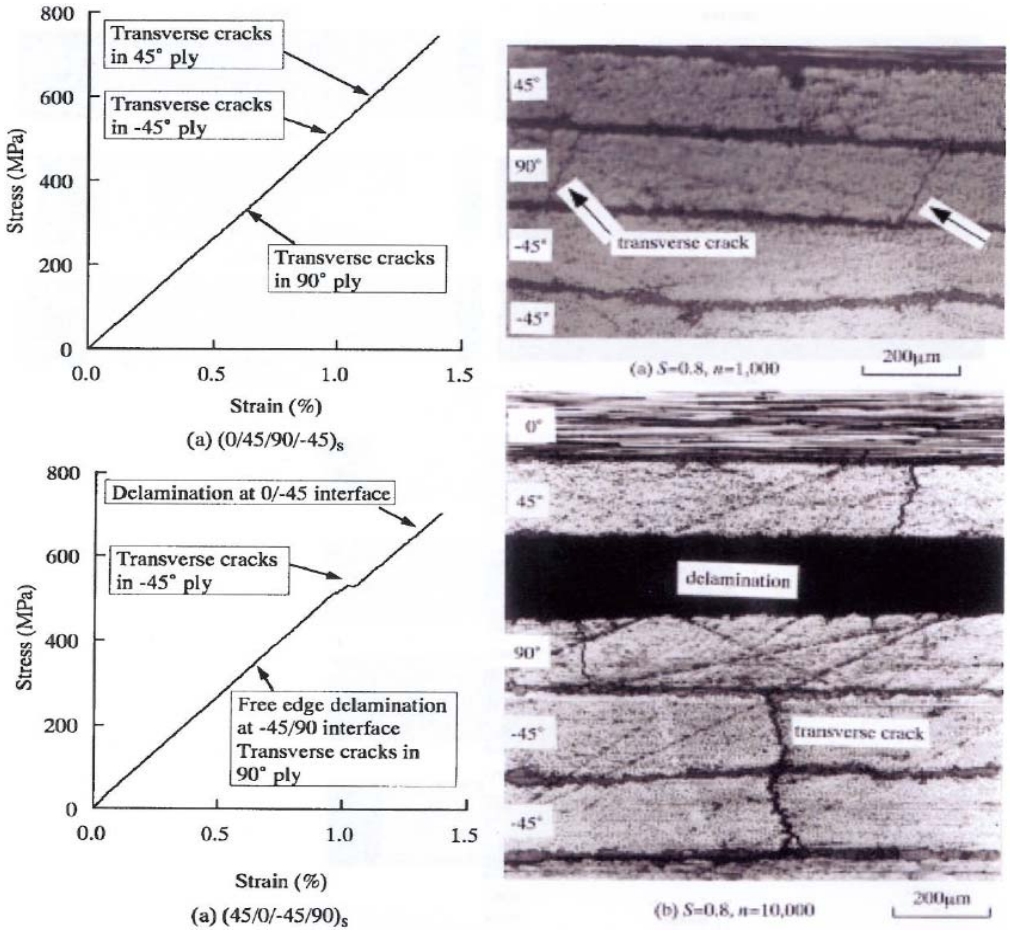

Figure 19 - Typical stress-strain damage onset on T800H/3900-2 quasi-isotropic laminates (plots) under a tensile test. At the right side of the image is shown the respective microscopic damage progress (Ogiharaa et al. 1999).

Phillips (1976) has studied the effect of hybrid composite laminates which consists of both glass and carbon plies within the same laminate. He has noticed that "hybrid composite materials appear to fail later than predicted, in a tough and fatigue resistant manner" due to the combination of glass plies and carbon plies in the composite laminate. Also, Dickson et al. (1989) has studied the fatigue behavior of hybrid composite laminates manufactured from glass and carbon plies. In his conclusions, he has noticed that "the fatigue stress for a life of 10^6 cycles and the fatigue ratio vary with the composition of the composite laminate in a manner that suggests a positive synergistic effect " which means that the combination of glass and carbon plies in a single composite laminate contributes for a better fatigue life, increasing the number of cycles is able to withstand the composite component.

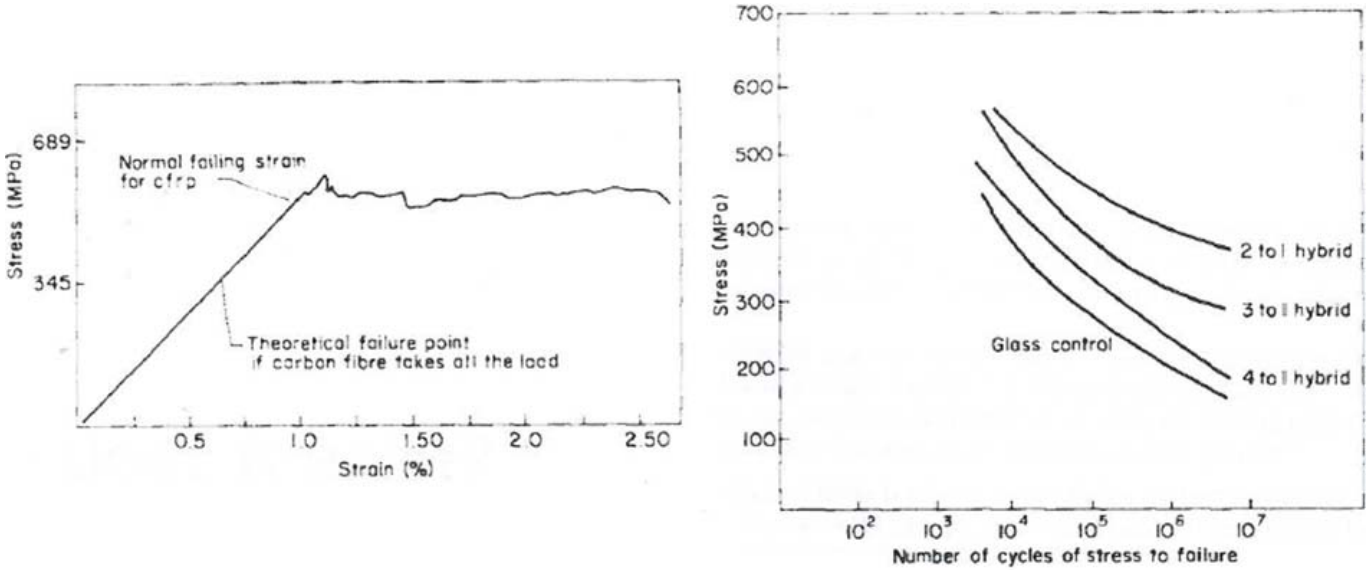

Figure 20 - Hybrid material stress/strain curve (left plot), and fatigue life of glass fibre composite and glass/carbon hybrids (right plot) (Phillips 1976).

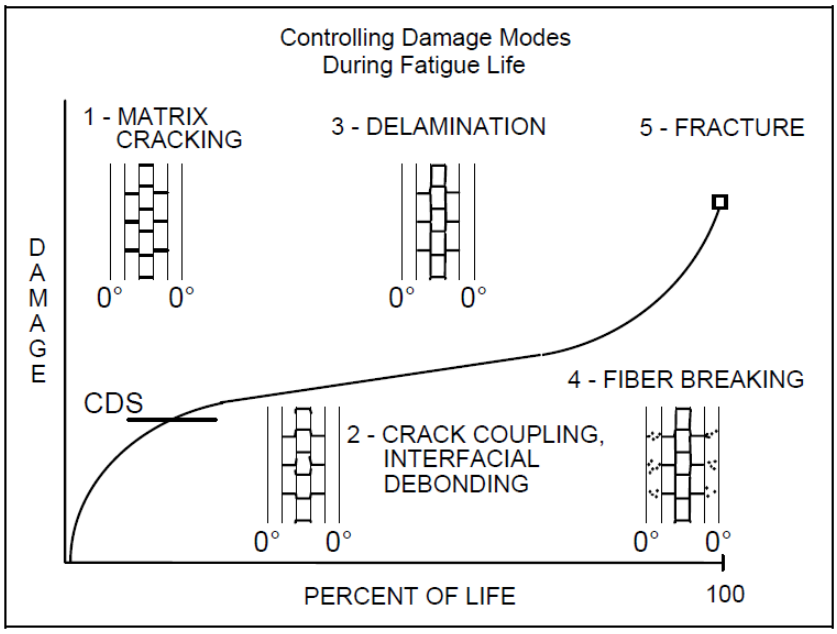

Figure 21 - Fatigue damage development in composite laminates (German 2004)

1.8. RESEARCH OBJECTIVES

The literature review has shown that fatigue life in terms of crack initiation can be improved by finding the best ply orientation for through-thickness performance by the use of hybrid composite laminates.

The purpose of this thesis is to report on the development of design rules to improve the interlaminar shear strength (ILSS), which will be needed to improve the fatigue life of a component under through-thickness loading. Through those rules, a delay in the crack initiation of the composite component will be achieved. By choosing an appropriate combination of through-thickness fibre arrangements, materials and geometry, a better fatigue behaviour of the component is expected under "in-service" conditions.

The objectives of this thesis can be summarized as follows:

- Development of an algorithm to find the best material disposition of an hybrid composite laminate made by carbon and glass plies, in which a maximum of 40% of the plies are made by glass material. This algorithm should run every possible combination of material position plus orientation.

- Instruct the algorithm to use the through-thickness shear stress equation for 2-D given in Chapter 2, and find the best stacking sequence of plies in order to minimize the damage in the middle of the composite laminate loaded subject to an SBS test (see Figure 13).

- Perform and assess experimental static and fatigue test to assess and confirm theory.

- Perform and assess CT scan of the best composite designs found.

- Compare three different designs and give the best design found which has an improvement in both fatigue and static properties.

1.9. THESIS SUMMARY

Chapter 1 is an introductory chapter which describes in general, what a composite laminate is and how it is made, types of damage that could be caused in the composite laminate loaded in a determined load condition, fatigue issues of a composite part, and a few research and developments that have been made on the through-thickness shear stress.

Chapter 2 demonstrates how to obtain the interlaminar shear strength for a two dimensional analysis.

Chapter 3 describes how the algorithm was built and the considerations taken in order to run all possible combinations of materials and ply orientations.

Chapter 4 gives an assessment of the static tests that have been performed in order to confirm the findings.

Chapter 5 describes the assessment that has been made of the fatigue experiments. Also, in this chapter is shown CT scan images of two composite components that were tested under a fatigue condition using a monotonic load.

The experimental work was carried out by an MSc student (Han 2013).

Chapter 2

THEORETICAL ASSESSMENT - DEMONSTRATION

2.1. INTRODUCTION

In order to achieve the best stacking sequence that will minimize the ILSS (τ_{xz} and τ_{zx}) in the middle of a composite laminate (central ply of the laminate) and in a four ply angle hybrid laminate, an optimization method has been developed in Matlab R2011b (Chapter 3), in order to find from all the possible combinations of angles and materials, the best result to minimize the damage in the middle of the laminate under a SBS test condition.

From the results obtained through the optimization method that has been created, two laminate designs were chosen, the first one, with a stacking sequence limited to a maximum angle of 45°, and the second one, with a maximum laminate ply orientation of 90°. In addition a quasi-isotropic laminate was considered.

All laminates have 24 plies. They are symmetric and balanced in regards to their middle surface in order to avoid laminate bending effects, resulting from the stretching of the midplane of the laminate as well as the enforcement of curvatures, which results in additional bending moments due to the internal strains (anticlastic bending) (Ashton et al. 1969, p.39).

This Chapter describes the method and analysis that have been used to assess the static strength condition of the three designs that were chosen. The laminates were assessed in a condition in which the right and left ends are simply supported.

2.2. CONVENTION

The reference system axis in use during this assessment is in accordance with the Figure 22 and Figure 23.

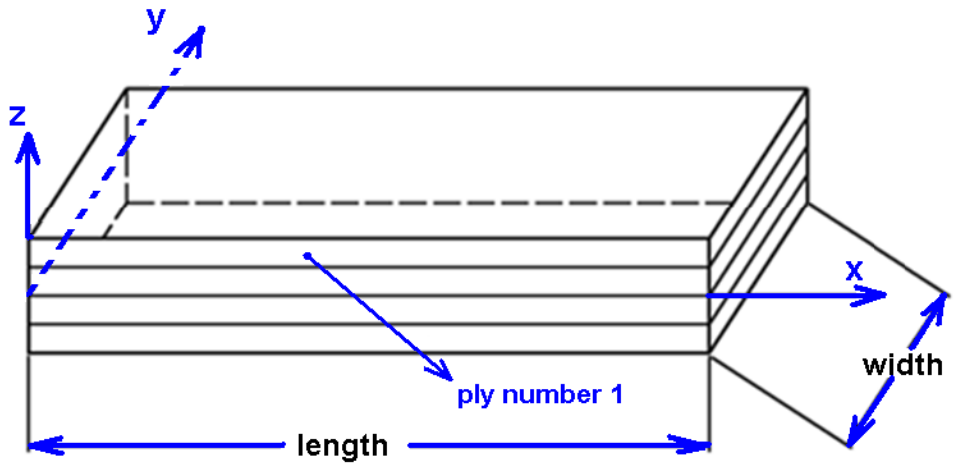

Figure 22 – Composite laminate coupon showing relevant axis system.

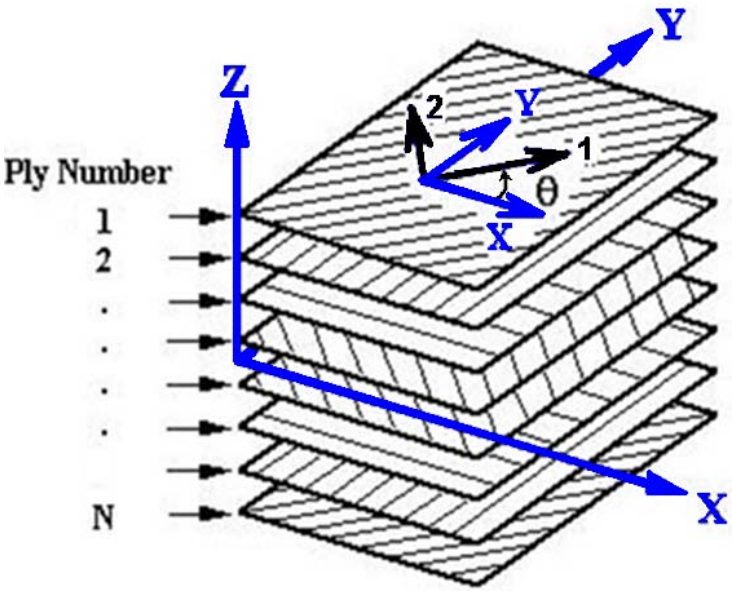

Figure 23 - Ply number and respective system axis used throughout this thesis (Delaware University 2005).

Note: The application of the Interlaminar Shear Strength equations that are presented in this work, should be applied from the top of the laminate shown on the image above, down to the bottom of the laminate.

2.3. ILSS IN ACCORDANCE WITH THE STANDARDS

As Han (2013, chapter 3) has demonstrated in his work, the ILSS equation which is given in the standards D2344/2344M (2006) and BS14130:1998 (2004) was derived for an isotropic short beam.

According to Han (2013), and changing the system axis in accordance with the convention shown on the section 2.2, the shear stress flow equation represented by the variable q_s is given by:

$$q_s = \frac{S_z}{I_y}\int_0^s t\,z\,ds + \frac{S_y}{I_z}\int_0^s t\,y\,ds \qquad (1)$$

In which, I_x and I_y are the moments of inertia in regards to the *x* axis and *y* axis respectively, and the variables S_z and S_y are the support loads, in which, S_z is equal to $\frac{P}{2}$ and S_y is equal to zero as will be explained later in this section.

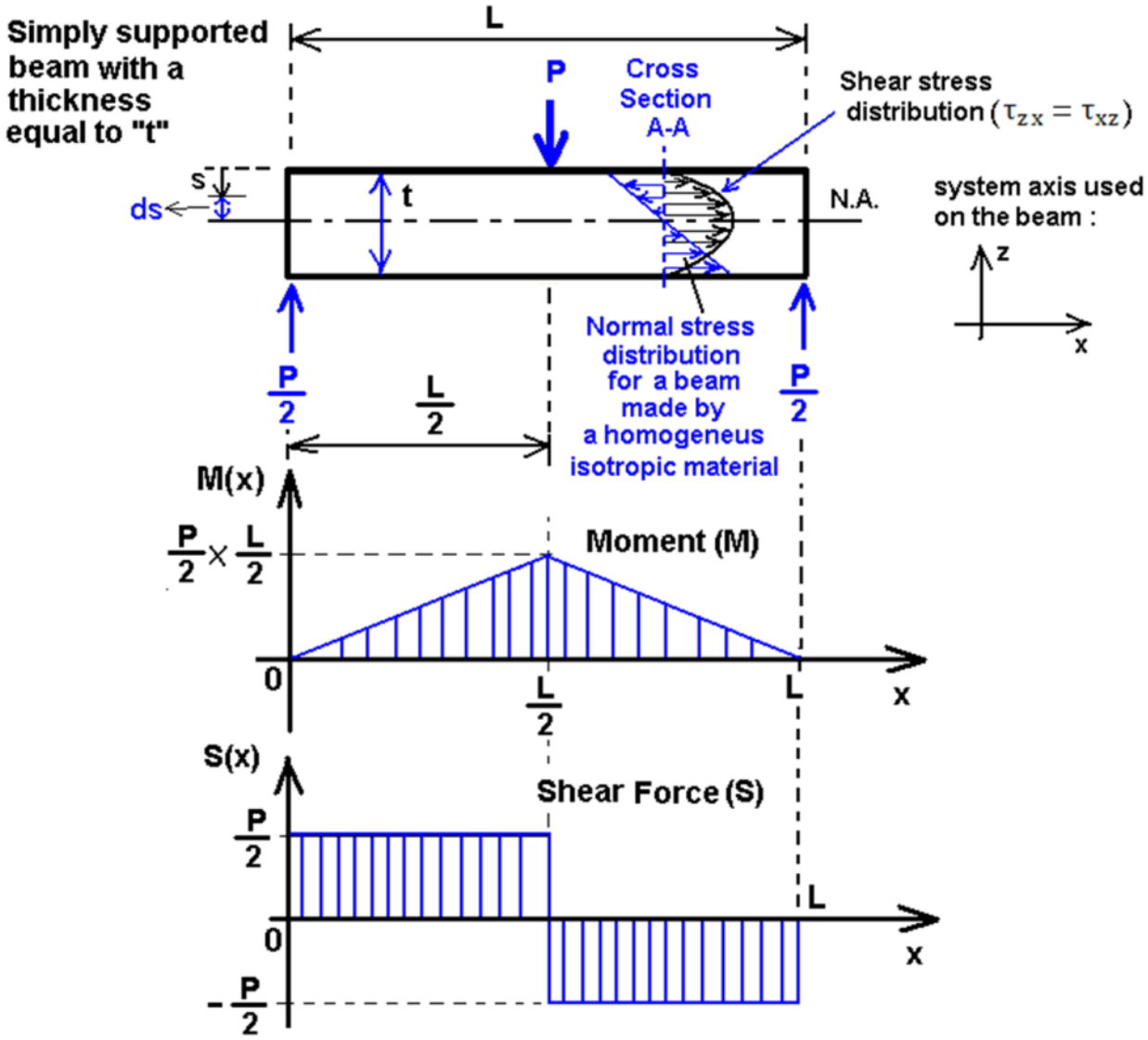

Figure 24 - Simply supported beam diagram

From the Figure 24, the constant *t* is the thickness of the beam, and, the variable *P* is the total *line load* applied over the top surface of the beam at the middle position of the specimen length, on a 3PB or SBS test condition.

Since there is no torsion in this short beam shear strength problem, then the load $S_y = 0$ (Han 2013) .

Applying the assumption given above to equation (1) gives shear flow, q_s as shown in equation (2).

$$q_s = \frac{S_z}{I_y}\int_0^s t\, z\, ds \tag{2}$$

For the distance from the middle of the cross section beam up to the point where the value of the Shear Stress is required ($z = \frac{t}{2} - s_1$), the equation (2) becomes:

$$q_s = \frac{S_z}{I_y}\int_0^s t\, z\, ds = \frac{S_z}{I_y}\int_0^s t\left(\frac{t}{2} - s_1\right) ds \tag{3}$$

As shown in Figure 24, *s* is limited to the interval: $0 < s < \frac{t}{2}$, thus the equation (3) will be:

$$q_s = \frac{S_z}{I_y}\int_0^{\frac{t}{2}} t\left(\frac{t}{2} - s_1\right) ds \tag{4}$$

When $s_1 = \frac{t}{2}$, then:

$$q_s = \frac{S_z}{I_y}\left[\frac{t^2}{2}.\frac{t}{2} - \frac{t}{2}.\frac{t^2}{4}\right] = \frac{S_z}{I_y}.\frac{t^3}{8} \tag{5}$$

Since $I_y = \frac{b \times t^3}{12}$, and, $S_z = \frac{P}{2}$ and $b = \text{width of the beam}$, then:

$$q_s = \frac{3 \times P}{4 \times b} \tag{6}$$

Since the shear flow is described as the shear force per unit length, then:

$$q_s = t \times \tau_{xz} \tag{7}$$

From the equation above, the equation for the ILSS in accordance with the standards D2344/2344M (2006) and BS14130:1998 (2004) is given by:

$$\mathbf{ILSS}_{Apparent} = \boldsymbol{\tau}_{\mathbf{xz}} = \frac{\mathbf{3P}}{\mathbf{4bt}} \tag{8}$$

NOTE: τ_{xz} will be equal to ILSS ($ILSS_{Apparent}$) when the variable P is equal to the ultimate load.

which is normally presented in the standards as:

$$F^{sbs} = 0.75 \times \frac{P}{bt} \tag{9}$$

NOTE: The constant *P* is the load applied (in Newtons) on a SBS test coupon according to standard D2344/2344M (2006) and BS14130:1998 (2004).

2.4. LAMINATE CONSTITUTIVE EQUATIONS

This section will provide the base theory required for the next sections, which is based on the *Laminate Constitutive Equations*.

Certain assumptions are made in the formulation of the laminate constitutive relationship theory. In accordance with Ashton et al. (1969, section 2.3) in the theory of bending of beams and plates, and, due to the geometry of the plate, the normal stress, σ_3, which is perpendicular to the plate midplane surface, is considered negligible in comparison to the normal stresses σ_1 and σ_2. Also, as referred by Ashton et al. (1969), another assumption that is made in this theory is that, any line perpendicular to the plate mid-plane surface before the deformation occurs, remains perpendicular to that surface after the deformation, and no extension or contraction occurs, as a result of this consideration, the shear strains γ_{13} and γ_{23}, and the normal strain, ε_3 will be equal to zero.

Through the considerations taken above, and considering that τ_{13} and τ_{23} are neglected, the lamina could be considered to be in a plane stress state as shown in Figure 25.

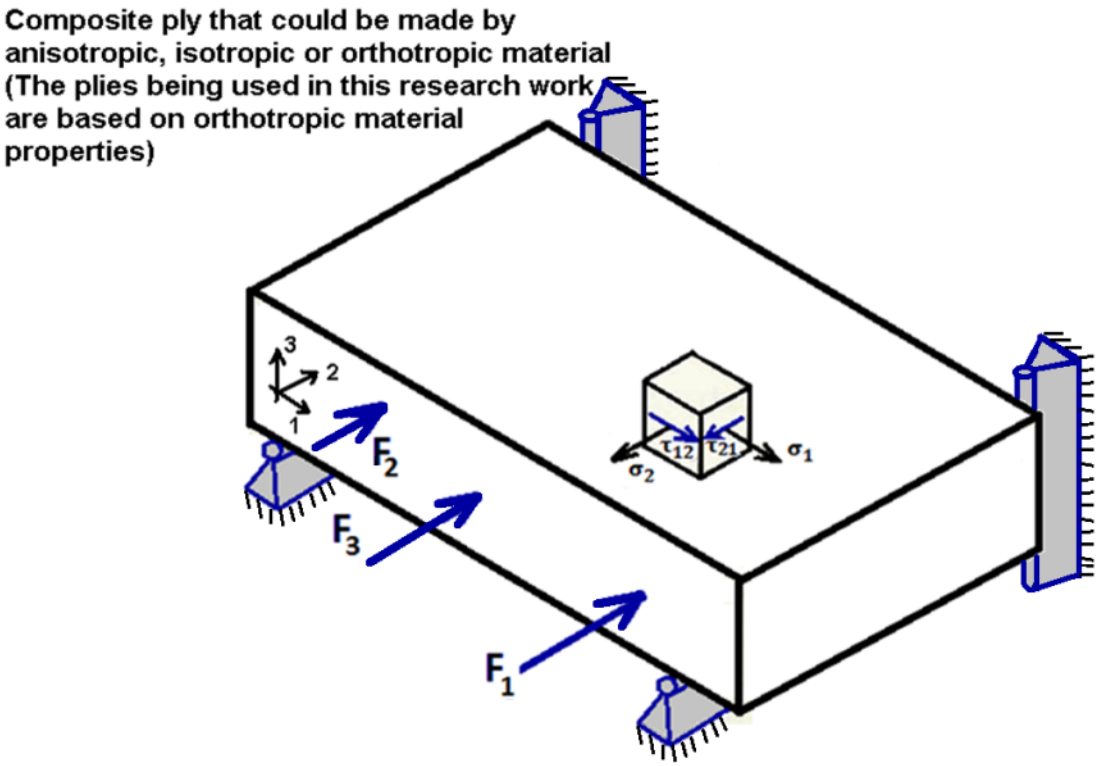

Figure 25 - Plane stress state on an element within the thin plate (each ply considered as a thin plate) simply supported. F_1; F_2 and F_3 are external forces.

Figure 25 shows the plane stress state of an element within the thin plate, in which, external forces (F_1; F_2; F_3; F_4 and F_5) are applied on the edges of the plate.

The assumption to apply this theory in composite laminates, is that, the plies, when in the composite laminate, are in a plane stress state. By making this assumption, the stress-strain relationships can be established for a composite part, however, "a plane stress state on a lamina is not merely an idealization of reality, but instead is a practical and achievable objective of how we must use a lamina with fibres in its plane" (Jones 1999, p.71).

In a three-dimensional stress state as shown in Figure 26, Hooke's law relationship for anisotropic materials is expressed as (Jones 1999) :

$$\sigma_{ij} = \sum_{k=1}^{3} \sum_{l=1}^{3} C_{ijkl} \times \varepsilon_{kl} \; ; \text{ for } \; \mathrm{i,j} = 1,2,3 \tag{10}$$

where the variable σ_{ij} (for $\mathrm{i,j} = 1,2,3$) is the stress tensor, ε_{kl} (for $\mathrm{k,l} = 1,2,3$) is the strain tensor of the elastic anisotropic material, and the variables C_{ijkl} (for $\mathrm{i,j,k,l} = 1,2,3$) are the elastic constants of the material.

For a linearly elastic medium in which the strain energy function given by the equation (12) satisfies the relationship shown in the equation (11), then the stress tensor σ_{ij} and the strain tensor ε_{kl} are symmetric, and the conditions given by the equation (13) are verified in the anisotropic material properties.

$$\sigma_{\mathrm{ij}} = \frac{\partial \mathrm{U}}{\partial \varepsilon_{\mathrm{ij}}} \quad \text{and} \quad \mathrm{i,j} = 1,2,3 \tag{11}$$

in which:

$$U = \frac{1}{2} \times C_{ijkl} \times \varepsilon_{ij} \times \varepsilon_{kl} \quad (\text{for } \mathrm{i,j,k,l} = 1,2,3) \tag{12}$$

then,

$$\sigma_{ij} = \sigma_{ji} \; ; \; \varepsilon_{kl} = \varepsilon_{lk}; C_{ijkl} = C_{jikl} = C_{ijlk} = C_{jilk} \text{ and } C_{ijkl} = C_{klij} \quad (\text{for } \mathrm{i,j,k,l} = 1,2,3) \tag{13}$$

For an equality shown by the expression number (14) :

$$\begin{bmatrix} \sigma_{11} \\ \sigma_{22} \\ \sigma_{33} \\ \sigma_{23} \\ \sigma_{13} \\ \sigma_{12} \end{bmatrix} = \begin{bmatrix} \sigma_1 \\ \sigma_2 \\ \sigma_3 \\ \tau_{23} \\ \tau_{13} \\ \tau_{12} \end{bmatrix} \quad \text{and} \quad \begin{bmatrix} \varepsilon_{11} \\ \varepsilon_{22} \\ \varepsilon_{33} \\ 2 \times \varepsilon_{23} \\ 2 \times \varepsilon_{13} \\ 2 \times \varepsilon_{12} \end{bmatrix} = \begin{bmatrix} \varepsilon_1 \\ \varepsilon_2 \\ \varepsilon_3 \\ \gamma_{23} \\ \gamma_{13} \\ \gamma_{12} \end{bmatrix} \tag{14}$$

the constitutive relationship for the general case of an anisotropic material is given by the equation (15) (Halpin 1992).

$$\begin{bmatrix} \varepsilon_1 \\ \varepsilon_2 \\ \varepsilon_3 \\ \gamma_{23} \\ \gamma_{13} \\ \gamma_{12} \end{bmatrix} = \begin{bmatrix} S_{11} & S_{12} & S_{13} & S_{14} & S_{15} & S_{16} \\ S_{12} & S_{22} & S_{23} & S_{24} & S_{25} & S_{26} \\ S_{13} & S_{23} & S_{33} & S_{34} & S_{35} & S_{36} \\ S_{14} & S_{24} & S_{34} & S_{44} & S_{45} & S_{46} \\ S_{15} & S_{25} & S_{35} & S_{45} & S_{55} & S_{56} \\ S_{16} & S_{26} & S_{36} & S_{46} & S_{56} & S_{66} \end{bmatrix} \times \begin{bmatrix} \sigma_1 \\ \sigma_2 \\ \sigma_3 \\ \tau_{23} \\ \tau_{13} \\ \tau_{12} \end{bmatrix} \tag{15}$$

in which the compliance matrix $[S_{ij}]$ is equal to $[C_{ij}]^{-1}$; for $\mathrm{i,j} = 1,2,3,4,5 \text{ and } 6$.

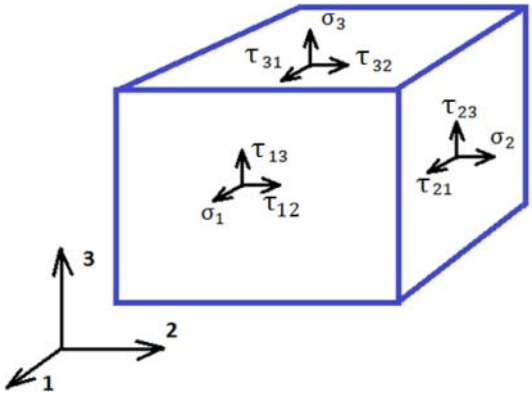

Figure 26 – Three-dimensional state of stress for an element taken from a single ply (lamina) as shown in Figure 7

For an orthotropic material in which there are three mutually orthogonal planes of symmetry, the equation (15) is reduced to equation (16) (Halpin 1992).

$$\begin{bmatrix} \varepsilon_1 \\ \varepsilon_2 \\ \varepsilon_3 \\ \gamma_{23} \\ \gamma_{13} \\ \gamma_{12} \end{bmatrix} = \begin{bmatrix} S_{11} & S_{12} & S_{13} & 0 & 0 & 0 \\ S_{12} & S_{22} & S_{23} & 0 & 0 & 0 \\ S_{13} & S_{23} & S_{33} & 0 & 0 & 0 \\ 0 & 0 & 0 & S_{44} & 0 & 0 \\ 0 & 0 & 0 & 0 & S_{55} & 0 \\ 0 & 0 & 0 & 0 & 0 & S_{66} \end{bmatrix} \times \begin{bmatrix} \sigma_1 \\ \sigma_2 \\ \sigma_3 \\ \tau_{23} \\ \tau_{13} \\ \tau_{12} \end{bmatrix} \tag{16}$$

For a plane stress state on a orthotropic thin plate as shown in Figure 25, the normal stress σ_3 and the shear stresses τ_{23} and τ_{13} are equal to zero as shown in the equation (17). Since the stresses σ_3; τ_{23} and τ_{13} are equal to zero, then γ_{23} and γ_{13} will also be equal to zero.

$$\sigma_3 = \tau_{23} = \tau_{13} = \gamma_{23} = \gamma_{13} = 0 \tag{17}$$

This also verifies the condition given in equation (18).

$$\varepsilon_3 = S_{13} \times \sigma_1 + S_{23} \times \sigma_2 \tag{18}$$

Thus, by substituting the equations (17) and (18) into the equation (16), the equation (19) for a orthotropic material is obtained.

$$\begin{bmatrix} \varepsilon_1 \\ \varepsilon_2 \\ \gamma_{12} \end{bmatrix} = \begin{bmatrix} \mathrm{S}_{11} & \mathrm{S}_{21} & 0 \\ \mathrm{S}_{12} & \mathrm{S}_{22} & 0 \\ 0 & 0 & \mathrm{S}_{66} \end{bmatrix} \times \begin{bmatrix} \sigma_1 \\ \sigma_2 \\ \tau_{12} \end{bmatrix} \tag{19}$$

According to Reddy (2004, p.30), the compliance coefficients S_{11}, S_{21}, S_{12}, S_{22} and S_{66} are related to the engineering constants E_1, E_2, ν_{21}, ν_{21} and G_{12} as shown in equation (20).

$$\begin{cases} \mathrm{S}_{11} = \dfrac{1}{E_1} \\ \mathrm{S}_{21} = -\dfrac{\nu_{21}}{E_2} \\ \mathrm{S}_{12} = -\dfrac{\nu_{12}}{E_1} \\ \mathrm{S}_{22} = \dfrac{1}{E_2} \\ \mathrm{S}_{66} = \dfrac{1}{G_{12}} \end{cases} \tag{20}$$

For a homogeneous isotropic lamina (ply) in a plane stress state, in which the elastic constants are: $\mathrm{E}_1 = \mathrm{E}_2 = \mathrm{E}$ and $\nu_{12} = \nu_{21} = \nu$, equation (19) will be equivalent to equation (21) (Jones 1999).

$$\begin{cases} \sigma_1 = (\varepsilon_1 + \nu_{21} \times \varepsilon_2) \dfrac{\mathrm{E}_1}{1 - \nu_{12} \times \nu_{21}} \\ \sigma_2 = (\varepsilon_2 + \nu_{12} \times \varepsilon_1) \dfrac{\mathrm{E}_2}{1 - \nu_{12} \times \nu_{21}} \\ \tau_{12} = (\gamma_{12}) \times G_{12} \end{cases} \tag{21}$$

The Hooke's law relationship given by equation (21) will be expressed in a matrix form for the j^{th} ply, in which: $1 \leq j \leq$number of plies in the laminate (Jones 1999). Thus, equation (21) in the matrix form will be given by equation (22).

$$\begin{bmatrix} \sigma_1 \\ \sigma_2 \\ \tau_{12} \end{bmatrix}_{j^{th}\, ply} = \begin{bmatrix} \mathrm{Q}_{11} & \mathrm{Q}_{21} & 0 \\ \mathrm{Q}_{12} & \mathrm{Q}_{22} & 0 \\ 0 & 0 & \mathrm{Q}_{66} \end{bmatrix}_{j^{th}\, ply} \times \begin{bmatrix} \varepsilon_1 \\ \varepsilon_2 \\ \gamma_{12} \end{bmatrix}_{j^{th}\, ply} \tag{22}$$

According to Jones (1999), the coefficients Q_{mn} (in which each of the subscripts m,n are equal to 1, 2 or 6) are given by equations (23), (24), (25), (26) and (27).

$$\begin{cases} Q_{11} = \dfrac{E_1}{1 - v_{12} \times v_{21}} & (23) \\ Q_{12} = \dfrac{v_{12} \times E_2}{1 - v_{12} \times v_{21}} & (24) \\ Q_{21} = \dfrac{v_{21} \times E_1}{1 - v_{12} \times v_{21}} & (25) \\ Q_{22} = \dfrac{E_2}{1 - v_{12} \times v_{21}} & (26) \\ Q_{66} = G_{12} & (27) \end{cases}$$

The matrix that contains the coefficients Q_{mn} is also called the stiffness matrix ($[Q_{mn}]$) for a lamina in natural coordinate system (as shown in Figure 25).

The equations number (22), (23), (24), (25), (26) and (27), demonstrated previously, can be established for a single homogeneous orthotropic ply, in which the filamentary lamina can be unidirectional (UD) or woven (this research is based in UD plies), and assuming that each lamina (ply) is in a plane stress state as shown in Figure 25.

As explained by Ashton, et al. (1969, p.18), "the macromechanics approach to the problem ignores the fibre-resin geometry and interactions and assumes the lamina is a homogeneous medium". In this basis, Hooke's law relationship for a homogeneous material with orthotropic properties (as shown in Figure 27), and, in a plane stress state can be expressed by the equation (28).

$$\begin{cases} \sigma_1 = Q_{11}\,\varepsilon_1 + Q_{12}\,\varepsilon_2 \\ \sigma_2 = Q_{12}\,\varepsilon_1 + Q_{22}\,\varepsilon_2 \\ \tau_{12} = Q_{66} \times \gamma_{12} \end{cases} \quad (28)$$

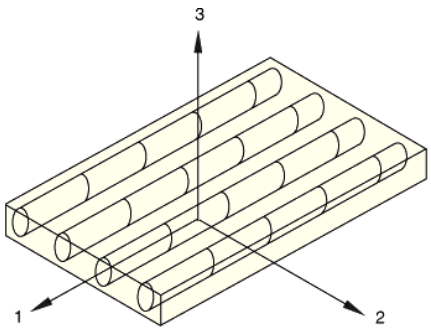

Figure 27 - Example of an orthotropic lamina (single ply), which, in a macroscopic view can be approximated to a homogeneous material with orthotropic properties.

In the equation (21) the properties of the orthotropic material given by E_1; E_2; ν_{12}; ν_{21} and G_{12} could be determined experimentally, using test specimens made up with the required material.

In order to determine the Young's Modulus E_1 and the Poisson's ratio ν_{12} of the laminate it is necessary to perform an uniaxial experimental test with UD composite laminates made up with a single material type as shown in Figure 28.

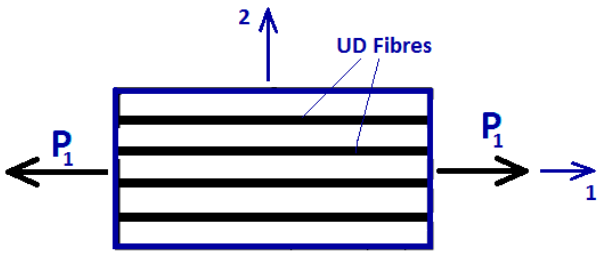

Figure 28 – Top view of an UD orthotropic composite laminate subjected to an uniaxial tensile load P_1 in the direction *1*.

In order to define Young's Modulus, E_1 and the Poisson's ratio, ν_{12} using the test setup shown in Figure 28, the following measurements must be taken: applied load, P_1, cross-section area, *A* with regards to the system axis *1* direction, longitudinal strain, ε_1 and transverse strain, ε_2. Equations (29) and (30) may then be applied (Reddy 2004).

$$\begin{cases} \mathrm{E}_1 = \dfrac{\mathrm{P}_1}{A \times \varepsilon_1} & (29) \\ \nu_{12} = -\dfrac{\varepsilon_2}{\varepsilon_1} & (30) \end{cases}$$

To define the Young's Modulus E_2, the process is repeated with the test load, P_1 applied in the *2* direction of the ply system axis as shown in Figure 29.

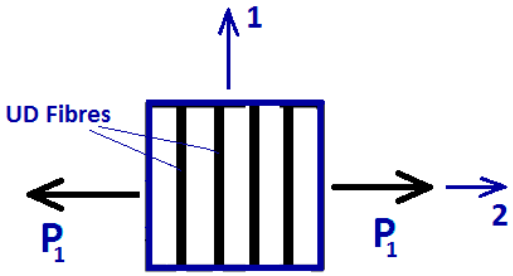

Figure 29 - Top view of an UD orthotropic composite laminate subjected to an uniaxial tensile load P_1 in the direction *2*.

In order to define Young's Modulus, E_2 using the test setup shown in Figure 29, the following measurements must be taken: applied load, P_1, cross-section area, *A* with regards to the system axis *2* direction and transverse strain, ε_2 (measured on the system axis *2* direction). Equation (31) may then be applied (Reddy 2004).

$$\mathrm{E}_2 = \frac{\mathrm{P}_1}{A \times \varepsilon_2} \tag{31}$$

With the values for the Young's Modulus E_1 and E_2 and the Poisson's ratio ν_{12} given by the experimental tests (Figure 28 and Figure 29), and since the material is homogeneous with orthotropic properties it is possible to determine the value for the Poisson's ratio ν_{12} by applying Maxuell's reciprocal theorem (Hoff 1956, p.373) given by the equation (32).

$$\frac{\mathrm{v}_{12}}{\mathrm{E}_1} = \frac{\mathrm{v}_{21}}{\mathrm{E}_2} \tag{32}$$

In order to obtain the value of the Shear Modulus G_{12} an experimental test is required in which the orthotropic composite laminate is pure subjected to a shear force on the edges of the laminate as shown in Figure 30.

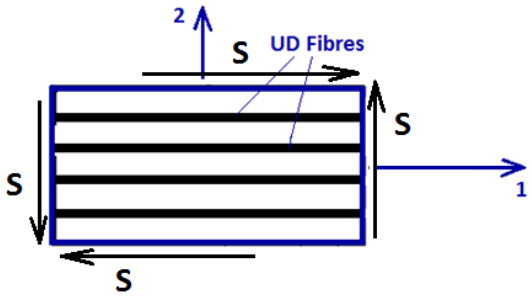

Figure 30-Top view of the orthotropic composite ply. Shear force *S* acting on the ends of the composite ply.

The experimental test shown in Figure 30 is equivalent to the experimental test shown on the right side of the Figure 31.

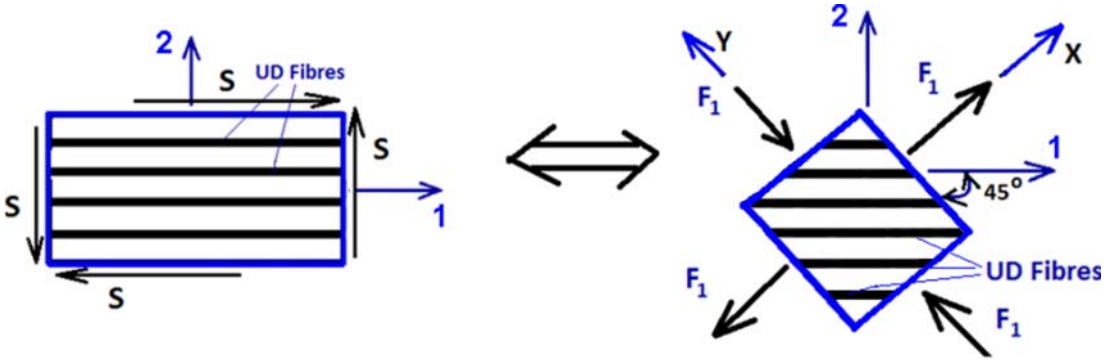

Figure 31 – Equivalence between experimental tests. Constants *S* and F_1 are the shear force and the normal force respectively.

Then, taking this into consideration, the Shear Modulus, G_{12} may be defined using the test setup shown in Figure 32, in which a uniaxial load is applied at 45 degrees to the *1* direction of the orthotropic ply system axis.

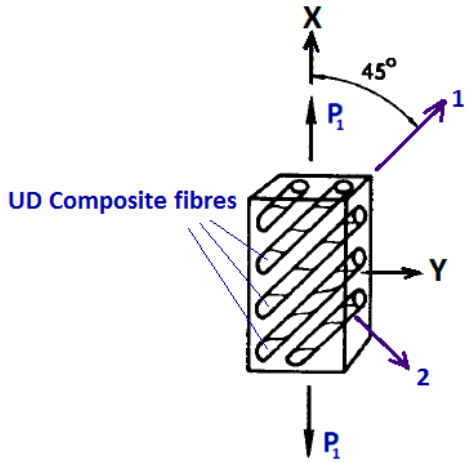

Figure 32 – Uniaxial loading at 45 degrees to the 1 direction of the orthotropic composite ply Jones (1999).

According to Craig & Summerscales (1988, p.178), the equation for the Shear Modulus that provides optimum results when comparing theory (equation (33)) with the experiments (see Craig & Summerscales (1988, p.180)) is given by the Huber's equation (33).

$$G_{xy} = \frac{\sqrt{E_x \times E_y}}{2 \times \left(1 + \sqrt{\nu_{xy} \times \nu_{yx}}\right)} \tag{33}$$

Thus, for a homogeneous isotropic ply, equation (33) reduces to equation (34) because $E_1 = E_2 = E$; $\nu_{12} = \nu_{21} = \nu$.

$$G_{12} = \frac{E}{2 \times (1 + \nu)} \tag{34}$$

In the case of a single orthotropic composite ply, since G_{12} is a constant that comes from an experimental test under uniaxial loading at 45 degrees to the *1* direction of the orthotropic composite ply, as shown in Figure 32, meaning that the fibres are at an angle of 45 degrees to the loading axis, then in this circumstance the use of the Huber's equation (33) will give the optimum correlation between theory and experiment as referred by Craig & Summerscales (1988, p.178).

For a single orthotropic composite ply the Huber's equation (33) is defined as follows: (Craig & Summerscales 1988)

$$G_{12\ \textbf{Shear test}-\text{ Figure 30}} = G_{xy\ \textbf{45 degree tensile test}-\text{ Figure 32}} = G_{12} \tag{35}$$

giving,

$$G_{12} = \frac{\sqrt{E_{x\ 45\text{ degree tensile test– Figure 32}} \times E_{y\ 45\text{ degree tensile test– Figure 32}}}}{2 \times \left(1 + \sqrt{\nu_{xy\ 45\text{ degree tensile test– Figure 32}} \times \nu_{yx\ 45\text{ degree tensile test– Figure 32}}}\right)} \quad (36)$$

Since the fibres of the orthotropic composite ply are at an angle of 45 degrees with regards to the axis system *x*, then :

$$E_{x\ 45\text{ degree tensile test– Figure 32}} = E_{y\ 45\text{ degree tensile test– Figure 32}} \quad (37)$$

and also, according to Maxwell's reciprocal theorem (Hoff 1956, p.373) the relationship given by the equation (32) will be valid for a single orthotropic composite ply, so substituting equation (37) into the equation (32) gives:

$$\nu_{xy\ 45\text{ degree tensile test– Figure 32}} = \nu_{yx\ 45\text{ degree tensile test– Figure 32}} \quad (38)$$

Thus, for a single orthotropic composite ply, Huber's equation (Craig & Summerscales 1988) will be transformed into the expression (39)

$$G_{12} = \frac{E_{x\ 45\text{ degree tensile test– Figure 32}}}{2 \times \left(1 + \nu_{xy\ 45\text{ degree tensile test– Figure 32}}\right)} \quad (39)$$

NOTE: In this thesis, the value for the Shear Modulus G_{12} that has been used was given by the manufactures's data for the carbon and glass UD materials (CIBA-GEICY 1983). This value is shown in Table 20.

With the demonstration given previously, in which the relation given by equations number (28) and (32) were obtained for a plane stress state applied on a single ply (lamina), a general formulation for a whole laminate can be demonstrated, by transforming the constitutive relations of each single ply of a laminate to the laminate reference axes system (X,Y) as shown in Figure 23.
After the application of trigonometric functions, and through algebraic modifications made on the constitutive relation for a single ply (equation: (28)), the constitutive equation for an orthotropic ply that makes an angle of θ degrees in regards to the laminate system axis *X* can be expressed as:

$$\begin{bmatrix}\sigma_x\\ \sigma_y\\ \tau_{xy}\end{bmatrix}_{j^{th}\ ply} = \begin{bmatrix}Q_{11}^{*} & Q_{12}^{*} & Q_{16}^{*}\\ Q_{12}^{*} & Q_{22}^{*} & Q_{26}^{*}\\ Q_{16}^{*} & Q_{26}^{*} & Q_{66}^{*}\end{bmatrix}_{j^{th}\ ply} \begin{bmatrix}\varepsilon_x\\ \varepsilon_y\\ \gamma_{xy}\end{bmatrix}_{j^{th}\ ply} \quad (40)$$

Where:

$$
\begin{cases}
\bar{Q}_{11} = Q_{11}\cos^4\theta + 2(Q_{12} + 2Q_{66})\sin^2\theta\cos^2\theta + Q_{22}\sin^4\theta & (41)\\
\bar{Q}_{22} = Q_{11}\sin^4\theta + 2(Q_{12} + 2Q_{66})\sin^2\theta\cos^2\theta + Q_{22}\cos^4\theta & (42)\\
\bar{Q}_{12} = (Q_{11} + Q_{22} - 4\times Q_{66})\sin^2\theta\cos^2\theta + Q_{12}(\sin^4\theta + \cos^4\theta) & (43)\\
\bar{Q}_{66} = (Q_{11} + Q_{22} - 2Q_{12} - 2Q_{66})\sin^2\theta\cos^2\theta + Q_{66}(\sin^4\theta + \cos^4\theta) & (44)\\
\bar{Q}_{16} = (Q_{11} - Q_{12} - 2Q_{66})\cos^3\theta\sin\theta - (Q_{22} - Q_{12} - 2Q_{66})\cos\theta\sin^3\theta & (45)\\
\bar{Q}_{26} = (Q_{11} - Q_{12} - 2Q_{66})\cos\theta\sin^3\theta - (Q_{22} - Q_{12} - 2Q_{66})\cos^3\theta\sin\theta & (46)
\end{cases}
$$

The terms $\bar{Q}_{mn}$, which are the components of the lamina stiffness matrix (equation: (40)) are now expressed in terms of an arbitrary system axis.

Note: each of the indices m and n are equal to 1, 2 or 6.

Considering the strain at any point in a laminate undergoing some deformation as shown in Figure 33.

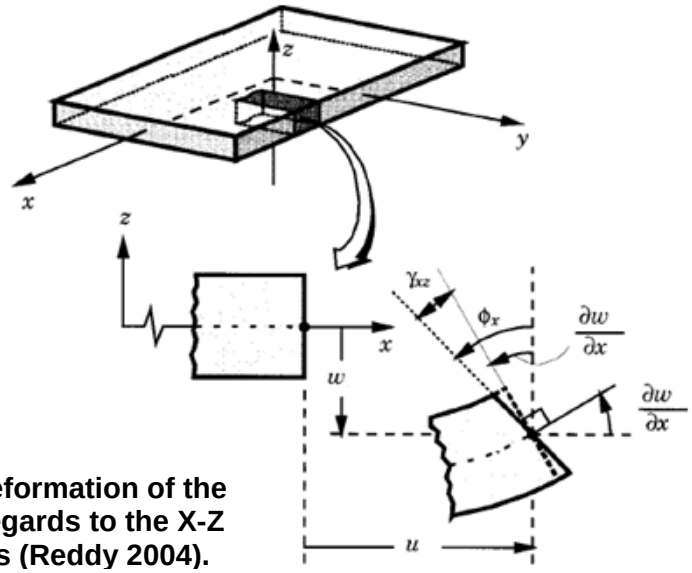

Figure 33 - Deformation of the laminate in regards to the X-Z laminate axis (Reddy 2004).

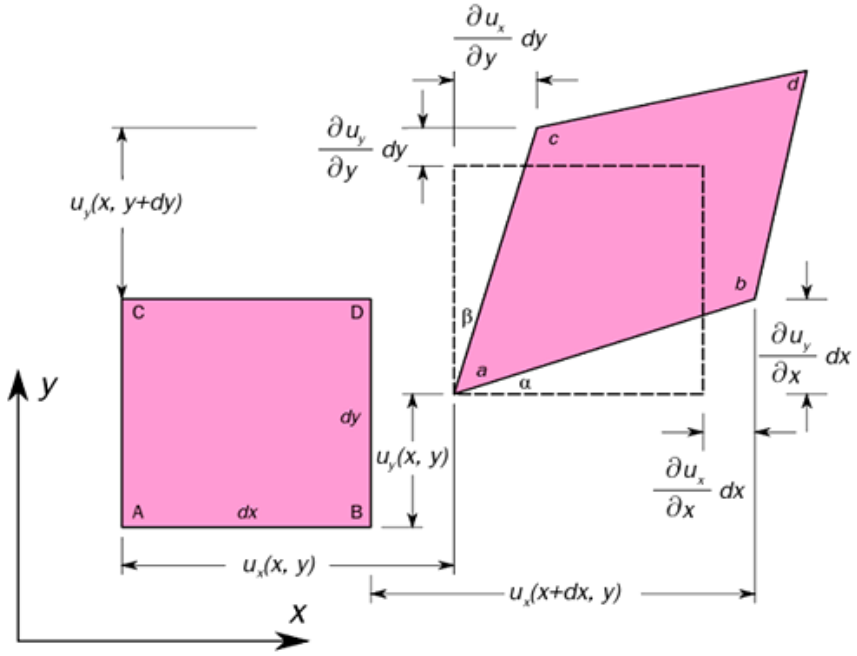

Figure 34- Deformation of the mid-plane laminate in regards to the Y-Z laminate axis (source: (Wikipedia 2009)).

The equation (40) becomes:

$$\begin{bmatrix}\sigma_x\\ \sigma_y\\ \tau_{xy}\end{bmatrix}_{j^{th}\,ply} = \begin{bmatrix}Q_{11}^{*} & Q_{12}^{*} & Q_{16}^{*}\\ Q_{12}^{*} & Q_{22}^{*} & Q_{26}^{*}\\ Q_{16}^{*} & Q_{26}^{*} & Q_{66}^{*}\end{bmatrix}_{j^{th}\,ply} \begin{bmatrix}\varepsilon_x^{0}\\ \varepsilon_y^{0}\\ \gamma_{xy}^{0}\end{bmatrix} + \begin{bmatrix}Q_{11}^{*} & Q_{12}^{*} & Q_{16}^{*}\\ Q_{12}^{*} & Q_{22}^{*} & Q_{26}^{*}\\ Q_{16}^{*} & Q_{26}^{*} & Q_{66}^{*}\end{bmatrix}_{j^{th}\,ply} \begin{bmatrix}k_x\\ k_y\\ k_{xy}\end{bmatrix} \quad (47)$$

in which:

$$\begin{cases}\varepsilon_x^{0} = \frac{\partial u_x}{\partial x}\\ \varepsilon_y^{0} = \frac{\partial u_y}{\partial y}\\ \gamma_{xy}^{0} = \frac{\partial u_x}{\partial x} + \frac{\partial u_y}{\partial y}\end{cases} \quad \text{and} \quad \begin{cases}k_x = -\frac{\partial^2 w}{\partial x^2}\\ k_y = -\frac{\partial^2 w}{\partial y^2}\\ k_{xy} = -2\frac{\partial^2 w}{\partial x\,\partial y}\end{cases} \quad (48)$$

Laminate Constitutive Equations:

For a finite element, cut from a laminate, as shown Figure 35, in which stresses are acting on it ($\sigma_x, \sigma_y, \sigma_z, \tau_{xy}, \tau_{xz}$ and τ_{yz}), the resultant forces and moments acting on the whole laminate will be given by the following matrices:

$$\begin{bmatrix}N_x\\ N_y\\ N_{xy}\end{bmatrix} = \int_{-h/2}^{h/2} \begin{bmatrix}\sigma_x\\ \sigma_y\\ \tau_{xy}\end{bmatrix} dz \quad (49)$$

and,

$$\begin{bmatrix}M_{x\,\text{around y axis}}\\ M_{y\,\text{around X axis}}\\ M_{xy\,\text{around Z axis}}\end{bmatrix} = \int_{-h/2}^{h/2} \left(\begin{bmatrix}\sigma_x\\ \sigma_y\\ \tau_{xy}\end{bmatrix} z \right) dz \quad (50)$$

NOTE: Presented below is a description of the variables given in the the equations (49) and (50) :

- $\mathbf{M_{x\ around\ y\ axis}}$ - Resultant of the bending moment per unit width that acts around the *y* axis, perpendicular to the plane x-z. Its vector is located on the plane y-z (Figure 35).

- $\mathbf{M_{y\ around\ X\ axis}}$ - Resultant of the bending moment per unit length that acts around the *x* axis, perpendicular to the plane y-z. Its vector is located on the plane x-z (Figure 35).

- $\mathbf{M_{xy\ around\ y\ axis}}$ - Resultant of the bending moment per unit length that acts around the *y* axis. Its vector is perpendicular to the plane x-z (Figure 35).

- $\mathbf{M_{yx\ around\ X\ axis}}$ - Resultant of the bending moment per unit width that acts around the *x* axis. Its vector is perpendicular to the plane y-z (Figure 35).

- $\mathbf{N_x}$ - Resultant of the force per unit width that acts in the *x* direction. Its vector is perpendicular to the plane y-z (Figure 35).

- $\mathbf{N_y}$ - Resultant of the force per unit length that acts in the *y* direction. Its vector is perpendicular to the plane x-z (Figure 35).

- $\mathbf{N_{xy}}$ - Resultant of the force per unit width that acts in the *y* direction. Its vector is on the plane y-z (Figure 35).

- $\mathbf{N_{yx}}$ - Resultant of the force per unit length that acts in the *x* direction. Its vector is on the plane x-z (Figure 35).

Figure 35 shows how the moments $M_{x\,\text{around y axis}}$; $M_{y\,\text{around X axis}}$; $M_{xy\,\text{around y axis}}$ and $M_{yx\,\text{around X axis}}$ and the forces $N_x; N_y$ and N_{xy} are placed on a composite laminate finite element made by a limited number of plies laid up in the through-thickness direction.

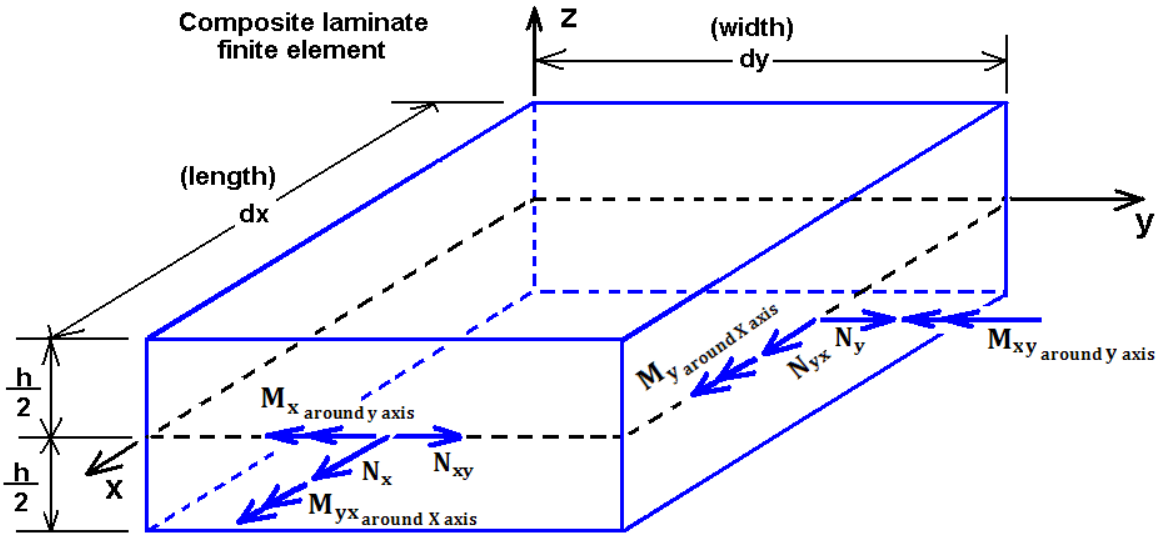

Figure 35 - Composite laminate finite element with the forces and moments applied on it (Ashton et al. 1969, p. 35).

Separating the continuous integral from the equations (49) and (50), and performing the integration over each of the *N* plies (layers), as is shown in Figure 36, the stress and moment resultants can be expressed by equations (51) and (52).

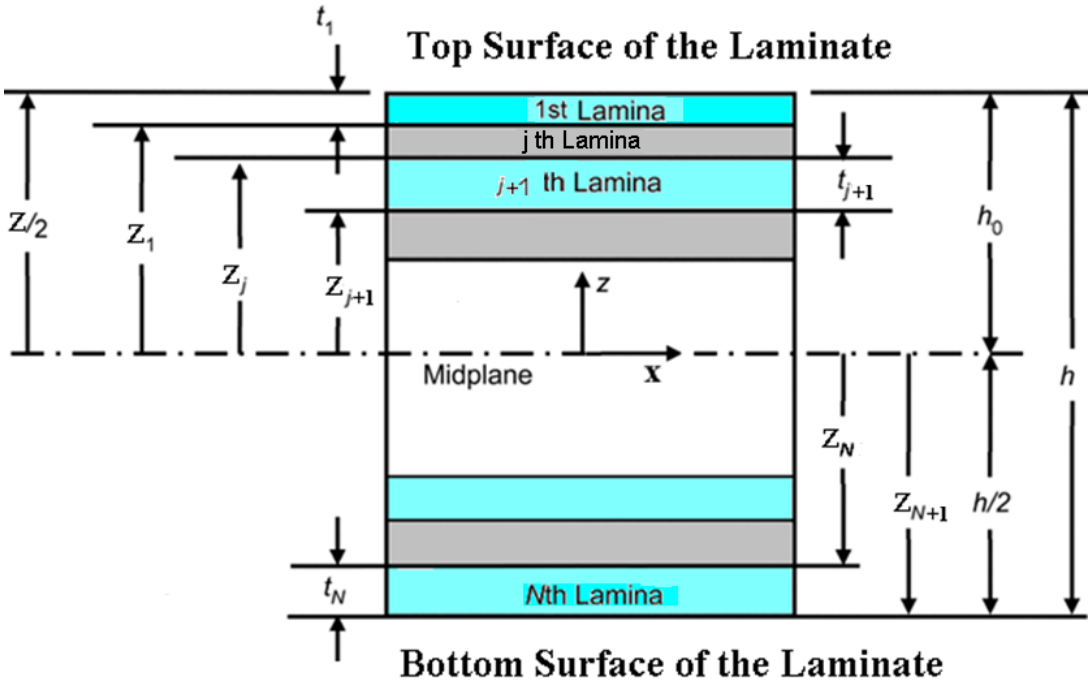

Figure 36 - Laminate stacking sequence notation (Campbell 2010, p.431)

$$\begin{bmatrix} N_x \\ N_y \\ N_{xy} \end{bmatrix} = \sum_{j=1}^{N} \left\{ \begin{bmatrix} Q_{11}^{*} & Q_{12}^{*} & Q_{16}^{*} \\ Q_{12}^{*} & Q_{22}^{*} & Q_{26}^{*} \\ Q_{16}^{*} & Q_{26}^{*} & Q_{66}^{*} \end{bmatrix}_{j^{th}\, ply} \begin{bmatrix} \varepsilon_x^{0} \\ \varepsilon_y^{0} \\ \gamma_{xy}^{0} \end{bmatrix} \int_{h_{j-1}}^{h_j} dz + \right.$$
$$\left. + \begin{bmatrix} Q_{11}^{*} & Q_{12}^{*} & Q_{16}^{*} \\ Q_{12}^{*} & Q_{22}^{*} & Q_{26}^{*} \\ Q_{16}^{*} & Q_{26}^{*} & Q_{66}^{*} \end{bmatrix}_{j^{th}\, ply} \begin{bmatrix} k_x \\ k_y \\ k_{xy} \end{bmatrix} \int_{h_{j-1}}^{h_j} z\ dz \right\} \tag{51}$$

and,

$$\begin{bmatrix} M_{x\ \text{around y axis}} \\ M_{y\ \text{around X axis}} \\ M_{xy\ \text{around y axis}} \end{bmatrix} = \sum_{j=1}^{N} \left\{ \begin{bmatrix} Q_{11}^{*} & Q_{12}^{*} & Q_{16}^{*} \\ Q_{12}^{*} & Q_{22}^{*} & Q_{26}^{*} \\ Q_{16}^{*} & Q_{26}^{*} & Q_{66}^{*} \end{bmatrix}_{j^{th}\, ply} \begin{bmatrix} \varepsilon_x^{0} \\ \varepsilon_y^{0} \\ \gamma_{xy}^{0} \end{bmatrix} \int_{h_{j-1}}^{h_j} z\ dz + \right.$$
$$\left. + \begin{bmatrix} Q_{11}^{*} & Q_{12}^{*} & Q_{16}^{*} \\ Q_{12}^{*} & Q_{22}^{*} & Q_{26}^{*} \\ Q_{16}^{*} & Q_{26}^{*} & Q_{66}^{*} \end{bmatrix}_{j^{th}\, ply} \begin{bmatrix} k_x \\ k_y \\ k_{xy} \end{bmatrix} \int_{h_{j-1}}^{h_j} z^2\ dz \right\} \tag{52}$$

Since the matrices $[\varepsilon^0]$ and $[k]$ are not a function of the number of plies, then, the equations (53) and (54) can be reduced respectively to:

$$\begin{bmatrix} N_x \\ N_y \\ N_{xy} \end{bmatrix} = \begin{bmatrix} A_{11} & A_{12} & A_{16} \\ A_{12} & A_{22} & A_{26} \\ A_{16} & A_{26} & A_{66} \end{bmatrix} \begin{bmatrix} \varepsilon_x^{0} \\ \varepsilon_y^{0} \\ \gamma_{xy}^{0} \end{bmatrix} + \begin{bmatrix} B_{11} & B_{12} & B_{16} \\ B_{12} & B_{22} & B_{26} \\ B_{16} & B_{26} & B_{66} \end{bmatrix} \begin{bmatrix} k_x \\ k_y \\ k_{xy} \end{bmatrix} \tag{53}$$

and,

$$\begin{bmatrix} M_{x\ \text{around y axis}} \\ M_{y\ \text{around X axis}} \\ M_{xy\ \text{around y axis}} \end{bmatrix} = \begin{bmatrix} B_{11} & B_{12} & B_{16} \\ B_{12} & B_{22} & B_{26} \\ B_{16} & B_{26} & B_{66} \end{bmatrix} \begin{bmatrix} \varepsilon_x^{0} \\ \varepsilon_y^{0} \\ \gamma_{xy}^{0} \end{bmatrix} + \begin{bmatrix} D_{11} & D_{12} & D_{16} \\ D_{12} & D_{22} & D_{26} \\ D_{16} & D_{26} & D_{66} \end{bmatrix} \begin{bmatrix} k_x \\ k_y \\ k_{xy} \end{bmatrix} \tag{54}$$

Where, the extensional-shear couplings for the whole laminate are described as:

$$A_{mn} = \sum_{j=1}^{N} (Q_{mn}^{*})_j \times (h_j - h_{j-1}) \tag{55}$$

the bending membrane couplings for the whole laminate are defined as:

$$B_{mn} = \frac{1}{2} \sum_{j=1}^{N} (Q_{mn}^{*})_j \times (h_j^2 - h_{j-1}^2) \tag{56}$$

and, the Bending Stiffness couplings for the whole laminate are:

$$D_{mn} = \frac{1}{3} \sum_{j=1}^{N} (Q_{mn}^{*})_j \times (h_j^3 - h_{j-1}^3) \tag{57}$$

For each single ply, the equations referred above should be transformed to:

$$A_{mn_{Each\ Ply}} = (Q^*_{mn})_j \times (h_j - h_{j-1}) \tag{58}$$

$$B_{mn_{Each\ Ply}} = \frac{1}{2} \times (Q^*_{mn})_j \times (h_j^2 - h_{j-1}^2) \tag{59}$$

$$D_{mn_{Each\ Ply}} = \frac{1}{3} \times (Q^*_{mn})_j \times (h_j^3 - h_{j-1}^3) \tag{60}$$

Note: the subscript *j* refers to the $j^{th}\ ply$.

As mentioned by Ashton et al. (1969, p.37, chapter 3.5), the equation (53) indicates that, "for a general laminated plate the mid-plane stress resultants are given in terms of the mid-plane strains and the plate curvatures for small normal curvatures", while equation (54) indicates that, "for a general laminated plate bending moments arise or are given in terms of mid-plane strains and the plate curvatures. That is, compressing the mid-plane, as well as enforcing curvatures, results in bending moments".

Combining the equations (53) and (54), the constitutive equation for the whole laminate can be written as follows:

Laminate Constitutive Equation:

$$\begin{bmatrix} N_x \\ N_y \\ N_{xy} \\ M_{x\ \text{around y axis}} \\ M_{y\ \text{around X axis}} \\ M_{xy\ \text{around y axis}} \end{bmatrix} = \left[\begin{array}{ccc:ccc} A_{11} & A_{12} & A_{16} & B_{11} & B_{12} & B_{16} \\ A_{12} & A_{22} & A_{26} & B_{12} & B_{22} & B_{26} \\ A_{16} & A_{26} & A_{66} & B_{16} & B_{26} & B_{66} \\ \hdashline B_{11} & B_{12} & B_{16} & D_{11} & D_{12} & D_{16} \\ B_{12} & B_{22} & B_{26} & D_{12} & D_{22} & D_{26} \\ B_{16} & B_{26} & B_{66} & D_{16} & D_{26} & D_{66} \end{array}\right] \times \begin{bmatrix} {\varepsilon_x}^0 \\ {\varepsilon_y}^0 \\ {\gamma_{xy}}^0 \\ k_x \\ k_y \\ k_{xy} \end{bmatrix} \tag{61}$$

In which, the ABD matrix is given by:

$$ABD_{Matrix} = \left[\begin{array}{ccc:ccc} A_{11} & A_{12} & A_{16} & B_{11} & B_{12} & B_{16} \\ A_{12} & A_{22} & A_{26} & B_{12} & B_{22} & B_{26} \\ A_{16} & A_{26} & A_{66} & B_{16} & B_{26} & B_{66} \\ \hdashline B_{11} & B_{12} & B_{16} & D_{11} & D_{12} & D_{16} \\ B_{12} & B_{22} & B_{26} & D_{12} & D_{22} & D_{26} \\ B_{16} & B_{26} & B_{66} & D_{16} & D_{26} & D_{66} \end{array}\right] \tag{62}$$

The constitutive equation (61) is coupled between bending and stretching, and, also between normal stress, shearing and twisting deformations.
For equation (61) and following the explanations given by Campbell (2010, p. 433, chapter 16), some conclusions can be drawn:

- If the laminate is balanced and symmetric in regards to the mid-plane, then the terms $A_{16} = A_{26} = 0$, and in addition all the bending membrane couplings that are shown in equation (61) will be equal to zero ($[B_{mn}] = 0$; and indices $m, n = 1,2,6$).

- The bending stiffness coupling terms : D_{11}; D_{12}; D_{22}; and D_{66} are always positive.

- The bending stiffness coupling terms: D_{16} and D_{26} will be equal to zero if the laminate is balanced and NOT symmetric, which means that, "for each ply oriented at $+\theta$ and at a given distance above the mid-plane, there is an identical ply oriented at $-\theta$ at the same distance below the mid-plane. However such laminate will not be symmetric and $[B_{mn}] \neq 0$" (Campbell 2010, p.433, chapter 16).

- In general the bending stiffness coupling terms: D_{16} and D_{26} will not be zero if the laminate is symmetric in regards to its mid-plane. However, If the composite laminate is made of UD orthotropic plies laid up at an angle equal to zero degrees or 90 degrees in regards to the *x* axis of the composite laminate, then the terms D_{16} and D_{26} will be equal to zero. Also, this is applicable ($D_{16} = 0$ and $D_{26} = 0$) for a cross-ply composite laminate made by both plies laid up at an angle equal to 0 degrees or 90 degrees in the thorough-thickness direction.

- According to Campbell (2010), the coupling terms D_{16} and D_{26} , "become small when a large number of plies are stacked at $\pm\theta$. Generally, D_{16} and D_{26}, become insignificant for thicknesses of more than 16 plies".

2.5. ILSS IN ACCORDANCE WITH REDDY (2004)

In this section the demonstration given by Reddy (2004), to achieve the interlaminar shear strength ($ILSS_{Reddy} = \tau_{xz}$) in a composite laminate will be described.

According to Reddy (2004, chapter 4.1), "when the width (variable *b* with its length along the *y* axis) of a laminated plate is very small compared to the length along the *x* axis and lamination scheme, and loading is such that the displacements are functions of *x* only, the laminate is treated as a beam".

Considering the bending of a symmetrically laminated beam according to the classical laminated plate theory (CLPT), the equations for bending deflection are uncoupled from those of stretching displacements.

For a symmetric laminate, in which no in-plane forces are acting (which means that the in-plane displacements (u_x, u_y) are zero) the constitutive equation (61) for a laminate (CLPT), will be given by:

$$\begin{bmatrix} \mathrm{M_{x\ around\ y\ axis}} \\ \mathrm{M_{y\ around\ X\ axis}} \\ \mathrm{M_{xy\ around\ y\ axis}} \end{bmatrix} = \begin{bmatrix} \mathrm{D_{11}} & \mathrm{D_{12}} & \mathrm{D_{16}} \\ \mathrm{D_{12}} & \mathrm{D_{22}} & \mathrm{D_{26}} \\ \mathrm{D_{16}} & \mathrm{D_{26}} & \mathrm{D_{66}} \end{bmatrix} \begin{bmatrix} \mathrm{k_x} \\ \mathrm{k_y} \\ \mathrm{k_{xy}} \end{bmatrix} \tag{63}$$

In the inverse form, equation (63) will be expressed as:

$$\begin{bmatrix} \mathrm{k_x} \\ \mathrm{k_y} \\ \mathrm{k_{xy}} \end{bmatrix} = \begin{bmatrix} \mathrm{D_{11}}^{-1} & \mathrm{D_{12}}^{-1} & \mathrm{D_{16}}^{-1} \\ \mathrm{D_{12}}^{-1} & \mathrm{D_{22}}^{-1} & \mathrm{D_{26}}^{-1} \\ \mathrm{D_{16}}^{-1} & \mathrm{D_{26}}^{-1} & \mathrm{D_{66}}^{-1} \end{bmatrix} \begin{bmatrix} \mathrm{M_{x\ around\ y\ axis}} \\ \mathrm{M_{y\ around\ X\ axis}} \\ \mathrm{M_{xy\ around\ y\ axis}} \end{bmatrix} \tag{64}$$

Since the bending of a symmetrically laminated beam in accordance with CLPT has been considered, in deriving the laminated beam theory, the following assumption have been considered everywhere in the beam (according with the system axis shown in Figure 22):

$$\mathrm{M_{y\ around\ X\ axis}} = \mathrm{M_{xy\ around\ y\ axis}} = 0$$

Based on this assumption, the equation (64) becomes:

$$\begin{cases} \mathrm{k_x} = \mathrm{D_{11}}^{-1} \times \mathrm{M_{x\ around\ y\ axis}} \\ \mathrm{k_y} = \mathrm{D_{12}}^{-1} \times \mathrm{M_{x\ around\ y\ axis}} \\ \mathrm{k_{xy}} = \mathrm{D_{16}}^{-1} \times \mathrm{M_{x\ around\ y\ axis}} \end{cases} \tag{65}$$

where:

$$\begin{cases} \mathrm{D_{11}}^{-1} = \dfrac{\mathrm{D_{22}D_{66}} - \mathrm{D_{26}^2}}{\mathrm{D^{**}}} \\ \mathrm{D_{12}}^{-1} = -\dfrac{\mathrm{D_{12}D_{66}} - \mathrm{D_{16}D_{26}}}{\mathrm{D^{**}}} \\ \mathrm{D_{16}}^{-1} = \dfrac{\mathrm{D_{12}D_{26}} - \mathrm{D_{22}D_{16}}}{\mathrm{D^{**}}} \end{cases}$$

$$\mathrm{D^{**}} = \mathrm{D_{11}(D_{22}D_{66} - D_{26}^2) - D_{12}(D_{12}D_{66} - D_{16}D_{26}) + D_{16}(D_{12}D_{26} - D_{22}D_{16})}$$

Equation (48), shows that $\mathrm{k_x}$, $\mathrm{k_y}$ and $\mathrm{k_{xy}}$ are equal to:

$$\begin{cases} \mathrm{k_x} = -\dfrac{\partial^2 \mathrm{w}}{\partial \mathrm{x}^2} \\ \mathrm{k_y} = -\dfrac{\partial^2 \mathrm{w}}{\partial \mathrm{y}^2} \\ \mathrm{k_{xy}} = -2\dfrac{\partial^2 \mathrm{w}}{\partial \mathrm{x}\,\partial \mathrm{y}} \end{cases} \tag{66}$$

According to Reddy (2004, p.167), equation (66) shows that w (transverse deflection) is dependent on the coordinate *y* due to both the Poisson effect ($\mathrm{D_{12}}^{-1}$) and anisotropic shear coupling ($\mathrm{D_{16}}^{-1}$). These effects can be neglected only when the length-to-width ratio is large (transverse deflection independent of the coordinate *y*), which is a consideration that will be taken in this demonstration. This consideration will simplify the use of the classical laminated plate theory (CLPT) constitutive equations (53) and (54) in which the in-plane forces are equal to zero ($\mathrm{N_x}$= $\mathrm{N_y}$=$\mathrm{N_{xy}} = 0$). The simplified CLPT will be combined with equation (47) in order to obtain the stress equations $\sigma_{\mathrm{x}\,_{j^{th}\,ply}}(\mathrm{x,z})$; $\sigma_{\mathrm{y}\,_{j^{th}\,ply}}(\mathrm{x,z})$ and $\tau_{\mathrm{xy}\,_{j^{th}\,ply}}(\mathrm{x,z})$ (equation (73)) for the laminated composite beam under a bending loading condition (Reddy 2004), while the thorugh-thickness shear stress equations will be computed using the equilibrium equations of 3-D elasticity (Chapter 2, section 2.5, sub-section iii).

According to Reddy (2004), "for angle-ply laminates this ratio must be rather large to make the twisting curvature negligible".

i. Bending Moment Equation in terms of Applied Loads

By applying the considerations in section 2.5, the transverse deflection will be a function only of the coordinate *x* of the laminate on an instant of time equal to *t* ($\mathrm{w} = \mathrm{w(x,t)}$) , by doing so, the equations reduce to:

$$\frac{\partial^2 \mathrm{w}}{\partial \mathrm{x}^2} = -\mathrm{D_{11}}^{-1} \times \mathrm{M_{x\ around\ y\ axis}} \tag{67}$$

The transverse deflection given by the composite laminate beam equation (67) is treated only as a function of the coordinate *x*.

Notes:

- Equation (67) is based on the consideration that the laminated beam "is long enough to make the effects of the Poisson's ratio and shear coupling on the deflection negligible" Reddy (2004).

- Equation (67) could be used with the classical Euler-Bernoulli beam theory if the term $\frac{\partial^2 \mathrm{w}}{\partial \mathrm{x}^2}$ of the equation (67) is substituted by the equation (70).

Introducing the following quantities:

$$\begin{cases} M_{(x)} = b \times M_{x\ \text{around y axis}}\ ; \\ Q_{x_{(x)}} = \int_{x_1}^{x_2} q_{(x)}\, dx \\ Q_{(x)} = b \times Q_{x_{(x)}} \\ E_x = \dfrac{12}{h^3 \times {D_{11}}^{-1}} = \dfrac{b}{I_y \times {D_{11}}^{-1}} \\ I_y = \frac{b \times h^3}{12} \end{cases} \tag{68}$$

Note: $M_{x\ \text{around y axis}}$ is the resultant of the bending moment per unit width that acts around the *y* axis which is perpendicular to the plane x-z and its vector is located on the plane y-z (Figure 35). The constants b and h are the total width and thickness of the laminate respectively. The variable $q_{(x)}$ is the shear flow per unit area of the composite laminate (see Figure 37), while $Q_{x_{(x)}}$ is the resultant shear flow per unit width as a function of the *x* coordinate of the composite laminate, and $Q_{(x)}$ is the resultant shear flow as a function of the x coordinate of the composite laminate system axis (see Figure 37). The variables x_1 and x_2 are coordinates taken along the length of the laminate along the *x* axis of the composite laminate axis system.

The equation (67) can be written in the familiar form as used in the classical Euler-Bernoulli beam theory:

$$M_{(x)} = -E_x \times I_y \times \frac{\partial^2 w}{\partial x^2} \tag{69}$$

Then,

$$\frac{\partial^2 w}{\partial x^2} = -\frac{M_{(x)}}{E_x \times I_y} \tag{70}$$

And, the resultant shear flow will be expressed by:

$$Q_{(x)} = \frac{\partial M_{(x)}}{\partial x} \tag{71}$$

ii. In-Plane Stresses

By considering the assumptions that have been taken during this section 2.5, and given that $M_{(x)} = b \times M_{x\ \text{around y axis}}$, the equations (47) and (64) will generate the following Matrix:

$$\begin{bmatrix}\sigma_x\\ \sigma_y\\ \tau_{xy}\end{bmatrix}_{j^{th}\ ply} = \frac{z}{b}\begin{bmatrix}Q_{11}^{*} & Q_{12}^{*} & Q_{16}^{*}\\ Q_{12}^{*} & Q_{22}^{*} & Q_{26}^{*}\\ Q_{16}^{*} & Q_{26}^{*} & Q_{66}^{*}\end{bmatrix}_{j^{th}\ ply}\begin{bmatrix}D_{11}^{-1} & D_{12}^{-1} & D_{16}^{-1}\\ D_{12}^{-1} & D_{22}^{-1} & D_{26}^{-1}\\ D_{16}^{-1} & D_{26}^{-1} & D_{66}^{-1}\end{bmatrix}\begin{bmatrix}M\\ 0\\ 0\end{bmatrix} \quad (72)$$

Which will yield the following equations for the in-plane stresses of a laminated composite beam:

$$\begin{cases}\sigma_{x\ j^{th}\ ply}(x,z) = \dfrac{M_{(x)} \times z}{b} \times \left(Q_{11}^{*}{}_{j^{th}ply} \times D_{11}^{-1} + Q_{12}^{*}{}_{j^{th}ply} \times D_{12}^{-1} + Q_{16}^{*}{}_{j^{th}ply} \times D_{16}^{-1}\right)\\ \sigma_{y\ j^{th}\ ply}(x,z) = \dfrac{M_{(x)} \times z}{b} \times \left(Q_{12}^{*}{}_{j^{th}ply} \times D_{11}^{-1} + Q_{22}^{*}{}_{j^{th}ply} \times D_{12}^{-1} + Q_{26}^{*}{}_{j^{th}ply} \times D_{16}^{-1}\right)\\ \tau_{xy\ j^{th}\ ply}(x,z) = \dfrac{M_{(x)} \times z}{b} \times \left(Q_{16}^{*}{}_{j^{th}ply} \times D_{11}^{-1} + Q_{26}^{*}{}_{j^{th}ply} \times D_{12}^{-1} + Q_{66}^{*}{}_{j^{th}ply} \times D_{16}^{-1}\right)\end{cases} \quad (73)$$

Notes: - The *z* coordinate is as shown in Figure 36.
- Equations (73) are derived from the classical laminated plate theory constitutive equations for symmetric laminates (see equations (47) and (64)) and are applicable for laminated composite beams under a bending condition.

iii. Through-thickness shear stress

Despite the laminate constitutive equations being based in an assumption in which τ_{xz} and τ_{yz} are neglected, in reality, those stresses do exist, and can be responsible for failures in composite laminates, because of the relatively low shear and transverse normal strengths of the materials used at the interface that exist between the plies (resin or matrix).

According to Reddy (2004), "the interlaminar stresses may be computed using the equilibrium equations of 3-D elasticity" which will give the following expressions:

$$\begin{aligned}0 &= \frac{\partial\sigma_x}{\partial x} + \frac{\partial\tau_{xy}}{\partial y} + \frac{\partial\tau_{xz}}{\partial z}\\ 0 &= \frac{\partial\tau_{xy}}{\partial x} + \frac{\partial\sigma_y}{\partial y} + \frac{\partial\tau_{yz}}{\partial z}\\ 0 &= \frac{\partial\tau_{xz}}{\partial x} + \frac{\partial\tau_{yz}}{\partial y} + \frac{\partial\sigma_z}{\partial z}\end{aligned} \quad (74)$$

Integrating the equation above for each ply with respect to the *z* coordinate, the interlaminar stresses will be obtained ($z_k \leq z \leq z_{k+1}$), as a result:

$$\begin{cases} \tau_{xz_{\,j^{th}\,ply}} = -\int_{z_{j^{th}\,ply}}^{z} \left(\dfrac{\partial \sigma_{x_{\,j^{th}\,ply}}}{\partial x} + \dfrac{\partial \tau_{xy_{\,j^{th}\,ply}}}{\partial y} \right) dz + G_{\,j^{th}ply} \\ \tau_{yz_{\,j^{th}\,ply}} = -\int_{z_{j^{th}\,ply}}^{z} \left(\dfrac{\partial \tau_{xy_{\,j^{th}\,ply}}}{\partial x} + \dfrac{\partial \sigma_{y_{\,j^{th}\,ply}}}{\partial y} \right) dz + F_{\,j^{th}ply} \\ \sigma_{z_{\,j^{th}\,ply}} = -\int_{z_{j^{th}\,ply}}^{z} \left(\dfrac{\partial \tau_{xz_{\,j^{th}\,ply}}}{\partial x} + \dfrac{\partial \tau_{yz_{\,j^{th}\,ply}}}{\partial y} \right) dz + H_{\,j^{th}ply} \end{cases} \quad (75)$$

Where the variables $\tau_{xz_{\,j^{th}\,ply}}$; $\tau_{yz_{\,j^{th}\,ply}}$ and $\sigma_{z_{\,j^{th}\,ply}}$ are known from equation (74), and, $G_{\,j^{th}ply}$, $F_{\,j^{th}ply}$ and $H_{\,j^{th}ply}$ are constants.

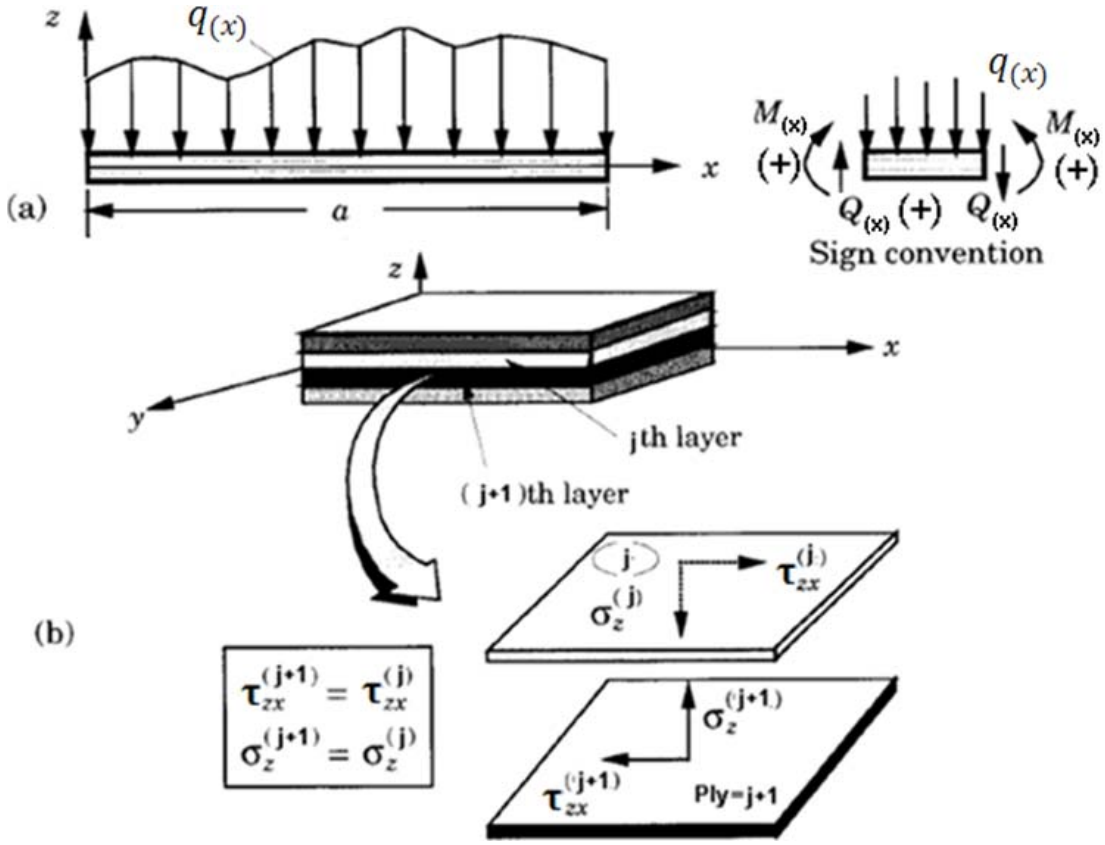

Figure 37 - Figure taken from Reddy (2004, p.171), and modified in accordance with the variables that have been used during this work. (a) denotes the sign convention of the internal forces of the beam, and (b) denotes the equilibrium of the interlaminar stresses in a laminated beam

Figure 37 presents a laminate in which the plies are numbered from the top to the bottom surface.

For laminated composite beams, all variables are independent of the coordinate *y* of the laminate system axis which means that in equation (73) the laminate composite beam stresses given by: $\sigma_{x_{j^{th}\,ply}}(x,z)$; $\sigma_{y_{j^{th}\,ply}}(x,z)$ and $\tau_{xy_{j^{th}\,ply}}(x,z)$ are only functions of the coordinates *x* and *z*, and since $u_y = 0$, the derivatives of the equation (74) with respect to the *y* coordinate are zero (Reddy 2004).

Through the equations (73) and (75), and considering the assumptions given above:

$$\begin{cases} \tau_{xz_{j^{th}ply}}(x,z) = -Q_{x_{(x)}}\left(Q_{11}^{*}{}_{j^{th}ply}{D_{11}}^{-1} + Q_{12}^{*}{}_{j^{th}ply}{D_{12}}^{-1} + Q_{16}^{*}{}_{j^{th}ply}{D_{16}}^{-1}\right)\left(\frac{z^2 - z_{j^{th}ply}^2}{2}\right) + G_{j^{th}ply} \\ \sigma_{z_{j^{th}ply}}(x,z) = -\frac{dQ_x}{dx}\left(Q_{11}^{*}{}_{j^{th}ply}{D_{11}}^{-1} + Q_{12}^{*}{}_{j^{th}ply}{D_{12}}^{-1} + Q_{16}^{*}{}_{j^{th}ply}{D_{16}}^{-1}\right)\left(\frac{z^3 - z_{j^{th}ply}^3}{6}\right) + H_{j^{th}ply} \end{cases} \quad (76)$$

in which, equation (71) has been used to replace the ratio $\frac{dM_{(x)}}{dx}$ with $Q_{(x)} = b \times Q_{x_{(x)}}$, and, $G_{j^{th}ply}$ and $H_{j^{th}ply}$ are integration constants which will depend on the boundary and interface continuity conditions.

According to Reddy (2004, p. 171), for layer number one (1st ply), the constants G_1 and H_1 will be equal to zero if the laminate at the bottom surface is stress free, while the constants $G_{j^{th}ply}$ and $H_{j^{th}ply}$ for $j^{th}ply = 2,3,\ldots$ are determined by considering that $\tau_{xz_{j^{th}ply}}$ and $\sigma_{z_{j^{th}ply}}$ are continuous at the layer interfaces, thus:

$$\begin{cases} \tau_{xz_j}(x, z_{j+1}) = \tau_{xz_{j+1}}(x, z_{j+1}) \\ \sigma_{z_j}(x, z_{j+1}) = \sigma_{z_{j+1}}(x, z_{j+1}) \end{cases}$$

Note: Subscript has been changed from $j^{th}\,ply$ to j.

And also,

$$\begin{cases} \frac{dM_{(x)}}{dx} - Q = 0 \\ \frac{dQ_{(x)}}{dx} + q_{(x)} = 0 \end{cases}$$

As a result, for j=1,2, ...,N , the equations (76) will become:

$$\begin{cases} \tau_{xz_j}(x, z_{j+1}) = G_{j+1} = -Q_{x_{(x)}}\left({Q_{11}}_j^* {D_{11}}^{-1} + {Q_{12}}_j^* {D_{12}}^{-1} + {Q_{16}}_j^* {D_{16}}^{-1}\right)\left(\frac{z_{j+1}^2 - z_j^2}{2}\right) + G_j & (77) \\ \sigma_{z_j}(x, z_{j+1}) = H_{j+1} = -\frac{dQ_x}{dx}\left({Q_{11}}_j^* {D_{11}}^{-1} + {Q_{12}}_j^* {D_{12}}^{-1} + {Q_{16}}_j^* {D_{16}}^{-1}\right)\left(\frac{z_{j+1}^3 - z_j^3}{6}\right) + H_j & (78) \end{cases}$$

Equations (77) and (78) show that the transverse shear stress τ_{xz_j} is quadratic, and the normal stress σ_{zz_j} is cubic through-thickness of each ply (lamina) (Reddy 2004).

In order to compare equation (77) with the next demonstration (chapter 2.6), a modification has been done incorporating the ply thickness, so,

Since:

$$\frac{z_{j+1}^2 - z_j^2}{2} = \frac{(t_{ply} + z_j)^2 - z_j^2}{2} = \frac{{t_{ply}}^2 + 2 \times t_{ply} \times z_j + {z_j}^2 - z_j^2}{2} = t_{ply} \times \left(\frac{t_{ply}}{2} + z_j\right)$$

then the equation for the interlaminar shear stress (77) according to Reddy (2004), which has been derived from the CLPT (equations (47) and (64)) with the equilibrium equations of 3-D elasticity (equation (74)) becomes:

$$\boldsymbol{\tau_{xz_j}(x, z_{j+1}) = -Q_{x_{(x)}}\left({Q_{11}}_j^* {D_{11}}^{-1} + {Q_{12}}_j^* {D_{12}}^{-1} + {Q_{16}}_j^* {D_{16}}^{-1}\right)\left(t_{ply} \times \left(\frac{t_{ply}}{2} + z_j\right)\right) + \tau_{xz_j}(x, z_j)} \quad (79)$$

Note: If the variable $Q_{x_{(x)}}$ is a function of the ultimate load, then, equation (79) is treated as the ILSS of the laminate; otherwise it will be treated as through-thickness shear stress, or, interlaminar shear stress.

When $Q_{x_{(x)}}$ is a function of the ultimate load the equation (79) will be defined as:

$$\begin{aligned} \boldsymbol{ILSS_{Reddy}(x, z_{j+1})} &= \boldsymbol{\tau_{xz_j}(x, z_{j+1})} \\ &= \boldsymbol{-Q_{x_{(x)}}\left({Q_{11}}_j^* {D_{11}}^{-1} + {Q_{12}}_j^* {D_{12}}^{-1} + {Q_{16}}_j^* {D_{16}}^{-1}\right)\left(t_{ply} \times \left(\frac{t_{ply}}{2} + z_j\right)\right)} \\ &+ \boldsymbol{ILSS_{Reddy}(x, z_j)} \end{aligned} \quad (80)$$

2.6. 2-D ILSS EQUATION

The method that has been used by Hua (2011) to derive interlaminar shear stress on a laminated composite beam was based on some assumptions, such as:

- The laminate is balanced and symmetric in regards to its mid-plane.

- In-plane forces are zero, which means that $u_x(x, y)$ and $u_y(x, y)$ will be equal to zero (Figure 34).

- The laminate beam under consideration is long enough to make the Poisson ratio and shear coupling effects, caused during the deflection, negligible (similarly to the consideration taken by Reddy (2004) on his assessment of the ILSS equation).

- The dependency of the coordinate *y* of the laminate due to the Poisson effect ($\mathrm{D_{12}}^{-1}$) and anisotropic shear coupling ($\mathrm{D_{16}}^{-1}$), is neglected, because it is considered that the length-to-width ratio is large enough to make the twisting curvature negligible, thus, the transverse deflection ($\mathrm{w_o}$) will be independent of the coordinate *y*. So, by this assumption $\mathrm{D_{12}}^{-1}$ and $\mathrm{D_{16}}^{-1}$ are independent from the coordinate *y* (see equations (65) and (66)).

- This approach considers a thick laminate in which the values for the coupling terms: $\mathrm{D_{16}}$ and $\mathrm{D_{26}}$ could be neglected when compared to the remaining terms of the ABD matrix (equation (62)), so, those coefficients mentioned previously will generate small values, thus the difference in value of the interlaminar shear stress without those terms will be small for a thick laminate.

- In order to do a 2-D assessment, the coupling term $\mathrm{D_{12}}$ is neglected on the X-Z plane of the laminate axis system, as will be explained in section 2.7.

According to the considerations made previously and considering the Figure 38.

For a 2-D Assessment:

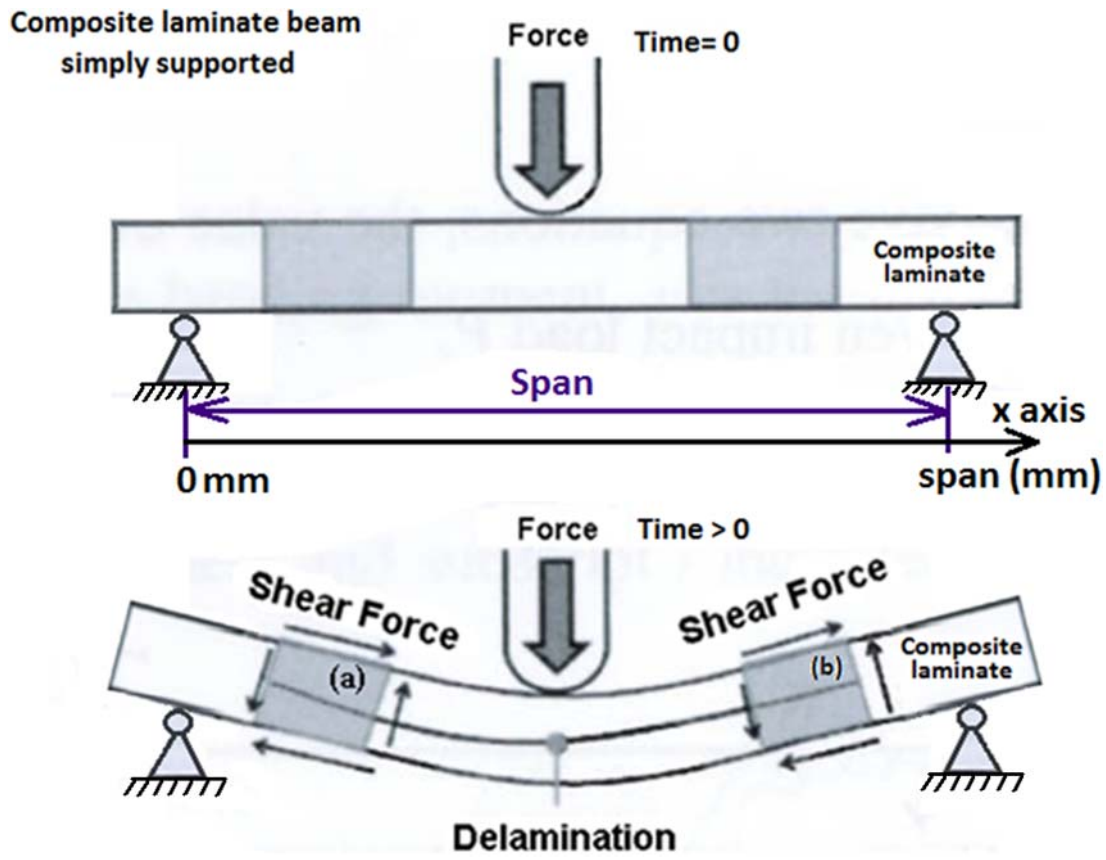

Figure 38 - Deflection caused by an external force on a composite laminate beam simply supported (Hua 2011).

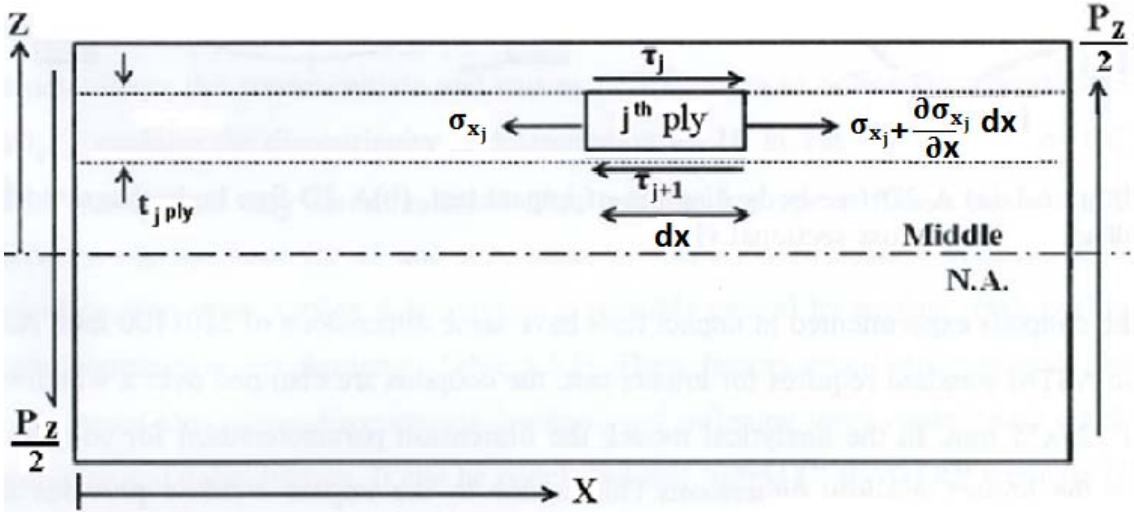

Figure 39 - Element (a) shown in Figure 38 (Hua 2011).

The 2-D ILSS equation (Hua 2011) has been derived as is shown below:

For a laminate in a three point bending loading (which includes the SBS test), in which the force, identified in Figure 38, is acting over the upper surface of the laminate, the following expressions will be considered:

$$\begin{cases} \text{Force} = \text{Line Force over the upper surface of the composite laminate} & (81) \\ \mathrm{P_z} = \dfrac{\text{Force}}{\text{Width of the Laminate}} & (82) \\ \mathrm{Q_{x_{(x)}}} = \mathrm{Q_x} = \dfrac{\mathrm{P_z}}{2} & (83) \end{cases}$$

In which, the variable $Q_{x_{(x)}}$ is the shear flow per unit width acting on the element (a) shown in Figure 39, which in the case of a line load (load equally distributed along the width on the laminated beam) will have the same value along the span of the composite beam assuming a constant value equal to $\mathrm{Q_x}$.

The expressions (81), (82) and (83) are valid for a system axis as shown in Figure 38 and Figure 39, and in the section 2.2, of Chapter 2.

Following the diagram of Figure 39, since the element is in equilibrium within the laminate, thus:

$$\left(\sigma_{\mathrm{x_j}} + \frac{\partial \sigma_{\mathrm{x_j}}}{\partial \mathrm{x}}\mathrm{dx} - \sigma_{\mathrm{x_j}}\right)\mathrm{t_{j\_ply}} - \left(\tau_j - \tau_{j+1}\right)\mathrm{dx} = 0 \quad \Leftrightarrow \tag{84}$$

$$\Leftrightarrow \quad \tau_{j+1} = \tau_j - \frac{\partial \sigma_{\mathrm{x_j}}}{\partial \mathrm{x}}\ \mathrm{t_{j\_ply}} \tag{85}$$

Where, $\mathrm{t_{j\_ply}}$ is the thickness of the ply number j .

From engineer's bending theory and stress relationship (Budynas 1998):

$$\begin{cases} \varepsilon_{\mathrm{x_{(x,z)}}} = -\mathrm{Z} \times \dfrac{\partial^2 \mathrm{w}}{\partial \mathrm{x}^2} & (86) \\ \sigma_{\mathrm{x}_{j\ (x,z)}} = -\mathrm{Z} \times \mathrm{E_{(x,z)}} \times \dfrac{\partial^2 \mathrm{w}}{\partial \mathrm{x}^2} & (87) \\ \mathrm{M_{x\ around\ y\ axis\ (x)}} = -\mathrm{D_{11}} \times \dfrac{\partial^2 \mathrm{w}}{\partial \mathrm{x}^2} & (88) \end{cases}$$

Additionally, according with Hua (2011), and applying the equation (88) in the equation (86):

$$\begin{cases} \varepsilon_{\mathrm{x_{(x,z)}}} = \left(\mathrm{M_{x\ around\ y\ axis\ (x)}} \times \mathrm{Z}\right) \times (\mathrm{D_{11}})^{-1} & (89) \\ \dfrac{\sigma_{x_{j\ (x,z)}}}{\varepsilon_{\mathrm{x_{(x,z)}}}} = \mathrm{E_{(x,z)}} & (90) \end{cases}$$

Where:

D_{11} - Bending stiffness coupling in the direction *1* of the composite laminate, which in this case it is coincident with the *x* axis shown in Figure 39 (coupling form of the ABD matrix, equation (62)).

Z - Distance from the mid-plane (neutral axis) of the composite laminate up to the ply number *j*

$M_{x_{\text{around y axis }(x)}}$ - Bending moment per unit width of the laminate, which is dependent on the *x* coordinate of the 2-D laminate system axis.

$\varepsilon_{x_{(x,z)}}$ - Strain in the *x* direction of the lamina, which is a function of the *z* coordinate.

w - Transverse displacement.

Through the equations (89) and (90) the stress along the *x* coordinate of the composite laminate will be:

$$\sigma_{x_{j\ (x,z)}} = \left(M_{x_{\text{around y axis }(x)}} \times Z \times E_{(x,z)}\right) . (D_{11})^{-1} \tag{91}$$

Note: Equation (91) will be used in chapter 4 in order to obtain the stress due to the bending moment $\sigma_{x_{j_{(x,z)}}}$ in the composite laminate beam.

The constant $E_{(x,z)}$ is obtained by through the equation (96)

Differentiating σ_{x_j} in respect to x equation (91) becomes:

$$\frac{\partial \sigma_{x_{j\ (x,z)}}}{\partial x} = \frac{\partial\left(\left(M_{x_{\text{around y axis }(x)}} \times Z \times E_{(x,z)}\right) . (D_{11})^{-1}\right)}{\partial x} \tag{92}$$

For a concentrated load acting in the middle of the laminate, the following expression is valid:

$$\frac{\partial\left(M_{x_{\text{around y axis }(x)}}\right)}{\partial x} = Q_x \tag{93}$$

Since $E_{(x,z)}$ will be constant along the *x* coordinate of the laminate system axis ($E_{(x,z)} = E_{(z)}$), and, since D_{11} will be constant along the *x* coordinate because the angle and the Stiffness along the *x* and *y* directions will be kept constant too, then, the equation (92) becomes:

$$\frac{\partial \sigma_{x_{j\ (x,z)}}}{\partial x} = \left(Z \times E_{(z)}\right) . (D_{11})^{-1} . \frac{\partial\left(M_{x_{\text{around y axis }(x)}}\right)}{\partial x} \tag{94}$$

then, for a small length in the *x* direction (*dx*), localized in the middle of the laminate in regards to the laminate span, the equation (94) becomes:

$$\frac{\partial \sigma_{x_{j\ (x,z)}}}{\partial x} = \left(Z \times E_{(z)}\right).\ (D_{11})^{-1}.\ \times Q_x \tag{95}$$

Substituting equation (95) into equation (85), and since:

$$A_{11_j} = k_j = E_{(z)} \times t_{j\_ply} \tag{96}$$

Then, considering the 2-D assessment, where the analysis is made on the x-z plane of the laminate coordinate axis system: $(D_{11})^{-1} = \frac{1}{D_{11}}$, thus:

$$\tau_{j+1} = \tau_j - \frac{A_{11_j} \times z_j}{D_{11}} \times Q_x$$

Which is the same as:

$$\boldsymbol{\tau_{xz_{j+1}} = \tau_{xz_j} - \frac{A_{11_j} \times z_j}{D_{11}} \times Q_x} \tag{97}$$

Note: If the variable Q_x is a function of the ultimate load (equation (81) equal to the ultimate load) then, the equation (97) is treated as the ILSS of the laminate; otherwise it will be treated as through-thickness shear stress, or, interlaminar shear stress.

When Q_x is a function of the ultimate load the equation (97) will be defined as:

$$ILSS_{2-D\ j+1} = \tau_{xz_{j+1}} = ILSS_{2-D\ j} - \frac{A_{11_j} \times z_j}{D_{11}} \times Q_x \tag{98}$$

Thus,

$$\boldsymbol{ILSS_{2-D\ j+1} = ILSS_{2-D\ j} - \frac{A_{11_j} \times z_j}{D_{11}} \times Q_x} \tag{99}$$

Note: Equation (99) will be used in chapter 4 in order to obtain the ILSS in the composite laminate beam.

2.7. THEORY APPLIED IN THIS WORK TO MINIMIZE THE DAMAGE IN THE MIDDLE OF THE COMPOSITE LAMINATE

From the three demonstrations that were given previously, in chapter 2.3 to obtain the equation (8); in the chapter 2.5 to obtain the equation (80) and in the chapter 2.6 to obtain the equation (99); the one that has been chosen for this research work is the 2-D ILSS equation (99), given in chapter 2.6.

Regarding the ILSS equation (8) in accordance with the standards (section 2.3 of Chapter 2), the theory takes an approach by considering the application of a load over an isotropic short beam, which is not applicable to the case of a composite laminate made by multiple plies.
This equation just works as a quick way to derive the ILSS from the experiments, however, when the result of ILSS must be assessed in more detail and not by approximation, another theory should be considered, that could be one of either ILSS in accordance with Reddy (2004) or the 2-D ILSS Equation.

Comparing the *2-D ILSS equation* theory (chapter 2.6; equation (99)) with the Reddy's theory (Reddy 2004) (chapter 2.5; equation (80)), both are similar (equations (105) and (106) show the similarity) when ignoring the effects due to the bending couplings D_{12} and D_{16} of the ABD matrix (equation (62)).

According to Reddy (2004), the through-thickness equation (80) is expressed as:

$$\mathbf{ILSS}_{Reddy}(\mathbf{x}, \mathbf{z}_{\mathbf{j+1}}) = -\mathbf{Q}_{\mathbf{x}_{(x)}}\left(\mathbf{Q}_{\mathbf{11}_{\mathbf{j}}}^{*}\,\mathbf{D}_{\mathbf{11}}{}^{-\mathbf{1}} + \mathbf{Q}_{\mathbf{12}_{\mathbf{j}}}^{*}\,\mathbf{D}_{\mathbf{12}}{}^{-\mathbf{1}} + \mathbf{Q}_{\mathbf{16}_{\mathbf{j}}}^{*}\,\mathbf{D}_{\mathbf{16}}{}^{-\mathbf{1}}\right)\left(\mathbf{t}_{\mathbf{ply}} \times \left(\frac{\mathbf{t}_{\mathbf{ply}}}{\mathbf{2}} + \mathbf{z}_{\mathbf{j}}\right)\right) + \mathbf{ILSS}_{Reddy}(\mathbf{x}, \mathbf{z}_{\mathbf{j}}) \quad (100)$$

According to the 2-D ILSS Equation theory (chapter 2.6; equation (99)), for a 2-D problem on the x-z plane of the composite laminate, the equation is expressed as:

$$\mathbf{ILSS}_{\mathbf{2-D}\ \mathbf{j+1}} = \mathbf{ILSS}_{\mathbf{2-D}\ \mathbf{j}} - \frac{\mathbf{A}_{\mathbf{11}_j} \times \mathbf{z}_j}{\mathbf{D_{11}}} \times \mathbf{Q_x} \quad (101)$$

In order to compare both equations, the following assumptions were considered:

- The resultant shear flow per unit width of the composite laminate $Q_{x_{(x)}}$ is a function of the ultimate load (line load as shown in Figure 38 from chapter 2.6 and Figure 42 from chapter 4).
- The assessment of the interlaminar shear strength (ILSS) is performed in the middle of the laminate, where the maximum ILSS could be found (in theory).
- The laminate is under a concentrated line load on the upper surface of the composite part at the middle of its length.

- The laminate designs under assessment are thick enough so that the effects of the bending couplings D_{16} and D_{26} are small (negligible), when compared to the remaining bending couplings values shown on the ABD matrix (equation: (62)). According to Campbell (2010, p.433), those couplings variables, generally become insignificant for such conditions.

- The length-to-width ratio of the composite laminate is large.

- No free-edge effect exists on the composite laminate. This means that the through-thickness shear stress τ_{xz} near to the free edges of the composite laminate beam will be equal to zero and the normal stress σ_3 on the free edges of the laminated beam will also be equal to zero. This assumption implies that no crack onset will start at the edges of the composite laminate to be confirmed.

- Additionally, the considerations taken on the sections 2.5 and 2.6 of this chapter to achieve equations (100) and (101) in this section remains valid.

Applying the considerations mentioned above on a symmetric and balanced composite laminate beam, the inverse of the bending couplings become:

$$
\begin{aligned}
{D_{11}}^{-1} &= \frac{D_{22}D_{66} - D_{26}^2}{D^{**}} = \frac{D_{22}D_{66} - 0}{D^{**}} = \frac{D_{22}D_{66}}{D^{**}} \\
{D_{12}}^{-1} &= -\frac{D_{12}D_{66} - D_{16}D_{26}}{D^{**}} = -\frac{D_{12} \times D_{66} - 0 \times 0}{D^{**}} \\
{D_{16}}^{-1} &= \frac{D_{12}D_{26} - D_{22}D_{16}}{D^{**}} = \frac{D_{12} \times 0 - D_{22} \times 0}{D^{**}} = 0
\end{aligned}
$$

$$
\begin{aligned}
D^{**} &= D_{11}(D_{22}D_{66} - D_{26}^2) - D_{12}(D_{12}D_{66} - D_{16}D_{26}) + D_{16}(D_{12}D_{26} - D_{22}D_{16}) \\
&= D_{11}(D_{22}D_{66} - 0) - D_{12} \times (D_{12} \times D_{66} - 0 \times 0) + 0 \times (D_{12} \times 0 - D_{22} \times 0) \\
&= D_{11}D_{22}D_{66} - {D_{12}}^2 D_{66}
\end{aligned}
$$

Continuing:

$$
\begin{cases}
{D_{11}}^{-1} = \dfrac{D_{22}D_{66}}{D_{11}D_{22}D_{66} - {D_{12}}^2 D_{66}} \\
{D_{12}}^{-1} = -\dfrac{D_{12} \times D_{66}}{D_{11}D_{22}D_{66} - {D_{12}}^2 D_{66}}
\end{cases}
$$

Thus,

$$\begin{cases} {D_{11}}^{-1} = \dfrac{1}{D_{11} - \dfrac{{D_{12}}^2}{D_{22}}} & (102) \\ {D_{12}}^{-1} = -\dfrac{1}{\dfrac{D_{11}D_{22}}{D_{12}} - D_{12}} = -\dfrac{D_{12}}{D_{11}D_{22} - {D_{12}}^2} & (103) \end{cases}$$

Since the analysis of this work is based on the X-Z plane of the laminate coordinate axis system (2-D assessment), in accordance with the convention shown in section: 2.2 of Chapter 2, the value for the bending coupling term: D_{12} will be considered equal to zero. By doing this, the symmetric and balanced laminate will be submitted to a condition in which only the normal curvature of the *X* direction of the composite laminate axis system is considered as presented in Figure 38 (for a time > 0). Laminate bending effects given by the stretching of the midplane of the laminate as well as the enforcement of curvatures will be avoided due to the symmetry and balance of the composite laminate which will result in an anticlastic bending when the laminate is under a condition of SBS test or 3PB test.

Then, for a 2-D problem in the X-Z plane of the laminate axis system (Figure 22):

$${D_{11}}^{-1} = \frac{1}{D_{11}} \quad (104)$$

Applying the considerations explained previously in this section, and considering that:

$$\begin{cases} Q_{x_{(x)}} = Q_x = \dfrac{P_z}{2} \\ A_{11_j} = k_j = E_{(z)} \times t_{j_{ply}} = {Q_{11}}^*_j \times t_{j_{ply}} \end{cases}$$

Note: Q_x is the shear flow per unit width of the composite laminate beam (see equations (81); (82) and (83)).

the equations (100) and (101) becomes:

Reddy's Equation (Reddy 2004):

$$ILSS_{Reddy}\left(\frac{span}{2}, z_{j+1}\right) = -Q_x \times \left({Q_{11}}^*_j \times \frac{1}{D_{11}} + {Q_{12}}^*_j \times 0 + {Q_{16}}^*_j \times 0\right)\left(t_{ply} \times \left(\frac{t_{ply}}{2} + z_j\right)\right) + ILSS_{Reddy}\left(\frac{span}{2}, z_j\right)$$

which is equal to:

$${ILSS_{Reddy}}_{j+1} = {ILSS_{Reddy}}_j - Q_x \times {Q_{11}}^*_j \times t_{ply} \times \frac{1}{D_{11}} \times \left(\frac{t_{ply}}{2} + z_j\right)$$

Thus:

$$\mathbf{{ILSS_{Reddy}}_{j+1} = {ILSS_{Reddy}}_j - \frac{A_{11_j} \times \left(\frac{t_{ply}}{2} + z_j\right)}{D_{11}} \times Q_x} \quad (105)$$

2-D ILSS Equation:

$$\mathbf{ILSS_{2-D\ j+1}} = \mathbf{ILSS_{2-D\ j}} - \frac{\mathbf{A_{11_j}} \times \mathbf{z_j}}{\mathbf{D_{11}}} \times \mathbf{Q_x} \tag{106}$$

Note: According to the equations (97); (98) and (99) $\mathrm{ILSS}_{2-D\ \mathrm{j+1}} = \tau_{\mathrm{xz\ j+1}}$ and $\mathrm{ILSS}_{2-D\ \mathrm{j}} = \tau_{\mathrm{xz\ j}}$

As can be seen on the equations (105) and (106), the difference between them is related to the distance given in the ***z*** axis.

Depending on how the distance z_j is attributed to the Reddy's equation (Reddy 2004), if z_j is equal to zero, then, the values for the ILSS will be given at the middle of each ply; on the other hand, if the minimum value of z_j is equal to a half of a ply, then, the ILSS at the middle plane of the composite laminate will be missed, and the values for the ILSS will be given at the upper surface of each ply.
In regards to the 2-D ILSS equation, the expression is derived in a way that the ILSS could be taken at the interface of each ply, or at the middle of each ply, without any restriction in terms of ply thickness, and also, another advantage of this equation, is that it captures the ILSS at the interface in the middle of the composite laminate.

Regarding the considerations and conclusions given previously, ***all of the research work has been based on the 2-D ILSS equation (106).***

Chapter 3

Optimization of Stacking Sequence for ILSS

3.1. INTRODUCTION

This work has been developed in order to get the best stacking sequence to improve the interlaminar shear strength (ILSS) in a short beam shear (SBS) test (SBS test).

An algorithm has been developed in MATLAB taking advantage of several considerations. Those considerations help reduce the total amount of possible combinations (ply orientations and material combinations) without loss of generality.

Hossein Ghiasi et al. (2009) described several optimization methods used to find the best fibre orientation of a composite laminate. From those methods, similar ideas were used in order to reduce the total amount of possible combinations (Ghiasi et al. 2009, sections 4.4 and 4.6).

The algorithm developed in the present thesis can consider between two and four different angles, and a maximum of two different UD fibre ply materials. To resolve the equations, the algorithm considers all possible combinations yielded by the angles and materials, to achieve the final result, which will be the best stacking sequence of the composite laminate.

In order to be less expensive in terms of computation time, the algorithm was created to use the functionality of parallel processing, through Matlab's function: *MatlabPool*.

3.2. PROGRAM OVERVIEW - METHOD FOR OPTIMIZATION OF LAMINATES

The Matlab algorithm is a program that runs every possible combination of layups generated through the mixture of two different materials with a determined number of angles (up to 3 different angles) on each ply that lies within a composite laminate to determine the optimum layup.

This tool receives user defined input for the desired material properties of a hybrid laminate composed of two different materials, as well as the desired number of angles that the user wants to vary in the through-thickness direction. It also receives the user defined input for the desired limits according to Figure 40.

Most of the sub-routines and functions that constitute the code are drawn from assumptions that have been explained in chapter 2. The methodology followed here is based on the elimination of the undesirable combinations that do not allow a symmetric and balanced laminate to be built.

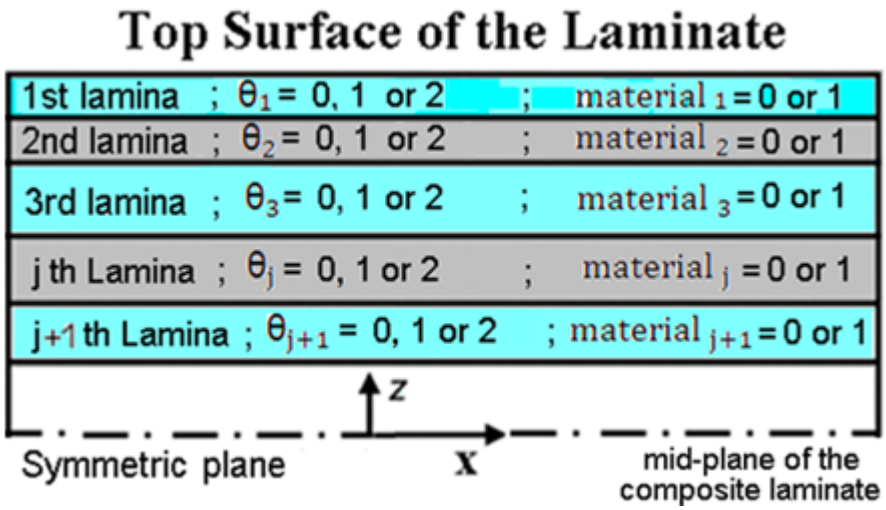

Figure 40 - Methodology used by the software to proceed with the optimization of the stacking sequence

3.3. GENERAL DESCRIPTION OF THE ALGORITHM PROCESS

Taking the input given by the user, the software will consider all the combinations of angles and materials that make the composite laminate symmetric and balanced. Additionally it will consider the combinations that have a minimum of 10% of zero degree plies within the laminate (BS14130:1998, 2004) and those combinations in which no more than 4 plies of the same orientation are joined together (in order to reduce thermal cracking and splitting along the fibre direction)

After considering the valid combinations resulting from this process, the software stores them in a bulk data file and proceeds with the optimization of the through-thickness damage in the middle of the composite laminate as shown in the flowchart given in Figure 41.

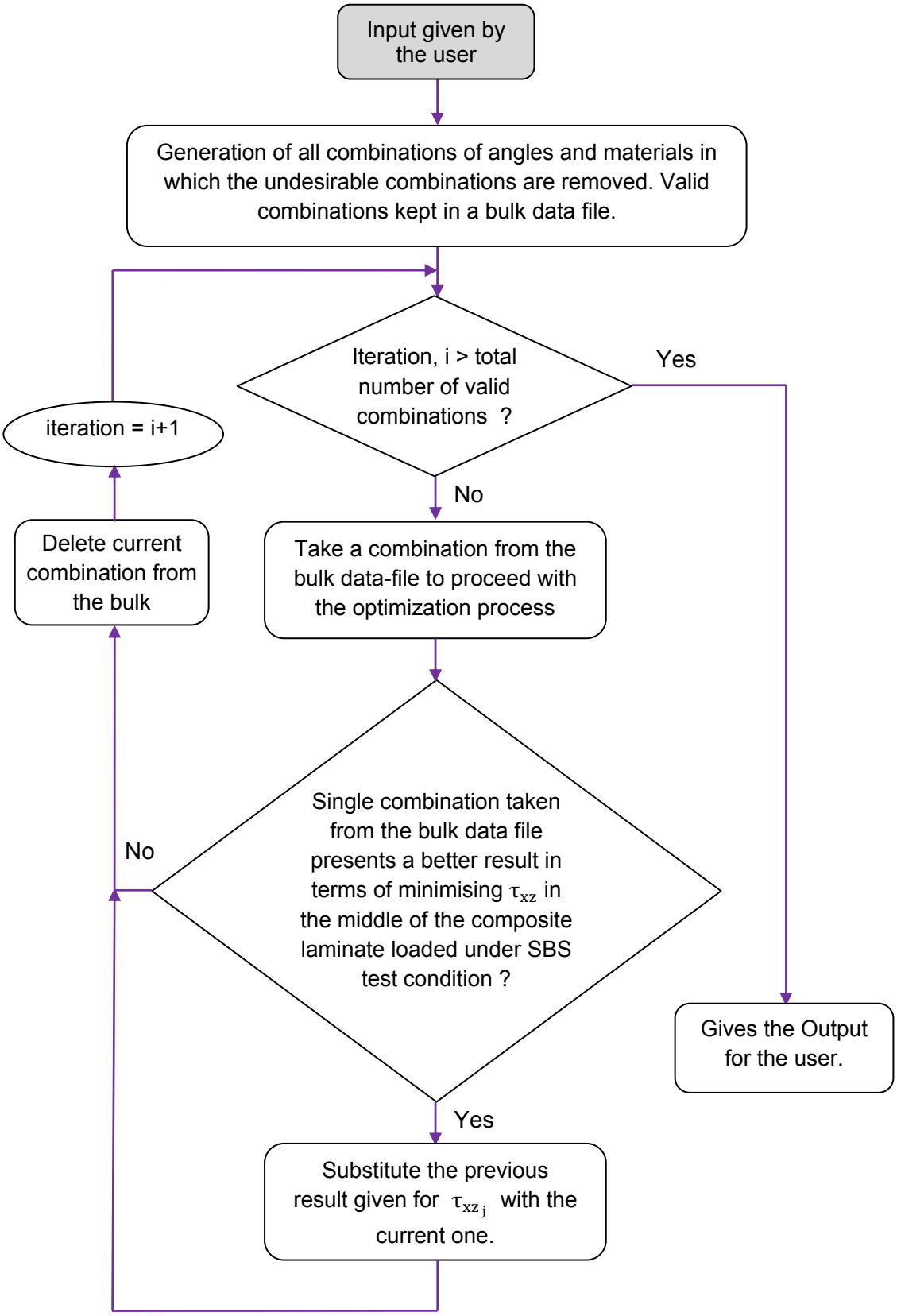

Figure 41 - Algorithm flowchart

Note: Some results given by this software are shown in Appendices A and B as an example.

The static experiments that were conducted (shown in Chapter 4) were essential to confirm the theory and the algorithm predictions about the Damage Minimization in the middle of the laminate. Based on the output given by the algorithm, two different hybrid designs were chosen and additionally a quasi-isotropic design laid up with a single material was considered, so three different designs were assessed in this work.

Chapter 4

EXPERIMENTAL TEST - STATIC

4.1. INTRODUCTION

This work has been developed to optimize the interlaminar shear strength (ILSS) in the middle of a thick composite laminate under a through-thickness loading, on a standard method of SBS test. The optimization method was based on the "Laminate Constitutive Laws".

By choosing an appropriate combination of through-thickness fibre arrangements and materials, a better static condition, as well as better fatigue behaviour of the component is expected under *in-service* conditions.

This chapter describes the static experiments that were realized in Bath University's laboratory by Han (2013), who has laid up and tested composite laminates based on three different stacking sequences. Those stacking sequences were generated by the algorithm that has been developed in this work (see Chapter 3).

The experimental work that has been performed on all the specimens has been done under a Short Beam Shear (SBS) test condition as shown on Figure 42 and in accordance with the standard D2344/2344M (2006) and BS14130:1998 (2004).

The experimental static test has been performed in accordance with Han (2013) at a speed of 0.1 mm/min. Further information about the experimental part of this work is given in Appendix C, D, E, F, G, H, I, J, K and L.

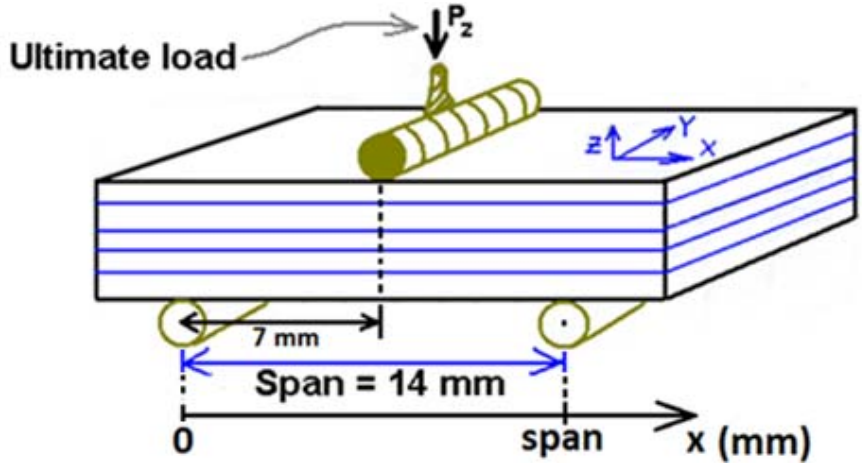

Figure 42 – Short Beam Shear (SBS) test representation.

4.2. STATIC EXPERIMENTS

4.2.1. STATIC TEST OF THE ALL CARBON DESIGN

The *All Carbon Design* is a 24 ply composite laminate laid up with the following stacking sequence:

$$[(0/45/90/-45)_3]_s$$

In his experimental work, Han (2013), has tested seven specimens with the stacking sequence shown above. The static tests that were performed in the *All Carbon Design*, were a standard method of SBS test in accordance with the ASTM D2344/2344M (2006). The experimental results of the static tests are shown in Table 1 (the values are taken from Han (2013), which are shown in Appendix C and I).

Table 1 - Experimental results of the static test performed for the composite laminate *All Carbon Design*

Specimens	Failure Load (N)	Failure Load per unit width (N/mm)		Thickness (mm)	Width (mm)	Length (mm)
1	2449.10	353.39		3.36	6.93	18.82
2	2622.79	381.80		3.37	6.87	18.58
3	2484.44	344.18		3.29	7.22	18.61
9	2524.28	367.93		3.39	6.86	18.62
10	2318.36	337.41		3.33	6.87	19.08
3L	2554.13	347.01		3.29	7.36	26.74
4L	2597.05	354.78		3.29	7.32	26.94
AVERAGE	2507.16	355.22		3.33	7.06	21
Standard Deviation	102.86	15		0.04	0.23	4

The first crack in Specimen 9 detected from the load-displacement data recovered by the testing machine occurred at 2503.89 N. After the first crack occurred there was small drop in load. The specimen subsequently failed at a load of 2524.28 N.

For the case of specimens 3L and 4L the specimen length was greater than 26 mm in order to see if the static and fatigue results would be affected. As can be seen in Table 1 the static results are within the range of results obtained for the *short* specimens (length of approximately 18 mm).

i. Assessment of the images taken from the Static Experiment

Based on the experiments given in Table 1, four specimens were assessed in more detail. The specimen numbers are: 1; 9; 2; 10 .

As can be seen in Figure 43 ((b); (c) and (d)), the crack starts in the compression side of each of the 24 ply specimens (above the mid-plane of the composite laminate). The images (Figure 43 - (b); (c) and (d)) were taken after the crack initiation has started, so, the crack propagation for a particular instant of time will be seen.

Due to the application of the ultimate load, several delaminations have occurred on each of the specimens during the failure process. All of the static tests that have been performed show similar characteristics, by a visual means of assessment, the intralaminar crack has started near to the middle plane of the specimen, within a single 90^0 ply, and at an angle of approximately 138^0 (as shown in Figure 49 (a)). After the crack initiation has started, it propagates to right side of the image, originating more cracks and consequent delaminations in other plies, which are due to the decrease in stiffness on the whole composite laminate that was originated by the first crack. The intralaminar failure has been initiated by principal stress. This is confirmed through the Figure 47 ((a); (b) and (c)) (Hybrid Design 2) showing the same pattern of failure as shown for the All Carbon Design.

Since the specimen has been subject to an ultimate load, the through-thickness shear stress that has been obtained through the static test will be obtained through the ILSS_{2-D} equation (106) and will be represented by the variable τ_{xz}. Also, by visual means of assessment, some of the specimens that were tested, present a failure underneath the loading roller due to the compression of the roller surface against the first ply of the composite laminate. This failure seems to have happened at the same time as the 90^0 plies have failed (see Figure 43 (b)).

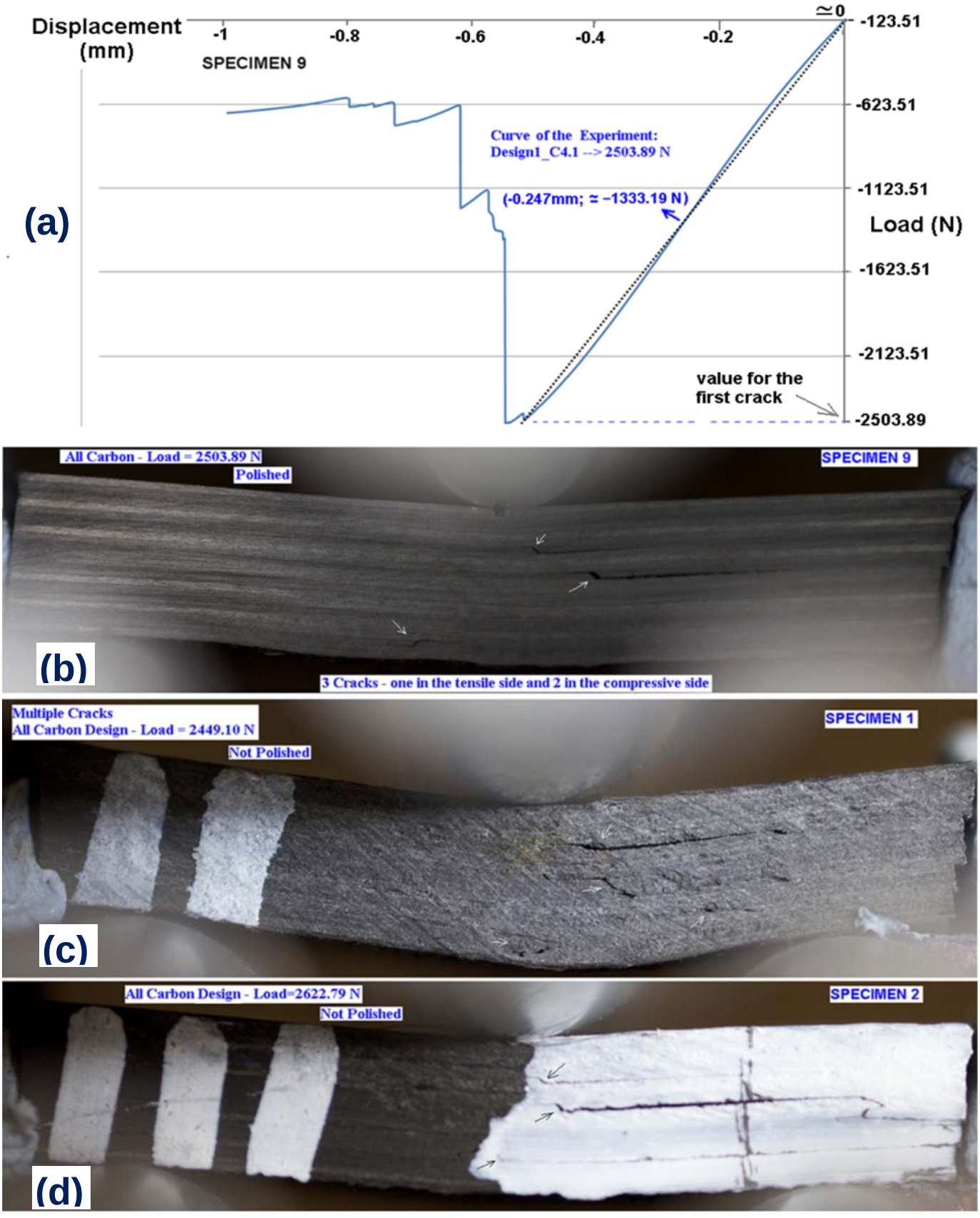

Figure 43 - All Carbon Design - Static test experiments showing: (a) load-displacement plot given by the SBS test performed on specimen 9; (b) SBS test performed on Specimen 9; (c) SBS test performed on Specimen 1; (d) SBS test performed on Specimen 2.

4.2.2. STATIC TEST OF THE HYBRID DESIGN 1 WITH $\theta_{max} = |\pm 45^o|$

The *Hybrid Design 1* is a 24 ply composite laminate, made of a maximum of 40% of glass plies (which allows 8 glass plies in the symmetric composite laminate), and which have been laid up with the following stacking sequence:

$$\left(\left[(0_C)_2 / (\pm 45_C)_2 / (\pm 45_g)_2 / (\pm 45_C) \right]_s \right)$$

Han (2013) has performed the experiments on the static test rig at a speed of 0.1mm/min, in this experimental work seven specimens have been tested with the stacking sequence shown above.

The static tests performed were of a standard method of SBS test in accordance with the ASTM D2344/2344M (2006). The experimental results of the static tests are shown in Table 2 (the values are taken from Han (2013), which are shown in Appendix D and I).

Table 2 - Experimental results of the static test done for the composite laminate *Hybrid Design 1* with $\theta_{max} = |\pm 45^o|$

Specimens	Failure Load (N)	Failure Load per unit width (N/mm)		Thickness (mm)	Width (mm)	Length (mm)
1	2551.83	369.86		3.38	6.90	18.60
2	2576.28	374.56		3.39	6.88	18.81
3	2534.99	366.33		3.31	6.92	18.62
9	2588.00	373.45		3.40	6.93	18.37
10	2506.02	361.10		3.40	6.94	17.97
3L	2718.98	373.87		3.34	7.27	25.26
4L	2436.53	369.65		3.35	6.59	24.97
AVERAGE	2558.95	369.83		3.37	6.92	20.37
Standard Deviation	86.76	4.83		0.04	0.20	3.25

Note: The highest and lowest failure loads presented in Table 2 correspond to the widest and narrowest samples respectively. Due to this, equation (164) from Appendix P has been used in order to achieve the average of the loads necessary to setup the fatigue rig to proceed with the fatigue experiments, as will be explained in Chapter 5.

i. Assessment of the images taken from the Static Experiment

Based on the experiments given in the Table 2, three specimens were assessed in more detail. The specimens number are: 3, 9, 10 .

During the static tests that have been performed under a condition of *SBS test*, some common characteristics have been noticed. One of these is in regards to the glass plies within the composite laminate. During the whole static test process it was noticed, by visual means (Figure 44 (b); (c); and Figure 45 (a), (b), (c), (d)), that after the crack has initiated it propagates and goes from near the middle of the specimen, between two carbon plies, upwards to the bottom surface of the glass ply, breaking the carbon plies in the through-thickness direction. This situation has been detected on all of the specimens that were tested, except for one. Through this finding it seems that the glass plies work well as a driver of the crack during the static test process, possibly because it is less stiff than the carbon ply absorbing the crack energy much better than the carbon does.

More common characteristics have been found during the static test process. Below is shown a description of each of those characteristics that by a visual means of assessment seems to accomplish with a regular pattern of this particular design (Hybrid Design 1):

Three of the seven specimens that were tested have presented the first crack in the upper surface of the composite laminate at the same time that the delamination has occurred near the middle of the composite laminate due to interlaminar failure. The failure on the upper surface of the laminate, which is underneath the loading roller, is due to the compression of the roller surface against the first ply of the composite laminate. This did not influence the results because they are within the range of results presented by the specimens that did not have the failure underneath the loading roller at the same time as the interlaminar failure that occurred on the specimens (see specimen 3 of Figure 45 (c) and Table 2 as an example).

All delaminations that have been verified on each of the seven static tests, have begun near the middle of the laminate due to interlaminar failure, in the compression side of the composite part (Above the middle plane of the laminate). Since the delamination is expected to occur in the middle of the laminate (between the plies number 12 and 13) or in its tensile side (not on the compression side), an explanation of this, is due to the laminate being balanced and symmetric, the middle plane will be shared by two plies with the same orientation (-45^{o}), one from the upper half of the specimen and other from the lower half. Since both plies have the same orientation, this could have an effect in terms of the interface stiffness between those plies. Since the failure has happened between the plies number 11 and 12 with orientations of 45^{o} and -45^{o} respectively, it means that the interface between those plies is weaker in regards to the interface between plies number 12 and 13.

The first delamination presented on Specimen 9 (see Figure 55 (a)) has appeared near the middle of the specimen, between the ply 11 and 12 (Han 2013).

According to the explanation given in section 4.2.1 i), and as will be shown in section 4.3.2 ii), the reason the crack initiates above the mid-plane of the composite laminate is due to the interlaminar shear stress distribution as shown in Figure 56 in which, the cross-sections (perpendicular to the *x* axis) that are near to the loading roller create hotspots of ILSS above the mid-plane of the laminate.

Since the specimen has been submitted to an ultimate load, the through-thickness shear stress that has been obtained through the static test will be obtained through the ILSS equation (106) and will be represented by the variable τ_{xz}.

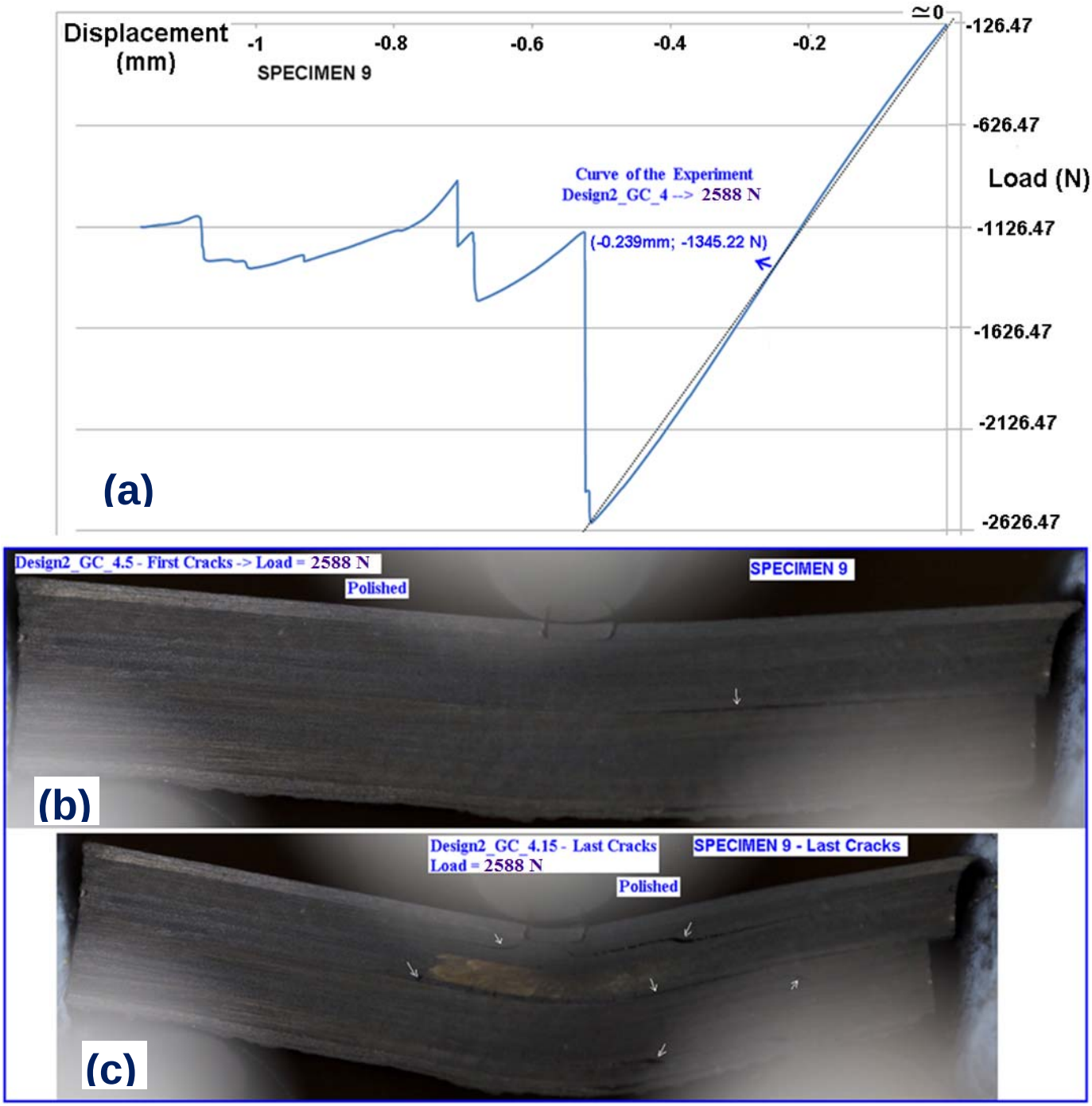

Figure 44 - Hybrid Design 1 - Static test experiments (SBS test) showing:
(a) load-displacement plot given by the SBS test performed on specimen 9;
(b) Specimen 9 - image captured after the first crack has initiated;
(c) Specimen 9 - image captured in the final stage of the SBS test.

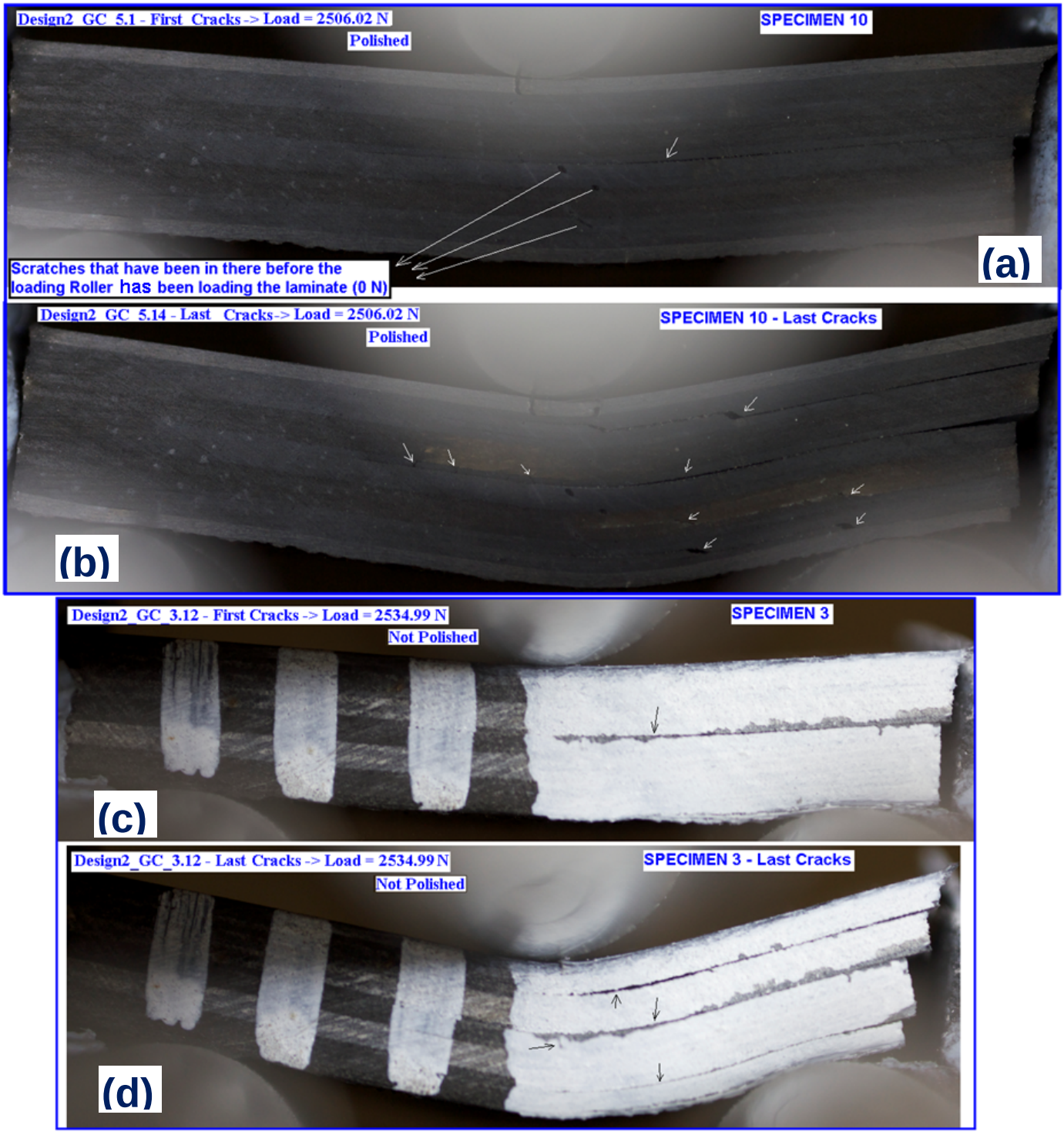

Figure 45 - Hybrid Design 1 - Static test experiments (SBS test) showing: (a) Specimen 10 – first image captured after the first crack has initiated; (b) Specimen 10 - image captured in the final stage of the SBS test; (c) Specimen 3 – first image captured after the first crack has initiated; (d) Specimen 3 - image captured in the final stage of the SBS test.

4.2.3. STATIC TEST OF THE HYBRID DESIGN 2 WITH $\theta_{max} = |90^o|$

The *Hybrid Design 2*, which is laid up with 24 plies, was made in order to allow a maximum of 40% of glass plies within the laminate (which is 8 glass plies in a symmetric composite laminate), and in order to allow ply orientations of $|\pm 45|$ degrees.

The stacking sequence of this laminate, and the glass and carbon plies disposition in the through-thickness direction of the laminate, were taken from the output given by the algorithm described in Chapter 3.

The stacking sequence of the Hybrid Design 2 is:

$$\left[(0_c)_2/(\pm 45_g)/(90_C)_4/(\pm 45_g)/(90_C)_2\right]_s$$

The static tests for this design, performed by Han (2013), were performed in a standard method of SBS test in accordance with the ASTM D2344/2344M (2006). Static tests failure loads and geometric characteristics of the *Hybrid Design 2* specimens are presented in Table 3 (these values are taken from Han (2013), and are shown in Appendix E and I).

Table 3 - Experimental results of the static test done for the composite laminate *Hybrid Design 2* with $\theta_{max} = |90^o|$

Specimens	Failure Load (N)	Failure Load per unit width (N/mm)		Thickness (mm)	Width (mm)	Length (mm)
1	2027.48	294.20		3.45	6.89	19.02
2	1876.40	269.54		3.43	6.96	18.22
3	1888.22	270.49		3.38	6.98	18.68
6	1826.81	265.55		3.47	6.88	18.54
7	1981.33	290.47		3.48	6.82	17.96
9	1668.00	242.44		3.48	6.88	18.28
10	2307.96	331.47		3.34	6.96	18.67
AVERAGE	1939.46	280.59		3.43	6.91	18.48
Standard Deviation	199.28	28.22		0.05	0.06	0.35

i. Assessment of the images taken from the Static Experiment

Based on the experiments given in Table 3, three Specimens were assessed more in detail. The Specimen Numbers were: 3, 9, 10 .

During the static tests that have been performed some common characteristics have been noticed. Below is shown a description of each of those characteristics that, by a visual means of assessment, seems to accomplish with a regular pattern:

Through Figure 47 ((a) and (b)), it was observed that the cracks in this design (Hybrid Design 2) have started in the tensile region of the composite laminate and on a 90^o ply orientation.

The crack initiation of each of the specimens that were tested have almost the same angle, this crack has occurred due to the principal stresses within a 90^0 ply (intralaminar failure).

Also, another characteristic that has been noticed, in comparison with the other designs is the low value of the ultimate load obtained from the experiments. This design (Hybrid Design 2) seems to be the worst in terms of static failure in comparison with the *All carbon Design* and *Hybrid Design 1*.

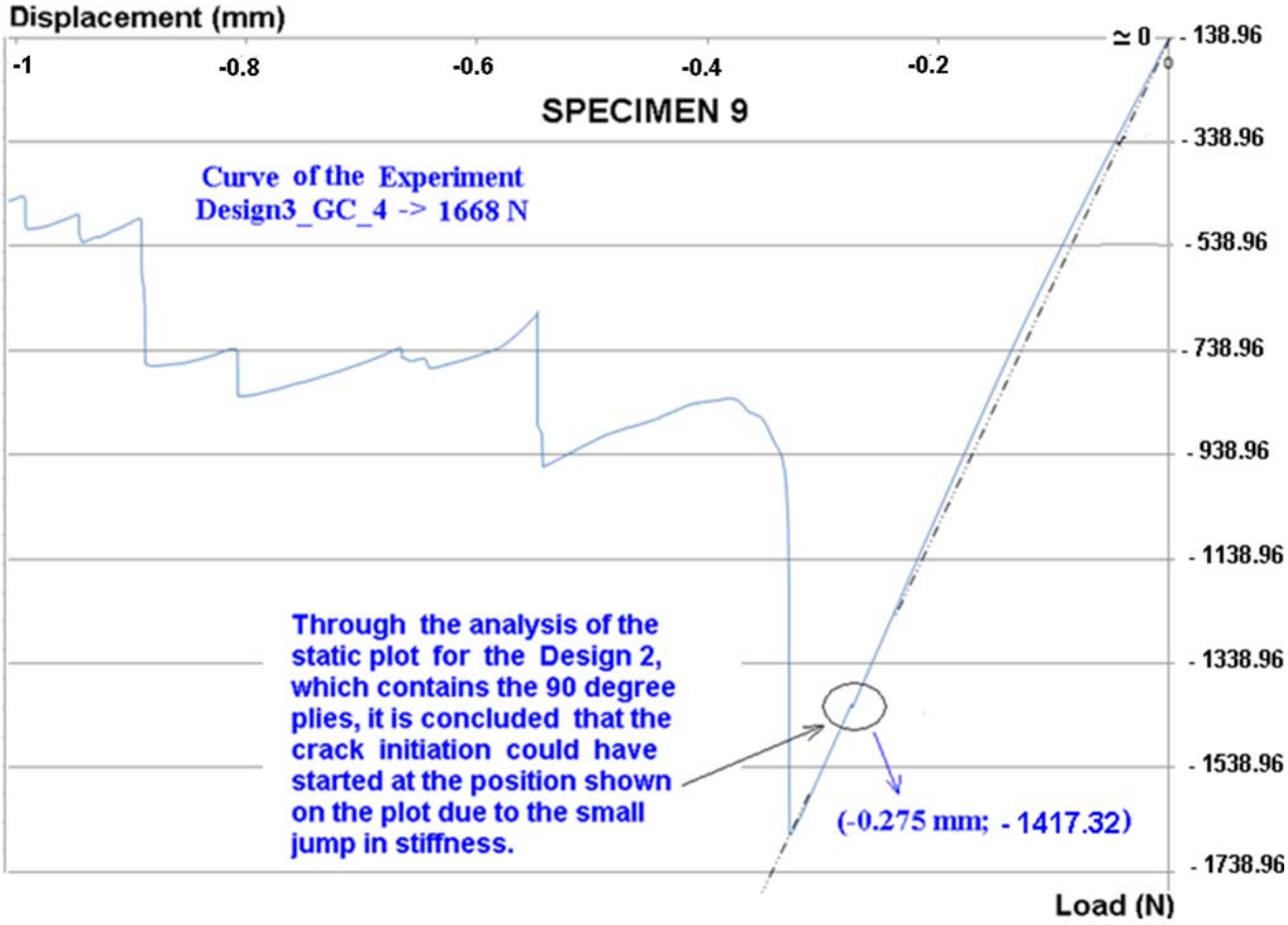

Figure 46 - Hybrid Design 2 -- Load-displacement plot given by the SBS test performed on specimen 9;

As can be seem in Figure 46, in the point of inflection, the *Hybrid Design 2* presents a small jump, which could mean that a crack initiation has started, and then, after that small jump, the laminate achieves its ultimate load. This point seems to have a direct connection with the matrix of a composite laminate, however it could be a rig error (machine compliance). Due to the uncertainty of this affirmation, further investigation is required.

Figure 47 - Hybrid Design 2 - Static test experiment (SBS test) showing: (a) Specimen 9 - shows the crack initiation captured by the camera at the instant of the crack onset; (b) Specimen 9 – zoomed-in image of the area in part at where the first crack has initiated; (c) Specimen 9 - image captured in the final stage of the SBS test, showing the crack propagation in the through-thickness direction at a determined angle, accompanied by the delamination of some plies.

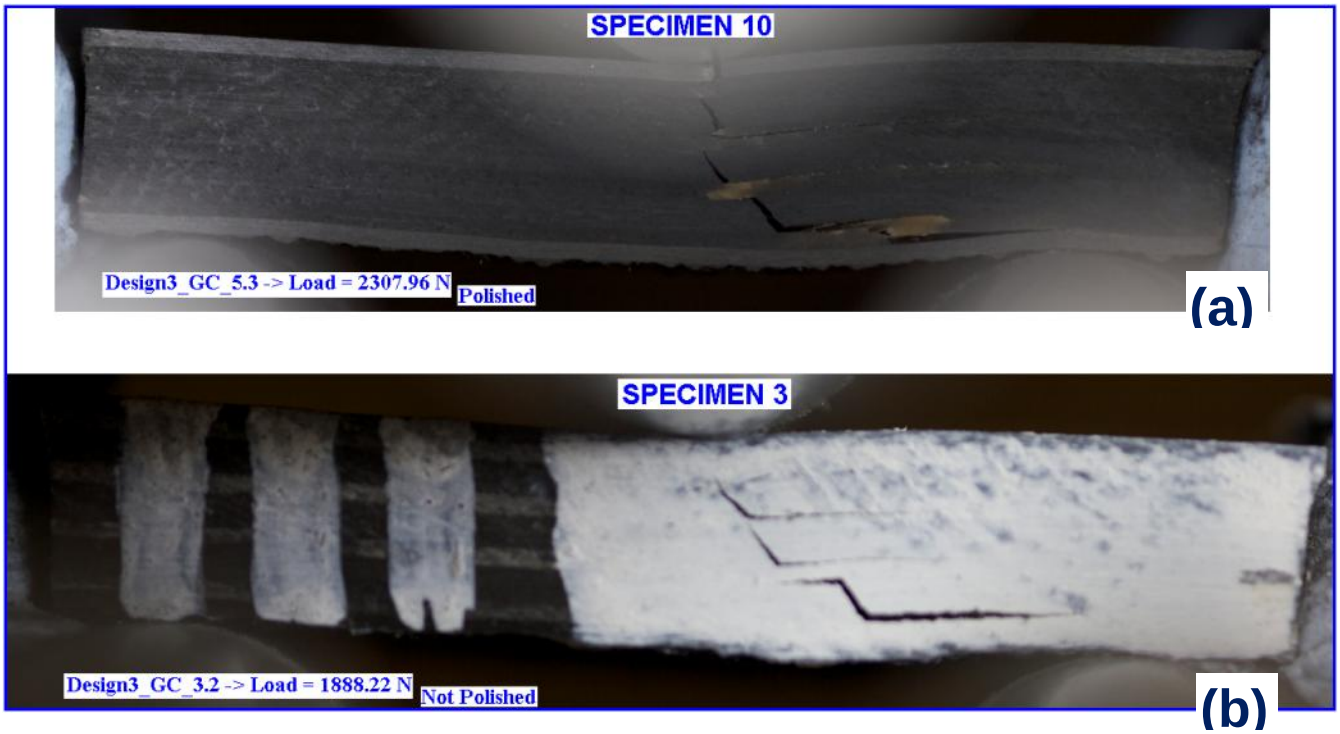

Figure 48 - Hybrid Design 2 - Static test experiments (SBS test) showing: (a) Specimen 10 - first image captured after the first crack has initiated; (b) Specimen 3 - first image captured after the first crack has initiated.

From the specimens shown in Figure 47, Figure 48 and Figure 59, one of the characteristics that could be seen is that the glass plies drive the crack propagation along its length, so it seems to be clear that glass plies within an hybrid composite laminate help to drive the crack propagation in a way that protects other adjacent plies.

4.3. ANALYSIS OF THE STATIC EXPERIMENTS

4.3.1. STRESS ANALYSIS OF ALL CARBON DESIGN

i. Theoretical Results

Using equations (89), (91), and (104) that were demonstrated in Chapter 2, the Table 4 shows the results for the static experiment that has been performed on Specimen number 10.

For a carbon ply thickness equal to 0.139mm (as shown by Han (2013) in Appendix I, table 3.4), with the width and length values equal to that shown on the Table 1 (Han 2013) and according to Young & Budynas (2002, section 8.17; table 8.1 - case 1c) (for a right and left end simply supported beam), Table 4 is presented.

Table 4 - Theoretical values found for specimen 10

SPECIMEN 10 - Line Load = 2318.36 N								
TOP OF THE LAMINATE								
Ply Number	**Angle (Degrees)**	**Material**	**Distance from the middle of the laminate (mm)**	ε_x (effective Strain) **where the crack has occurred, at x=11mm** (equation (89))	$\sigma_{x\left(\frac{Span}{2},z\right)}$ **Maximum axial stress value. At $x = 7$ mm** (equation (91)) **(MPa)**	$\sigma_{x\,(11mm,z)}$ **Axial stress on the spot where the first crack occurred (x=11 mm)** (equation (91)) **(MPa)**	τ_{xz} (equation (106)) **(MPa)**	$\tau_{Apparent}$ (equation (8)) **(MPa)**
Top Surface	**----**		1.668	-0.003879	- 1249.69	-535.58	0	75.87
1	**0**	Carbon	1.529	-0.003556	- 370.75	-158.89	24.82	
2	**45**	Carbon	1.390	-0.003233	- 92.66	-39.71	32.18	
3	**90**	Carbon	1.251	-0.002909	- 303.34	-130.00	34.02	
4	**- 45**	Carbon	1.112	-0.002586	- 833.13	-357.06	40.04	
5	**0**	Carbon	0.973	-0.002263	- 235.93	-101.11	56.58	
6	**45**	Carbon	0.834	-0.001940	- 55.60	-23.83	61.27	
7	**90**	Carbon	0.695	-0.001616	- 168.52	-72.22	62.37	
8	**- 45**	Carbon	0.556	-0.001293	- 416.56	-178.53	65.72	
9	**0**	Carbon	0.417	-0.000970	- 101.11	-43.33	73.99	
10	**45**	Carbon	0.278	-0.000647	- 18.53	-7.94	76.00	
11	**90**	Carbon	0.139	-0.000323	- 33.70	-14.44	76.37	
12	**- 45**	Carbon	0	0	0	0	77.04	
MIDDLE OF THE SYMMETRIC LAMINATE								

Figure 49 shows the Specimen 10 loaded under a SBS test condition.

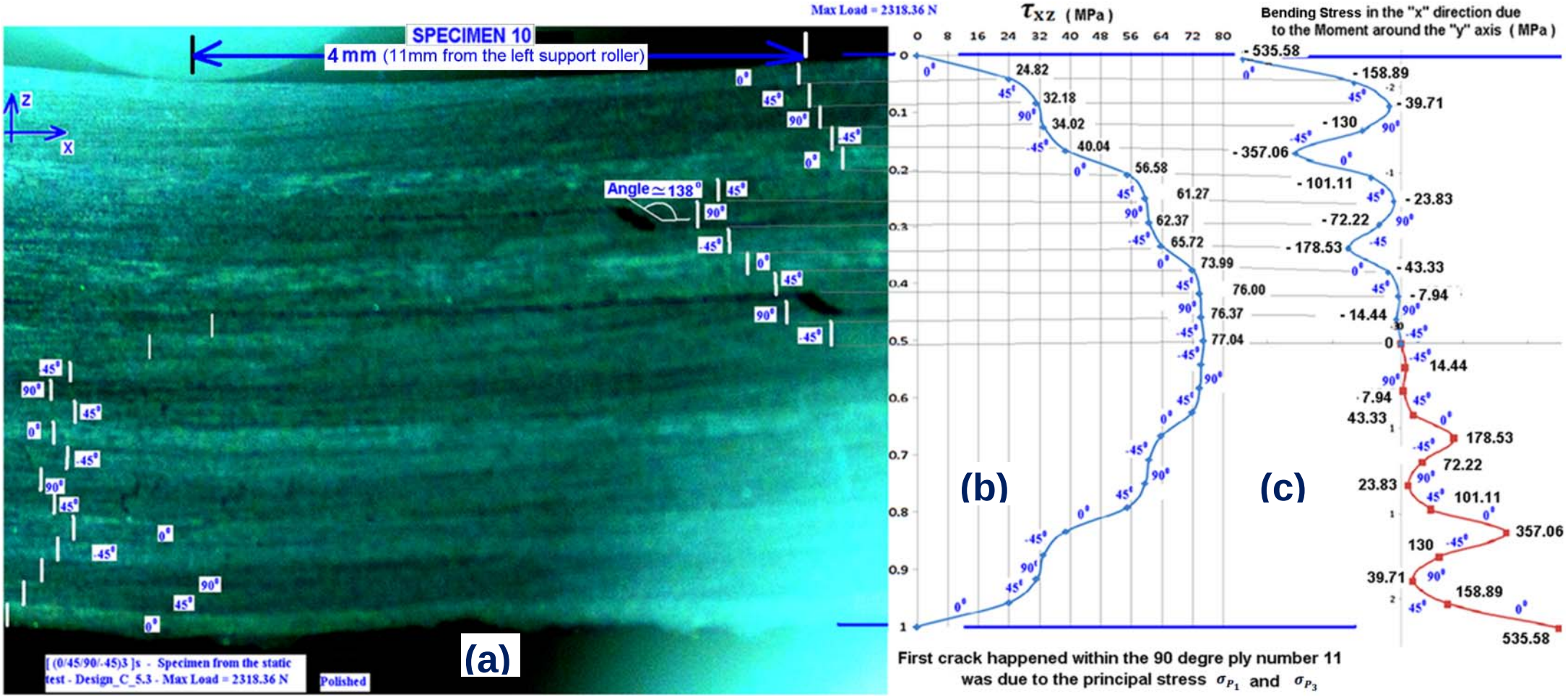

Figure 49 – Analysis of the theoretical results for *All Carbon Design.* Image showing: (a) central part of the Specimen 10; (b) through-thickness shear stress (τ_{xz}) (from Table 4); (c) bending stress in the *x* direction of the laminate ($\sigma_{x\,(x,z)}$) (from Table 4). Notes: 1) Each white line represents a ply thickness. 2) The First crack happened due to an *Intralaminar* failure in a 90 degree ply. 3) Figure 49 was taken when the first two cracks had started.

ii. FE Analysis for All Carbon Design

A brief explanation of the method applied during the FE Analysis

The continuum shell element offers a general view of the stresses around a composite part, however, 3-D Stress elements (brick elements) were used because they show in detail the stress in a determined region of the composite laminate and also because they use the full 3-D stress field to obtain the stresses.

Table 5 shows the dimensions and load that have been used in the *All Carbon Design* FE model.

Table 5 - Composite Laminate's Geometric Characteristic

DESIGN	Failure Load (values taken from Table 1) (N)	Thickness (according to Han (2013) in Appendix I, table 3.4) (mm)	Width (values taken from Table 1) (mm)	Length (values taken from Table 1) (mm)	Span (mm)
All Carbon (Specimen 10)	2318.36	24×0.139	6.87	19.08	14

The FE models have been created in order to achieve a better visualization in terms of the ILSS distribution of a specimen which has been subjected to an experimental test under SBS test conditions.

The diameter of the loading rollers and support roller is 6 mm (this is the same as that used in the experimental test).

The models have been built in order to achieve 24 elements in the through-thickness direction, in which each of the elements has the same thickness as the respective ply which it represents within the composite laminate. This means that if a single layer (orthotropic ply) is made by UD glass fibres then the thickness of the element will be the same as the glass ply thickness. Each of the orthotropic plies that have been created in the FE-model has a single material orientation as shown in Figure 7. Each ply has been given orthotropic elastic properties using the Abaqus input option type *Engineering Constants*. The material properties that have been used are in accordance with those given in the Appendix M.

Boundary conditions were applied to each of the FE-model in order to fix the specimen at two points located in the middle of its length (centre span) in order to allow a vertical movement of the laminate when a load is applied in the middle of the span. The support rollers were completely restrained with the Abaqus option *encastre* by fixing all the inner nodes in the inner cylinder of each roller (see Figure 50).

A multipoint constraint (MPC) has been created on the loading roller fixing all of the nodes that are in the inner cylinder of the roller. The MPC has been used to apply the single load presented in Table 5.

The elastic material properties of the AISI 4340 alloy steel in which the Young's Modulus is given as 199 948 MPa and the Poisson's Ratio as 0.32 has been used for the loading and support rollers.

Figure 50 shows an example of the FE-model that has been built.

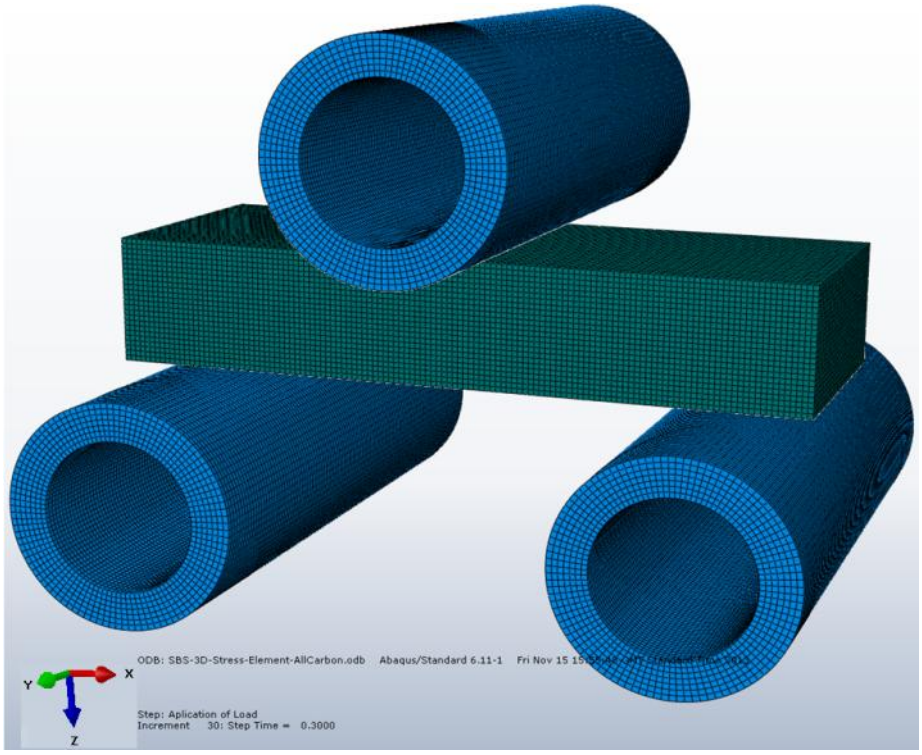

Figure 50 - SBS test - General assembly

Note: the explanation given in this section is also applicable to the sections 4.3.2 ii) and 4.3.3 ii).

The results from the final element analysis for *All Carbon Design* are given in Figure 51, Figure 52 and Figure 53.

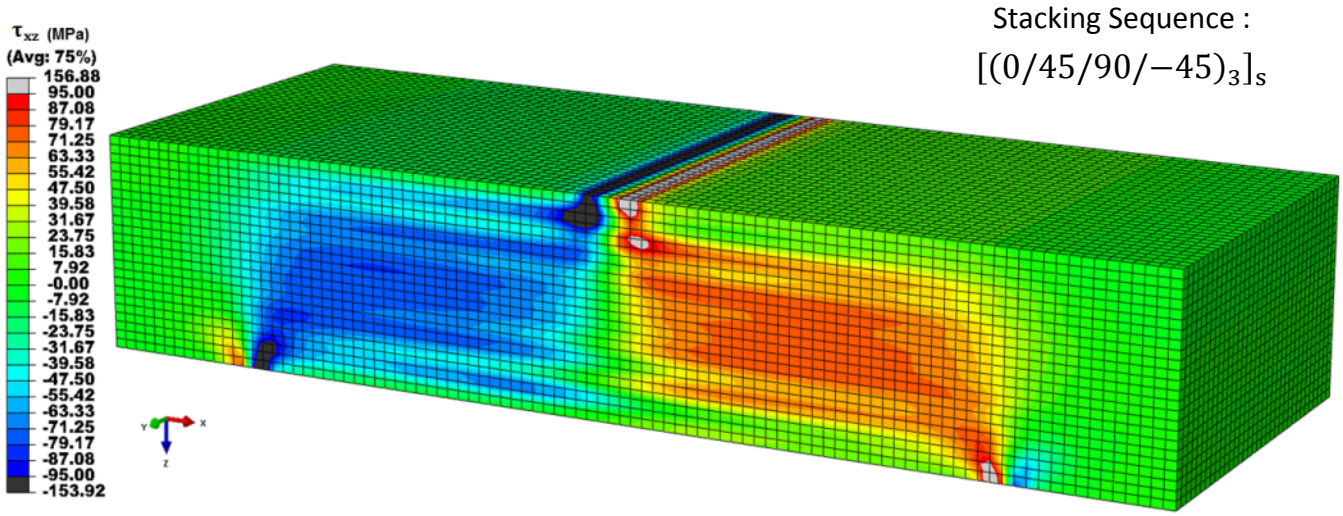

Figure 51 – Image showing the ILSS (τ_{xz}) FE results for the *All Carbon Design* specimen 10.

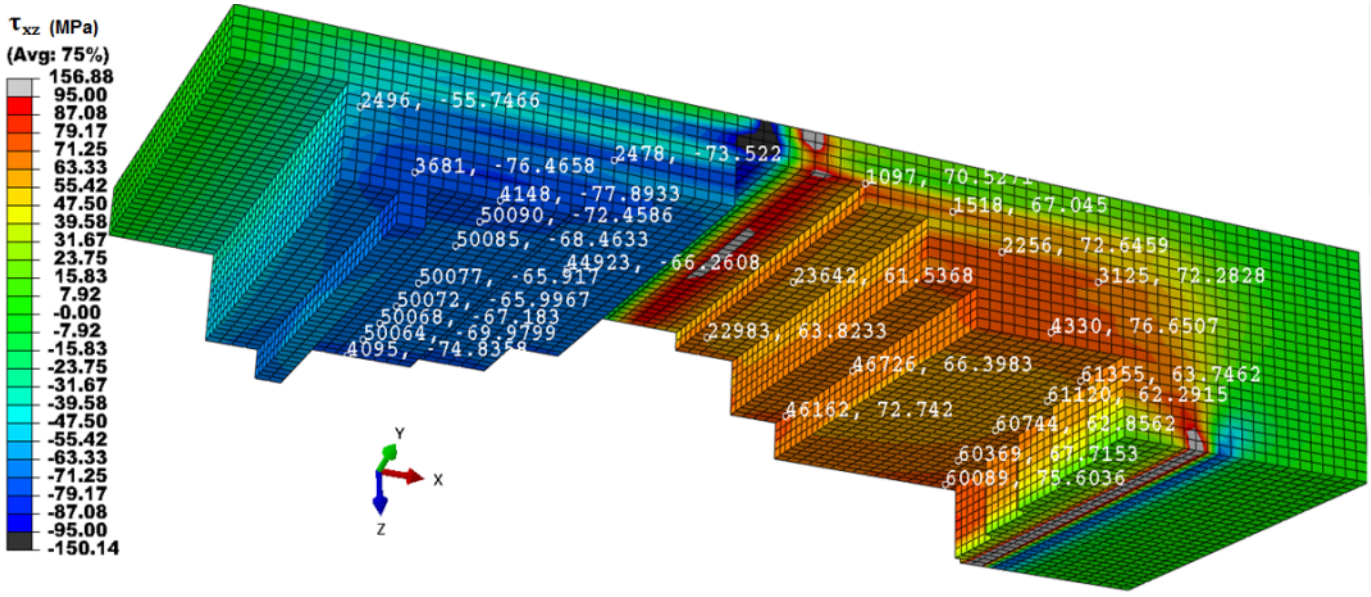

Figure 52 - Internal ILSS (τ_{xz}) presented for the All Carbon Design specimen 10. Note that the pair of values shown on the figure are the element number followed by the ILSS (τ_{xz}).

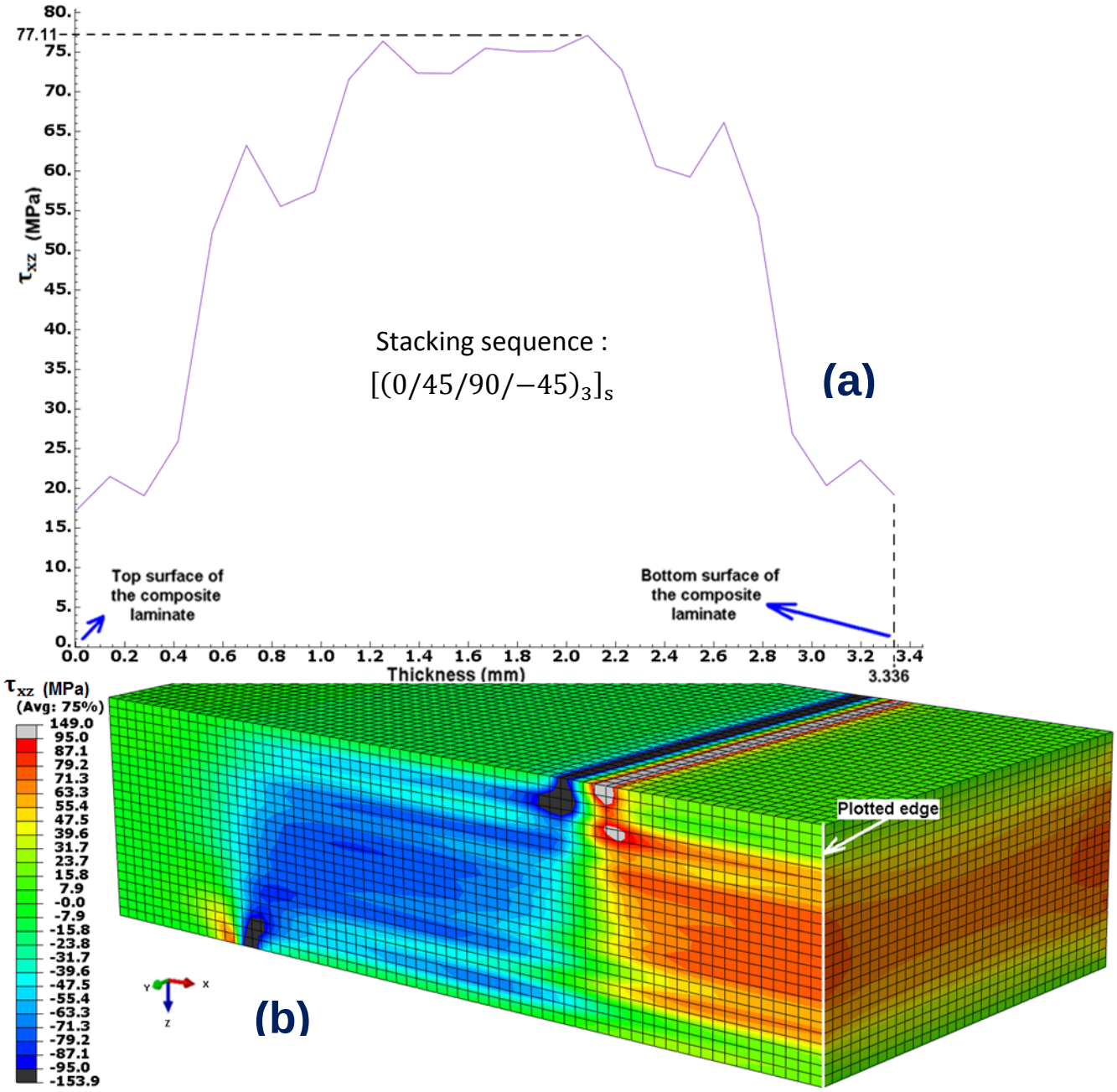

Figure 53 – Image showing the: (a) ILSS (τ_{xz}) Abaqus plot for *All Carbon Design*; (b) Specimen 10, shown in Figure 51, cut at the cross-section where the first crack has appeared (see Figure 43 and Figure 49).

iii. Resume of the Analytical Results for All Carbon Design

Table 6 shows the analytical results obtained from the three different methods that have been used to obtain the value of the ILSS (τ_{xz}). These methods are: FE-Analysis; the assessment of the ILSS using equation (106) and the assessment of the ILSS using equation (8).

Table 6 – Results for All Carbon Design

SPECIMEN 10 - Line Load = 2318.36 N - All Carbon Design $[(0/45/90/-45)_3]_s$					
TOP OF THE LAMINATE					
Ply Number	**Angle (Degrees)**	**Material**	**τ_{xz} applying equation (106) (MPa)**	**τ_{xz} from the FE-Model (for the cross-section shown in Figure 53) (MPa)**	**τ_{xz} applying equation (8) (MPa)**
Top Surface			0	0	
1	**0**	Carbon	24.82	19.33	
2	**45**	Carbon	32.18	20.28	
3	**90**	Carbon	34.02	22.50	
4	**- 45**	Carbon	40.04	39.10	
5	**0**	Carbon	56.58	57.76	
6	**45**	Carbon	61.27	59.39	
7	**90**	Carbon	62.37	56.48	
8	**- 45**	Carbon	65.72	64.49	
9	**0**	Carbon	73.99	73.97	
10	**45**	Carbon	76.00	74.37	
11	**90**	Carbon	76.37	72.33	
12	**- 45**	Carbon	**77.04**	74.58	
MIDDLE OF THE LAMINATE					**75.87**
13	**- 45**	Carbon	**77.04**	74.58	
14	**90**	Carbon	76.37	75.10	
15	**45**	Carbon	76.00	**77.11**	
16	**0**	Carbon	73.99	74.94	
17	**- 45**	Carbon	65.72	66.70	
18	**90**	Carbon	62.37	59.94	
19	**45**	Carbon	61.27	62.69	
20	**0**	Carbon	56.58	60.18	
21	**- 45**	Carbon	40.04	40.57	
22	**90**	Carbon	34.02	23.62	
23	**45**	Carbon	32.18	21.95	
24	**0**	Carbon	24.82	21.35	
Bottom surface			0	0	
BOTTOM OF THE LAMINATE					

iv. Principal Stresses for All Carbon Design

A brief explanation of the method applied

The failure criterion that has been implemented and assessed was in accordance with Tsai-Wu criterion (Tsai & Hahn 1980), however, the final results have shown that the laminates tested failed in a different mode. This difference could have been a result of the fact that Tsai-Wu (Tsai & Hahn 1980) is a failure criterion for plane stress state. The failure that has occurred on each specimen tested in laboratory was due to the ILSS (τ_{xz}) combined with the stress in the *x* direction ($\sigma_{x\,(x,z)}$) for each of the plies within a laminate. This thesis considers the principal stresses in order to assess the intralaminar failure on the 90^0 ply that has been found during the experiments performed by Han (2013).

Considering that for an SBS test, the normal stress σ_z acting on each ply is negligible (equal to zero), and considering also that on a 2-D assessment in the through-thickness direction the stresses in the *y* direction of each ply are equal to zero due to the explanation given in Chapter 2, section 2.6 ($\sigma_y = \tau_{yx} = \tau_{yz} = 0$), thus, the Figure 54 shows the stress state for a 2-D assessment in the through-thickness direction. The index *j* denotes the ply number. The accompanying equations are given in Appendix N (equations (119) up to (124)).

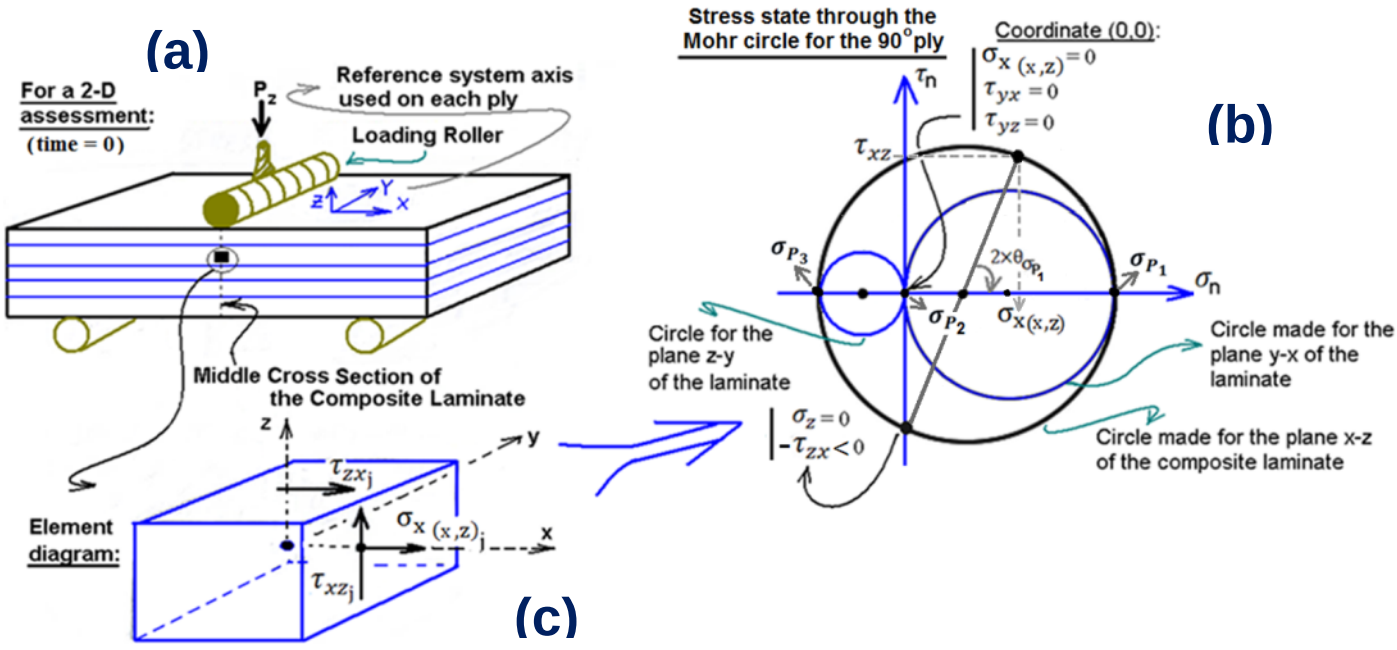

Figure 54 - Image showing the: (a) specimen under a SBS test condition; (b) Mohr's circle for the stress state element shown in (c); (c) stress state element taken from a single ply belonging to the specimen (a).

Results of the principal stresses:

Table 7 shows the results of applying equations (156) through (162) to the 90^0 plies in the *All Carbon Design* which can be found in Appendix N.

All Carbon Design

$$[(0/45/90/-45)_3]_s$$

Table 7 - Principal stresses for All Carbon Design (Specimen 10). Values for bending moment taken at the position where the first crack has occurred (x= 11 mm; see Figure 49).

For the Specimen 10 shown on the Table 1 (Specimen with 24 plies)							
TOP OF THE LAMINATE							
Ply Number	**Angle (Degrees)**	**Material**	σ_{P_1} **(MPa)**	σ_{P_3} **(MPa)**	$\theta_{\sigma_{P\,1}}$ **(Degrees)**	$\tau_{max\,x'z'}$ **(MPa)**	$\theta_{\tau_{max\,x'z'}}$ **(Degrees)**
3	**90**	Carbon	- 57.67	17.95	- 29.16	37.81	- 74.16
7	**90**	Carbon	- 74.33	50.50	- 39.50	62.42	- 84.50
11	**90**	Carbon	**- 80.07**	**72.13**	**- 43.50**	76.10	- 88.50
MIDDLE OF THE SYMMETRIC LAMINATE		Resin (Matrix)	77.04	-77.04	0	77.04	45
14	**90**	Carbon	80.07	- 72.13	43.50	76.10	88.50
18	**90**	Carbon	74.33	- 50.50	39.50	62.42	84.50
22	**90**	Carbon	57.67	- 17.95	29.16	37.81	74.16
BOTTOM OF THE LAMINATE							

Note: The black cells shown in Table 7 show the values for the spot where the first crack has occurred in the laminate due to an Intralaminar failure (Figure 49, ply number 11).

4.3.2. STRESS ANALYSIS OF HYBRID DESIGN 1 WITH $\theta_{max} = |\pm 45^o|$

i. Theoretical Results

Similarly to what has been done in section 4.3.1 i), by using the equations (89), (91), and (104) , Table 8 shows the results for the static experiment that has been performed on Specimen 9.

For a carbon ply thickness equal to 0.139mm, and a glass ply thickness equal to 0.143 mm (as shown by Han (2013) in Appendix I, table 3.4), and, according to Young & Budynas (2002, section 8.17; table 8.1 - case 1c) (for a right and left end simply supported beam), the Table 8 is presented.

Note: From Figure 44 and Figure 45. As it is not clear where the crack has initiated on this Hybrid Design 1, the maximum value of the moment per unit width, $M_{x\ around\ y\ axis}$ (used in the equation (91) to obtain the axial stress σ_{x_j}) has been used to calculate the axial stress ($\sigma_{x\ (x,z)}$).

Table 8 - Theoretical values found for specimen 9

SPECIMEN 9 - Line Load = 2588 N							
TOP OF THE LAMINATE							
Ply Number	**Angle (Degrees)**	**Material**	**Distance from the middle of the laminate (mm)**	ε_x (effective Strain) **At x=7mm** (equation (89))	$\sigma_x\left(\frac{Span}{2},z\right)$ **Maximum axial stress value. At $x = 7$ mm** (equation (91)) **(MPa)**	τ_{xz} (equation (106)) **(MPa)**	$\tau_{Apparent}$ (equation (8)) **(MPa)**
Top Surface	**----**		1.684	- 0.008581	- 1184.73	0	83.16
1	**0**	Carbon	1.545	- 0.007873	- 1086.94	23.53	
2	**0**	Carbon	1.406	- 0.007165	- 320.13	45.11	
3	**45**	Carbon	1.267	- 0.006456	- 288.48	51.47	
4	**- 45**	Carbon	1.128	- 0.005748	- 256.83	57.19	
5	**45**	Carbon	0.989	- 0.005039	- 225.18	62.29	
6	**- 45**	Carbon	0.850	- 0.004331	- 83.71	66.77	
7	**45**	Glass	0.707	- 0.003603	- 69.63	68.48	
8	**- 45**	Glass	0.564	- 0.002874	- 55.54	69.90	
9	**45**	Glass	0.421	- 0.002145	- 41.46	71.03	
10	**- 45**	Glass	0.278	- 0.001417	- 63.30	71.88	
11	**45**	Carbon	0.139	- 0.000708	- 31.65	73.14	
12	**- 45**	Carbon	0	0	0	73.77	
MIDDLE OF THE SYMMETRIC LAMINATE							

Figure 55 shows the Specimen 9 loaded under a SBS test condition. The picture was taken after the crack had started and on the last stage of the static test.

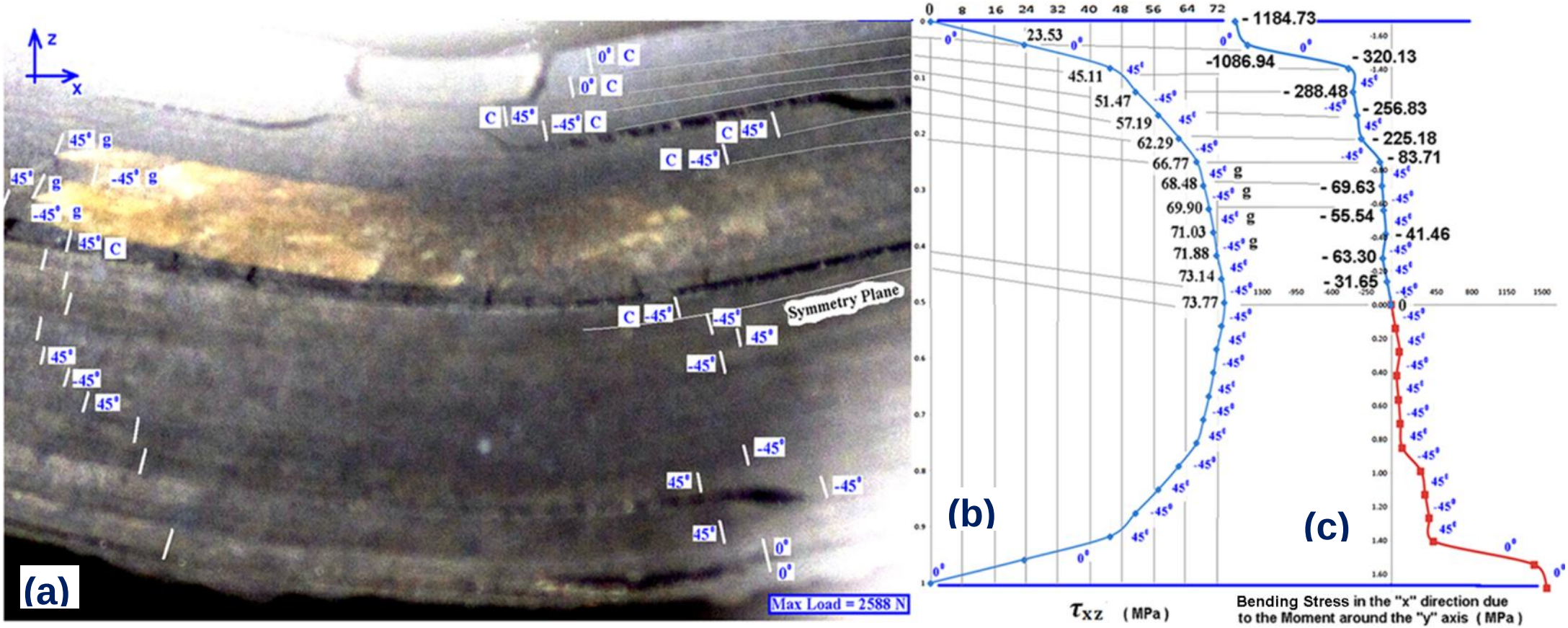

Figure 55 - Analysis of the theoretical results for *Hybrid Design 1.* Image showing: (a) Central part of the Specimen 9; (b) Through-thickness shear stress (τ_{xz}) (from Table 8); (c) bending stress in the *x* direction of the laminate ($\sigma_{x\,(x,z)}$) (from Table 8).

Notes: 1) Each white line represents the ply thickness at that level. 2) The initials *C* and *g* means: Carbon and Glass material respectively. 3) The First crack happened due to an *Interlaminar* failure between the ply number 11 and ply number 12.

ii. FE Analysis for Hybrid Design 1

Table 9 shows the dimensions and load that have been used in the *Hybrid Design 1* FE model.

Table 9 - Composite Laminate's Geometric Characteristic

DESIGN	Failure Load (values taken from Table 2) (N)	Thickness (According to Han (2013) in Appendix I, table 3.4) (mm)	Width (values taken from Table 2) (mm)	Length (values taken from Table 2) (mm)	Span (mm)
Hybrid Design 1 (Specimen 9)	2588.00	$16 \times 0.139 + 8 \times 0.143$	6.93	18.37	14

The results from the final element analysis for *Hybrid Design 1* are given in Figure 56, Figure 57 and Figure 58.

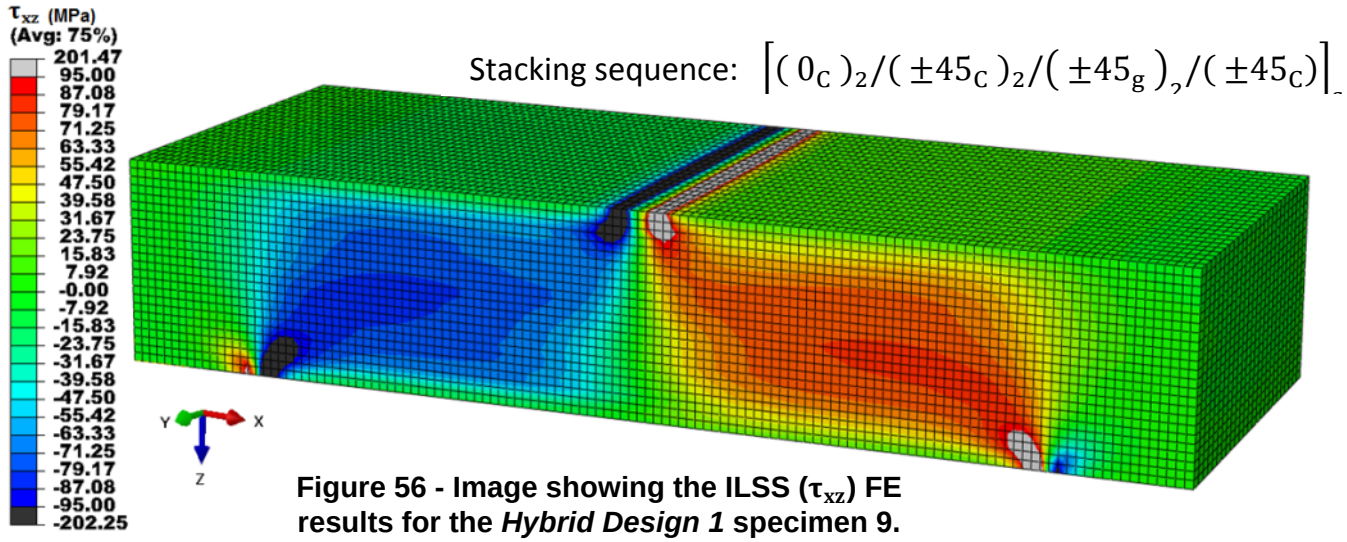

Figure 56 - Image showing the ILSS (τ_{xz}) FE results for the *Hybrid Design 1* specimen 9.

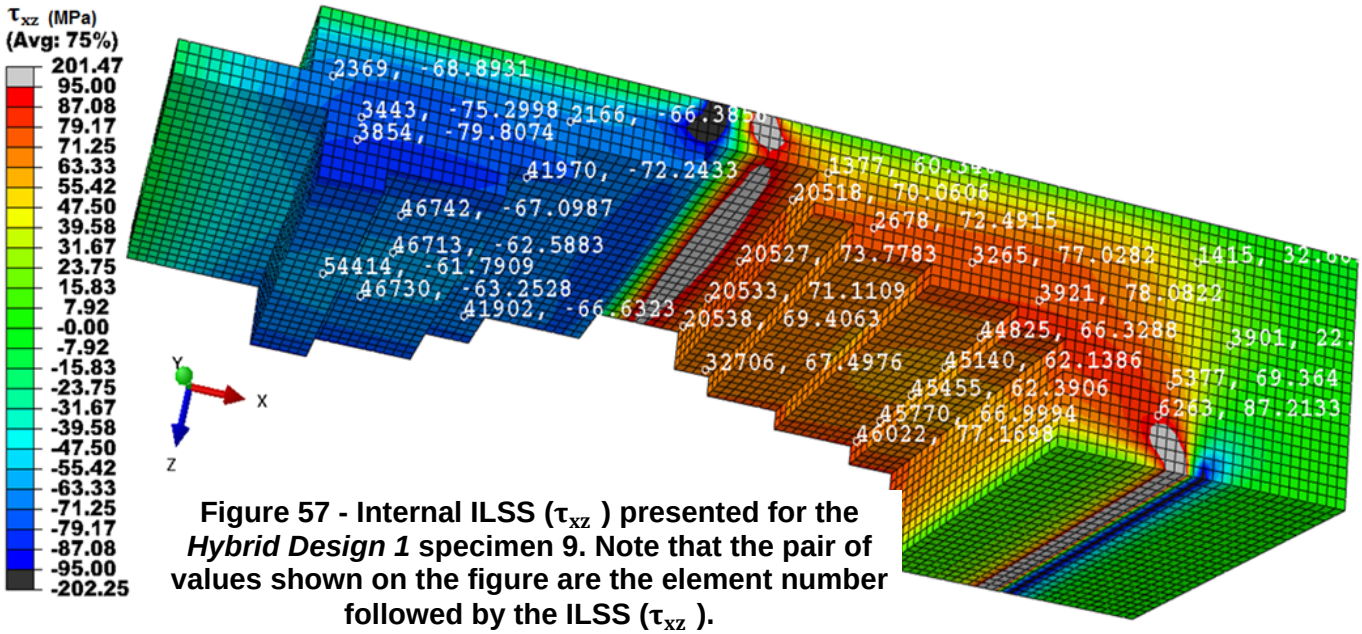

Figure 57 - Internal ILSS (τ_{xz}) presented for the *Hybrid Design 1* specimen 9. Note that the pair of values shown on the figure are the element number followed by the ILSS (τ_{xz}).

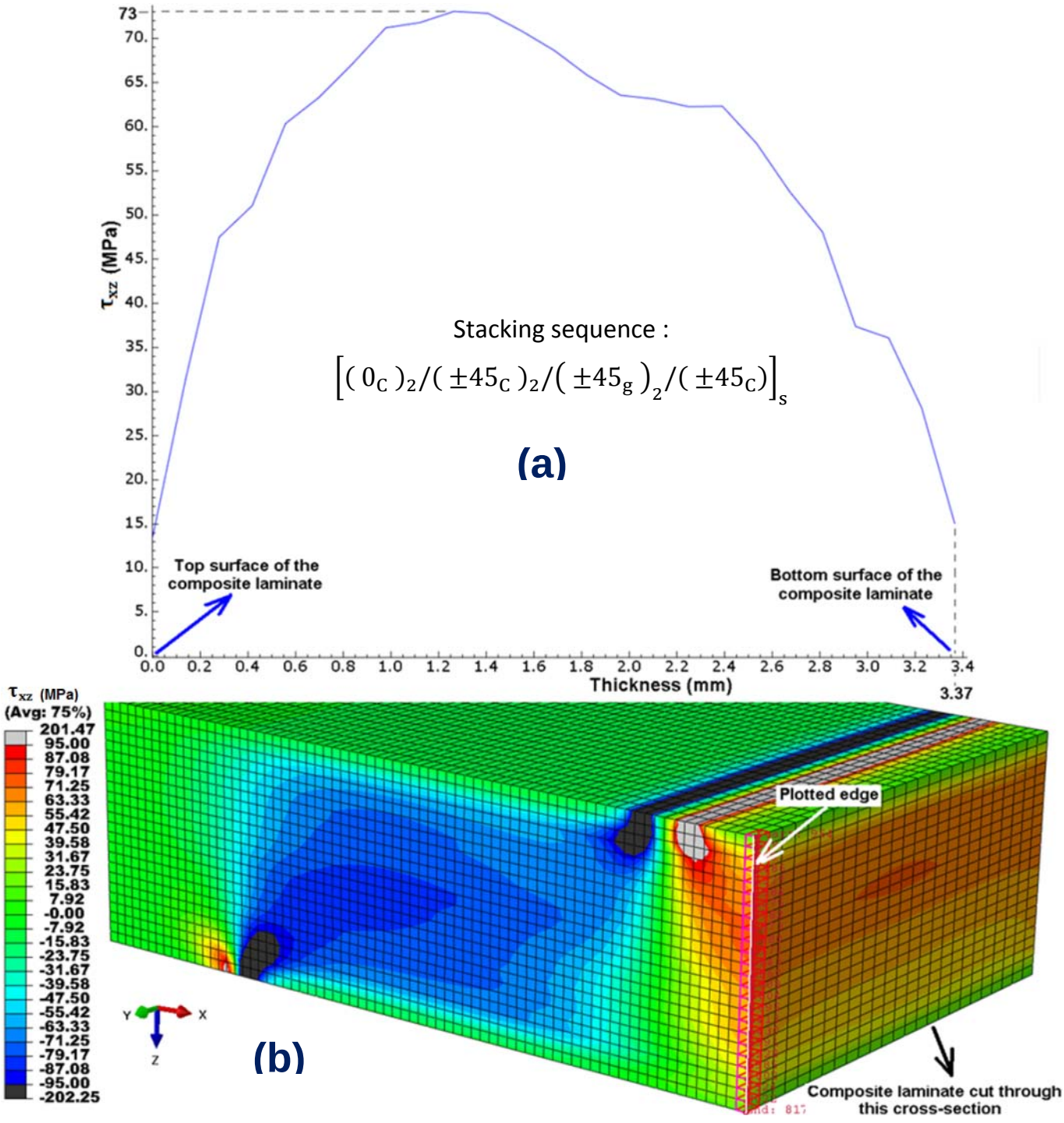

Figure 58 - Image showing the: (a) ILSS (τ_{xz}) Abaqus plot for *Hybrid Design 1*; (b) Specimen 9, shown in Figure 56, cut at the cross-section near to the middle of the laminate (middle of the span).

iii. Resume of the Analytical Results for Hybrid Design 1 with $\theta_{max} = |\pm 45^{o}|$

Table 10 shows the analytical results obtained from the three different methods that have been used to obtain the value of the ILSS (τ_{xz}).

Table 10 – Results for Hybrid Design 1

SPECIMEN 9 - Line Load = 2588 N - Hybrid Design 1 $\left[(0_c)_2/(\pm 45_c)_2/(\pm 45_g)_2/(\pm 45_c)\right]_s$					
TOP OF THE LAMINATE					
Ply Number	**Angle (Degrees)**	**Material**	**τ_{xz} applying equation (106) (MPa)**	**τ_{xz} from the FE-Model (for the cross-section shown in Figure 58) (MPa)**	**τ_{xz} applying equation (8) (MPa)**
Top Surface			0	0	
1	**0**	Carbon	23.53	22.56	
2	**0**	Carbon	45.11	39.52	
3	**45**	Carbon	51.47	49.28	
4	**- 45**	Carbon	57.19	55.7	
5	**45**	Carbon	62.29	61.81	
6	**- 45**	Carbon	66.77	65.16	
7	**45**	Glass	68.48	69.12	
8	**- 45**	Glass	69.90	71.50	
9	**45**	Glass	71.03	72.42	
10	**- 45**	Glass	71.88	**73.05**	
11	**45**	Carbon	73.14	71.86	
12	**- 45**	Carbon	**73.77**	68.49	
MIDDLE OF THE LAMINATE					**83.16**
13	**- 45**	Carbon	**73.77**	67.23	
14	**45**	Carbon	73.14	64.69	
15	**- 45**	Glass	71.88	63.35	
16	**45**	Glass	71.03	62.70	
17	**- 45**	Glass	69.90	62.29	
18	**45**	Glass	68.48	60.22	
19	**- 45**	Carbon	66.77	55.39	
20	**45**	Carbon	62.29	50.36	
21	**- 45**	Carbon	57.19	42.72	
22	**45**	Carbon	51.47	36.73	
23	**0**	Carbon	45.11	32.11	
24	**0**	Carbon	23.53	21.60	
Bottom surface			0	0	
BOTTOM OF THE LAMINATE					

Note: Since *Hybrid Design 1* has presented an interlaminar failure between ply number 11 and ply number 12, and since this design does not have 90^0 plies, the principal stresses will not be presented for this design.

4.3.3. STRESS ANALYSIS OF HYBRID DESIGN 2 WITH $\theta_{max} = |90^o|$

i. Theoretical Results

For this sub-section, the equations (89), (91), and (104) were applied.

The Table 11 shows the static experiment results that have been performed by Han (2013) on specimen 10 – Hybrid Design 2.

For a carbon and glass ply thickness equal to 0.139mm and 0.153mm respectively (as shown by Han (2013) in Appendix I, table 3.4), with the width and length values equal to those shown on Table 3, and, according to Young & Budynas (2002, section 8.17; table 8.1 - case 1c) (for a right and left end simply supported beam), The Table 11 is presented.

Table 11 - Theoretical values found for the specimen 10

SPECIMEN 10 - Line Load = 2307.96 N								
TOP OF THE LAMINATE								
Ply Number	**Angle (Degrees)**	**Material**	**Distance from the middle of the laminate (mm)**	ε_x (effective Strain) **where the crack has occurred, at x=9mm** (equation (89))	$\sigma_{x\left(\frac{Span}{2},z\right)}$ **Maximum axial stress value. At** $x = 7\ mm$ (equation (91)) **(MPa)**	$\sigma_{x\ (9mm,z)}$ **Axial stress on the location where the first crack occurred [x=9 mm]** (equation (91)) **(MPa)**	τ_{xz} (equation (106)) **(MPa)**	$\tau_{Apparent}$ (equation (8)) **(MPa)**
Top Surface	**----**		1.724	- 0.006319	- 1221.40	- 872.43	0	72.1
1	**0**	Carbon	1.585	- 0.005810	- 1122.92	- 802.09	24.25	
2	**0**	Carbon	1.446	- 0.005300	- 143.41	- 102.43	46.55	
3	**45**	Glass	1.293	- 0.004739	- 128.23	- 91.59	49.69	
4	**- 45**	Glass	1.140	- 0.004179	- 71.86	- 51.33	52.49	
5	**90**	Carbon	1.001	- 0.003670	- 63.10	- 45.07	53.92	
6	**90**	Carbon	0.862	- 0.003160	- 54.34	- 38.81	55.17	
7	**90**	Carbon	0.723	- 0.002650	- 45.58	- 32.55	56.25	
8	**90**	Carbon	0.584	- 0.002141	- 57.92	- 41.37	57.15	
9	**45**	Glass	0.431	- 0.001580	- 42.74	- 30.53	58.42	
10	**- 45**	Glass	0.278	- 0.001019	- 17.52	- 12.52	59.35	
11	**90**	Carbon	0.139	- 0.000510	- 8.76	- 6.26	59.70	
12	**90**	Carbon	0	0	0	0	59.87	
MIDDLE OF THE SYMMETRIC LAMINATE								

Figure 59 shows Specimen 10 loaded under a condition of SBS test. The picture was taken after the crack had started.

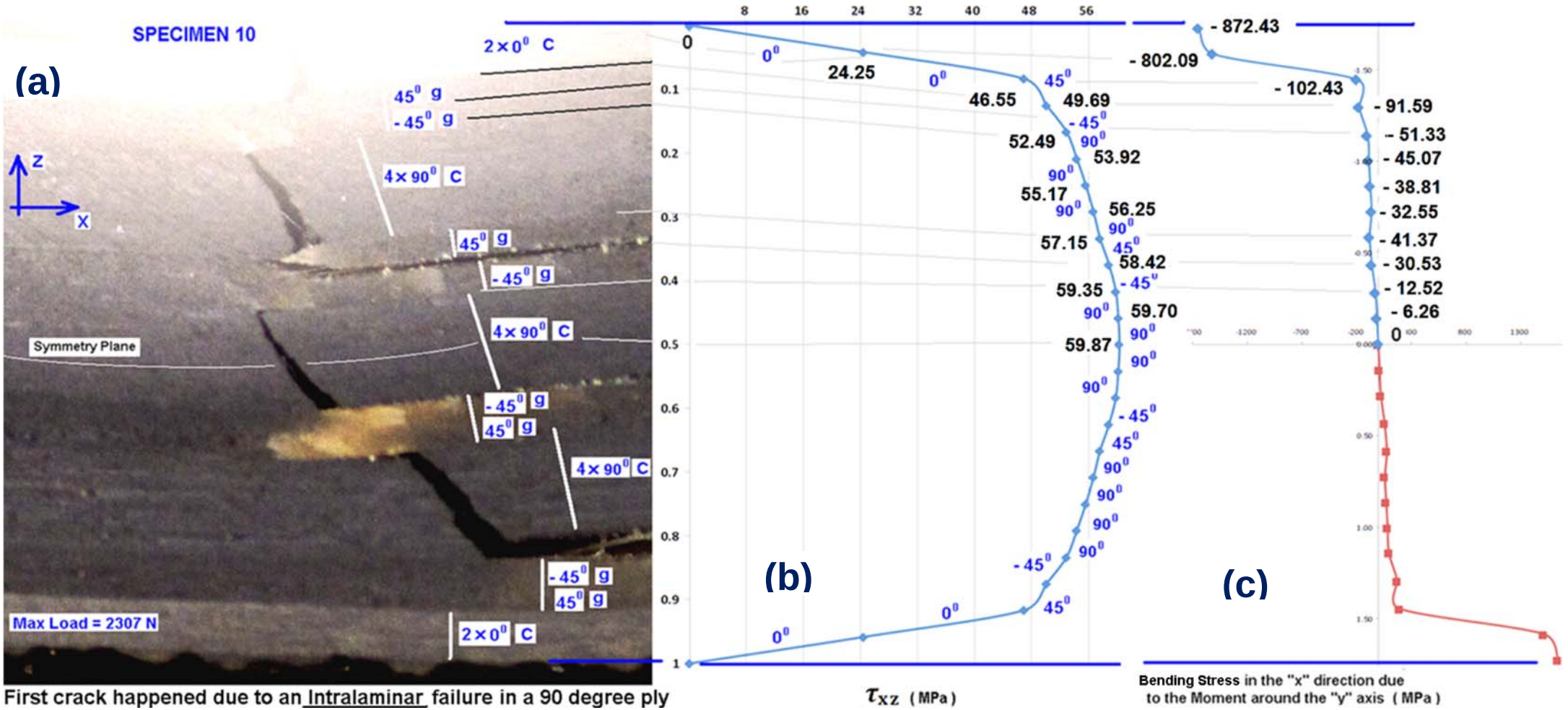

Figure 59 - Analysis of the theoretical results for *Hybrid Design 2.* Image showing: (a) Central part of the Specimen 10; (b) Through-thickness shear stress (τ_{xz}) (from Table 11); (c) bending stress in the *x* direction of the laminate ($\sigma_{x\,(x,z)}$) (from Table 11).

Notes: 1) Each white line represents a ply thickness. 2) The First crack happened due to an *Intralaminar* failure in a 90 degree ply (between the ply number 17 and ply 20). 3) Figure 59 was taken when the first two cracks had started.

ii. FE Analysis for Hybrid Design 2

Table 12 shows the dimensions and load that have been used in the *Hybrid Design 2* FE model.

Table 12 - Composite Laminate's Geometric Characteristic

DESIGN	Failure Load (values taken from Table 3) (N)	Thickness (According to Han (2013) in Appendix I, table 3.4) (mm)	Width (values taken from Table 3) (mm)	Length (values taken from Table 3) (mm)	Span (mm)
Hybrid Design 2 (Specimen 10)	2307.96	$16 \times 0.139 + 8 \times 0.153$	6.96	18.67	14

The results from the final element analysis for *Hybrid Design 2* are given in Figure 60, Figure 61 and Figure 62.

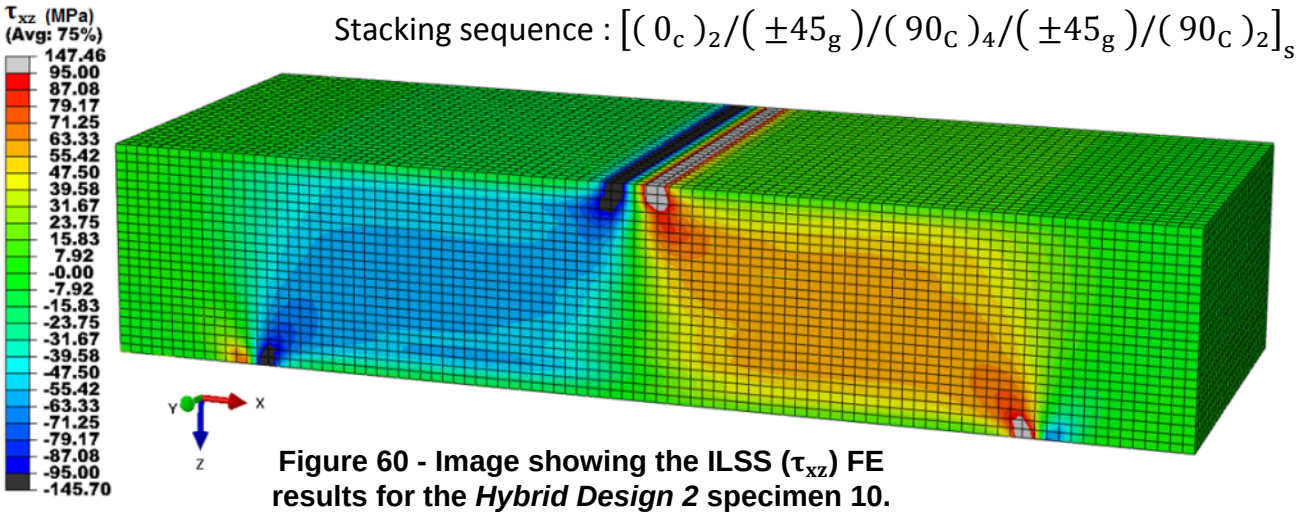

Figure 60 - Image showing the ILSS (τ_{xz}) FE results for the *Hybrid Design 2* specimen 10.

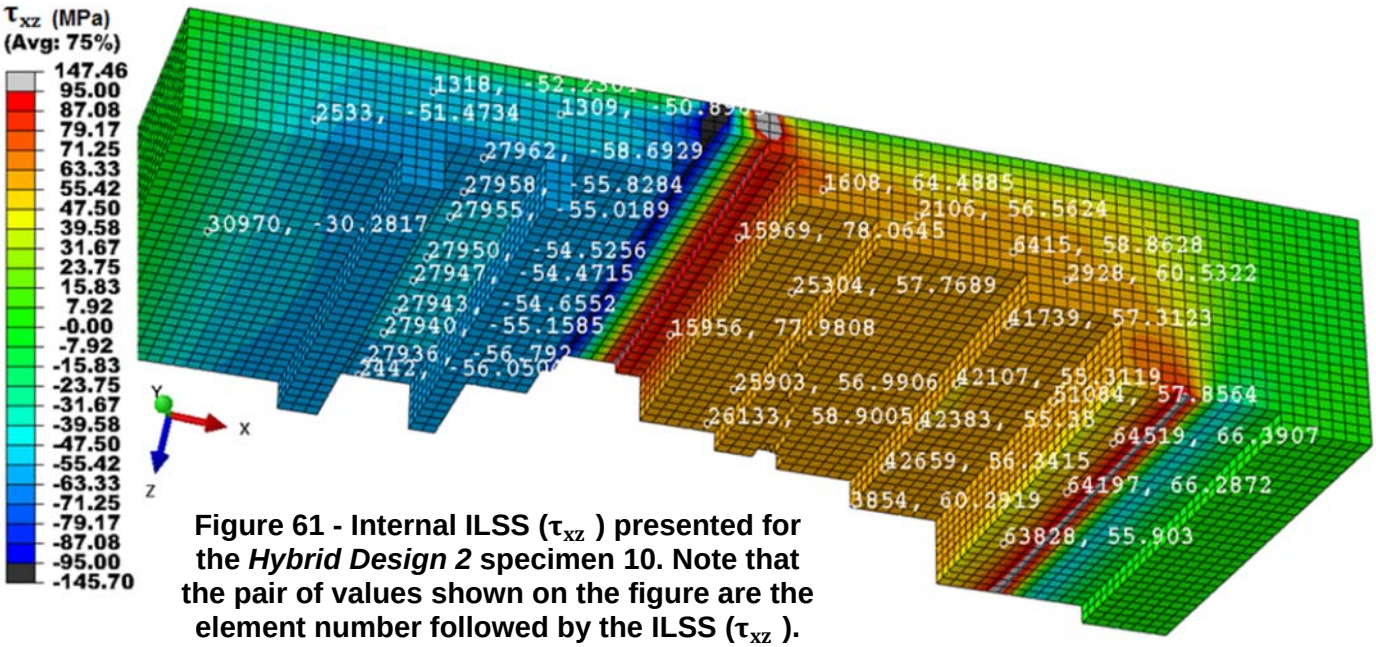

Figure 61 - Internal ILSS (τ_{xz}) presented for the *Hybrid Design 2* specimen 10. Note that the pair of values shown on the figure are the element number followed by the ILSS (τ_{xz}).

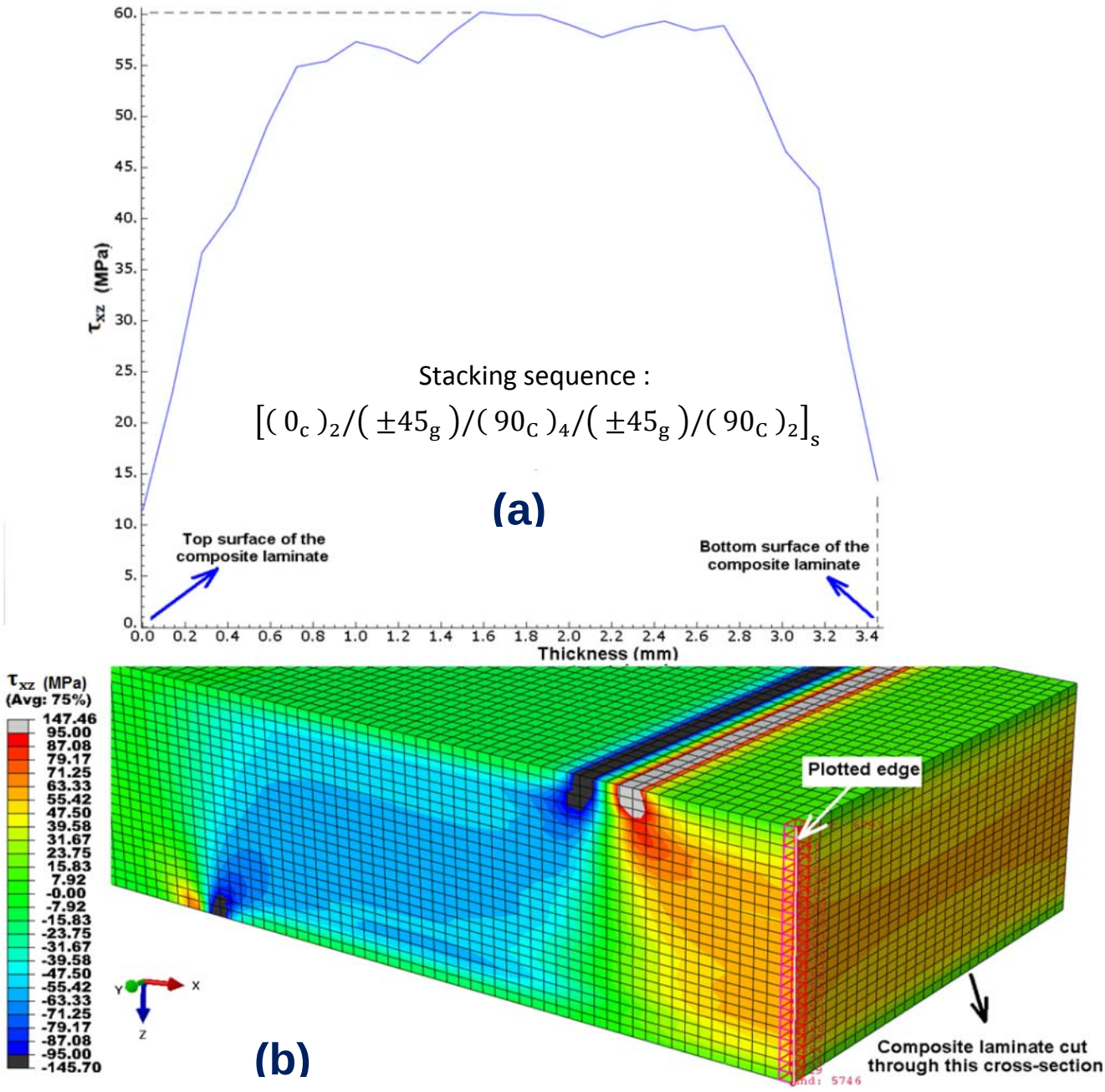

Figure 62 - Image showing the: (a) ILSS (τ_{xz}) Abaqus plot for *Hybrid Design 2*; (b) Specimen 10, shown in Figure 60, cut at the cross-section section where the first crack has appeared (see Figure 47).

iii. Resume of the Analytical Results for Hybrid Design 2 with $\theta_{max} = |90^o|$

Table 13 shows the analytical results obtained from the three different methods that have been used to obtain the value of the ILSS (τ_{xz}).

Table 13 – Results for Hybrid Design 2

SPECIMEN 10 - Line Load = 2307.96 N - Hybrid Design 2 $[(0_c)_2/(\pm 45_g)/(90_C)_4/(\pm 45_g)/(90_C)_2]_s$					
TOP OF THE LAMINATE					
Ply Number	**Angle (Degrees)**	**Material**	**τ_{xz} applying equation (106) (MPa)**	**τ_{xz} from the FE-Model (for the cross-section shown in Figure 62) (MPa)**	**τ_{xz} applying equation (8) (MPa)**
Top Surface			0	0	
1	**0**	Carbon	24.25	17.16	
2	**0**	Carbon	46.55	29.79	
3	**45**	Glass	49.69	38.87	
4	**- 45**	Glass	52.49	45.10	
5	**90**	Carbon	53.92	52.00	
6	**90**	Carbon	55.17	55.15	
7	**90**	Carbon	56.25	56.38	
8	**90**	Carbon	57.15	56.97	
9	**45**	Glass	58.42	55.92	
10	**- 45**	Glass	59.35	56.67	
11	**90**	Carbon	59.70	59.17	
12	**90**	Carbon	**59.87**	**60.22**	
MIDDLE OF THE LAMINATE					**72.1**
13	**90**	Carbon	**59.87**	**60.22**	
14	**90**	Carbon	59.70	59.45	
15	**-45**	Glass	59.35	58.36	
16	**45**	Glass	58.42	58.25	
17	**90**	Carbon	57.15	59.05	
18	**90**	Carbon	56.25	58.89	
19	**90**	Carbon	55.17	58.67	
20	**90**	Carbon	53.92	56.41	
21	**-45**	Glass	52.49	50.23	
22	**45**	Glass	49.69	44.75	
23	**0**	Carbon	46.55	35.32	
24	**0**	Carbon	24.25	20.99	
Bottom surface			0	0	
BOTTOM OF THE LAMINATE					

iv. Principal Stresses for Hybrid Design 2

Table 14 shows the results of applying equations (156) through (162) to the 90^0 plies located in the *Hybrid Design 2* which are found in Appendix N.

Hybrid Design 2

$$\left[\left(0_c\right)_2/\left(\pm45_g\right)/\left(90_C\right)_4/\left(\pm45_g\right)/\left(90_C\right)_2\right]_s$$

Table 14 - Principal stresses for the *Hybrid Design 2* (Specimen 10). Values for bending moment taken at the position where the first crack has occurred (x= 9 mm; see Figure 47 (a) and (b)).

For the Specimen 10 shown on the Table 11 (Specimen with 24 plies)							
TOP OF THE LAMINATE							
Ply Number	**Angle (Degrees)**	**Material**	σ_{P_1} **(MPa)**	σ_{P_3} **(MPa)**	$\theta_{\sigma_{P1}}$ **(Degrees)**	$\tau_{max\ x'z'}$ **(MPa)**	$\theta_{\tau_{max\ x'z'}}$ **(Degrees)**
5	**90**	Carbon	- 84.09	32.76	- 31.97	58.43	- 76.97
6	**90**	Carbon	- 80.97	35.90	- 33.66	58.44	- 78.66
7	**90**	Carbon	- 77.89	39.08	- 35.31	58.48	- 80.31
8	**90**	Carbon	- 74.83	42.28	- 36.93	58.56	- 81.93
11	**90**	Carbon	- 65.94	53.42	- 41.99	59.68	- 86.99
12	**90**	Carbon	- 62.91	56.65	- 43.50	59.78	- 88.50
MIDDLE OF THE SYMMETRIC LAMINATE		Resin (Matrix)	59.87	- 59.87	0	59.87	45
13	**90**	Carbon	62.91	- 56.65	43.50	59.78	88.50
14	**90**	Carbon	65.94	- 53.42	41.99	59.68	86.99
17	**90**	Carbon	**74.83**	**- 42.28**	**36.93**	58.56	81.93
18	**90**	Carbon	**77.89**	**- 39.08**	**35.31**	58.48	80.31
19	**90**	Carbon	**80.97**	**- 35.90**	**33.66**	58.44	78.66
20	**90**	Carbon	**84.09**	**- 32.76**	**31.97**	58.43	76.97
BOTTOM OF THE LAMINATE							

Note: The black cells shown in Table 14 show the values for the region where the first crack has occurred in the laminate (see Figure 47 and Figure 59). Since it is not clear where the crack has initiated in Figure 47 it was considered that the Intralaminar failure has initiated within one of the four plies between the ply number 17 and ply number 20.

4.4. DISCUSSION AND CONCLUSIONS - STATIC TEST

From the images shown in the previous section 4.2, it should be noted that during the static tests that have been performed, the load applied to each of the composite laminates that were tested under SBS test conditions was not a line of load, but spread over a contact surface approximately 1mm wide. However, it seems to have had a little influence on the results.

At the beginning of this research it was thought that the mode of failure of each of the composite laminates due to the ultimate static load of an SBS test, would always be due an interlaminar failure (a failure in between two plies), and this would be independent to the stacking sequence. However, sections 4.2 and 4.3 show that the stress due to the moment around the y axis of the composite laminate ($\sigma_{x\,(x,z)}$) gives a contribution to the failure of the composite laminate when an ultimate load P_Z is applied in accordance with Figure 42. This contribution of stress together with the ILSS (τ_{zx}) could cause an intralaminar failure (a failure within the ply) which will depend on the stacking sequence of the composite laminate.

All Carbon Design :

Sections 4.2.1 and 4.3.1 have shown that the All Carbon Design with the stacking sequence: $[(0/45/90/-45)_3]_s$ has always failed due to an intralaminar failure in the 90^0ply with a similar failure pattern as that shown in Figure 49 and whose characteristics are described in Figure 63. Despite it being difficult to predict through the images taken from the static tests that have been performed on the seven specimens for the *all carbon design* specimens, from Figure 49 it seems that the intralaminar failure starts in the first 90^0 ply counted from the middle of the composite laminate up to the top of the laminate (ply number 11), in the compression side of the composite laminate. According to Figure 49, the angle of the failure in the 90^0 plies always have almost the same value around 138^0 in regards to the *x* axis (see Figure 63).

From the results obtained for the principal stress which are given in Table 7, ply number 11 is likely to be the position where the first crack has occurred (see Figure 49). The values shown in Table 7, show that the principal stress σ_{P_3} (see Figure 63) on the position of ply number 11 creates an angle of $\theta_{\sigma_{P\,3}} = -43.5^0$ which is close to that which has been detected on Figure 49 on the ply number 11, which is equal to $138 - 180 = -42^0$ and which is represented in Figure 63.

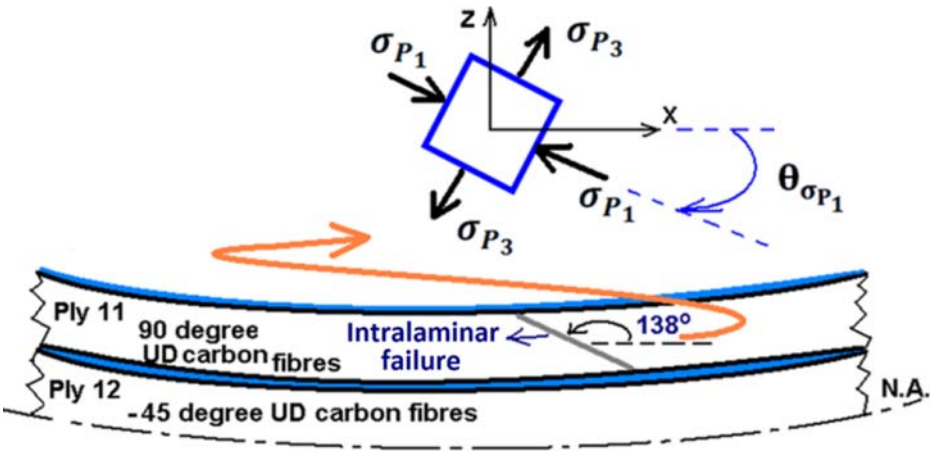

Figure 63 – Representation of the intralaminar failure within the ply number 11 as shown in Figure 49. Principal stresses are given in Table 7 and the angle given by the experimental test is shown on the Figure 49. Note: Test gives an angle $\theta_{\sigma_{P_1}} = -42^o$, Table 7 gives an angle $\theta_{\sigma_{P_1}} = -43.5^o$.

It is concluded that the failure in the design: *All Carbon Design* always occurs in the 90^0ply due to an intralaminar failure caused by the tensile principal stress σ_{P_3} (which includes the effects due to $\sigma_{x\,(x,z)}$ and ILSS ($\tau_{z\,x}$)).

Hybrid Design 1 :

In regards to Hybrid Design 1 that has a stacking sequence equal to $\left[(0_C)_2/(\pm45_C)_2/(\pm45_g)_2/(\pm45_C)\right]_s$, sections 4.2.2 and 4.3.2 show that, in this case it is likely that the failure is due to the interlaminar shear stress, because through Figure 44, Figure 45 and Figure 55 it could be seen that delamination has occurred near to the mid-plane of the composite laminate, which means that the crack initiation started in the matrix in the interface between ply number 11 and 12 according to Figure 55. Some explanations were given in section 4.2.2 i). Figure 64 shows the intralaminar failure as has occurred in the *Hybrid Design 1*.

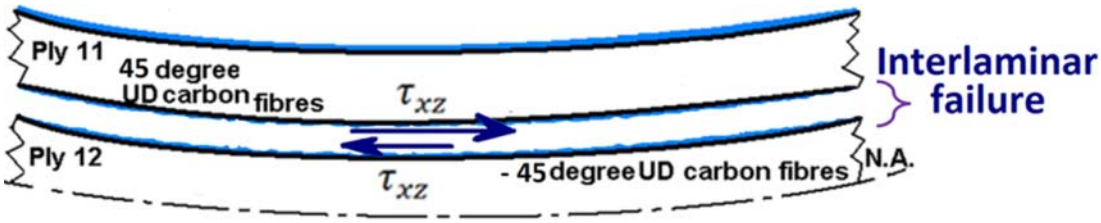

Figure 64 - Representation of the interlaminar failure as presented in Figure 45 and Figure 55.

Hybrid Design 2 :

Regarding to the Hybrid Design 2, which stacking sequence is given by : $[(0_c)_2/(\pm 45_g)/(90_C)_4/(\pm 45_g)/(90_C)_2]_s$, as is shown in Figure 47 and by a visual means of assessment, the first crack has occurred in the tensile side of the specimen on a 90^0 ply, it is not clear in which this has started, however it evident that was an intralaminar failure (within the ply) that has started in one of the 90^0 ply numbers: 17; 18; 19 or 20 (according to Table 11). As shown on the Figure 47, the crack was predicted to have started at an angle approximately equal to 34^0 and then propagates through the thickness until reaching the glass plies producing delaminations and consequent failure of the composite laminate.

According to Table 14, for the ply numbers 17 up to 20, the angle of the principal σ_{P_1} varies between $31.97^0$and 36.93^0 (see Figure 65 and Figure 95, this last from Appendix N), since those angles are near to the angle of 34^0 as shown in the Figure 47, It is concluded that the failure in the *Hybrid Design 2* always occurs in the 90^0 ply due to an intralaminar failure caused by the principal stress σ_{P_1} (which includes the effects due to $\sigma_{x\ (x,z)}$ and ILSS (τ_{zx})).

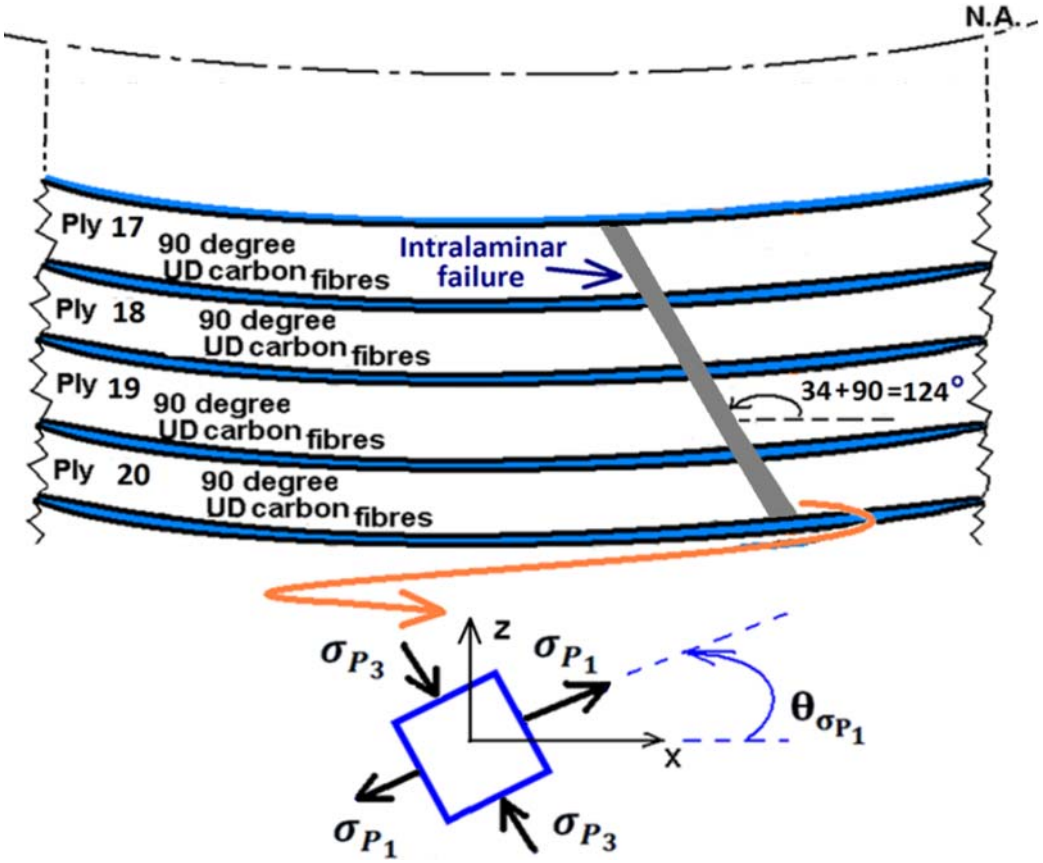

Figure 65 – Figure shows the intralaminar failure which occured in *Hybrid Design 2* (Figure 47). Note: Test gives an angle $\theta_{\sigma_{P_1}} = 34^o$, Table 14 gives an angle $\theta_{\sigma_{P_1}}$ between 31.97^0 and 36.93^0.

Summary :

Hybrid Design 1 has presented a better static failure behavior, because it allows the increase of the static failure load in regards to the remaining designs that were tested and because it is more stable in terms of static failure which may be due to the addition of glass plies within the composite laminate, which seems to drive the cracks along the length of the glass ply surface after it has started.

Due to the averaging method utilized by the software Abaqus on the FE-Models, some of the FE results could be higher than expected. However, in general the results show good compliance with the theory.

Note: Details about the experimental rig that has been used and test procedure are shown in Appendix C and I. After the experimental tests had been performed (Han 2013) it was noticed that the loading roller deviated from its central position by about 0.8 mm to the right. However, this measurement taken from Figure 43, Figure 44, Figure 45 and Figure 47 could lead to a larger value in reality because the load shown in the figures is spread over a contact surface of about 1mm width.

Chapter 5

EXPERIMENTAL TEST - FATIGUE

5.1. INTRODUCTION

Fatigue processes in composite materials are far more complex than those in homogeneous materials. In composite materials several damage modes, including fibre matrix debonding, matrix cracking, delamination and fibre fracture can occur. By a combination of these processes, widespread damage can propagate throughout the bulk of the composite leading to loss in strength and stiffness.

As Harris (2003) says: " the damage mechanisms in fibre composites vary both with the nature of the composite (the combination of fibres and matrices and reinforcement lay-up), and with the loading conditions (tension, bending, compression, etc.)."

It has been difficult up to now to exactly predict (at least, to the same extent that metal components are predictable) the endurance and other fatigue characteristics of a composite component, mainly due to the quantity of variables that are involved, and also due to it not being an isotropic material as metals are. It seems that all these fatigue laws as well as the failure criteria laws should be assessed in the microscopic level in order to define a consistent criteria, however, such affirmation requires many more investigations.

According to Harris (2003), the fatigue behavior of a composite laminate (number of cycles that a composite laminate can withstand under a determined loading condition, the endurance of the composite part, etc), is affected by factors such as: the fibre type, the matrix type (resin), the use of more than one material within a composite part (hybrid composite laminate), loading condition, etc. After a determined number of cycles there will be a degradation of the composite strength as shown in Figure 66, in which, σ_c is the normal composite static strength value.

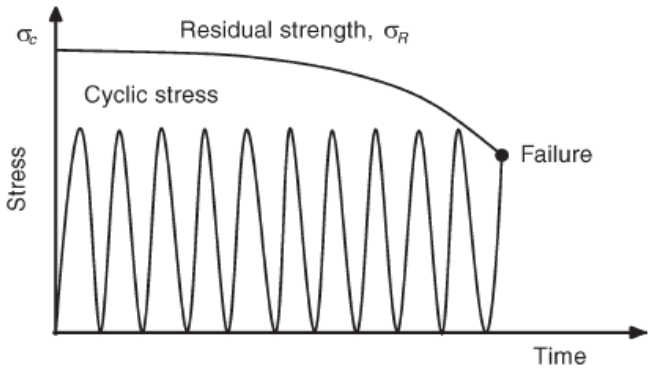

Figure 66 - Degradation of composite strength by wear-out - Example. Source: reference: (Harris 2003, p. 5)

This chapter presents the results and respective assessment of the specimens that have been tested under a monotonic fatigue load in a SBS test condition (according to (D2344/2344M 2006).

Ji Han (Han 2013) has conducted these experiments on two different designs provided by the theoretical part of this work. The designs that have been chosen were the best two of the three designs that have presented the best behavior in terms of the static ultimate load, crack initiation and crack propagation.

The designs are: All Carbon Design: $[(0/45/90/-45)_3]_s$ and Hybrid Design 1: $\left[(0_C)_2/(\pm 45_C)_2/(\pm 45_g)_2/(\pm 45_C)\right]_s$

According to ref. (Han 2013), the static results from the short ($\cong 18.6\, mm$) and long ($\cong 26\, mm$) specimens, which are described in chapter 4, were utilized to perform the fatigue tests at a 90%; 80%; and 70% of the ultimate average load given by the static experiments.

5.2. PROCEDURE

All fatigue tests were performed at a test frequency of 2 Hz (Han 2013).

The stress ratio, which is the ratio between the minimum load to the maximum load applied by the loading roller over the upper surface of the composite laminate is equal to 10 ($R=F_{z_{min}}/F_{z_{max}}$).

In the fatigue tests, a stress ratio of R=10 was chosen in order to keep all loads compressive as shown in Figure 67 (b).

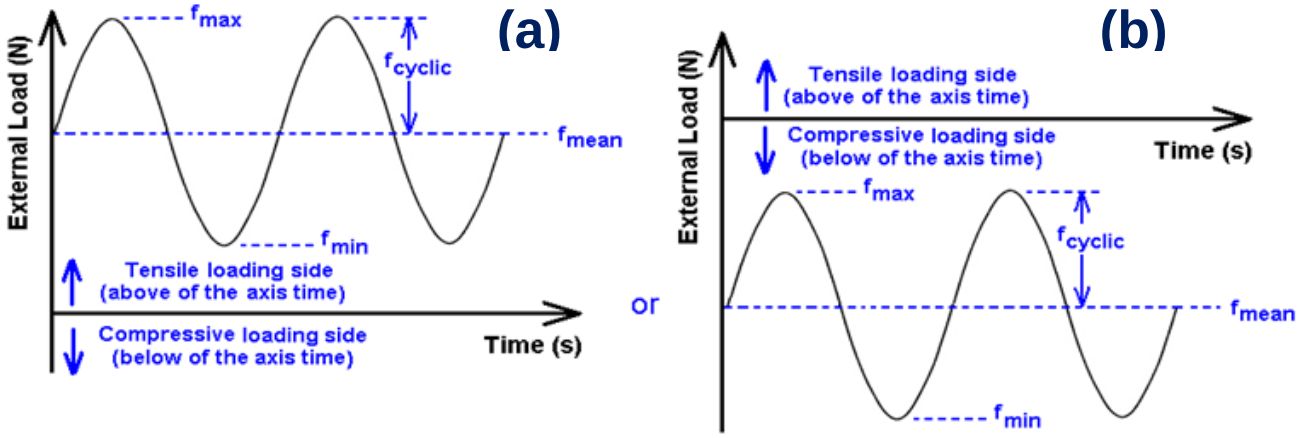

Figure 67 – Image showing: (a) Cyclic stress plot in which the external load is always positive (component always under a tensile load); (b) Cyclic stress plot in which the external load is always negative (component always under a compressive load). Meaning of the variables shown on the plot: $f_{max} = F_{z_{max}}$ is the maximum external load applied on the component; $f_{min} = F_{z_{min}}$ is the minimum external load applied on the component; f_{mean} is the mean load applied on the component; $f_{cyclic} = f_{max} - f_{mean}$

According to Figure 67, the amplitude value for a determined external load will be:

$$Amplitude = f_{max} - f_{min}$$

Further information about the fatigue experiments that were performed by Han (2013) is given in Appendix F; G; H; I and J.

5.3. ALL CARBON DESIGN - FATIGUE TEST RESULTS

This section will present the results and loads applied on each of the specimens that were tested under a fatigue condition of SBS test in accordance with the standard ASTM D2344/2344M (2006).

i. All Carbon Design - Rig Input Load

In order to find a reference value from which the loads to be applied on the fatigue testing will be estimated, the average of the thickness, width, and ultimate load of the specimens, obtained from the static test, will be applied to equation (164) from Appendix P (average values are shown in Table 1 of section 4.2.1, chapter 4).

As a result, by using equation (164) from Appendix P the maximum bending stress average will be:

$$\widehat{\sigma}_{x,iso}\left(\frac{span}{2},\frac{t}{2}\right) = 672.53\ \text{MPa}$$

In which:

$$\begin{cases} \text{span} = 14\text{mm} \\ \text{b} = \text{width average from the Table 1} = 7.06\ \text{mm} \\ \text{t} = \text{thickness average from Table 1} = 3.33\ \text{mm} \\ \text{P}_z = 2507.16\ \text{N (average load from Table 1)} \end{cases}$$

Note: - See Figure 42 for more details about the dimensions.
- See the explanation given in the first paragraph of the Appendix Q.

Since the value that has been calculated above has a small difference in regards to the value that has been obtained by Han (2013) (see Appendix J; table D.1 in the column showing the variable), which was $\widehat{\sigma}_{x,iso}\left(\frac{span}{2},\frac{t}{2}\right) = 670.63\ \text{MPa}$, then this last value will be applied because all the fatigue testing performed on the carbon laminate design was in accordance with that reference value.

The difference found above should be due to the change of the two ultimate load values in Table 1, in regards to the values shown by Han (2013) (see Appendix C, table 2). Also, rounding of the values during calculation could generate a small difference.

Table 15 presents the load values that were applied on each of the specimens that were tested under fatigue conditions.

Equation (164) from Appendix P will be applied again, but, in order to obtain P_z through the maximum bending stress calculated by Han (2013) and shown in Appendix J; table D.1, in the column showing the variable σ.

For:

$$\begin{cases} \hat{\sigma}_{x,iso}\left(\frac{span}{2},\frac{t}{2}\right) = 670.63\ \text{MPa} \\ \text{span} = 14\text{mm} \end{cases}$$

and applying the equation (164) from Appendix P, the value shown in Table 15, in the column titled: *initial load input on the rig*, will be equal to:

$$P_z = \frac{2 \times \hat{\sigma}_{x,iso}\left(\frac{span}{2},\frac{t}{2}\right) \times b \times t^2}{3 \times span} \times \text{Percentage to be applied}$$

As a result, the values in Table 15 are presented.

Table 15- Initial set up of the rig - All Carbon Design

Specimen	Percentage of Ultimate Load to be applied on the experiment	Initial Load Input on the Rig (N)	Thickness (from Appendix J; table D.1) (mm)	Width (from Appendix J; table D.1) (mm)	Length (from Appendix J; table D.1) (mm)
13	90%	2255.51	3.37	6.91	18.09
17	90%	2242.64	3.38	6.83	18.64
18	90%	2361.06	3.35	7.32	18.40
20	80%	1917.68	3.32	6.81	18.74
24	80%	1943.71	3.34	6.82	18.29
5L	80%	2104.45	3.35	7.34	26.03
1L	70%	1819.48	3.33	7.34	26.54
2L	70%	1831.87	3.33	7.39	26.50
6L	70%	1788.03	3.34	7.17	25.81

Regarding Table 15, the values shown in the column titled *initial load input on the rig* are the values that have been used to set up the rig before commencing the fatigue tests. The output load during the fatigue test will vary from the load used to set up the rig depending on the control type used during rig set up (displacement or loading control).

ii. Fatigue Experiment Results

Table 16 below shows the results obtained from the fatigue experiment (Han 2013).

As explained in section 5.3, sub-section i, the load output given by the rig computer (*load applied by the rig over the specimen*) is a little different to the load that has been used to set up the machine (see note below Table 15).

The results presented in Table 16 in column: *Maximum ISS at failure*, are the values obtained by the application of equation number (97), from Chapter 2.

For a carbon ply thickness equal to 0.139mm (according to Han (2013) (see Appendix I the table 3.4)), the results will be:

Table 16- Fatigue results - All Carbon Design

Specimen	Control type set up in the rig	Load applied by the rig over the specimen (N)	Peak Load per unit width (N/mm)	Number of cycles run	Maximum ISS at failure $\left(\tau_{xz}{}_{j=\frac{24}{2}}\right)$
18	Displacement	2210	301.91	279	68.92
17	Displacement	2045	299.41	319	68.35
13	Displacement	2055	297.39	134	67.89
5L	Load	2100	286.10	915	65.31
24	Load	1950	285.92	492	65.27
20	Displacement	1775	260.64	1095	59.50
6L	Load	1800	251.05	6967	57.31
1L	Load	1800	245.23	1140	55.98
2L	Load	1800	243.57	9500	55.60

As stated by Han (2013), "the peak loads of the specimen tests that were performed under displacement control were the average peak load during the test", because, when the test rig is set up to a displacement control type, the machine will vary the load in function of an imposed displacement, which is in the *z* direction of the laminate system axis.

iii. S-N curve for the *All Carbon Design*

As the failure has been considered a matrix dominated property, the S-N curve will be based on the maximum interlaminar shear stress (max ISS) as a function of the number of cycles, because the max ISS interacts directly on the interface between the two plies located at the middle of the composite laminate, which for a 24 ply laminate will be the interface between plies number 12 and 13.

Since there are not enough values to build an exact S-N curve, the following assumption was considered:

The endurance, S_e , which is the lower limit of the S-N curve (see as an example the Figure 99 shown in Appendix R), will be considered as achieved after 10^9 cycles have been completed.
Below this limit of the S-N curve, the composite laminate will have an infinite life (known as on-condition part), under the mode of testing that is being submitted.

According to the assumption given above and applying equation (176) from Appendix R. The constants of the equation: S_e, A', B and C were chosen in order to best fit the four parameter Weibull's curve (given by equation (176) from Appendix R) in between all the points that are placed individually on the plot (see the demonstration given in Appendix R). In order to do this arbitrary values were attributed to the constants of the equation (A',B and C) until a curve was seen that best fits all the points and an acceptable value for the variance given by equation (181) from Appendix R is achieved (this should be as close as zero as possible). A best fit curve was thus achieved.

The variables of the equation are:

$$\begin{cases} S_e = 25\ MPa \\ A' = 0.33 \\ B = 600 \\ C = 430 \\ \text{variance} = 0.0657 \end{cases}$$

Note: - An explanation of the *variance* is given in Appendix R.

- In order achieve a more accurate SN curve below 100 cycles and above 10^4 cycles (dashed part of the curve shown in Figure 68), many more fatigue data points would be required. However, Figure 68 gives a good visualization of the fatigue characteristic of the composite laminate.

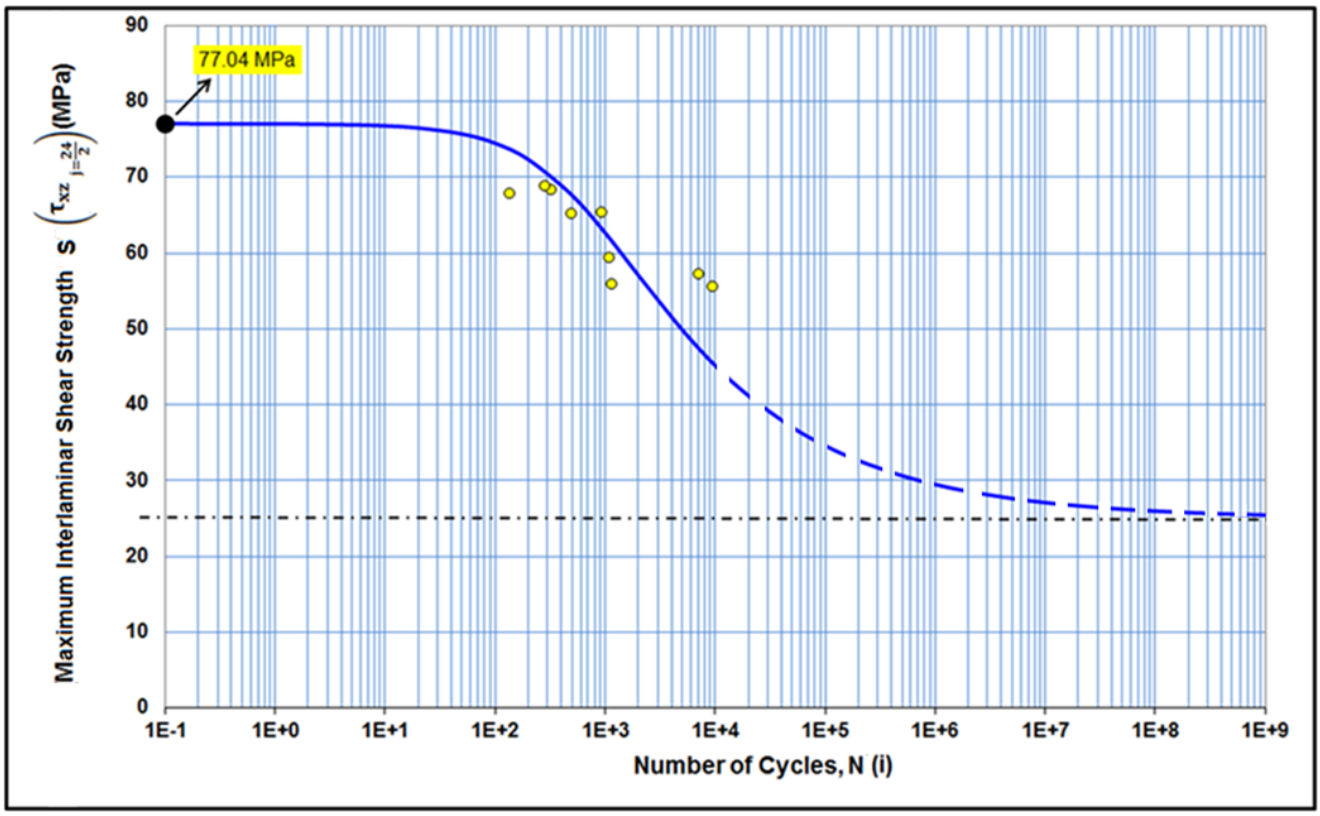

Figure 68- S/N curve for *All Carbon Design* $[(\mathbf{0/45/90/-45})_3]_s$

The yellow points shown on the Figure 68 are the coordinates of each of the specimens shown in Table 16, while the black point represents the fatigue static point on the S-N curve which is equal to the maximum value of the static ILSS τ_{xz} given in Table 4.

The plot related to the load per unit width function of the number of cycles was not created in this chapter, because, the composite laminates have different types of materials (glass and carbon plies), and also, different cross section areas. So, the ILSS τ_{xz} as a function of the number of cycles gives a better material definition in terms of fatigue rather than the load as a function of the number of cycles.

Due to the lack of fatigue data points, the discussion and conclusions that are given in section 5.5 are mainly based on the results given in Table 19.

iv. CT scan assessment for *All Carbon Design*

A CT Scan has been created on one of the nine specimens that were tested in fatigue. As has been described by Han (2013) (Appendix L of this thesis), the fatigue test that has been performed on specimen number 2L (for *All Carbon Design*), was stopped when a audible crack was heard. Specimen 2L, has performed 9500 cycles for nearly 70% of the ultimate static load obtained for the *All Carbon Design* (see section 4.2.1 for more details about the static test that has been performed). Figure 69 shows an image obtained from the CT scan assessment that has been assessed at Bath University.

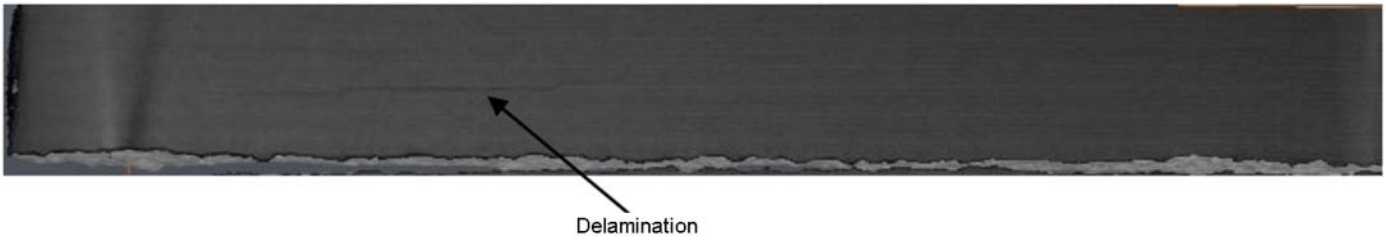

Figure 69 - Front view of specimen 2L of *All Carbon Design*. Image taken from Han (2013) after failure has occurred.

Figure 69 shows a delamination with an extension that goes from the middle of the specimen up to the left position where the support roller is located, which is close to the left side of the image. On the next pages more images are presented that were taken from the CT scan assessment.

The CT scan has been performed with a *Nikon XT H 225ST Micro CT system* machine running Nikon's own software named *CT inspect X*. *CT Pro 3D* software was used to capture images of the sample within the machine (*Nikon XT H 225ST Micro CT system*). Each image was taken through the x-ray technology used by the Nikon machine. After the CT scan process, the 3-D model of the laminate (*sample*) obtained was assessed with the *Avizo Fire software*. Several cross-sections with a distance from each other equal to one ply thickness has been made through the *Avizo Fire software*. These cross-sections have been made through the plane perpendicular to the *x* axis and through the plane perpendicular to the *z* axis. Each of the cross-sections that has been made was required to show the internal pattern of the laminate after the fatigue test has been performed.

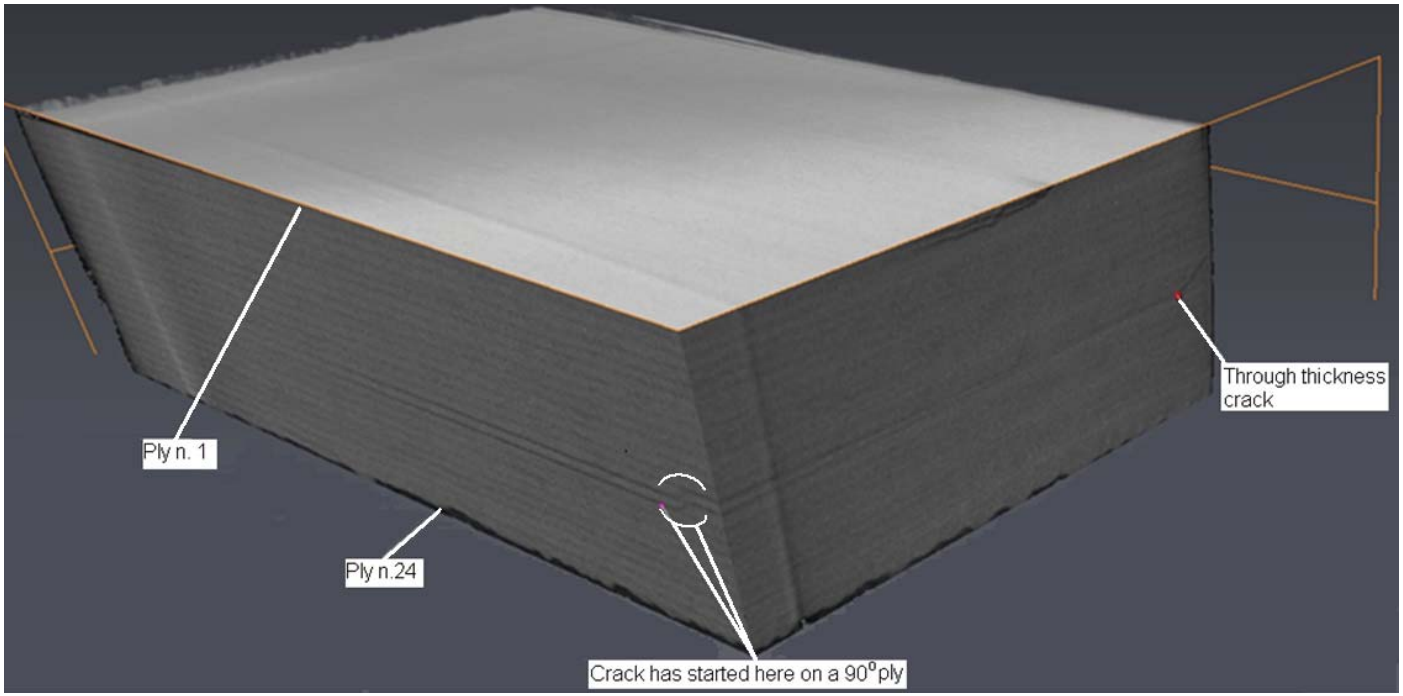

Figure 70 - Crack initiation and crack propagation

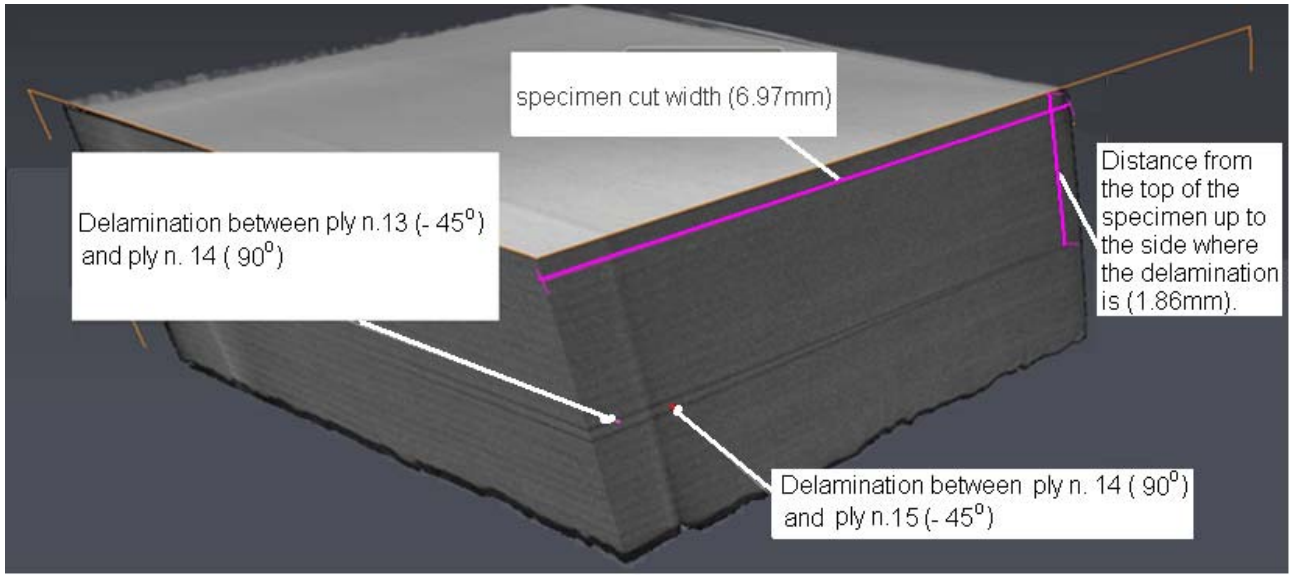

Figure 71 - Delaminations on the *All Carbon Design*

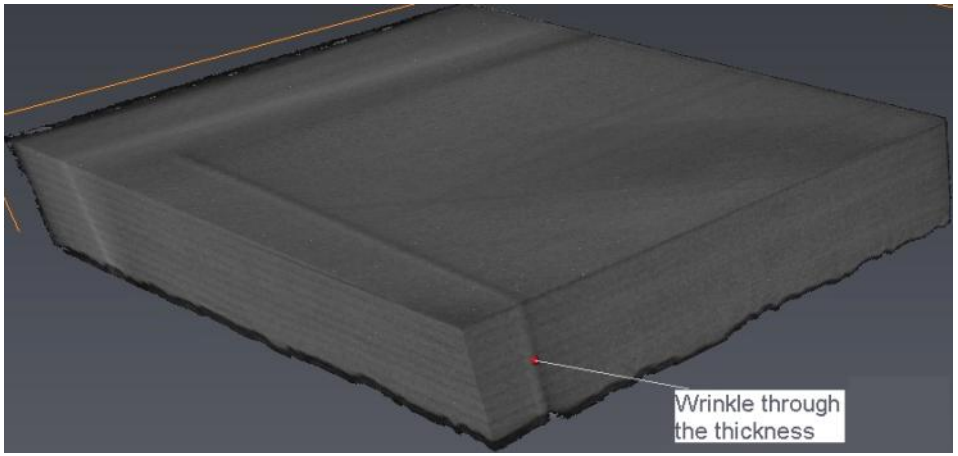

Figure 72 - Internal wrinkle (laminate defect) found in the *All Carbon Design*

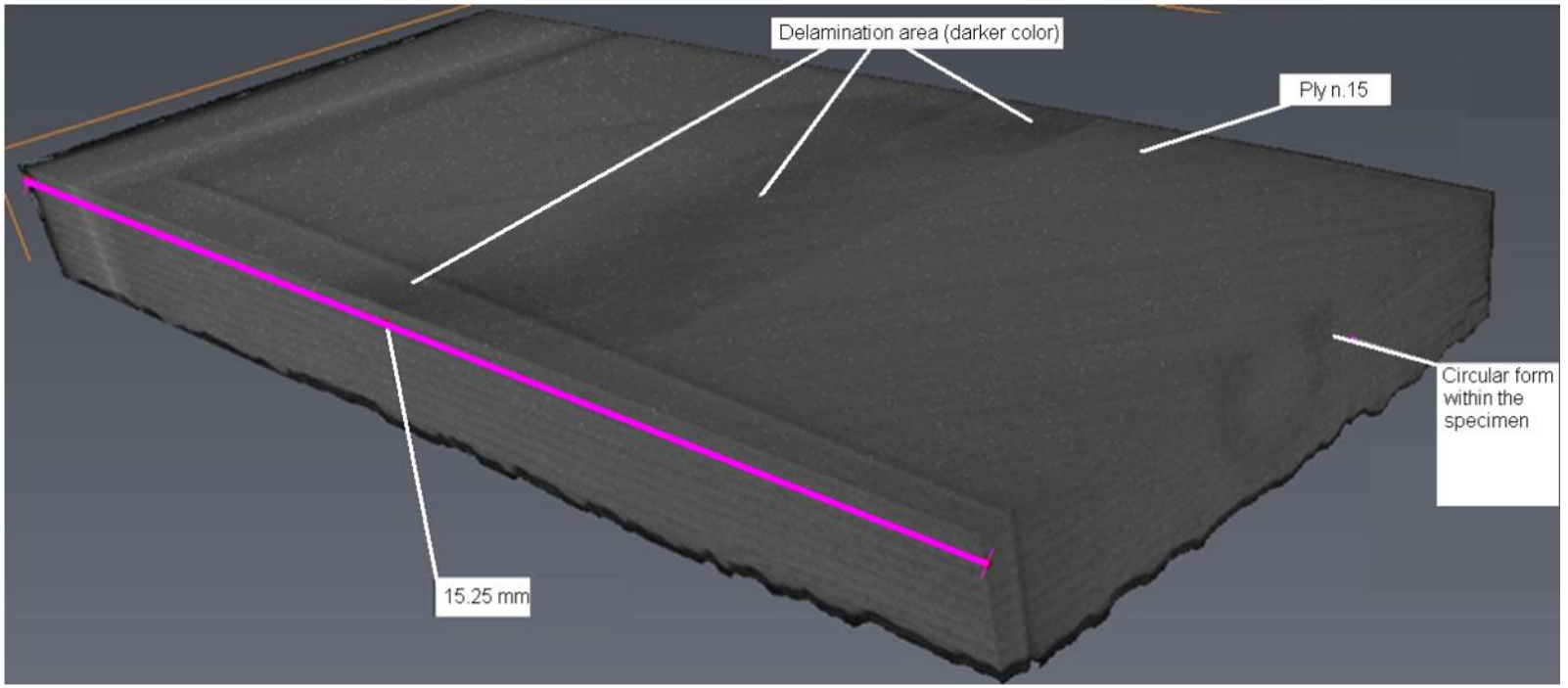

Figure 73 - Circular form found within the carbon laminate

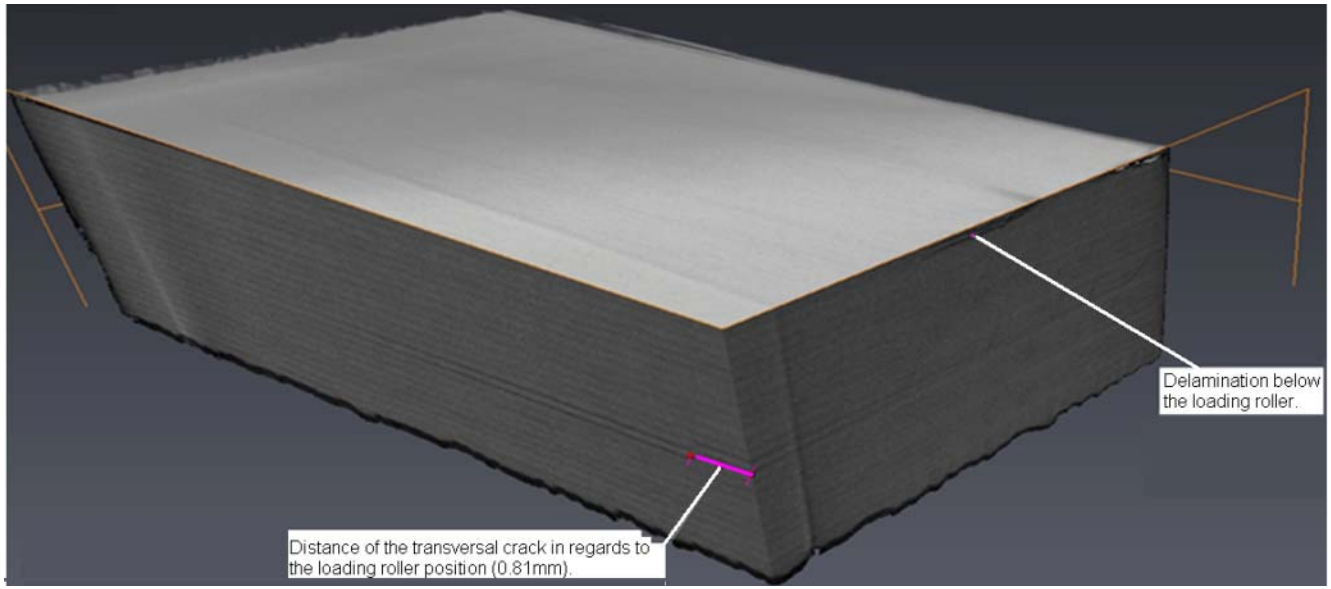

Figure 74 - Delamination underneath the loading roller

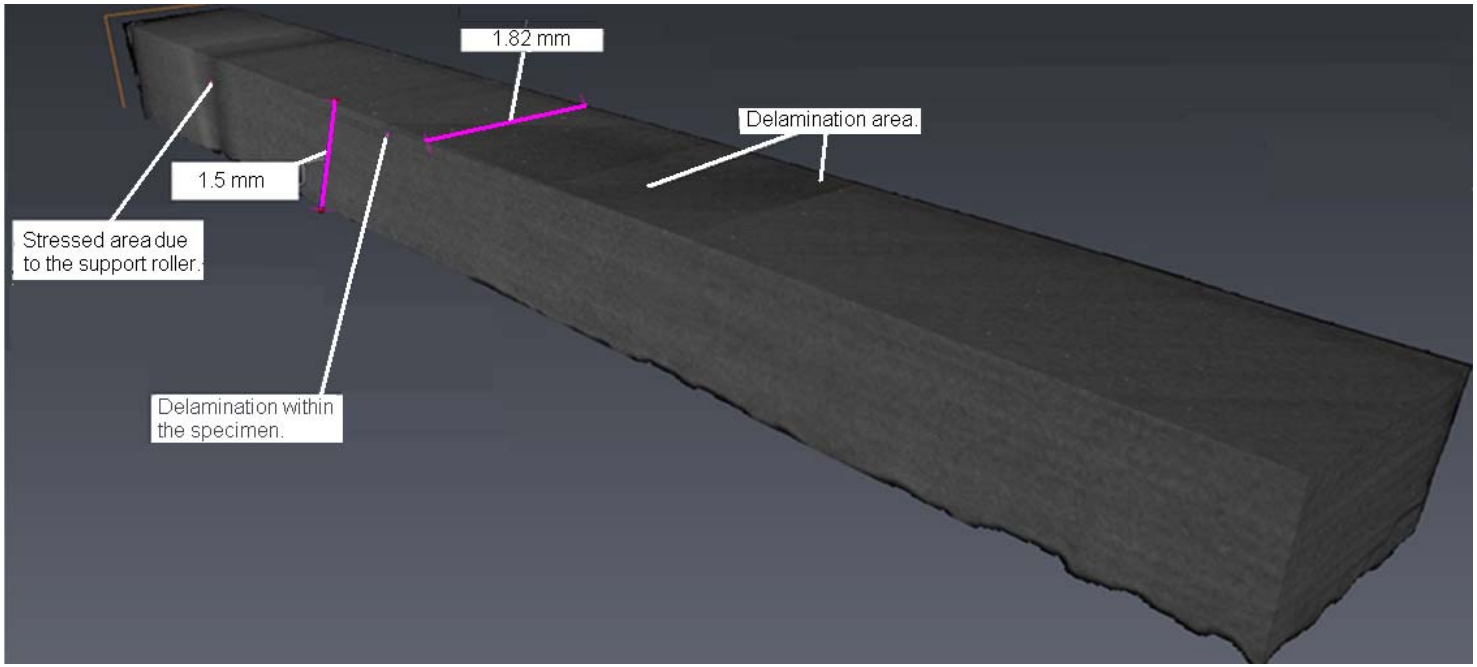

Figure 75 - Delamination on the upper surface of the cut specimen located at 1.5 mm from the bottom surface of the composite laminate. Delamination represented by a darker color.

v. Loading Roller

Figure 76 shows the effect that the loading roller had during the fatigue testing of the carbon laminate number 2L.

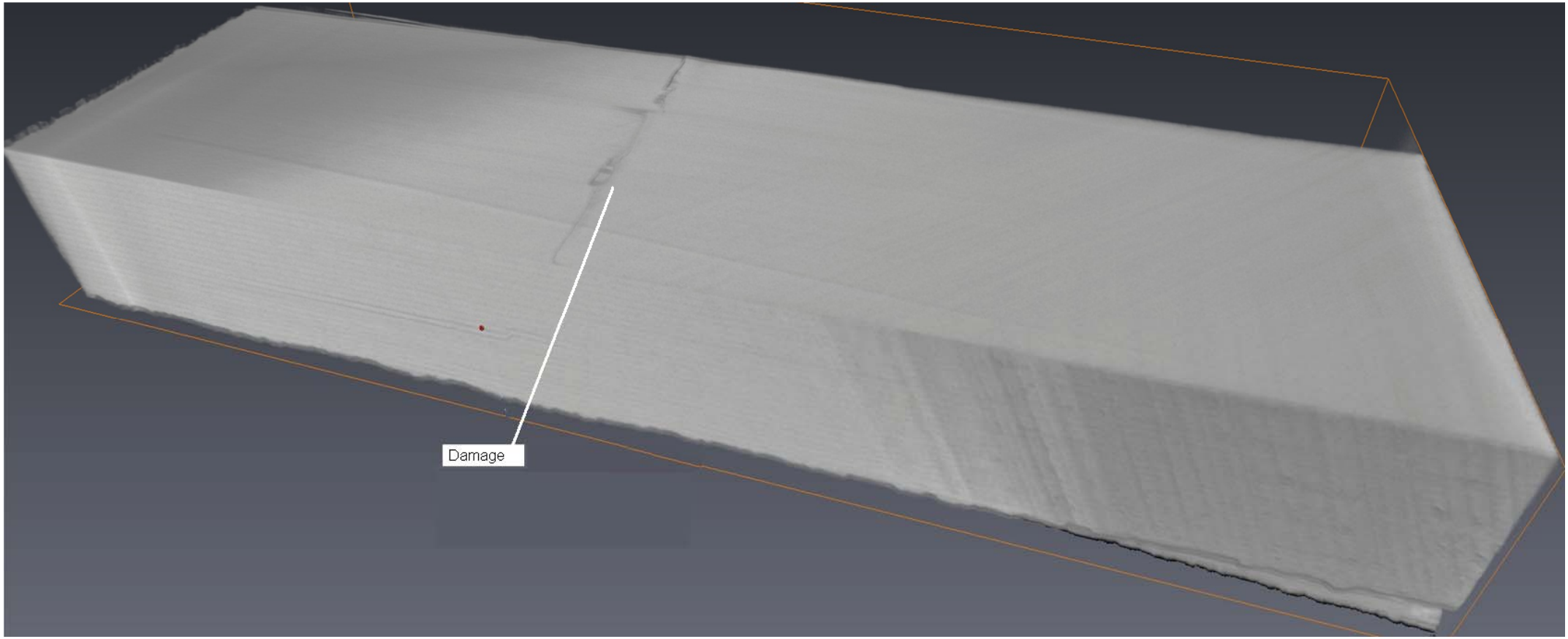

Figure 76 - Loading roller damage – All Carbon Design laminate. Note: This figure shows the part which has been cut at the left hand side of the image. The visible damage caused by the roller, labelled above, is in the centre of the part despite the 3D perspective of this image.

5.4. HYBRID DESIGN 1 - WITH $\theta_{max} = |\pm 45^o|$ - FATIGUE TEST RESULTS

Similarly to what has been done in the previous section (5.3), this section will present the results and loads applied on each of the specimens that have been tested under a fatigue condition of SBS test in accordance with the standard ASTM D2344/2344M (2006).

i. Hybrid Design 1 - Rig Input Load

The procedures that have been considered on the section 5.3, sub-section i, have been applied on this section too.
The average of the thickness, width, and ultimate load of the specimens, obtained from the static test (shown in Table 2 of section 4.2.2, chapter 4), will be applied in the equation (164) from Appendix P.

As a result, by using the equation (164) from Appendix P the maximum bending stress average will be:

$$\hat{\sigma}_{x,iso}\left(\frac{span}{2},\frac{t}{2}\right) = 683.78\ \text{MPa}$$

In which :

$$\begin{cases} \text{span} = 14\text{mm} \\ \text{b} = \text{width average from Table 2} = 6.92\ \text{mm} \\ \text{t} = \text{thickness average from Table 2} = 3.37\ \text{mm} \\ P_z = 2558.95\ \text{N (load average from Table 2)} \end{cases}$$

Note: See Figure 42 for more details about the dimensions.

According to table D.2 of Appendix J (see the column showing the variable σ), the value presented for the maximum bending stress average was: $\hat{\sigma}_{x,iso}\left(\frac{span}{2},\frac{t}{2}\right) = 679.11\ \text{MPa}$ for the static test that has been performed on the *Hybrid Design 1*, since that value has a small difference in regards to the value that has been obtained previously (683.78 MPa), then, the value used by Han (2013) will be applied, because, all the fatigue testing was performed in accordance with that reference value.

Table 17 presents the load values that were applied on each of the specimens that were tested under fatigue conditions.

In order to obtain P_z as a function of the maximum bending stress, equation (164) from Appendix P will be applied again.

Therefore, for:

$$\begin{cases} \hat{\sigma}_{x,iso}\left(\frac{span}{2}, \frac{t}{2}\right) = 685.15 \text{ MPa} \\ \text{span} = 14\text{mm} \end{cases}$$

Applying equation (164) from Appendix P, and according to Han (2013), the value shown in the column titled: *Initial load inputted on the rig* of Table 17 below:

$$P_z = \frac{2 \times \hat{\sigma}_{x,iso}\left(\frac{span}{2}, \frac{t}{2}\right) \times b \times t^2}{3 \times span} \times \text{Percentage to be applied}$$

As a result, the Table 17 is presented.

Table 17- Initial set up of the rig - Hybrid Design 1 with $\theta_{max} = |\pm 45^o|$

Specimen	Percentage of Ultimate Load to be applied on the experiment	Initial Load input on the rig (N)	Thickness (from Appendix J; table D.2) (mm)	Width (from Appendix J; table D.2) (mm)	Length (from Appendix J; table D.2) (mm)
4	90%	2602.11	3.39	6.94	17.71
6	90%	2575.99	3.40	6.83	17.99
11	90%	2432.47	3.28	6.93	18.41
15	80%	2552.57	3.36	6.93	18.27
16	80%	2549.26	3.37	6.88	18.26
5L	80%	2394.19	3.36	6.50	25.39
1L	70%	2362.78	3.31	6.61	24.41
2L	70%	2870.82	3.46	7.35	25.14
6L	70%	2788.45	3.41	7.35	24.91

Regarding Table 17, the values shown in the column titled *initial load input on the rig*, are the values that have been used to set up the rig before commencing the fatigue tests. As was explained previously in section 5.3, after the test has started, and depending on which kind of control type has been set up (see the comment shown underneath the Table 16), the output load during the fatigue test will be a little different than the load used to set up the rig before the commencing the test, due to rig compliance.

ii. Fatigue Experiment Results

The fatigue experiment results are shown in Table 18. The load output given by the rig computer entitled: *Load applied by the rig over the specimen*, will have a small difference in regards to the loads that have been used to set up the machine, due to the explanation given in section 5.4, sub-section i. The results presented in Table 18 in the column: *Maximum ISS at failure*, are the values obtained by the application of equation number (97), from Chapter 2.

Table 18- Fatigue results - Hybrid Design 1 with $\theta_{max} = |\pm 45^o|$

Specimen	Control type set up in the rig	Load applied by the rig over the specimen (N)	Peak Load per unit width (N/mm)	Number of cycles run	Maximum ISS at failure $\left(\tau_{xz}{}_{j=\frac{24}{2}}\right)$
6	Displacement	2240	327.96	130	64.78
4	Displacement	2170	312.68	99	61.76
16	Load	2000	290.70	1050	57.42
15	Load	2000	288.60	1700	57.01
11	Load	2000	288.60	73	57.01
5L	Load	1900	292.31	537	57.74
2L	Load	1950	265.31	13722	52.40
6L	Load	1900	258.50	6788	51.60
1L	Load	1600	242.06	19820	47.81

As referred by Han (2013): "The peak loads of the specimens that were tested under displacement control were the average peak load during the test".

iii. S-N curve for the *Hybrid Design 1* with $\theta_{max} = |\pm 45^o|$

Similarly to the S-N curve built in section 5.3, sub-section iii, the fatigue plot will be based on the maximum interlaminar shear stress (max ISS) as a function of the number of cycles, because the max ISS interacts directly on the interface between the two middle plies (ply number 12 and 13).

According to the assumptions explained in section 5.3, sub-section iii, and, applying equation (176) from Appendix R for the variable values as is shown below, the S-N curve has been built for the hybrid *Design1*.

The variables of the equation are:

$$\begin{cases} S_e = 43\ MPa \\ A' = 0.35 \\ B = 100 \\ C = 154 \\ \text{variance} = 0.1551 \end{cases}$$

The constants of the equation: S_e, A', B and C were chosen in order to achieve the best fit to the four parameter Weibull's curve (given by equation (176) from Appendix R). In order to do this, arbitrary values were attributed to the constants of the equation until a best fit curve was achieved and a variance (equation (181) from Appendix R) near to zero was achieved.

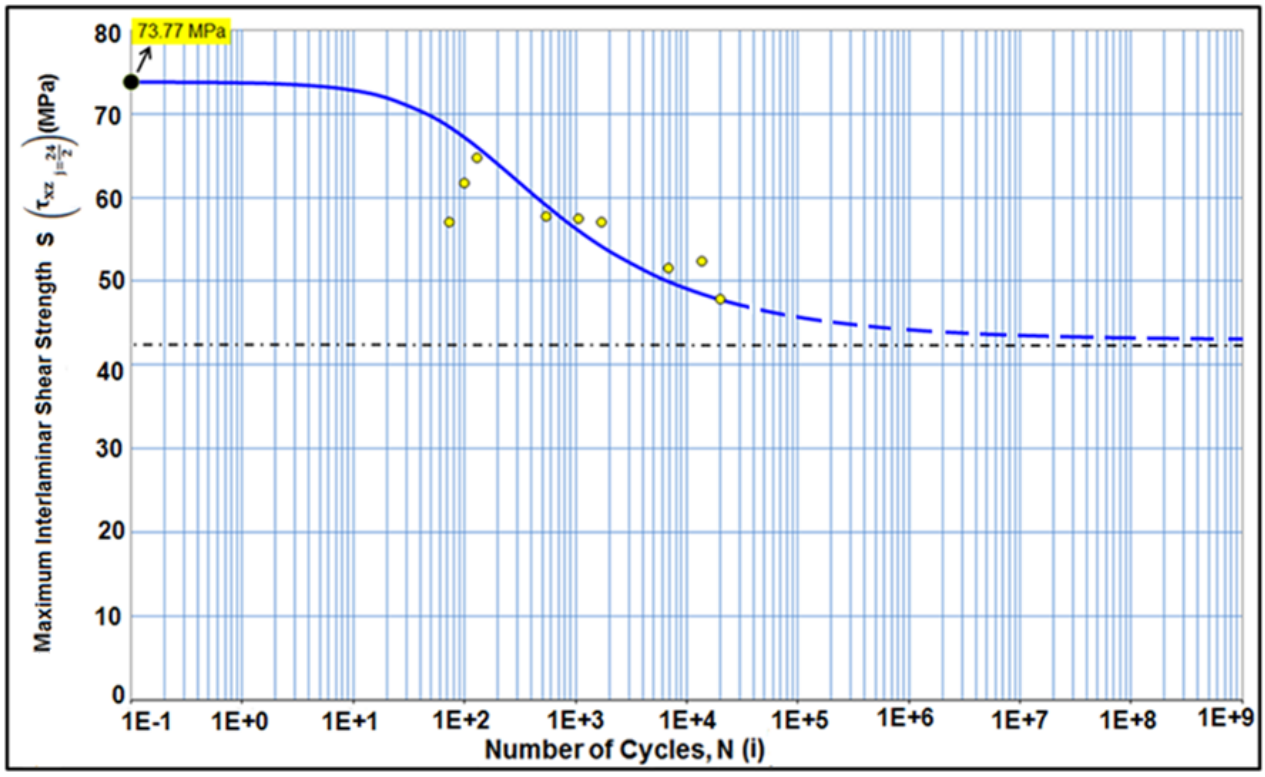

Figure 77- S/N curve for *Hybrid Design 1* $\left[(0_c)_2/(\pm 45_C)_2/(\pm 45_g)_2/(\pm 45_C)\right]_s$

Note: In order achieve a more accurate SN curve below 100 cycles and above 10^4 cycles (dashed part of the curve shown in Figure 77), many more fatigue data points would be required. However, Figure 77 gives a good visualization of the fatigue characteristic of the composite laminate.

The yellow points shown on the Figure 77 are the coordinates of each of the specimens shown on Table 18, while the black point represents the fatigue static point on the S-N curve which is equal to the maximum value of the static ILSS τ_{xz} given in Table 8.

iv. CT scan Assessment for *Hybrid Design 1*

A CT Scan has been performed on one of the nine specimens that has run a fatigue test.

As has been described by Han (2013) (Appendix L of this thesis), the fatigue test that has been performed on the specimen number 1L (for *Hybrid Design 1*), was stopped when an audible crack was heard. The composite laminate number 1L, has performed 19 820 cycles for nearly 70% of the ultimate static load obtained for the *Hybrid Design 1* (see section 4.2.2 for more details about the static test that has been performed).

Figure 78 shows an image obtained from the CT scan assessment that has been done at the University of Bath.

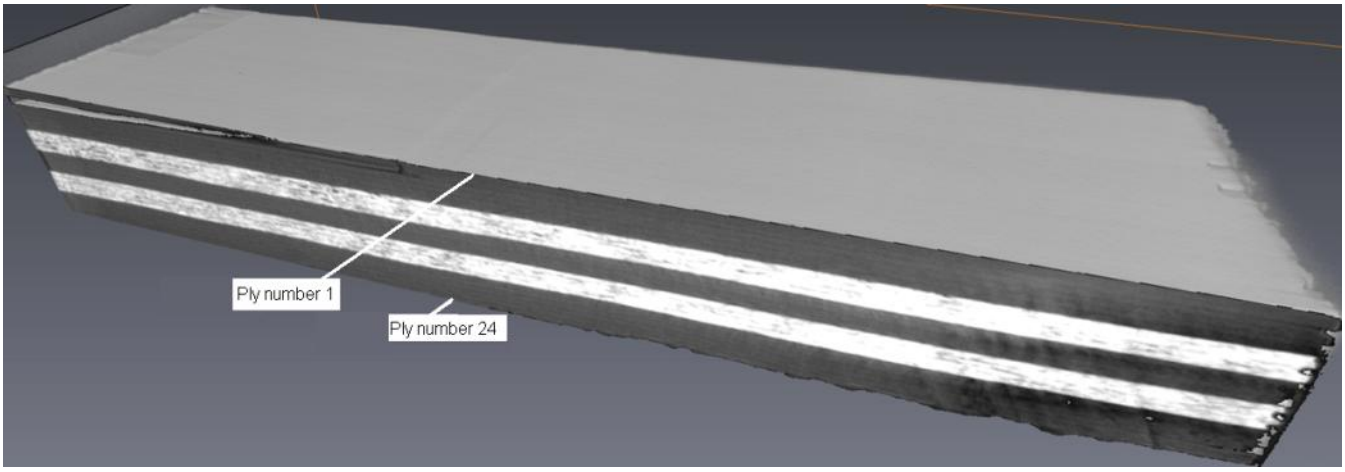

Figure 78 - 3D view of the composite laminate n. 1L; *Hybrid Design 1*.

Figure 78 shows a delamination that extends from the left side of the specimen up to the middle position, underneath the loading roller. As can be seen on the image, the delamination has begun in the compression region of the laminate that was submitted to a fatigue testing under a SBS test condition. A detailed assessment that has been done on the next images, indicates, that the crack has started at the left side of the specimen, due to this, it is likely that the crack initiation has begun due to free edge stress. The next pages show more images that were taken from the CT scan assessment.

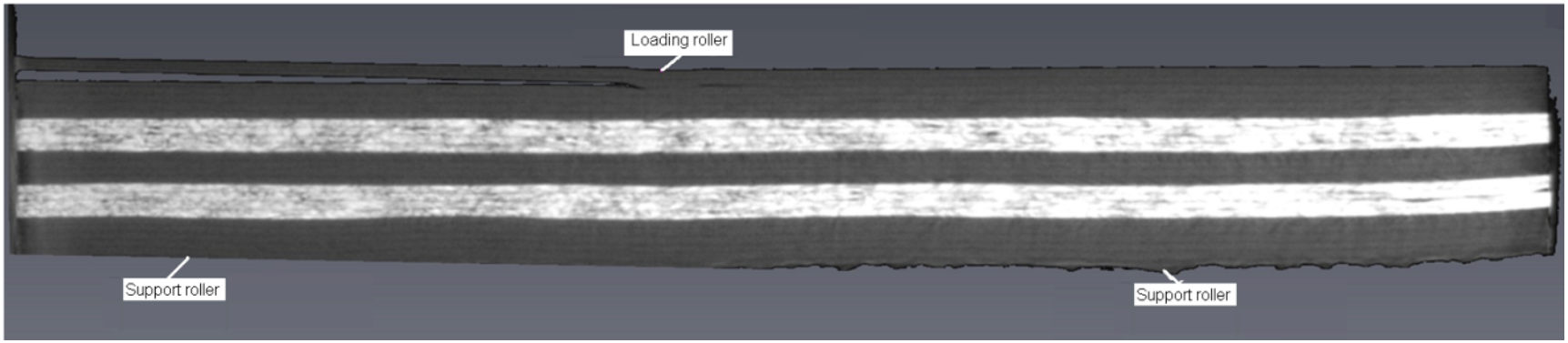

Figure 79 - Rollers Position.
Note: The loading roller shown on the image is in the centre of the part. This figure shows the part which has been cut at the left hand side of the image.

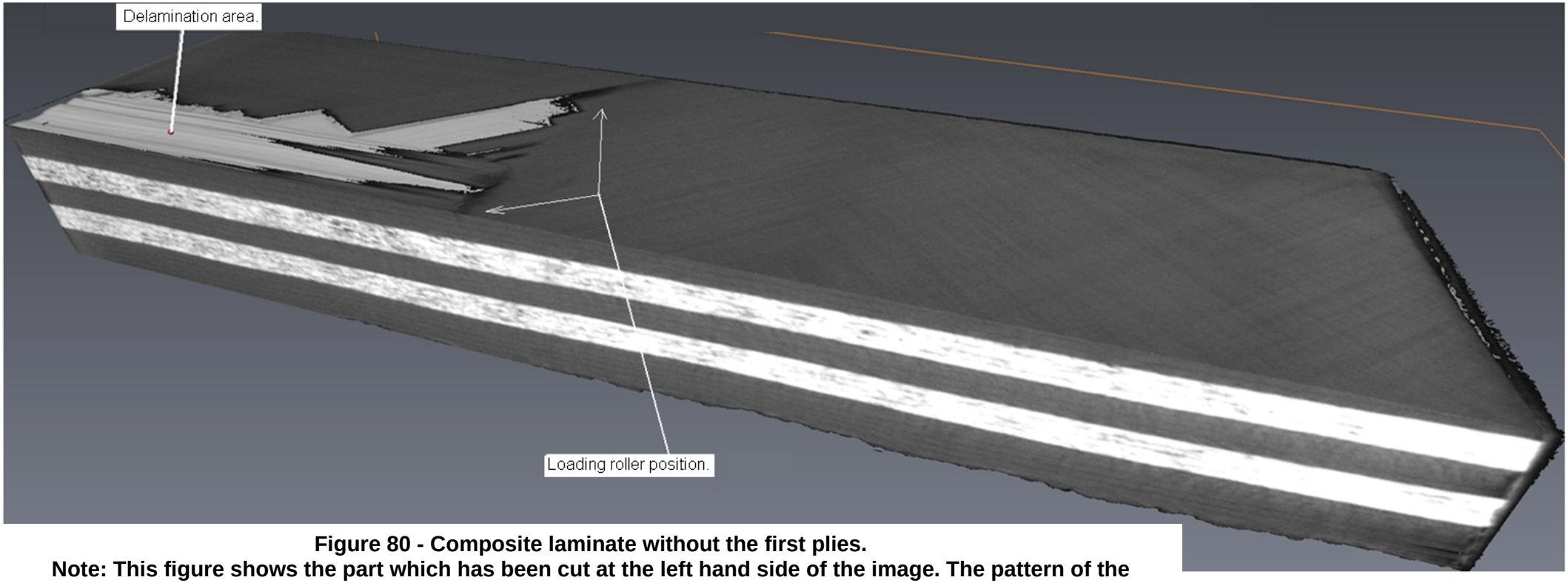

Figure 80 - Composite laminate without the first plies.
Note: This figure shows the part which has been cut at the left hand side of the image. The pattern of the delamination indicates that it could have started at the left edge of the composite laminate. The delamination presented in between the 2nd and 3rd ply, and it has propagated up to the 4th ply.

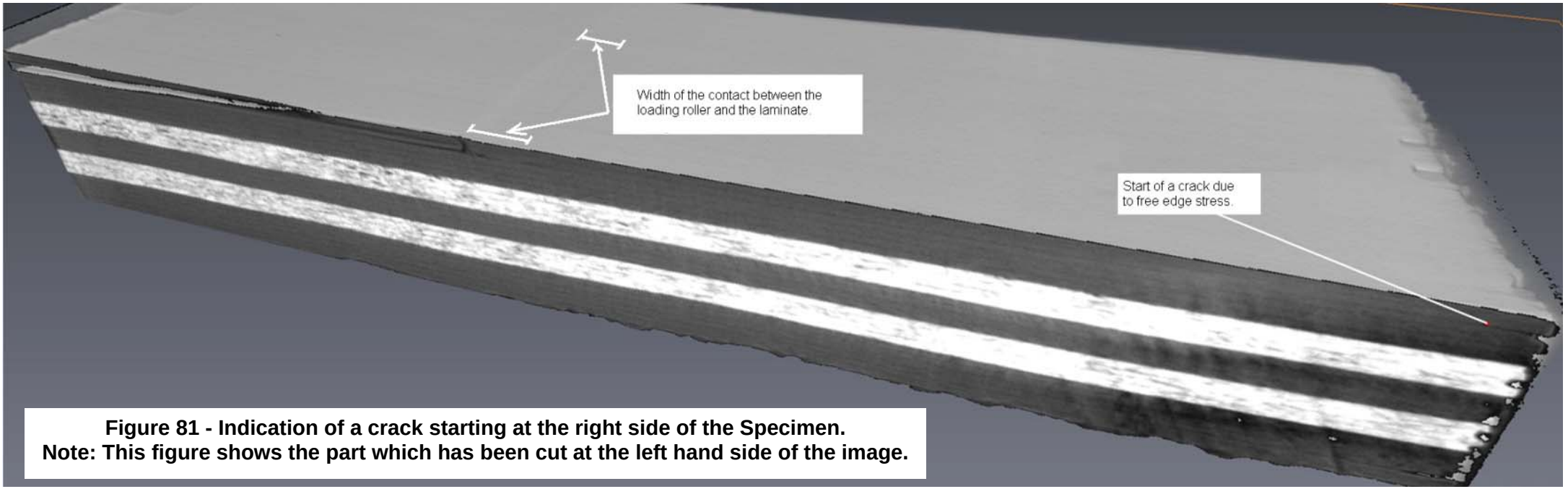

Figure 81 - Indication of a crack starting at the right side of the Specimen.
Note: This figure shows the part which has been cut at the left hand side of the image.

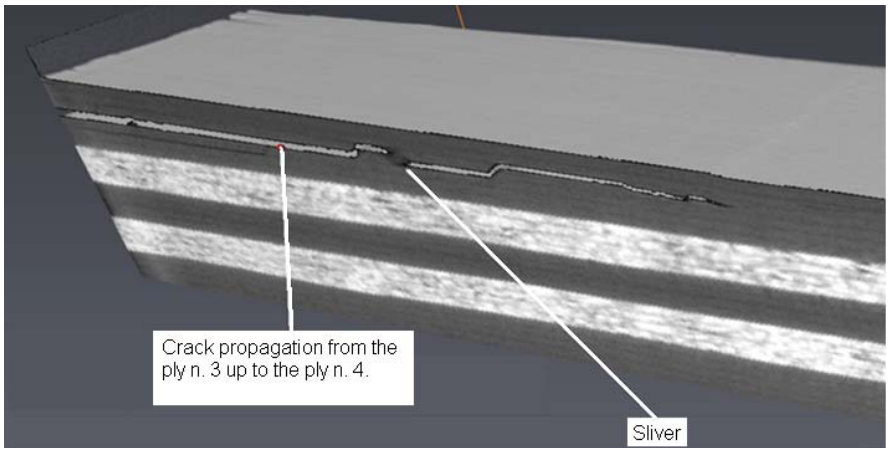

Figure 82 - Delamination that occurred at the left hand of the specimen. Part of the ply is still attached to the upper side of the laminate. This indicates that the delamination has begun at the left edge of the specimen, because the direction of the sliver is for an opening from the left to the right.

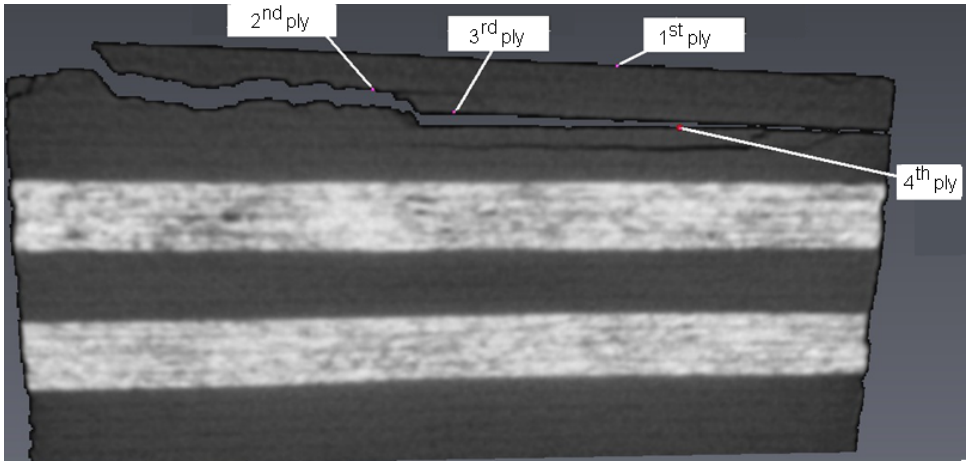

Figure 83 - Cross section of the laminate near to the left edge of the specimen.

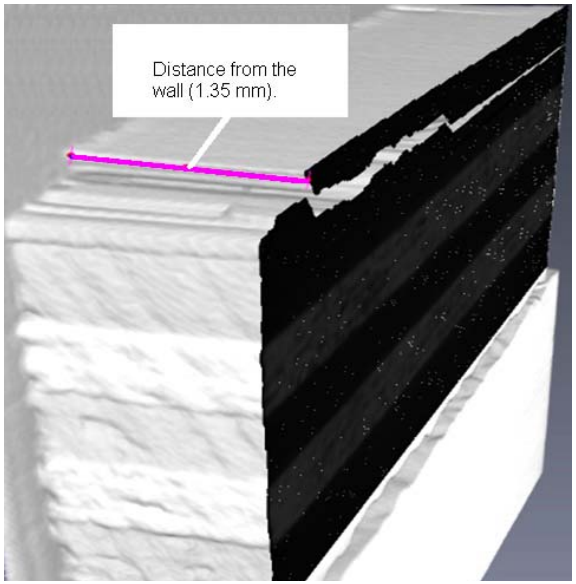

Figure 84 - Cut view of the Design 1 specimen n. 1L.

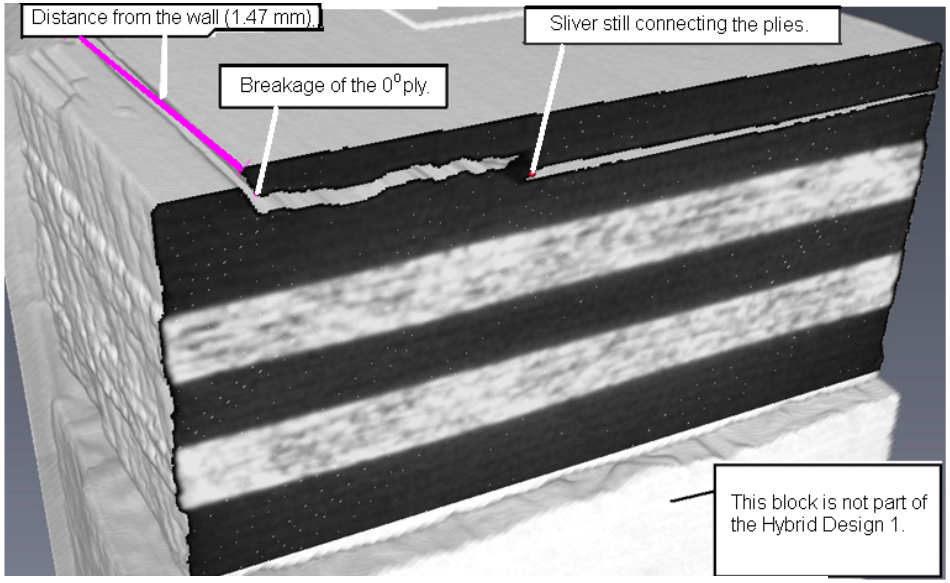

Figure 85 - Transverse cut on specimen n. 1L.

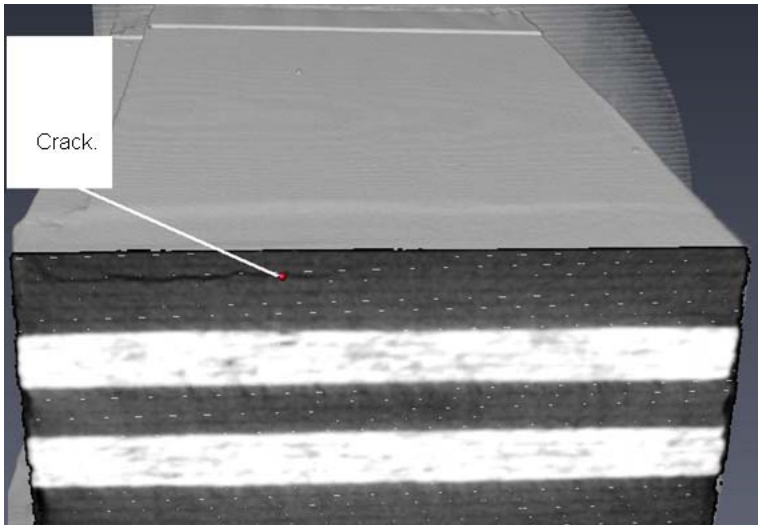

Figure 86 - Loading roller middle position. Image showing the crack underneath the position in where the loading roller was.

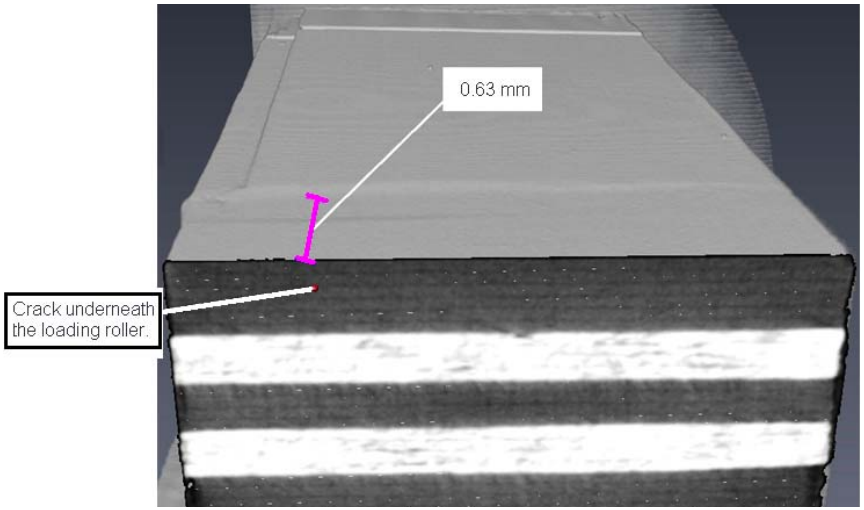

Figure 87 - 0.63mm from the loading roller middle position. Crack that was underneath the loading roller and that cames from the left side of the specimen have stopped after 0.63 mm from the loading roller position, in the direction of the right support roller.

v. Loading Roller

The Figure 88 and Figure 89, show the effect that the loading roller had during the fatigue testing of the Hybrid Design 1 :

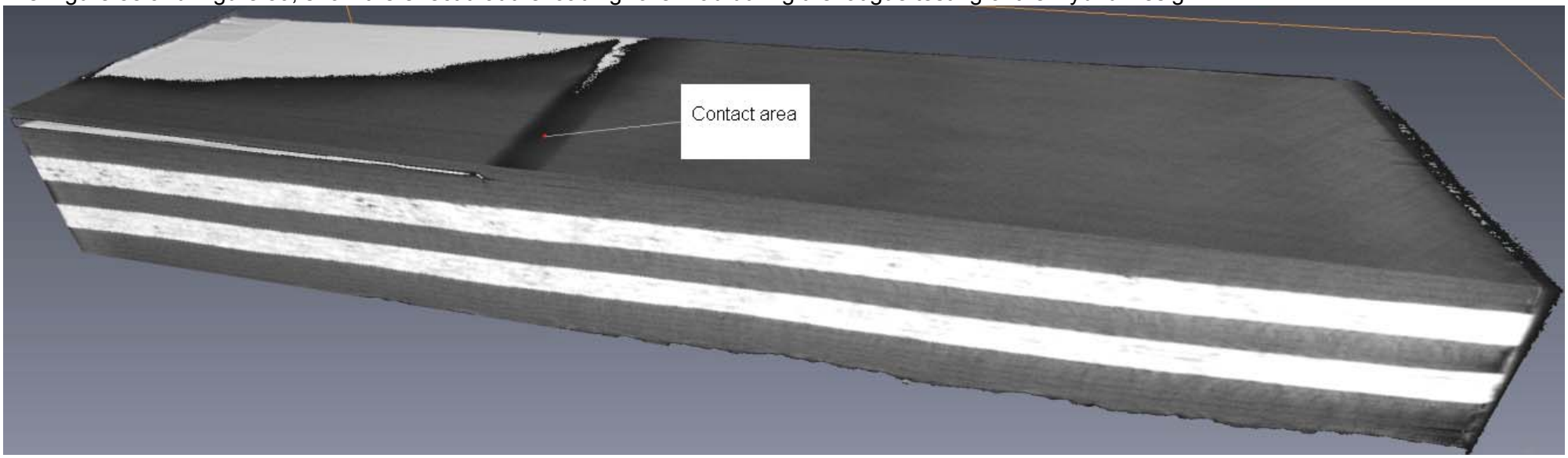

Figure 88 - Contact area between the loading roller and the upper surface of Hybrid Design 1 (removed part of the first ply). Note: This figure shows the part which has been cut at the left hand side of the image.

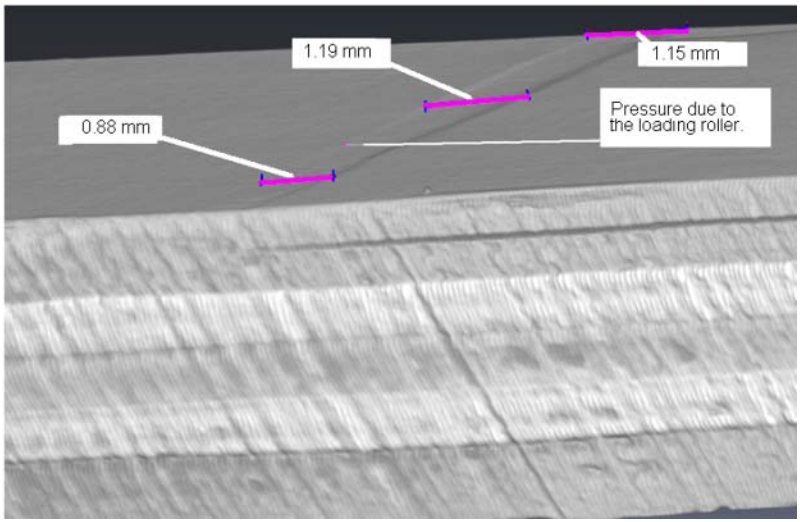

Figure 89 - Dimensions of the contact area - Hybrid Design 1.

5.5. DISCUSSION AND CONCLUSIONS - FATIGUE TEST

From the results that have been shown in the previous sections 5.3 and 5.4, in the Table 16 and Table 18, the table shown below (Table 19) was created with average values.

Table 19- Fatigue results - *All Carbon Design* Vs *Hybrid Design 1*

DESIGN	Percentage of Ultimate Load applied on the experiment	Control type set up in the rig	Average peak Load per unit width (N/mm)	Average ISS at failure	Average of the number of cycles run
$\left[(\mathbf{0_c})_2/(\pm\mathbf{45_C})_2/(\pm\mathbf{45_g})_2/(\pm\mathbf{45_C})\right]_s$					
Hybrid Design 1	90% (Specimens 4; 6; 11)	Displacement control (2 Specimens) and load control (1 Specimen)	309.74	61.18	100
	80% (Specimens 15; 16; 5L)	Load	277.55	57.39	834
	70% (Specimens 1L; 2L; 6L)	Load	255.29	50.60	13443
$[(\mathbf{0/45/90/-45})_3]_s$					
All Carbon Design	90% (Specimens 13; 17; 18)	Displacement	299.57	68.39	244
	80% (Specimens 20; 24; 5L)	Displacement control (1 Specimens) and load control (2 Specimen)	290.54	63.36	1096
	70% (Specimens 1L; 2L; 6L)	Load	246.67	56.30	5869

As can be seen in the average results shown in Table 19, in general, *Hybrid Design 1* withstood more cycles than the *All Carbon Design* for a percentage of the static ultimate load below 80%. In average, for 70 % of the static ultimate load, the *Hybrid Design 1* can run 7500 cycles more than the *All Carbon Design* for a load per unit width of 10 N above the load applied on the *All carbon design*.

In contrast, for a percentage of the static ultimate load above 80%, *Hybrid Design 1* withstood approximately 200 cycles less than the *All Carbon Design* for an average load per unit width which was almost the same. However, since the Rig was working under a displacement control on most of the specimens that were tested at a value of 90 % of the static load, then, this could have affected the total number of cycles that both specimens could have run, mainly because, for a displacement control, the rig will load the composite laminate under a non monotonic load (variable load), which could have affected the total number of cycles that the specimens could run if the rig was set up to a *load control* (quasi monotonic load). This situation could affect any conclusion taken for the region above the 90% of the ultimate static load.

Figure 90 shows the S/N curve in which both *Hybrid Design 1* and *All Carbon Design* are plotted. The logarithmic plot has been built by combining Figure 68 and Figure 77, and refers to the maximum interlaminar shear strength as a function of the number of cycles. Since there are not enough points on the plot to exactly define which are better in terms of the *endurance* (limit between an on-condition composite laminate and a laminate with a defined life), then, a conclusion could be taken by probability, and through the curves plotted in Figure 90, under the conditions defined in sections 5.3 (sub-section iii) and 5.4 (sub-section iii).

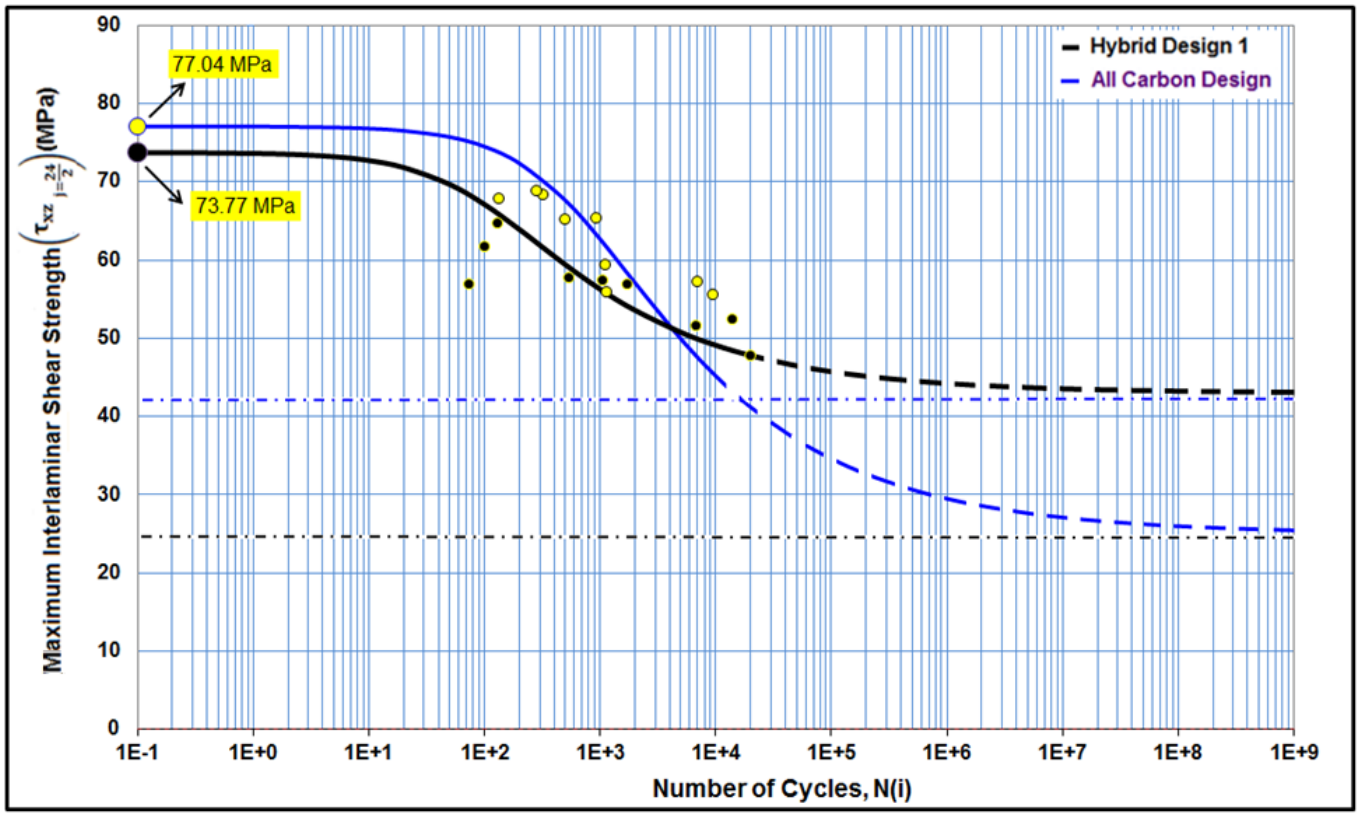

Figure 90 - S/N curve - *All Carbon Design* Vs *Hybrid Design 1*

Note that comparison of load is given in Table 19.

Also, after 10^5 cycles, the *Hybrid Design 1* can run more cycles for a lower ISS than the *All Carbon Design*, which means that, after a determined number of cycles the hybrid design 1 could withstand more load without failure than the carbon design.

Through the assessment that has been done on Figure 78 up to Figure 89, it has been concluded that the *Hybrid Design 1* was not long enough to prevent the failure due to free-edge stress (*Hybrid Design 1* has failed due to free-edge stress), and could withstand more cycles without failure occurring. Since this situation has been noticed on Figure 78 up to Figure 89, this could be a factor in producing an early failure on the remaining hybrid specimens that were tested under fatigue conditions. The free edge stress concentration was mainly due to the transition of the stiffness in the principal direction between the 0^0 ply and 45^0 ply.

In regards to the *All Carbon Design*, through Figure 69 up to the Figure 75, it has been noticed that the main reason for this design to not withstand more cycles without failure is due to the 90^0 plies that are within the laminate. The images have shown that the failure has happened on the 90^0 ply, in the tensile side of the laminate, nearest to the mid-plane, which means that for a 3PB or SBS test condition there is a negative influence in terms of fatigue when a composite laminate has 90^0 plies within it.

Also, as has been noticed by Han (2013), "*Hybrid Design 1* was more reliable and more stable than *All Carbon Design*". In general the *Hybrid Design 1* has been the best design developed among the three designs.

CONCLUSION

In this research three laminate designs were assessed for static and fatigue interlaminar shear strength (ILSS). These three laminates were the *All Carbon Design* with a stacking sequence $[(0/45/90/-45)_3]_s$, *Hybrid Design 1* with a stacking sequence $\left[(0_C)_2/(\pm45_C)_2/(\pm45_g)_2/(\pm45_C)\right]_s$ and *Hybrid Design 2* with a stacking sequence $\left[(0_c)_2/(\pm45_g)/(90_C)_4/(\pm45_g)/(90_C)_2\right]_s$, from which the last two designs were obtained through an algorithm that has been developed in order to proceed with an optimization of the stacking sequence for ILSS in a composite laminate. Static and fatigue tests were performed by an MSc student (Han 2013) on the three designs in order to validate the analytical results and confirm which of the specimens presents a better static and fatigue behaviour when loaded under a condition of short beam shear (SBS) test.

Through the analysis that has been developed and considering the discussions given during this thesis, it has been concluded that 90^0 plies within a composite laminate loaded in a SBS test condition give rise to an intralaminar failure due to excessive principal stresses. This does not allow the composite laminate to reach an ultimate load value equal or greater to the value verified in the *Hybrid Design 1* which has presented an interlaminar failure due to ILSS during the static test (in accordance with the images taken from the static experiments).

It has been noticed that with the addition of glass plies within a laminate there is a tendency to drive the cracks along the length of the composite component near to the surface of the glass ply, which results in a more stable static failure.

In addition, since *Hybrid Design 2* has presented an average ultimate static load that was much lower that the ultimate static load values obtained for *All Carbon Design* and *Hybrid Design 1*, then the fatigue tests were only performed just the latter two designs.

Through the S-N curves that have been constructed for *Hybrid Design 1* and *All Carbon Design*, it was noticed that for a value below 80% of the ultimate static load, *Hybrid Design 1* can withstand more cycles than the *All Carbon Design* when the same load is applied. It has been noticed that the fatigue failure that occurred in the *All Carbon Design* was in the middle of the laminate due to a combination of principal and shear stresses, while the failure in the *Hybrid Design 1* occurred due to free edge stress (according to the CT scan images), which means that it may be able to withstand even more cycles when edge effects are not present.

In general, the *Hybrid Design 1* laminate has shown to be the best among the three designs. This was due to the absence of 90^0 plies in the layup, which tend to produce an intralaminar failure instead of an interlaminar failure. The use of 90^0

plies within a composite laminate loaded under a SBS or 3PB conditions, produces an intralaminar failure due to principal stresses.

It is concluded that 90^0 plies should be avoided in a design of a composite component which will be submitted to a similar loading condition as the SBS test.

From the laminate design algorithm that has been created in which all possible combinations are considered, it was shown that for an hybrid laminate with a maximum of 40% of glass plies, the best material combination that minimises the damage in the middle of the composite laminate, should have carbon plies (instead of glass plies) in the centre of the laminate.

FUTURE WORK

Optimization software has been developed in this thesis in order to run all the possible material combinations and ply orientations to give the best composite component that minimizes the damage in the middle of the laminate, loaded on a short beam shear (SBS) test (D2344/2344M 2006). The optimization method developed is a function of the through-thickness equation for a 2-D laminate (τ_{xz} equation). Further assessment could be done in order to complement the work that has been performed in this thesis.

A 3-D optimization method in which the entire stress state is considered could be performed on an SBS test, in which will be found the stresses that have a direct influence on the interfaces of a composite laminate. Those stresses are: the stress in the *z* direction (σ_z), the interlaminar shear stress (τ_{xz}) and the bending stress in both *x* and *y* directions of the laminate.

Beyond the loading condition that has been applied in this thesis, there are other types of loading cases that could be studied in order to achieve the same purpose of this thesis. A load case in which torsion, bending and tension are combined, could be interesting work to be developed in future.

The failure criterion according to Tsai-Wu (Tsai & Hahn 1980) has been considered in this research, which did not show to work well on a loading condition of SBS test. Also it was considered the application of the failure criterion according to NLR (Creemers 2010). However, since it was missing the strength values in both directions x-z and y-z of the composite laminate, the criterion was discarded. A future consistent failure criterion for composite laminates is required.

In order to achieve a less expensive algorithm in terms of computation time, a generic algorithm should be considered in future work, also it should include the intraply laminar failure equations (given in Appendix N).

Finally, in parallel to this thesis, a study involving the strain energy in a composite laminate could be considered.

REFERENCES

1. Abaqus, 2010. *Analysis of Composite Materials with Abaqus.* s.l.:Dessault Systemes.
2. Anon., 1994. *Military Handbook (MIL-HDBK-17-3E) - Polymer Matrix Composites, Volume 3.* USA: Department of defence of the United States of America.
3. Anon., 1996. In: *Accelerated Aging of Materials and Structures.* Washington, D.C.: NATIONAL ACADEMY PRESS, p. 24.
4. Anon., 2011. *Reinforced plastics.com.* [Online]
   Available at: http://www.reinforcedplastics.com/view/21336/motorcycle-swingarm-redesigned-in-carbon-composite/
   [Accessed 12 December 2013].
5. Anon., n.d. *Linear Elastic Laminate Plate Problem: NPIB.* [Online]
   Available at: http://www.jwave.vt.edu/crcd/kriz/modules/module05a/start.html
   [Accessed 12 December 2013].
6. Ashton, J., Halpin, J. & Petit, P., 1969, Volume III. *Primer on composite materials analysis.* U.S.A.: TECHNOMIC Publishing Co., Inc.
7. Beng, Y. K., Noor, A. & Dalimin, M. N., 2001. Mode-I Interlaminar Fracture Toughness of Unidirectional Carbon Fibre Epoxy Composite. *Borneo Science data base,* Volume 10, pp. 1-9.
8. BS14130:1998, 2004. Fibre-reinforced plastic composites - Determination of apparent interlaminar shear strength by short-beam method. *BSI*.
9. Budynas, R. G., 1998. *Advanced Strength and Applied Stress Analysis.* 2nd ed. NYC: McGraw Hill Higher Education.
10. Campbell, F., 2010. *Structural Composite Materials.* Ohio: ASM International.
11. Choi, H. J. & Thangjitham, S., 1994. The interlaminar crack-tip response in a fibre-reinforced composite laminate. *International Journal of Fracture,* Volume 66, pp. 121-138.
12. Craig, P. D. & Summerscales, J., 1988. Poisson's Ratios in Glass Fibre Reinforced Plastics. *Composite Structures,* Volume 9, pp. 173-188.
13. Creemers, R., 2010. *Interlaminar shear strength criteria for composites (Report no. NLR-TP-2009-262),* Nederlands: NLR.
14. D2344/2344M, 2006. Standard test method for short-beam strength of polymer matrix composite materials and their laminates. *ASTM International*.
15. Davila, C. G., Camanho, P. P. & Rose, C. A., 2005. Failure Criteria for FRP Laminates. *SAGE,* Volume 39, pp. 323-343.
16. Delaware University, 2005. *CDS LAM 3D.* [Online]
   Available at: http://www.ccm.udel.edu/Tech/Lam3D/Theory.htm
   [Accessed 27 November 2013].
17. DICKSON, R. et al., 1989. Fatigue behaviour of hybrid composites - Part 2. *Journal of Materials Science,* Volume 24, pp. 227-233.

18. Freudenthal, A. M., Weibull, W. & Payne, A., 1963. *First Seminar on Fatigue and Fatigue Design,* New York: Columbia University.

19. German, J., 2004. Intralaminar Damage in fibre-reinforced polymeric matrix laminates. *KWM IMB PK.*

20. Ghiasi, H., Pasini, D. & Lessard, L., 2009. Optimum stacking sequence design of composite materials Part I: Constant stiffness design. *Composite Structures,* 90(1), p. Pages 1–11.

21. Ghugal, Y. M. & Sharma, R., 2011. A refined shear deformation theory for flexure of thick beams. *Latin American Journal of Solids and Structures,* Volume 8, pp. 183-195.

22. CIBA-GEICY, 1983. *Fibredux 913,* s.l.: Information Sheet No. FTA.46d.

23. Halpin, J. C., 1992. *Primer on Composite Materials Analysis.* 2nd ed. Pennsylvania: Technomic Publishing Company, Inc..

24. Han, J., 2013. *Fatigue Testing of Thick Composite Laminates (MSc thesis),* Bath: Bath University.

25. Harris, B., 1999. In: *Engineering Composite Materials.* London: The Institute of Materials.

26. Harris, B., 2003. *Fatigue in composites.* New York: Woodhead Publishing Limited.

27. Hashin, Z., 1980. Failure Criteria for Unidirectional Fiber Composites. *Journal of Applied Mechanics,* Volume 47, pp. 329-334.

28. Hoff, N. J., 1956. *The Analysis of Structures.* New York: John Wiley.

29. Hua, S., 2011. *Functionally sorted laminated material for damage resistance and damage tolerance,* United Kingdom: University of Bath.

30. Jones, R. M., 1975. *Mechanics of Composite Materials.* New York: Hemisphere Publishing Corporation.

31. Jones, R. M., 1999. *Mechanics of Composite Materials.* 2nd ed. Virginia: Taylor & Francis.

32. Kim, R. & Soni, S. R., 1984. Experimental and analytical studies on the onset of delamination in laminated composites. *Journal of Composite Materials,* 18(4), pp. 70-80.

33. Kinawy, M., n.d. *Static and fatigue propagation of buckle-driven delaminations under bending and compressive loads. Thesis (P.H.D.),.* United Kingdom: University of Bath.

34. Makeev, A., Ignatius, C., He, Y. & Shonkwiler, B., 2009. A Test Method for Assessment of Shear Properties for Thick Composites. *Journal of Materials,* Volume 43, pp. 3091-3105.

35. May, M., 2010. *A new model for initiation of damage in composites under fatigue loading for cohesive elements,* Bristol: University of Bristol.

36. Nishimura, A., 2008. Effect of the radius of loading nose and supports in short beam test fixture on fracture mode and interlaminar shear strength of GFRP at 77K. *AIP Proceedings,* Volume 986, pp. 50-59.

37. Niu, M. C. Y., 1996. *Composite Airframe Structure.* Hong Kong: Hong Kong Conmilit Press Ltd.

38. Ogiharaa, S., Takedab, N., Kobayashib, S. & Kobayashia, A., 1999. Effects of stacking sequence on microscopic fatigue damage development in quasi-isotropic CFRP laminates with interlaminar toughened layers. *Elsevier,* Volume 59, pp. 1387-1398.

39. Phillips, L., 1976. The hybrid effect - does it exist?. *Composites,* 7(1), pp. 7-8.

40. Reddy, J., 2004. *Mechanics of laminated composite plates and shells theory and analysis.* 2nd ed. U.S.A.: CRC Press.

41. Schijve, J., 2003. Fatigue of structures and materials in the 20th century and the state of art. *International Journal of Fatigue,* 25(Elsevier), pp. 679-702.

42. Sierakowski, R., 1995. *Damage Tolerance in Advance Composites.* Basel, Switzerland: Technomic.

43. Soutis, C. & Fleck, N., 1990. Static compression failure of carbon fibre T800/924C composite plate with single hole. *Journal of Composite Materials,* Volume 24, pp. 536-558.

44. Timoshenko, S., 1948. *Strength of Materials.* 2nd ed. United States of America: D. Van Nostrand Company Inc..

45. Tsai, S. W. & Hahn, H. T., 1980. *Introduction to composite materials.* USA: Technomic Publishing Company, Inc..

46. Vassilopoulos, A. P. & Keller, T., 2011. *Fatigue of Fiber-reinforced Composites.* London: Springer.

47. Voyiadjis, G. Z. & Woelke, P., 2008. Determination of Transverse Shear Stresses and Delamination in Composite Laminates Using Finite Elements. *Springer Link,* pp. 163-183.

48. Wikipedia, 2009. *Deformation (mechanics).* [Online]
Available at: http://en.wikipedia.org/wiki/File:2D_geometric_strain.svg
[Accessed 30 November 2013].

49. Young, W. C. & Budynas, R. G., 2002. *ROARK'S Formulas for Stress and Strain.* 7th ed. USA: McGraw Hill.

APPENDIX A

TITLE Results obtained from the algorithm for 24 Plies
BEST 100 SOLUTIONS when the variable angle θ in $\pm\theta$ plies is limited in the algorithm to have a maximum value of 45 degrees.

For an input equal to (Just the main variables are shown):

$[\theta_{1_{\min}}; \theta_{1_{\max}}] = [5^{\circ}; 45^{\circ}]$

$[\theta_{2_{\min}}; \theta_{2_{\max}}] = [10^{\circ}; 40^{\circ}]$

$\theta_{\text{increment\_1}} = 5^{\circ}$

$\theta_{\text{increment\_2}} = 10^{\circ}$

$N_{solution} = 100$

$\text{Plies}_{\text{\_n}} = 24$

$\text{Glass}_{\text{ply \%}} = 40\%$

width=6.92 mm

$\text{angles}_{\text{\_n}} = 3$

Without any 90^0 plies and without fix the angles $\boldsymbol{\theta_1}$ and $\boldsymbol{\theta_2}$

Accepted all the materials defaults except for the plies thicknesses which are:
t_{glass}= 0.143 mm and t_{carbon}= 0.139 mm

Load=2559 N

Note: For the tables that will be shown in this appendix: each of those columns represents a single composite laminate. The first column will be the best result found to minimize the damage in the middle of the composite laminate (best τ_{xz}), while the last column will be the worse value in terms of τ_{xz} in between the columns shown. The columns are in a crescent order. See also Appendix T for further information.

- COMPUTING TIME REQUIRED TO RUN THE SOFTWARE UNDER THE CONDITIONS IMPOSED DURING THE INPUT PROCESS

1h20min

for a computer with an i7 processor and with two core at 2.20 GHz each one and 8GB memory

- TOTAL NUMBER OF MAIN COMBINATIONS GENERATED

(Valid Angle Combinations × All the Material Combinations)

6 930 432 Combinations

- TOTAL NUMBER OF VALID ANGLE COMBINATIONS GENERATED

1 692 Valid Combinations

- INTERLAMINAR SHEAR STRENGHT RESULTS (MPa)

```
taufinal =

  Columns 1 through 14

         0         0         0         0         0         0         0         0         0         0         0         0         0         0
    23.295    22.37    23.267    23.217    24.373    22.344    22.298    20.498    23.189     23.28    23.362    23.932    24.208    22.272
    44.668    42.894    44.613    44.518    46.734    42.843    42.755    39.304    44.463    44.638    44.795    45.888    46.417    42.705
    50.963     50.54     50.9    50.791    53.319    50.481    50.377    49.685    50.729    50.929     52.78    52.355    52.959    50.318
    56.635    57.431    56.566    56.444    59.254    57.363    57.245     59.04    56.376    56.598    59.976    58.182    58.853    57.178
    61.685     62.28     61.61    61.478    61.605    62.207    62.079    63.484    61.403    61.644     62.23    60.491     61.55    62.006
    66.113    66.532    66.032     65.89    63.658    66.454    66.317     67.38     65.81    66.069    64.198    62.507    63.904    66.239
    67.806    68.158    67.723    67.839    65.413    68.078    68.188     68.87    67.756    67.761     65.88     66.38    65.647    68.108
    69.215    69.511     69.13     69.46     66.87    69.429    69.745    70.109    69.375    69.169    67.276    69.613    67.094    69.663
    70.338    70.589    70.426     70.58    69.475    70.673     70.82    71.098    70.666    70.292    69.773    70.767    69.681    70.903
    71.177    71.395    71.393    71.415    71.428    71.602    71.623    71.836     71.63     71.13    71.645    71.629    71.621    71.829
    72.422     72.59    72.636    72.656     72.73    72.796    72.814    72.931    72.869    72.703    72.893    72.907    72.914    73.019
    73.044    73.188    73.257    73.276    73.381    73.393     73.41    73.478    73.489     73.49    73.517    73.547    73.561    73.614

  Columns 15 through 28

         0         0         0         0         0         0         0         0         0         0         0         0         0         0
    22.356    24.289    22.956     23.21    22.721    23.251    23.202    23.773    18.927    23.201    23.285    23.902    21.327    24.125
    42.866    46.573    44.018    44.505    43.567    44.584    44.488    45.584    36.291    44.488    44.647    45.831    40.894    46.259
    50.508    53.136    51.865    52.438    49.707    50.867    50.758    52.007    48.968    50.757    52.606    52.289    51.696    52.778
    57.394     59.05    58.936    59.587    55.239    56.528    56.407    57.796    60.391    56.406    59.778    58.109    61.429    58.652
     62.24    61.393     61.15    62.172     61.47    61.569    61.437    60.444    64.494    61.436    62.025    60.415    63.487    61.339
     66.49    63.439    63.084     64.43    66.933    65.988    65.847    62.756    68.091    65.846    63.986    62.428    65.283    63.685
    68.115    65.459    66.799    66.101    68.585    67.679    67.794    66.603    69.467    67.532    65.922    66.296    66.819    65.691
    69.466    67.135      69.9    67.488    69.958    69.084    69.414    69.815    70.611    68.935    67.529    69.525    68.094    67.356
    70.545     69.73    71.008    69.969    71.054    70.379    70.533    70.961    71.524    70.626    70.017    70.856    70.373    69.934
     71.35    71.677    71.834    71.829    71.872    71.346    71.368    71.817    72.206    71.888    71.883     71.85    72.082    71.868
     72.86    72.975    73.061    73.069    73.086    72.917    72.936    73.087    73.217    73.128    73.127    73.127    73.221    73.156
    73.616    73.623    73.674    73.689    73.693    73.703    73.721    73.722    73.722    73.748    73.749    73.766    73.791    73.801

Columns 29 through 42

         0         0         0         0         0         0         0         0         0         0         0         0         0         0
   23.0383   21.8401   22.3296   22.2837   22.8100   23.0907   24.3558   17.9124   22.9287   22.6941   22.6467   23.1341   20.9889   23.1734
   44.1749   41.8775   42.8161   42.7280   43.7373   44.2754   46.7013   34.3462   43.9648   43.5150   43.4241   44.3586   40.2454   44.4340
   50.4002   49.3428   50.4486   50.3449   51.5341   50.5148   53.2826   48.5044   51.8021   49.6472   49.5435   52.2662   50.8757   50.6958
   56.0100   56.0700   57.3266   57.2087   58.5601   56.1373   59.2132   61.2628   58.8646   55.1732   55.0580   59.3920   60.4549   56.3385
   61.0043   62.0592   62.1673   62.0395   61.1006   61.1430   61.5627   65.1460   61.0764   61.3966   61.2683   61.9686   62.4796   61.3622
   65.3833   67.3104   66.4116   66.2750   63.3190   65.5319   63.6143   68.5506   63.0078   66.8531   66.7134   64.2185   64.2476   65.7668
   67.9138   68.8979   68.0347   68.1452   67.0102   67.2104   65.3681   69.8526   66.7181   68.5028   68.6141   66.1418   67.6441   67.7116
   70.0185   70.2184   69.3848   69.7008   70.0920   68.6065   66.8240   70.9356   69.8159   69.8749   70.1950   67.7385   70.4798   69.3293
   71.1297   71.2718   70.6283   70.7756   71.1921   71.1093   69.4265   71.7996   71.0928   71.1387   71.2873   70.2105   71.4921   70.6198
   71.9592   72.0581   71.5565   71.5779   72.0134   72.9954   71.3784   72.4445   72.0459   72.0820   72.1027   72.0645   72.2478   71.5831
   73.1901   73.2250   73.0656   73.0839   73.2320   73.5601   73.0245   73.4015   73.2709   73.2945   73.3126   73.3005   73.3692   73.1493
   73.8055   73.8084   73.8202   73.8369   73.8414   73.8425   73.8476   73.8800   73.8834   73.9008   73.9176   73.9185   73.9299   73.9324
```

Columns 43 through 56

0	0	0	0	0	0	0	0	0	0	0	0	0	0
17.565	23.743	22.181	23.087	23.346	23.836	22.689	23.916	21.815	19.632	21.771	24.191	22.258	22.783
33.68	45.527	42.532	44.267	44.765	45.705	43.505	45.857	41.829	37.643	41.745	46.386	42.678	43.685
48.346	51.942	50.113	50.506	52.745	52.145	49.636	52.32	49.286	50.792	49.187	52.922	50.286	51.472
61.561	57.724	56.946	56.127	59.937	57.949	55.161	58.143	56.006	62.64	55.893	58.813	57.142	58.49
65.369	60.368	61.754	61.132	62.189	61.424	60.08	60.45	61.988	64.534	61.863	61.507	61.967	61.027
68.708	62.677	65.97	65.52	64.155	64.458	64.392	62.465	67.233	66.188	67.098	63.86	66.197	63.243
69.985	66.519	67.583	67.198	65.836	66.174	68.099	66.335	68.819	67.601	68.925	65.602	68.065	66.93
71.047	69.727	68.924	68.594	67.232	67.599	71.199	69.566	70.138	68.775	70.445	67.048	69.619	70.008
71.894	71.05	71.328	71.097	69.726	70.146	72.309	70.719	71.353	70.873	71.495	69.633	70.859	71.277
72.526	72.037	73.14	72.982	71.597	72.056	73.141	71.58	72.259	72.446	72.279	71.572	71.784	72.224
73.465	73.305	73.682	73.634	73.175	73.33	73.696	73.197	73.425	73.495	73.442	73.207	73.288	73.441
73.934	73.939	73.954	73.96	73.964	73.966	73.974	74.005	74.008	74.019	74.024	74.024	74.04	74.05

Columns 57 through 70

0	0	0	0	0	0	0	0	0	0	0	0	0	0
17.994	22.177	23.014	20.053	21.81	24.272	22.685	17.549	20.425	17.521	22.941	23.414	22.62	22.707
33.623	42.524	44.128	38.451	41.821	46.541	43.498	33.649	39.164	33.595	43.989	44.896	43.372	43.539
47.846	50.105	50.346	55.194	49.276	53.099	49.627	48.301	49.508	48.223	51.831	51.223	49.485	49.675
61.385	56.936	55.95	60.077	55.994	59.01	55.151	61.504	58.83	61.405	58.897	56.924	54.992	55.204
65.286	61.744	60.939	64.424	60.722	61.351	60.069	65.309	63.258	65.203	61.11	60.337	61.195	61.43
68.706	65.959	65.313	66.12	64.867	63.396	64.381	68.644	67.14	68.533	63.043	63.317	66.634	66.89
70.014	67.571	67.245	67.571	68.43	65.413	68.087	69.92	68.625	70.004	66.755	67.106	68.532	68.54
71.102	68.912	68.851	68.777	71.411	67.089	71.186	70.981	69.86	71.227	69.855	70.27	70.111	69.913
71.97	71.316	71.346	69.737	72.477	69.682	72.296	71.958	71.348	72.072	70.961	71.399	71.371	71.009
72.618	73.127	73.226	71.344	73.278	71.627	73.128	72.688	72.46	72.703	71.787	72.242	72.311	71.826
73.579	73.753	73.789	72.416	73.811	73.268	73.769	73.625	73.551	73.639	73.338	73.493	73.52	73.361
74.06	74.067	74.07	74.071	74.078	74.088	74.089	74.094	74.097	74.107	74.113	74.118	74.124	74.128

Columns 71 through 84

0	0	0	0	0	0	0	0	0	0	0	0	0	0
23.195	19.345	20.298	18.543	22.11	24.098	23.757	20.339	22.661	23.01	21.807	23.269	18.171	20.615
44.475	37.093	38.921	35.555	42.395	46.206	45.553	38.999	43.452	44.12	41.813	44.618	34.842	38.52
52.404	50.049	49.202	50.211	49.953	52.718	51.972	49.3	49.575	50.337	49.267	52.572	50.013	54.814
59.548	61.725	58.466	63.418	56.763	58.585	57.757	58.583	55.093	55.94	55.984	59.739	63.684	59.833
62.131	63.591	62.866	65.207	61.556	60.91	60.403	62.992	60.005	60.928	60.712	61.984	65.437	64.302
64.387	65.22	66.725	66.769	65.759	62.94	62.713	66.858	64.313	65.302	64.856	63.944	66.967	66.046
66.057	68.35	68.954	68.104	67.615	65.562	66.558	68.337	68.014	67.233	68.419	65.878	68.276	67.537
67.444	70.964	70.809	69.212	69.158	67.738	69.768	69.566	71.111	68.839	71.398	67.484	69.362	68.777
69.922	71.897	71.788	71.194	71.555	70.313	70.913	71.771	72.391	71.333	72.465	69.971	71.304	69.764
71.781	72.594	72.518	72.68	73.361	72.245	71.769	73.432	73.351	73.213	73.265	71.835	72.76	71.416
73.349	73.627	73.603	73.671	73.901	73.532	73.374	73.93	73.905	73.862	73.881	73.408	73.731	72.517
74.133	74.144	74.145	74.166	74.172	74.176	74.177	74.178	74.182	74.187	74.189	74.194	74.216	74.219

Columns 85 through 98

0	0	0	0	0	0	0	0	0	0	0	0	0	0
21.746	23.886	21.827	24.255	23.077	23.137	19.971	24.109	17.504	23.833	20.016	17.556	17.122	22.795
41.698	45.8	41.852	46.508	44.249	44.363	38.293	46.227	33.564	45.698	38.381	33.664	32.83	43.709
49.131	52.254	49.312	53.063	50.485	50.615	54.966	52.742	48.179	52.138	55.093	48.322	47.93	51.501
55.829	58.07	56.035	58.969	56.104	56.249	59.829	58.612	61.348	57.941	59.967	61.531	61.538	58.522
61.793	60.374	62.021	61.308	61.107	61.265	64.158	61.297	65.143	60.24	64.306	65.337	65.458	61.061
67.021	62.386	67.269	63.352	65.493	65.662	66.109	63.642	68.47	62.248	65.999	68.674	68.896	63.278
68.846	66.251	68.855	65.098	67.17	67.344	67.777	65.646	69.939	66.104	67.447	69.95	70.211	66.967
70.364	69.478	70.175	66.548	68.566	68.743	68.977	67.31	71.161	69.324	68.837	71.011	71.304	70.047
71.575	70.808	71.228	69.827	71.067	70.824	69.934	69.886	72.136	71.061	69.943	71.858	72.176	71.146
72.479	71.801	72.013	72.285	72.952	72.378	71.534	71.818	72.864	72.358	71.548	72.49	72.828	71.967
73.641	73.416	73.489	73.581	73.805	73.614	72.601	73.448	73.799	73.631	72.617	73.677	73.794	73.507
74.222	74.223	74.226	74.229	74.231	74.232	74.25	74.262	74.267	74.268	74.269	74.27	74.277	74.278

Columns 99 through 100

0	0
21.784	18.286
41.771	35.063
49.217	49.517
55.927	62.542
60.65	64.306
64.79	65.846
68.349	68.805
71.326	71.276
72.556	72.158
73.479	72.816
74.012	73.793
74.278	74.282

Note that the difference between the value obtained for the 100th laminate and the value obtained for the first laminate is 1.226 MPa, despite to be a small difference, this value is for an ultimate load of 2559 N, which means that, if the load is increased, then this difference becomes higher, however, to increase the load requires that the laminate can withstand it, at least, until the ultimate load.

- MATERIAL COMBINATION CHOSEN

```
materialchosen =
Columns 1 through 21
  'C' 'C' 'C' 'C' 'C' 'C' 'C' 'C' 'C' 'C' 'C' 'C' 'C' 'C' 'C' 'C' 'C' 'C' 'C' 'C' 'C'
  'C' 'C' 'C' 'C' 'C' 'C' 'C' 'C' 'C' 'C' 'C' 'C' 'C' 'C' 'C' 'C' 'C' 'C' 'C' 'C' 'C'
  'C' 'C' 'C' 'C' 'C' 'C' 'C' 'C' 'C' 'C' 'C' 'C' 'C' 'C' 'C' 'C' 'C' 'C' 'C' 'C' 'C'
  'C' 'C' 'C' 'C' 'C' 'C' 'C' 'C' 'C' 'C' 'C' 'C' 'C' 'C' 'C' 'C' 'C' 'C' 'C' 'C' 'C'
  'C' 'C' 'C' 'C' 'G' 'C' 'C' 'C' 'C' 'C' 'G' 'G' 'G' 'C' 'C' 'G' 'G' 'G' 'C' 'C' 'C'
  'C' 'C' 'C' 'C' 'G' 'C' 'C' 'C' 'C' 'C' 'G' 'G' 'G' 'C' 'C' 'G' 'G' 'G' 'C' 'C' 'C'
  'G' 'G' 'G' 'G' 'G' 'G' 'G' 'G' 'G' 'G' 'G' 'C' 'G' 'G' 'G' 'G' 'C' 'G' 'G' 'G' 'G'
  'G' 'G' 'G' 'G' 'G' 'G' 'G' 'G' 'G' 'G' 'G' 'C' 'G' 'G' 'G' 'G' 'C' 'G' 'G' 'G' 'G'
  'G' 'G' 'G' 'G' 'C' 'G' 'G' 'G' 'G' 'G' 'C' 'G' 'C' 'G' 'G' 'C' 'G' 'C' 'G' 'G' 'G'
  'G' 'G' 'G' 'G' 'C' 'G' 'G' 'G' 'G' 'G' 'C' 'G' 'C' 'G' 'G' 'C' 'G' 'C' 'G' 'G' 'G'
  'C' 'C' 'C' 'C' 'C' 'C' 'C' 'C' 'C' 'C' 'C' 'C' 'C' 'C' 'C' 'C' 'C' 'C' 'C' 'C' 'C'
  'C' 'C' 'C' 'C' 'C' 'C' 'C' 'C' 'C' 'C' 'C' 'C' 'C' 'C' 'C' 'C' 'C' 'C' 'C' 'C' 'C'
Columns 22 through 42
  'C' 'C' 'C' 'C' 'C' 'C' 'C' 'C' 'C' 'C' 'C' 'C' 'C' 'C' 'C' 'C' 'C' 'C' 'C' 'C' 'C'
  'C' 'C' 'C' 'C' 'C' 'C' 'C' 'C' 'C' 'C' 'C' 'C' 'C' 'C' 'C' 'C' 'C' 'C' 'C' 'C' 'C'
  'C' 'C' 'C' 'C' 'C' 'C' 'C' 'C' 'C' 'C' 'C' 'C' 'C' 'C' 'C' 'C' 'C' 'C' 'C' 'C' 'C'
  'C' 'C' 'C' 'C' 'C' 'C' 'C' 'C' 'C' 'C' 'C' 'C' 'C' 'C' 'C' 'C' 'C' 'C' 'C' 'C' 'C'
  'G' 'C' 'C' 'G' 'G' 'G' 'G' 'C' 'C' 'C' 'C' 'G' 'C' 'G' 'C' 'G' 'C' 'C' 'G' 'G' 'C'
  'G' 'C' 'C' 'G' 'G' 'G' 'G' 'C' 'C' 'C' 'C' 'G' 'C' 'G' 'C' 'G' 'C' 'C' 'G' 'G' 'C'
  'C' 'G' 'G' 'G' 'C' 'G' 'G' 'G' 'G' 'G' 'G' 'C' 'G' 'G' 'G' 'C' 'G' 'G' 'G' 'C' 'G'
  'C' 'G' 'G' 'G' 'C' 'G' 'G' 'G' 'G' 'G' 'G' 'C' 'G' 'G' 'G' 'C' 'G' 'G' 'G' 'C' 'G'
  'G' 'G' 'G' 'C' 'G' 'C' 'C' 'G' 'G' 'G' 'G' 'G' 'C' 'C' 'G' 'G' 'G' 'G' 'C' 'G' 'G'
  'G' 'G' 'G' 'C' 'G' 'C' 'C' 'G' 'G' 'G' 'G' 'G' 'C' 'C' 'G' 'G' 'G' 'G' 'C' 'G' 'G'
  'C' 'C' 'C' 'C' 'C' 'C' 'C' 'C' 'C' 'C' 'C' 'C' 'G' 'C' 'C' 'C' 'C' 'C' 'C' 'C' 'C'
  'C' 'C' 'C' 'C' 'C' 'C' 'C' 'C' 'C' 'C' 'C' 'C' 'G' 'C' 'C' 'C' 'C' 'C' 'C' 'C' 'C'
```

```
Columns 43 through 63

  'C' 'C' 'C' 'C'  'C' 'C' 'C' 'C'  'C' 'C' 'C' 'C' 'C' 'C' 'C' 'C' 'C' 'C' 'C' 'C' 'C' 'C' 'C'
  'C' 'C' 'C' 'C'  'C' 'C' 'C' 'C'  'C' 'C' 'C' 'C' 'C' 'C' 'C' 'C' 'C' 'C' 'C' 'C' 'C' 'C' 'C'
  'C' 'C' 'C' 'C'  'C' 'C' 'C' 'C'  'C' 'C' 'C' 'C' 'C' 'C' 'C' 'C' 'C' 'C' 'C' 'C' 'C' 'C' 'C'
  'C' 'C' 'C' 'C'  'C' 'C' 'C' 'C'  'C' 'C' 'C' 'C' 'C' 'C' 'C' 'C' 'C' 'C' 'C' 'C' 'C' 'C' 'C'
  'C' 'G' 'C' 'C'  'G' 'G' 'C' 'G'  'C' 'G' 'C' 'G' 'C' 'G' 'C' 'C' 'C' 'C' 'C' 'G' 'C'
  'C' 'G' 'C' 'C'  'G' 'G' 'C' 'G'  'C' 'G' 'C' 'G' 'C' 'G' 'C' 'C' 'C' 'G' 'C' 'G' 'C'
  'G' 'C' 'G' 'G'  'G' 'G' 'C' 'C'  'G' 'G' 'G' 'G' 'G' 'C' 'G' 'G' 'G' 'G' 'C' 'G' 'C'
  'G' 'C' 'G' 'G'  'G' 'G' 'C' 'C'  'G' 'G' 'G' 'G' 'G' 'C' 'G' 'G' 'G' 'G' 'C' 'G' 'C'
  'G' 'G' 'C' 'C'  'C' 'C' 'G' 'G'  'G' 'C' 'G' 'C' 'G' 'G' 'C' 'C' 'G' 'C' 'G' 'C' 'G'
  'G' 'G' 'C' 'C'  'C' 'C' 'G' 'G'  'G' 'C' 'G' 'C' 'G' 'G' 'C' 'C' 'C' 'G' 'C' 'C' 'G'
  'C' 'C' 'G' 'G'  'C' 'C' 'G' 'C'  'C' 'C' 'C' 'C' 'C' 'C' 'C' 'G' 'G' 'C' 'G' 'C' 'G'
  'C' 'C' 'G' 'G'  'C' 'C' 'G' 'C'  'C' 'C' 'C' 'C' 'C' 'C' 'C' 'G' 'G' 'C' 'G' 'C' 'G'

Columns 64 through 84

  'C' 'C' 'C' 'C'  'C' 'C' 'C' 'C'  'C' 'C' 'C' 'C' 'C' 'C' 'C' 'C' 'C' 'C' 'C' 'C' 'C' 'C' 'C'
  'C' 'C' 'C' 'C'  'C' 'C' 'C' 'C'  'C' 'C' 'C' 'C' 'C' 'C' 'C' 'C' 'C' 'C' 'C' 'C' 'C' 'C' 'C'
  'C' 'C' 'C' 'C'  'C' 'C' 'C' 'C'  'C' 'C' 'C' 'C' 'C' 'C' 'C' 'C' 'C' 'C' 'C' 'C' 'C' 'C' 'C'
  'C' 'C' 'C' 'C'  'C' 'C' 'C' 'C'  'C' 'C' 'C' 'C' 'C' 'C' 'C' 'C' 'C' 'C' 'C' 'C' 'C' 'C' 'C'
  'C' 'C' 'C' 'G'  'G' 'C' 'C' 'G'  'G' 'C' 'G' 'C' 'G' 'G' 'C' 'C' 'C' 'C' 'G' 'G' 'C'
  'C' 'C' 'C' 'G'  'G' 'C' 'C' 'G'  'G' 'C' 'G' 'C' 'G' 'G' 'C' 'C' 'C' 'C' 'G' 'G' 'G'
  'G' 'G' 'G' 'C'  'C' 'G' 'G' 'G'  'C' 'G' 'G' 'G' 'G' 'C' 'G' 'C' 'G' 'C' 'G' 'G' 'G'
  'G' 'G' 'G' 'C'  'C' 'G' 'G' 'G'  'C' 'G' 'G' 'G' 'G' 'C' 'G' 'C' 'G' 'C' 'G' 'G' 'G'
  'G' 'G' 'G' 'G'  'G' 'G' 'G' 'C'  'G' 'G' 'C' 'C' 'C' 'G' 'C' 'G' 'C' 'G' 'C' 'C' 'G'
  'C' 'C' 'C' 'C'  'C' 'C' 'C' 'C'  'C' 'C' 'C' 'C' 'G' 'G' 'G' 'G' 'C' 'C' 'C' 'C'
  'C' 'C' 'C' 'C'  'C' 'C' 'C' 'C'  'C' 'C' 'C' 'C' 'G' 'C' 'C' 'G' 'G' 'G' 'G' 'C' 'C' 'C'

Columns 85 through 100

  'C' 'C' 'C' 'C'  'C' 'C' 'C' 'C'  'C' 'C' 'C' 'C' 'C' 'C' 'C' 'C'
  'C' 'C' 'C' 'C'  'C' 'C' 'C' 'C'  'C' 'C' 'C' 'C' 'C' 'C' 'C' 'C'
  'C' 'C' 'C' 'C'  'C' 'C' 'C' 'C'  'C' 'C' 'C' 'C' 'C' 'C' 'C' 'C'
  'C' 'C' 'C' 'C'  'C' 'C' 'C' 'C'  'C' 'C' 'C' 'C' 'C' 'C' 'C' 'C'
  'C' 'G' 'C' 'G'  'C' 'C' 'C' 'G'  'C' 'G' 'C' 'C' 'C' 'G' 'C' 'G'
  'C' 'G' 'C' 'G'  'C' 'C' 'G' 'G'  'C' 'G' 'G' 'C' 'C' 'G' 'C' 'G'
  'G' 'C' 'G' 'G'  'G' 'G' 'G' 'G'  'G' 'C' 'G' 'G' 'G' 'C' 'C' 'C'
  'G' 'C' 'G' 'G'  'G' 'G' 'G' 'G'  'G' 'C' 'G' 'G' 'G' 'C' 'C' 'C'
  'G' 'G' 'G' 'C'  'C' 'G' 'G' 'C'  'G' 'G' 'G' 'G' 'G' 'G' 'G' 'G'
  'G' 'G' 'G' 'C'  'C' 'G' 'C' 'C'  'G' 'G' 'C' 'G' 'G' 'G' 'G' 'G'
  'C' 'C' 'C' 'C'  'G' 'C' 'C' 'C'  'C' 'C' 'C' 'C' 'C' 'C' 'G' 'C'
  'C' 'C' 'C' 'C'  'G' 'C' 'C' 'C'  'C' 'C' 'C' 'C' 'C' 'C' 'G' 'C'
```

- PLIES ORIENTATION CHOSEN (Degrees)

```
anglechosen =
 Columns 1 through 32
   0     0     0     0     0     0     0     0     0     0     0     0     0     0     0     0     0     0     0     0     0     0     0     0     0     0     0     0     0     0     0     0
   0     0     0     0     0     0     0     0     0     0     0     0     0     0     0     0     0     0     0     0     0     0     0     0     0     0     0     0     0     0     0     0
  45    40    45    45    45    40    40    30    45    45    40    45    45    40    40    45    40    40    45    45    45    45    20    45    40    45    30    45    45    40    40    40
 -45   -40   -45   -45   -45   -40   -40   -30   -45   -45   -40   -45   -45   -40   -40   -45   -40   -40   -45   -45   -45   -45   -20   -45   -40   -45   -30   -45   -45   -40   -40   -40
  45    45    45    45    45    45    45    45    45    45    45    45    40    45    45    45    45    40    40    45    45    40    45    45    45    45    45    40    45    40    45    45
 -45   -45   -45   -45   -45   -45   -45   -45   -45   -45   -45   -45   -40   -45   -45   -45   -45   -40   -40   -45   -45   -40   -45   -45   -45   -45   -45   -40   -45   -40   -45   -45
  45    45    45    40    45    45    40    45    40    45    45    45    45    40    45    40    45    45    45    45    40    45    45    45    40    45    45    40    30    45    45    40
 -45   -45   -45   -40   -45   -45   -40   -45   -40   -45   -45   -45   -45   -40   -45   -40   -45   -45   -45   -45   -40   -45   -45   -45   -40   -45   -45   -40   -30   -45   -45   -40
  45    45    40    45    45    40    45    45    40    45    45    45    45    40    45    45    45    45    45    40    45    45    45    30    45    40    45    45    45    45    40    45
 -45   -45   -40   -45   -45   -40   -45   -45   -40   -45   -45   -45   -45   -40   -45   -45   -45   -45   -45   -40   -45   -45   -45   -30   -45   -40   -45   -45   -45   -45   -40   -45
  45    45    45    45    45    45    45    45    45    40    45    45    45    45    40    45    45    45    45    40    40    45    45    45    45    45    45    45    45    45    40    40
 -45   -45   -45   -45   -45   -45   -45   -45   -45   -40   -45   -45   -45   -45   -40   -45   -45   -45   -45   -40   -40   -45   -45   -45   -45   -45   -45   -45   -45   -45   -40   -40
 Columns 33 through 64
   0     0     0     0     0     0     0     0     0     0     0     0     0     0     0     0     0     0     0     0     0     0     0     0     0     0     0     0     0     0     0     0
   0     0     0     0     0     0     0     0     0     0     0     0     0     0     0     0     0     0     0     0     0     0     0     0     0    10     0     0     0     0     0     0
  40    45    45    10    40    45    45    40    30    45     0    45    40    45    40    45    45    45    40    20    40    45    40    40   -10    40    45     0    40    45    45     0
 -40   -45   -45   -10   -40   -45   -45   -40   -30   -45     0   -45   -40   -45   -40   -45   -45   -45   -40   -20   -40   -45   -40   -40     0   -40   -45    45   -40   -45   -45     0
  40    45    45    45    45    40    40    40    45    45    45    40    45    45    45    30    45    45    40    45    40    40    45    40    45    45    45   -45    45    45    45    45
 -40   -45   -45   -45   -45   -40   -40   -40   -45   -45   -45   -40   -45   -45   -45   -30   -45   -45   -40   -45   -40   -40   -45   -40   -45   -45   -45    45   -45   -45   -45   -45
  45    45    45    45    45    45    40    40    45    40    45    45    45    45    45    45    45    45    45    45    40    45    40    45    45    45    40   -45    45    40    45    45
 -45   -45   -45   -45   -45   -45   -40   -40   -45   -40   -45   -45   -45   -45   -45   -45   -45   -45   -45   -45   -40   -45   -40   -45   -45   -45   -40    45   -45   -40   -45   -45
  45    45    45    45    40    40    45    45    45    40    45    40    45    45    45    45    45    45    45    40    45    45    45    40    40    45    45    45   -45    45    45    45    40
 -45   -45   -45   -45   -40   -40   -45   -45   -45   -40   -45   -40   -45   -45   -45   -45   -45   -45   -45   -40   -45   -45   -45   -40   -40   -45   -45   -45    45   -45   -45   -45   -40
  45    45    40    45    45    45    45    45    45    40    45    45    45    40    40    45    45    40    45    45    45    40    40    45    45    40    45   -45    45    40    40    45
 -45   -45   -40   -45   -45   -45   -45   -45   -45   -40   -45   -45   -45   -40   -40   -45   -45   -40   -45   -45   -45   -40   -40   -45   -45   -40   -45     0   -45   -40   -40   -45
```

Columns 65 through 96

```
   0     0     0     0     0     0     0     0     0     0     0     0     0     0     0     0     0     0     0     0     0     0     0     0     0     0     0     0     0     0     0     0
   0     0     0     0     0     0     0     0     0     0     0     0     0     0     0     0     0     0     0     0    10     0     0     0     0     0     0     0     0     0     0     0
  30     0    40    45    45    45    40    20    30    10    40    45    45    30    45    45    40    40     0   -10    40    45    40    45    45    45     0    45     0    45     0     0
 -30     0   -40   -45   -45   -45   -40   -20   -30   -10   -40   -45   -45   -30   -45   -45   -40   -40     0    45   -40   -45   -40   -45   -45   -45    45   -45     0   -45    45     0
  45    45    45    30    40    40    40    45    45    45    45    45    40    45    45    45    45    45    45   -45    40    45    40    45    45    45   -45    40    45    45   -45    45
 -45   -45   -45   -30   -40   -40   -40   -45   -45   -45   -45   -45   -40   -45   -45   -45   -45   -45   -45    45   -40   -45   -40   -45   -45   -45    40   -40   -45   -45    45   -45
  45    40    45    45    40    45    45    45    30    45    40    30    45    45    45    40    45    40    45   -45    40    45    45    45    45    45   -40    40    40    45   -45    45
 -45   -40   -45   -45   -40   -45   -45   -45   -30   -45   -40   -30   -45   -45   -45   -40   -45   -40   -45    45   -40   -45   -45   -45   -45   -45    45   -40   -40   -45    40   -45
  30    45    45    45    40    45    45    45    45    45    45    45    45    45    40    45    45    45    45   -45    40    40    45    40    45    20   -45    45    40    30   -40    45
 -30   -45   -45   -45   -40   -45   -45   -45   -45   -45   -45   -45   -45   -45   -40   -45   -45   -45   -45    45   -40   -40   -45   -40   -45   -20    45   -45   -40   -30    45   -45
  45    45    40    45    45    40    40    45    45    45    45    45    40    45    45    40    40    40    45   -45    45    40    40    45    30    45   -45    40    45    45   -45    40
 -45   -45   -40   -45   -45   -40   -40   -45   -45   -45   -45   -45   -40   -45   -45   -40   -40   -40   -45     0   -45   -40   -40   -45   -30   -45     0   -40   -45   -45     0   -40
```

Columns 97 through 100

```
  10     0     0     0
 -10     0     0     0
   0    40    40    10
   0   -40   -40   -10
  45    40    45    45
 -45   -40   -45   -45
  45    45    45    45
 -45   -45   -45   -45
  45    45    40    45
 -45   -45   -40   -45
  45    40    45    45
 -45   -40   -45   -45
```

- YOUNG MODULUS IN THE DIRECTION 1 OF THE LAMINATE IN ACCORDANCE WITH THE RULE OF MIXTURES (MPa):

```
xxmodulus =
 Columns 1 through 14
    48639  51005   49286   49286   48639  51651  51651  56473   49932   51005  51005  48639  49286  52297
 Columns 15 through 28
    53370  49286   51005   51651   51005  51651  51651  49286   61918   50779  51651  49286  56473  49932
 Columns 29 through 42
    50779  53370   54016   54016   51651  48639  51005  65951   51651   51651  51651  52297  56473  52297
 Columns 43 through 56
    67440  49932   51005   49286   53370  50779  48639  51005   54016   61918  54016  51651  54662  52297
 Columns 57 through 70
    65951  51651   49286   67440   51005  51651  49286  68086   58613   68086  53370  50779  52297  53370
Columns 71 through 84
    54016  61918   58613   65951   51651  50779  51651  56473   49286   49932  51651  54016  67440  65951
Columns 85 through 98
    54662  51651   55736   51005   50779  52267  68086  52297   68732   50779  68086  69805  65951  54016
Columns 99 through 100
    51651  65951
```

- PLOT SHOWING THE BEST 100 SOLUTIONS PROVIDED BY THE ALGORITHM, AS A RESULT OF THE PARAMETER INPUT GIVEN BY THE USER:

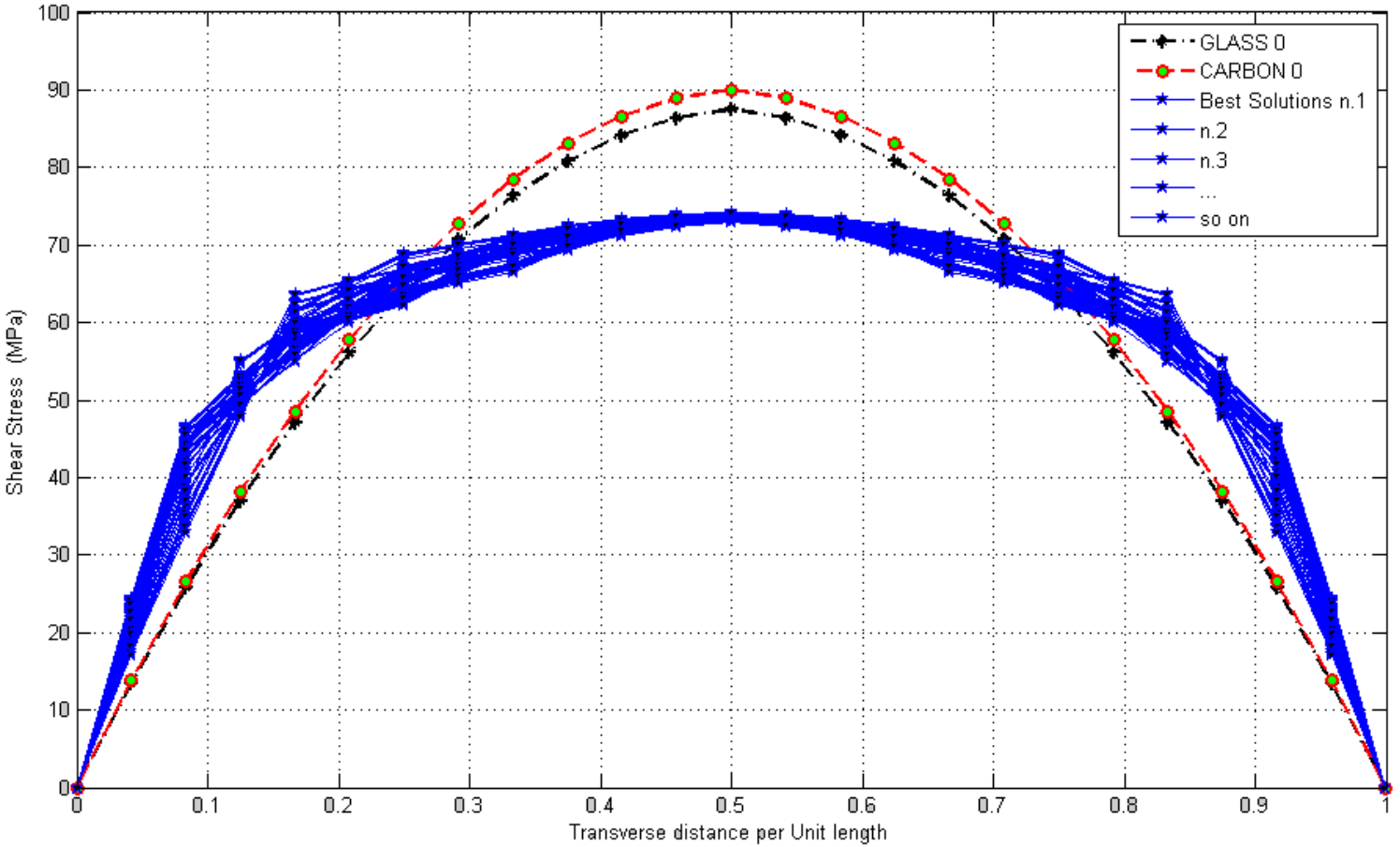

Figure 91 - Plot for the best 100 Solutions in terms of ILSS obtained for 24 Plies (For a Matlab input in which $[\theta_{min}\,;\theta_{max}] = [5^{\circ}\,;\,45^{\circ}]$)

APPENDIX B

TITLE Plot with the best 1500 results for the ILSS (24 Plies)

For an input equal to (just the main variables are shown):

$[\theta_{1_{min}}; \theta_{1_{max}}] = [5^{\circ}; 45^{\circ}]$

$[\theta_{2_{min}}; \theta_{2_{max}}] = [10^{\circ}; 40^{\circ}]$

$\theta_{\ increment\_1} = 5^{\circ}$

$\theta_{\ increment\_2} = 10^{\circ}$

$N_{solution} = 1500$

$Plies_{\_n} = 24$

$Glass_{ply\ \%} = 40\%$

width=6.92 mm

$angles_{\_n} = 3$

Without any 90° plies and without fix the angles θ_1 and θ_2

Accepted all the materials defaults except for the plies thicknesses which are:
t_{glass}= 0.143 mm and t_{carbon}= 0.139 mm

Load=2559 N

Note: For the tables that will be shown in this appendix: each of those columns represents a single composite laminate. The first column will be the best result found to minimize the damage in the middle of the composite laminate (best τ_{xz}), while the last column will be the worse value in terms of τ_{xz} in between the columns shown. The columns are in a crescent order. See also Appendix T for further information.

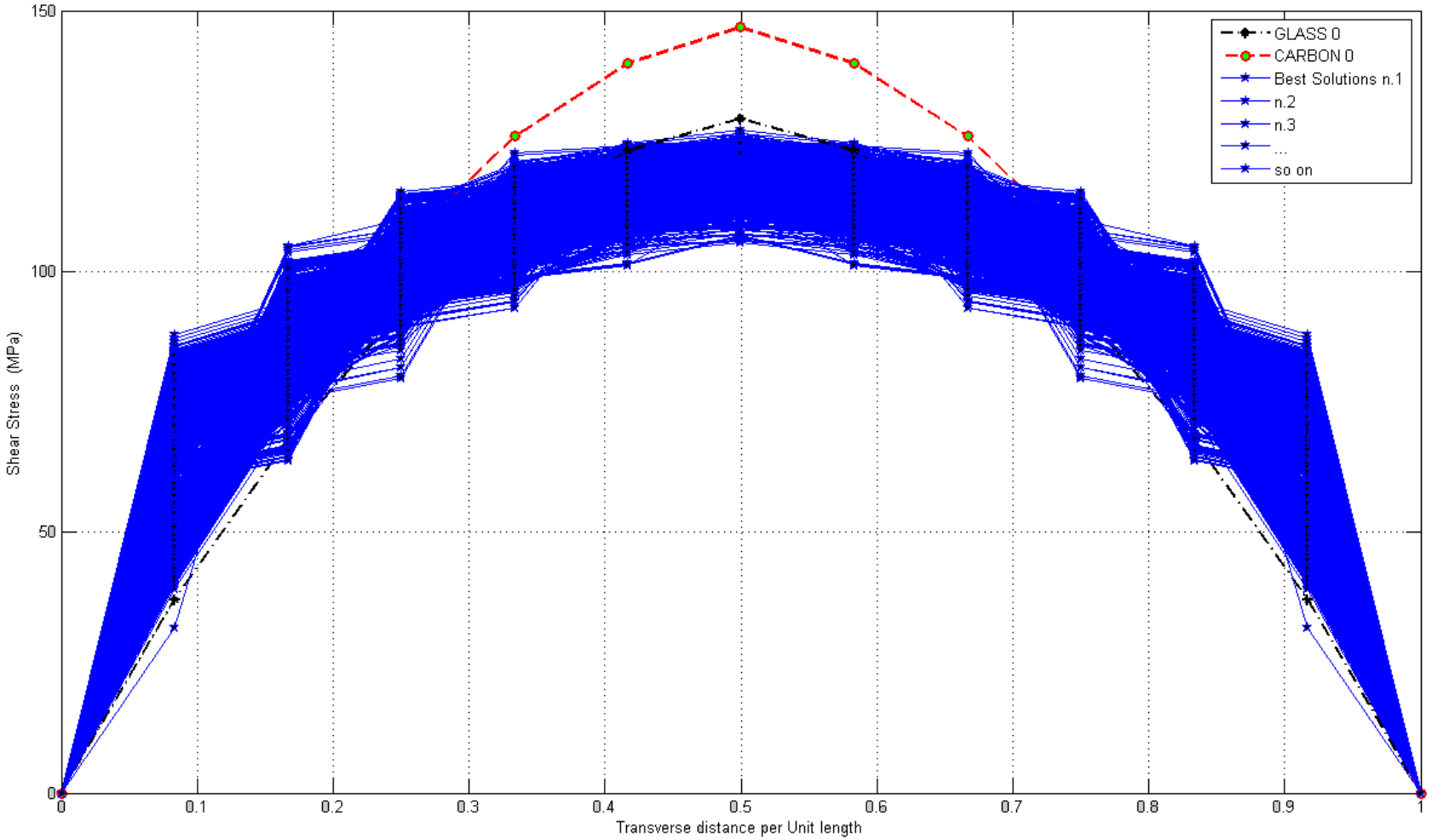
GLASS 0
CARBON 0
Best Solutions n.1
n.2
n.3
...
so on
Shear Stress (MPa)
Transverse distance per Unit length
0
50
100
150
0
0.1
0.2
0.3
0.4
0.5
0.6
0.7
0.8
0.9
1

APPENDIX C

TITLE **Ji Han's MSc thesis (Han 2013) - Chapter 2 - Experimental work.**
Static test results.
All Carbon Design

Chapter 2 (Han 2013)

Static Test – All Carbon Design

"2.1 Introduction and Objectives" (Han 2013)

"The static test was established to investigate the mechanics of compressive failure in the laminated composites, to acquire relevant load levels for fatigue test, and to study the static failure behaviour of the laminates (Kinawy 2011) (Soutis and Fleck 1990). Seven specimens from each design (All Carbon Design, Hybrid Design 1, and Hybrid Design 2) were selected randomly, in order to perform the static tests. The static tests were performed on the Instron 3369 Dual Colum Tabletop Universal Testing System with the utilisation of a 50 kN load cell. Moreover, a digital camera equipped with micro lens was utilised to record the failure of the composite laminates.

Performing the static test was not only for providing required data for the fatigue test, but also for showing the static failure behaviour of the laminates and presenting the mechanics of compressive failure in the composites. Therefore, the objectives of performing the static test are list below:

1. Measure the failure load of the specimens, and provide data for the fatigue test.
2. Study the static failure behaviour of the designed laminated composites.
3. Record and analyse the mechanics of the failure in the composite laminates.
4. Test and verify whether the design is qualified. " (Han 2013)

"2.2 Static Test of <u>All Carbon Design"</u> (Han 2013)

"As illustrated in Appendix H, the All Carbon Design is an all carbon layer composite laminate with a stacking sequence of $[(0/45/90/-45)_3]_s$. Seven specimens in total from All Carbon Design were selected to perform the static test. Among these seven specimens, five of them were short specimens that were short specimen 1, 2, 3, 9, and 10, and the other two were long specimens which were long specimen 3 and 4. Furthermore, short specimen 9 and 10 were polished before performing the static test, for showing a smooth side surface image. In this section, how the static tests of All Carbon Design were performed and the results of the static test are presented, as well as the discussion and conclusion of the results." (Han 2013)

"2.2.1 Static Test 1 -Static Test of <u>All Carbon Design</u>" (Han 2013)

"The static tests were performed on the Instron 3369 Dual Colum Tabletop Universal Testing System at room temperature. The specimens were performed under the three point bending rig as shown in the Appendix H. Moreover, the free-body diagram and bending moment diagram of the specimen under the testing rig are shown in Figure 2.1 and Figure 2.2 respectively (of this Appendix). The specimen was placed on the two supports with assistant tools to ensure the specimen was perpendicular to the loading nose and supports. Moreover, some blue tacks were place at each side of the specimen for preventing the specimen from moving during the test. A digital camera equipped with micro lens was established at the back of the machine, in order to record the failures and their propagation during the static test. Before starting the test, a pre-load was added on the specimen to make sure the loading nose was touched with the specimen. Then the test was performed at a test speed of 0.1 mm/min." (Han 2013)

"The results of the static test were analysed and converted into line chart with the utilisation of Matlab.

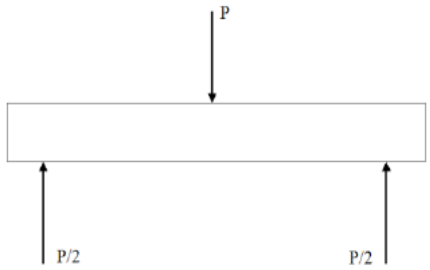

Figure 2.1. Free-body diagram of specimen

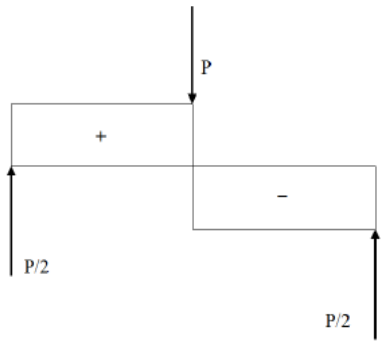

Figure 2.2. Bending moment diagram of specimen

" (Han 2013)

"2.2.2 Results of Static Test 1" (Han 2013) – <u>All Carbon Design</u>

"After the test, the data were collected and then analysed with Excel and Matlab. As the initial displacement of each specimen were different due to the thickness of each specimen varies. Therefore, the initial displacement of each specimen was returned to zero, in order to compare the results of the seven specimens in the same plot. Figure 2.3 (of this Appendix) shows the results of static test 1, which is a load versus displacement plot. In the plot, the seven curves in seven different colours represent the seven specimens, in which specimen 1 is in red, specimen 2 is in purple, specimen 3 is in green, specimen 9 is in black, specimen 10 is in cyan, specimen 3L is in pink, and specimen 4L is in blue." (Han 2013)

"Through Figure 2.3 (of this Appendix), we could find that the first load drops of all the specimens occurred between -0.45 mm to -0.55 mm. And Table 2.1 (of this Appendix) shows that failure loads of the seven specimens, including both short and long specimen, which were nearly the same with an average failure load of 2515 N. The standard deviation of the failure loads listed in the table was calculated as 103N. Moreover, most of the displacement versus load plots of the specimen shares a similar trend.

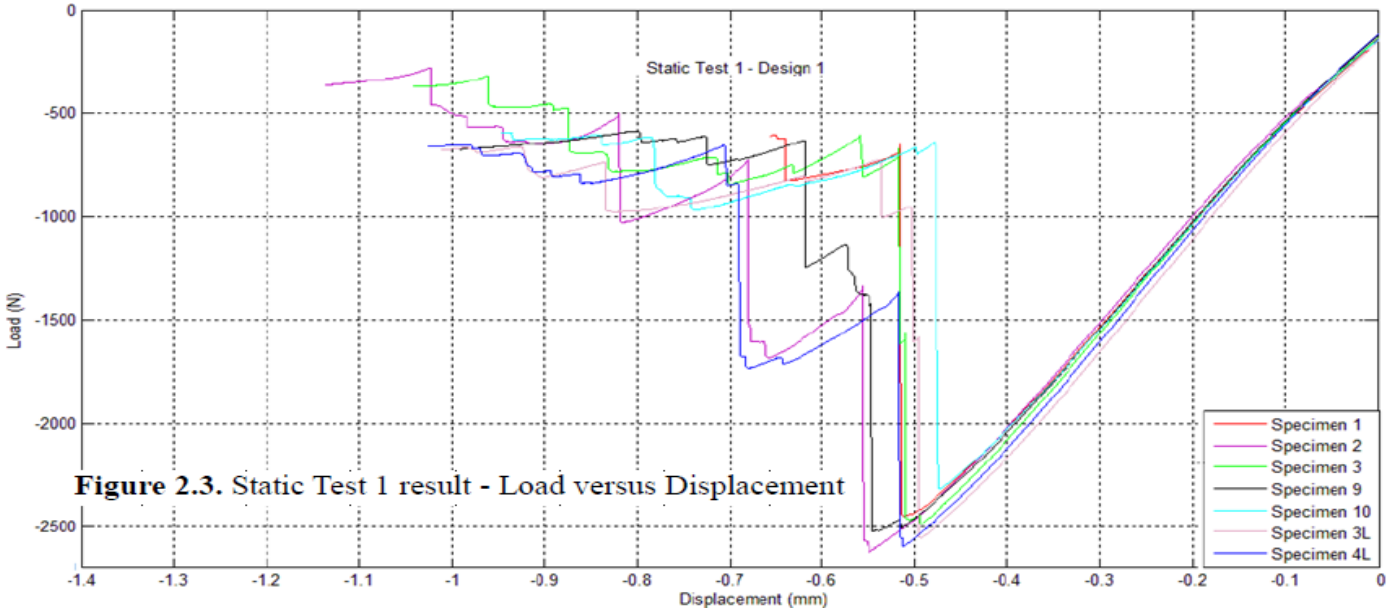

Figure 2.3. Static Test 1 result - Load versus Displacement

Table 2.1. Static Test 1 result - Failure load

Specimens	Failure Load (N)
1	2449
2	2663
3	2485
9	2542
10	2318
3L	2554
4L	2597
Average	2515
S.D.	103

" (Han 2013)

"The static test was recorded with a micro lens digital camera, in order to record the failures in the laminated composite. Photos were taken while a crack occurs and before the next failure occurs, as well as at the start of the test and at the end of the test. For specimen 10 was polished before testing, thus images of specimen 10 and its load versus displacement plot were used to illustrate the static failure behaviour of All Carbon Design, as shown in Figure 2.4 (of this Appendix). The plies of the specimen were pointed out in a clear image shown as Figure 2.5 (of this Appendix)." (Han 2013)

”

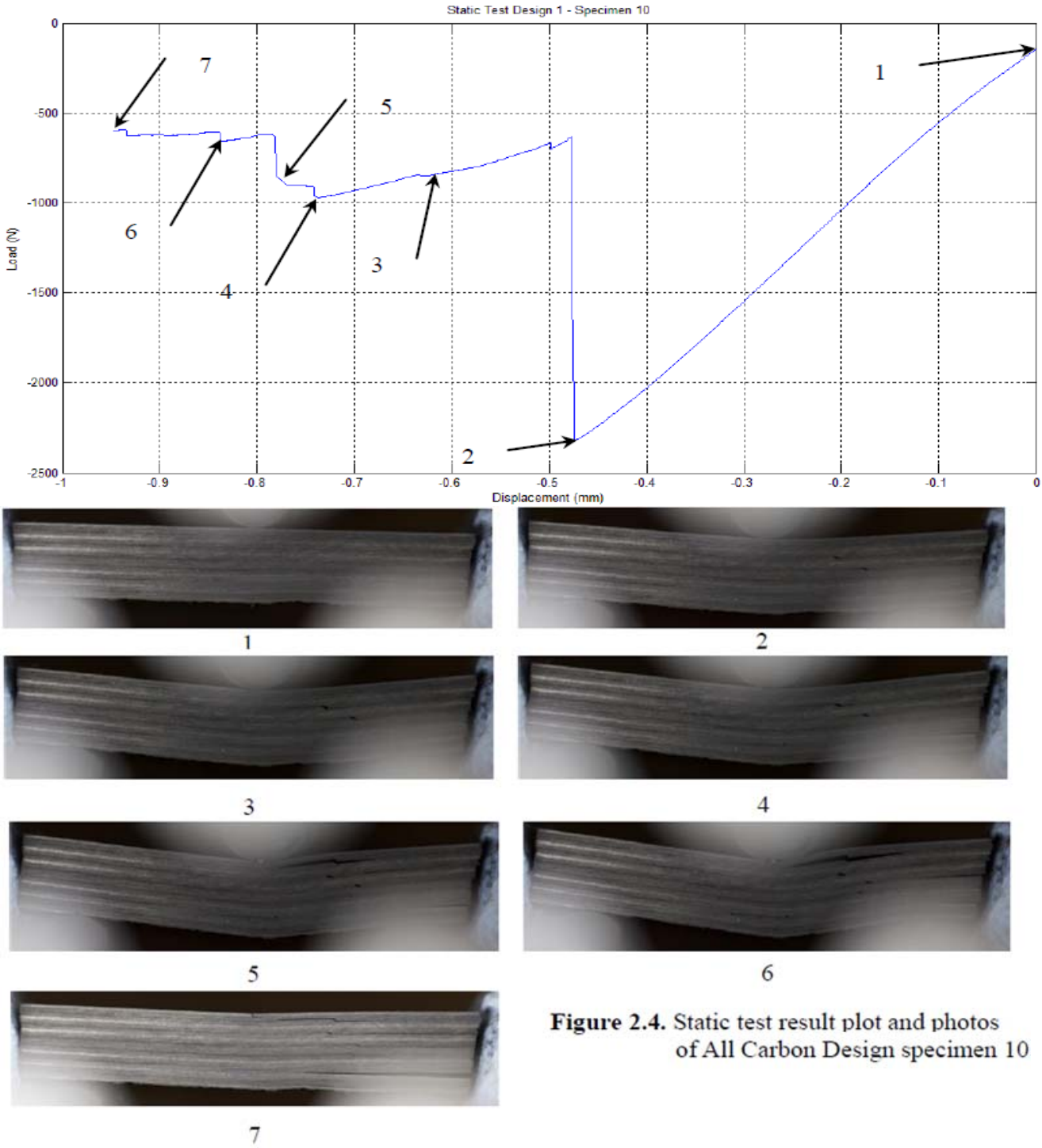

Figure 2.4. Static test result plot and photos of All Carbon Design specimen 10

”

(Han 2013)

APPENDIX D

TITLE **Ji Han's MSc thesis (Han 2013) - Chapter 2 - Experimental work.**
Static test results.
Hybrid Design 1

Chapter 2 (Han 2013)

Static Test – Hybrid Design 1

"2.3 Static Test of Hybrid Design 1" (Han 2013)

"Hybrid Design 1 is the laminate composite that is composed of 16 carbon fibre plies and 8 glass fibre plies. The lay-up of the design is $[(0_C)_2/(\pm45_C)_2/(\pm45_G)_2/(\pm45_C)]_s$. As the same as All Carbon Design, seven specimens, five short specimen (1, 2, 3, 9 and 10) and two long specimen (3 and 4), in total from Hybrid Design 1 were selected to perform the static test. Also, two short specimens (9 and 10) were polished before performing the static test. This section illustrates how the static tests of Hybrid Design 1 were performed and discusses the results of the static test." (Han 2013)

"2.3.1 Static Test 2 – Hybrid Design 1" (Han 2013)

"The static tests were performed on the Instron 3369 Dual Colum Tabletop Universal Testing System at room temperature with the three point bending rig. The specimen was placed on the two support cylinders with some blue tacks placing beside the supports to prevent the specimen from moving during the test. A digital camera with micro lens was established to record the static test. As the same as static test 1, a pre-load was added on the specimen before beginning the test. The test was also performed at a test speed of 0.1 mm/min. Static tests were stopped when the load versus displacement plot was tending to be stable. Matlab was used to analyse the results and convert them into line chart. "(Han 2013)

"2.3.2 Results of Static Test 2 – Hybrid Design 1" (Han 2013)

"As same as Static Test 1, the data were collected and then analysed with Excel and Matlab. The initial displacement of each specimen was returned to zero as well using Excel. As shown in figure 2.6 (of this Appendix), the seven curves in different colours represent the seven specimens, specimen 1 in red colour, specimen 2 in purple colour, specimen 3 in green colour, specimen 9 in black colour, specimen 10 in cyan, specimen 3L in pink, and specimen 4L in blue. " (Han 2013)

"

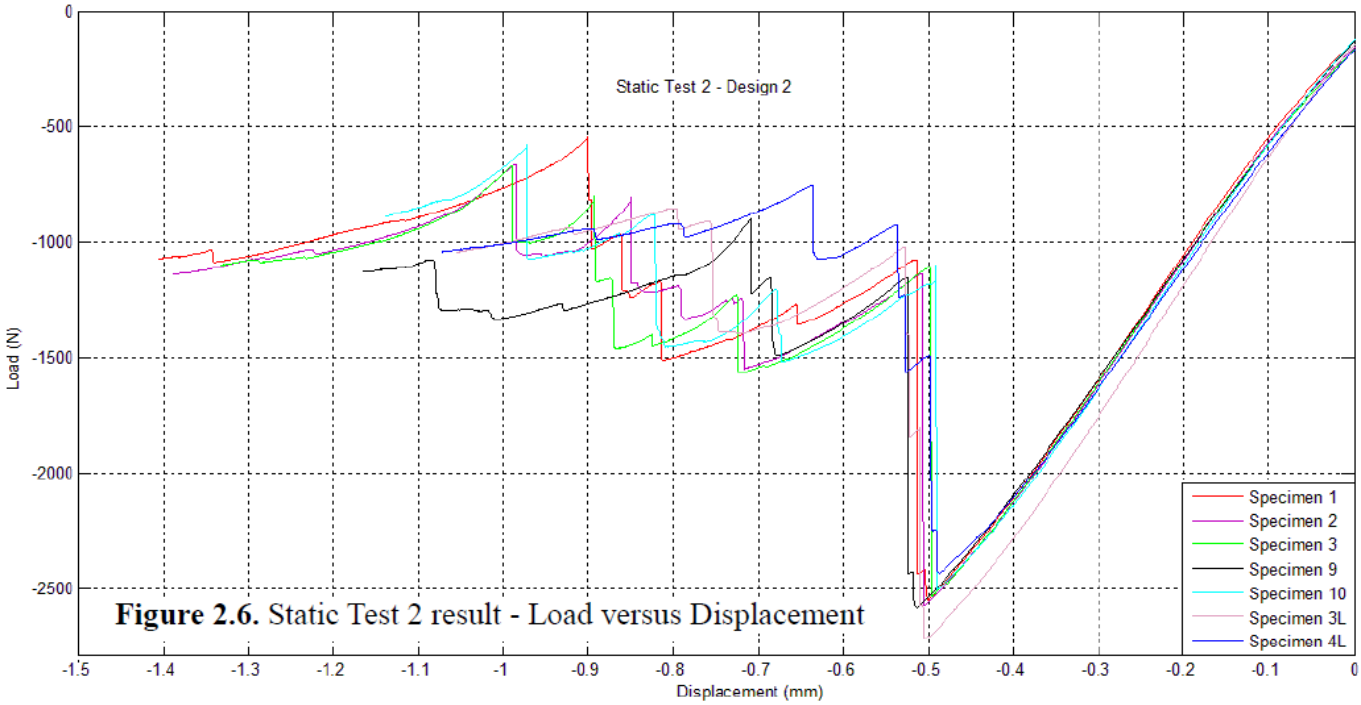

Figure 2.6. Static Test 2 result - Load versus Displacement

Table 2.2. Static Test 2 result - Failure load

Specimens	Failure Load (N)
1	2552
2	2577
3	2535
9	2588
10	2506
3L	2718
4L	2436
Average	2559
S.D.	80

" (Han 2013)

"Figure 2.6 (of this Appendix) presented that the first failure of all the seven laminates appeared at around -0.5 mm. Moreover, all the curves present a same trend. From table 2.2 (of this Appendix), the failure load of the specimens, including both short and long specimens, were nearly the same with an average failure load of 2559 N, which was higher than All Carbon Design. Furthermore, the standard deviation of the failure loads was 80N.

The static test 2 was recorded with a digital camera as well, and photos were taken while a crack occurs and before the next failure occurs as well as at the start of the test and at the end of the test. Images of the polished specimen 10 and its load versus displacement plot were utilised to demonstrate the failure behaviour of Hybrid Design 1, as shown in figure 2.7 (of this Appendix). Moreover, figure 2.8 (of this Appendix) presented the plies of specimen 10 in a photo." (Han 2013)

"

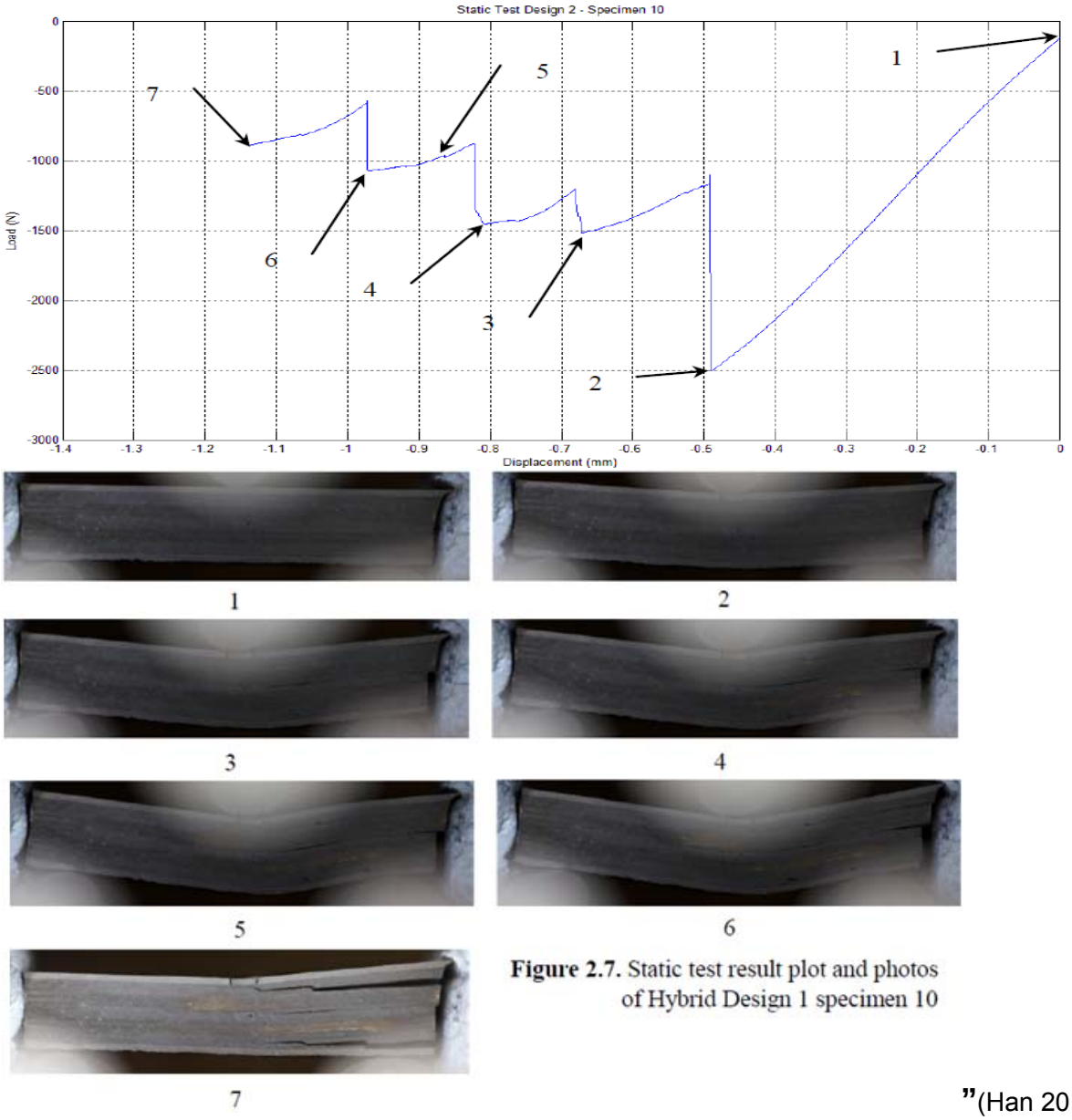

Figure 2.7. Static test result plot and photos of Hybrid Design 1 specimen 10

"(Han 2013)

APPENDIX E

TITLE **Ji Han's MSc thesis (Han 2013) - Chapter 2 - Experimental work**
Static test results.
Hybrid Design 2

Chapter 2 (Han 2013)

Static Test – Hybrid Design 2

"2.4 Static Test of Hybrid Design 2" (Han 2013)

"As presented in Appendix A, Hybrid Design 2 is a 24 plies composite laminate composed of 16 plies of carbon fibre reinforced laminate and 8 plies of glass fibre reinforced laminate as well as Hybrid Design 1, but possesses a $[(0_C)_2/(\pm 45_G)/(90_C)_4/(\pm 45_G)/(90_C)_2]_s$ stacking sequence. Seven short specimens were selected to perform the static test, which were 1, 2, 3, 6, 7, 9, and 10. Furthermore, specimen 9 and 10 were polished before performing the static test. How the static tests of Hybrid Design 2 were performed and the discussion of the results is demonstrated in this section." (Han 2013)

"2.4.1 Static Test 3 - Hybrid Design 2" (Han 2013)

" The same as All Carbon Design and Hybrid Design 1, the static tests were performed on the Instron 3369 at room temperature with the three point bending rig. The specimen was placed on the two supports, and some blue tacks were used to prevent it from moving. A digital camera equipped with micro lens was also utilised during the test to record the failure. A pre-load, about 150 N, was added on the specimen to make sure the loading nose was touched with the specimen. Then the static test was performed at a speed of 0.1 mm/min. Tests were stopped when the load versus displacement plot was becoming stable. The results of the static test were analysed using Matlab as well." (Han 2013)

"2.4.2 Results of Static Test 3- Hybrid Design 2" (Han 2013)

" As same as the previous static tests, the data were collected and then analysed with Excel and Matlab. The initial displacement of each specimen was returned to zero using Excel. As shown in figure 2.9 (of this Appendix), the seven curves in different colours represent the seven specimens, specimen 1 in red, specimen 2 in purple, specimen 3 in green, specimen 6 in pink, specimen 7 in blue, specimen 9 in black, and specimen 10 in cyan." (Han 2013)

“

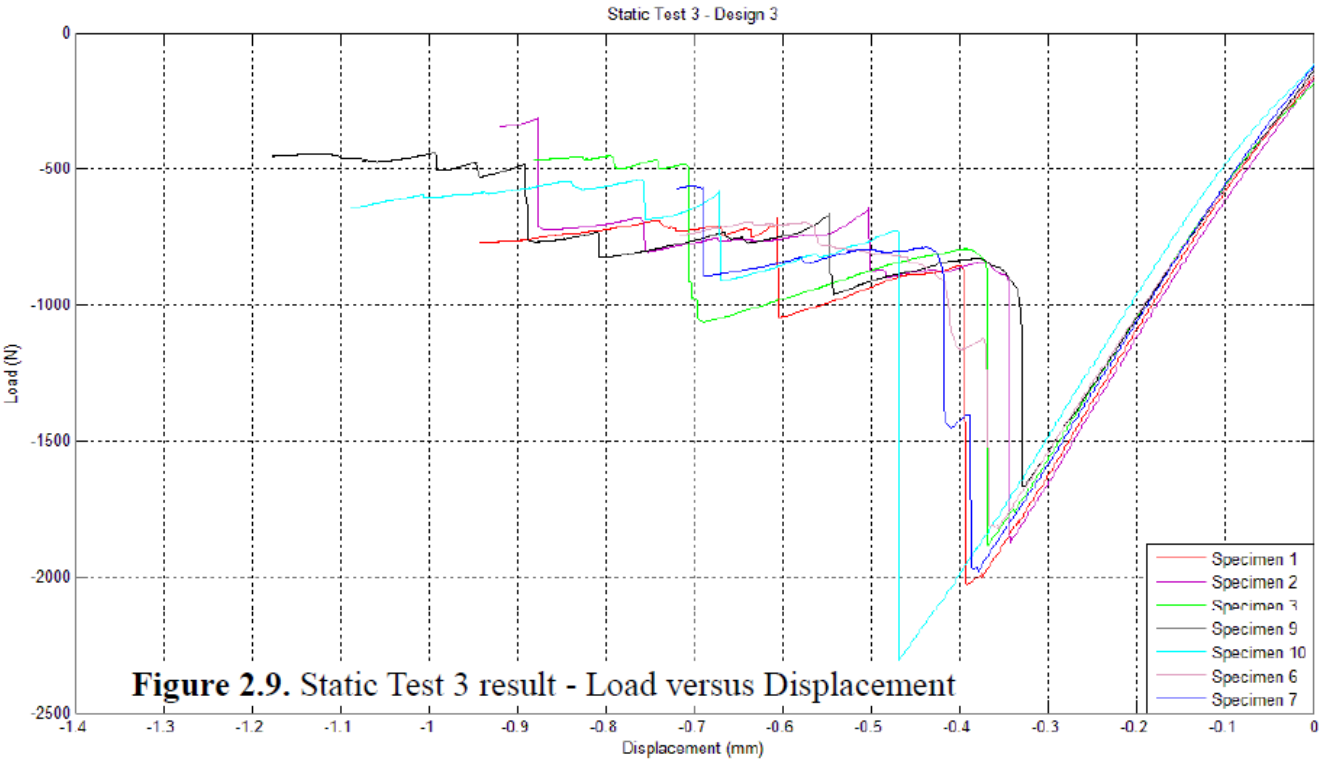

Figure 2.9. Static Test 3 result - Load versus Displacement

Table 2.3. Static Test 3 result - Failure load

Specimens	Failure Load (N)
1	2027
2	1876
3	1888
6	1827
7	1981
9	1668
10	2307
Average	1939
S.D.	184

“ (Han 2013)

“ As shown in figure 2.9 (of this Appendix) that the first failure of all the seven laminates occurred from -0.3 mm to -0.5 mm. But, all the curves show a same trend. From table 2.3 (of this Appendix), the failure load of the specimens differed one from another, for the lowest at 1668 N and the highest at 2307 N. The average failure load was 1939 N that was about 500 N

lower than All Carbon Design and Hybrid Design 1.The standard deviation of the failure loads listed above was calculated as 184N.

A digital camera was used to record the Static Test 3, and photos were taken while a crack occurs and before the next failure occurs as well as at the start of the test and at the end of the test. Images of specimen 10, which was polished before the test, and its load versus displacement plot were utilised to demonstrate the failure behaviour of Hybrid Design 2, as shown in figure 2.10 (of this Appendix). The plies of specimen 10 were pointed out in a photo shown as figure 2.11 (from this Appendix).

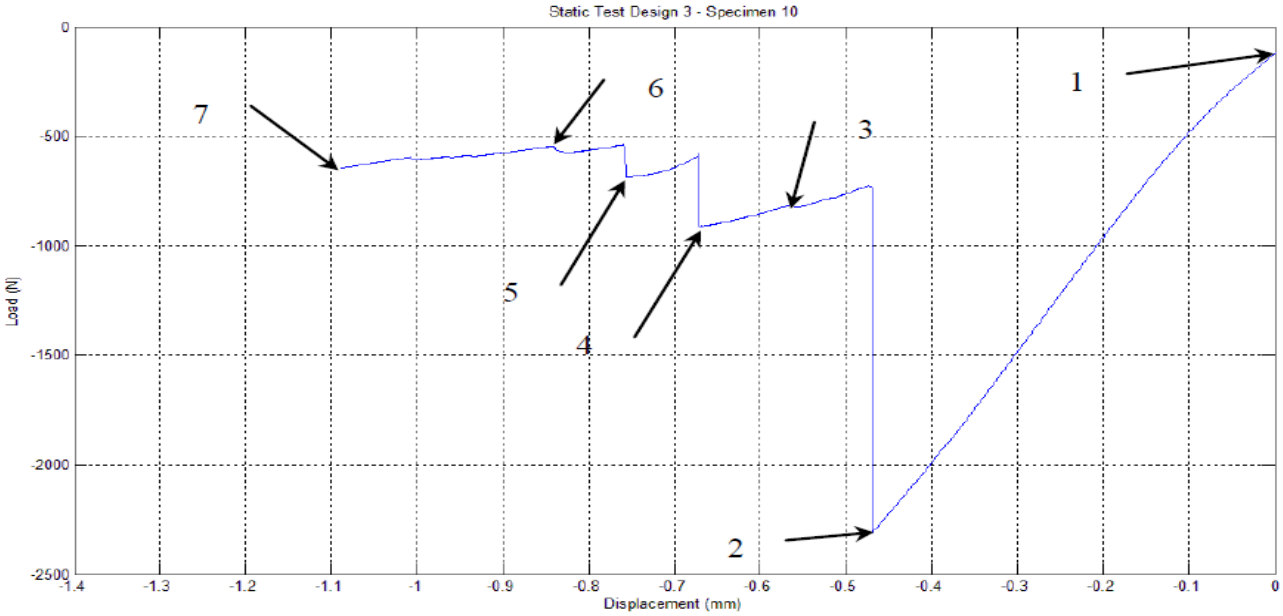

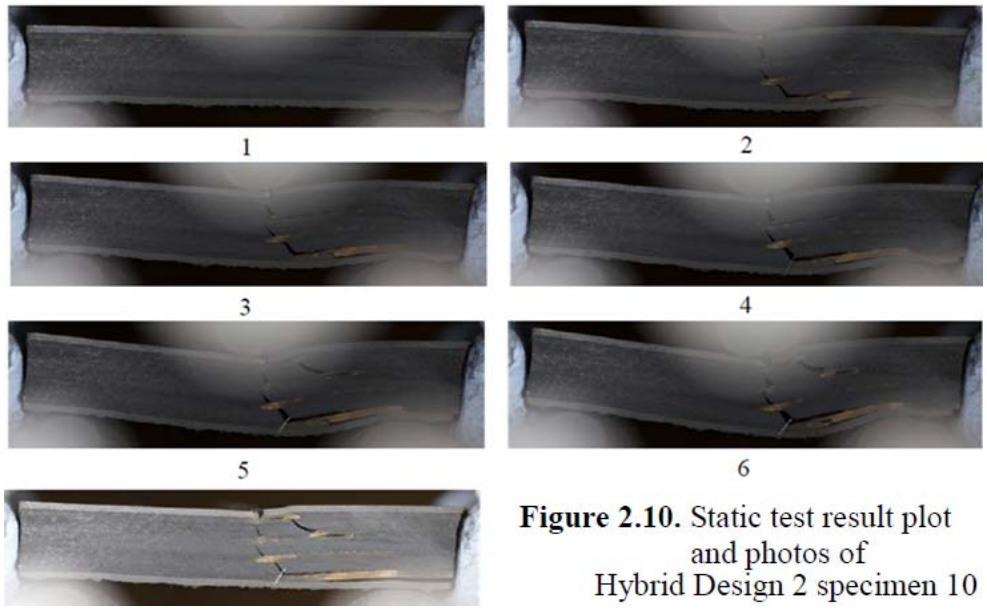

Figure 2.10. Static test result plot and photos of Hybrid Design 2 specimen 10 " (Han 2013)

APPENDIX F

TITLE **Ji Han's MSc thesis (Han 2013) - Chapter 4 - Experimental work**
Fatigue test results.
All Carbon Design

Chapter 4 (Han 2013)

Fatigue Test – All Carbon Design

"4.1 Introduction and Objectives" (Han 2013)

"Fatigue is known as brittle failure under cyclic stress below the level of general yield, and it is a significantly important parameter while designing composite laminates. The fatigue test was established to investigate the fatigue behaviour and work out the S-N curves of the design laminated composites. Both short specimens and long specimens were utilised to perform the fatigue tests at 90%, 80%, and 70% of the failure stress. The fatigue tests were performed on the Dartec HC10, with a 10 kN crosshead. The objectives of performing the fatigue tests are listed below:

1. Study the fatigue behaviour of All Carbon Design and Hybrid Design 1.
2. Work out the S-N curves of the two designs.
3. Observe the crack initiation in the specimens with the utilisation of CT-scan.
4. Compare the fatigue behaviour of All Carbon Design and Hybrid Design 1." (Han 2013)

"4.2 Fatigue Test of All Carbon Design" (Han 2013)

"All Carbon Design is an all carbon layers laminate, which possesses a lay-up of $[(0/45/90/-45)_3]_s$. This section illustrates how the fatigue test was performed and presents the result of the test. Moreover, the fatigue behavior and the loading capacity of All Carbon Design are demonstrated in the section, as a result of analyzing the S-N (Failure Shear Stress –Cycles to Failure) curve and L-N (Peak Load –Cycles to Failure) curve." (Han 2013)

"4.2.1Fatigue Test 1 - Fatigue Test of All Carbon Design" (Han 2013)

"In order to study the fatigue behaviour of All Carbon Design, a series fatigue tests were performed with the utilisation of the Dartec HC10. Furthermore, the fatigue tests were performed under the same three point bending rig as used in the static test. Three 100 cycles test, three 1,000 cycles test, and three 10,000 cycles test were required to be accomplished in the fatigue test 1. Therefore, the applied loads of 100, 1000, 10000 cycle fatigue tests were required to be calculated before starting the test, which should be obtained respectively form 90%, 80%, and 70% of the failure stress of All Carbon Design. Due to the experimental dimensions of the specimens were not the same, which had caused that different specimens have different failure stresses. Therefore, engineer's bending theory was utilised in order to calculate or predict the applied load of each specimen simply and quickly. As shown in equation (5.1) (of this Appendix)

that was used to calculate the bending stress σ of the specimen, in which *M* is the moment about the neutral axis, *z* is the perpendicular distance to the neutral axis, and I is the second moment of area.

$$\sigma = \frac{M \times z}{I} \tag{5.1}$$

In this three point bending problem, assume that *F* is the applied load and *L* is the span length, thus the bending moment $M=FL/4$, the perpendicular *y* equals to halve the thickness *t*, and the second moment of area I is known as $I=bt^3/12$. Therefore, we obtain equation (5.2) (of this Appendix) for calculating the bending stress in this problem. The maximum stress of All Carbon Design, σ_x=670.63 MPa, is calculated while *F* is the average failure load of the seven specimens obtained from the static test, *b* and *t* are the average width and thickness of the specimens, and the span length *L* is 14 mm.

$$\sigma = \frac{3FL}{2bt^2} \tag{5.2}$$

Equation (5.3) (of this Appendix) could be transformed from (5.3) (of this Appendix), which is used to calculate the applied loads of different specimens while σ equals to 90%, 80%, and 70% of the maximum stress.

$$F = \frac{2\sigma bt^2}{3L} \tag{5.3}$$ **“** (Han 2013)

“All the fatigue tests were performed at a test frequency of 2 Hz, with the applied loads listed in the Table D.1 (Appendix J). Moreover, the loading ratio R, which is the ratio between the maximum load to the minimum load in a cycle, was kept at R=10. After the specimen was placed properly on the support rollers with some blue sticks preventing the specimen from moving during the test, a pre-load (about 10% of the applied load) was added on the specimen to make sure the loading nose was touching the specimen. Due to the data was collected by the software which required to set an offset after the pre-load was added, thus the applied load data collected by the software was the applied load without the pre-load. Therefore, the pre-load value should be added on the collected applied load to obtain the actual applied load while analysing the result. The test was stopped while the specimen failure occurred, and the number of cycles to the failure was read from the computer and then collected.

The short specimens were utilised to perform the 100 and 1,000 cycles fatigue tests, while the long specimens were selected to perform the 10,000 cycles test. Both displacement control and load control were utilised in the fatigue test. The 100 cycles tests were performed under displacement control, while the 1,000 cycles and 10,000 cycles tests were performed under load control. This was due to the deformation of the specimen caused by the cyclic loading. If the test

was performed under load control, the specimen would not be totally destructed, as the test was stopped while the failures just occurred in the laminate. But the actual peak load was not able to reach the required value while the loading nose had reached its required displacement, and the cyclic load was dropping continuously while the cycle number was increasing. As presented in Figure 4.1 (of this Appendix), the peak load of specimen 17 was dropping persistently from 1960 N to 1770 N in about 300 cycles till a load drop appeared when the specimen was destructed. If the number of cycles increased, the cyclic load would drop more, which had caused the problem that some specimens did not show any failures while they had already significantly exceeded the cycles when they should break. If the test was performed under load control, the applied load would not drop during the test. But the specimen might be totally broken, for the loading nose was still trying to reach the required value while failures had already occurred. Therefore, low cycle tests such as 100 cycles tests were performed under displacement control, while 1,000 cycles and 10,000 cycles tests were performed under load control.

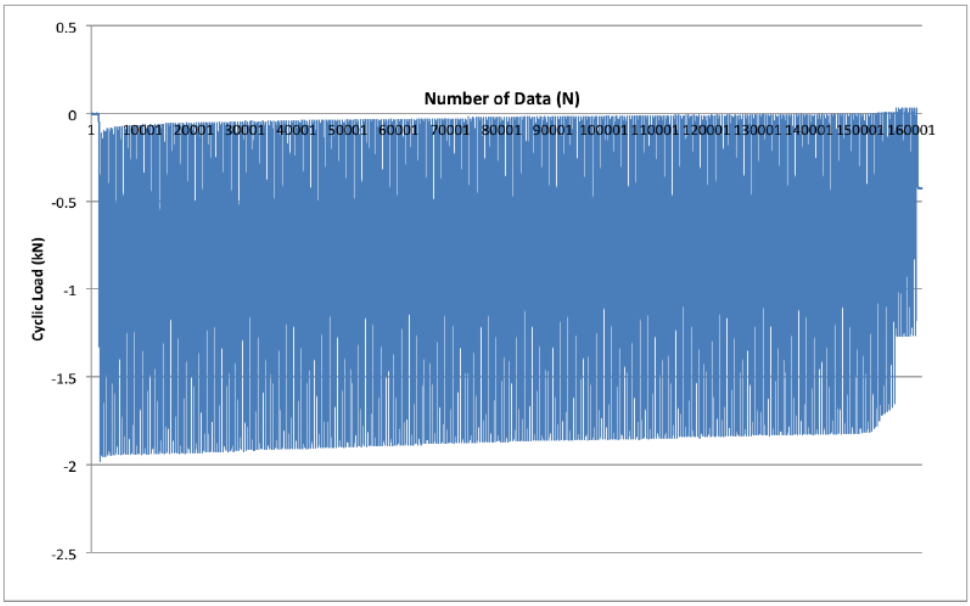

Figure 4.1. Cyclic load plot of specimen 17

" (Han 2013)

“4.2.2 Results of Fatigue Test 1” (Han 2013)

”

Table 4.1. peak load per unit width of Static Test 1 specimens

Specimen	Failure Load (N)	Cycle	Peak Load per Unit Width (N/mm)
1	2449	1	353.39
2	2663	1	387.63
3	2485	1	344.18
9	2542	1	370.55
10	2318	1	337.41
3L	2554	1	347.01
4L	2597	1	354.78

Table 4.2. Failure stress and peak load per unit width of Fatigue Test 1 specimens

Specimen	Percentage of Stress	Control Type	Applied Load (N)	Cycle	Peak Load per Unit Width (N/mm)
13	90%	Displacement	2055	134	297.40
17	90%	Displacement	2045	319	299.41
18	90%	Displacement	2210	279	301.91
20	80%	Displacement	1775	1095	260.65
24	80%	Load	1950	492	285.92
5L	80%	Load	2100	915	286.10
1L	70%	Load	1800	1140	245.23
2L	70%	Load	1800	9500	243.57
6L	70%	Load	1800	6967	251.05

“(Han 2013)

APPENDIX G

TITLE **Ji Han's MSc thesis (Han 2013) - Chapter 4 - Experimental work**
Fatigue test results.
Hybrid Design 1

Chapter 4 (Han 2013)

Fatigue Test – Hybrid Design 1

" 4.3 Fatigue Test of Hybrid Design 1" (Han 2013)

"Hybrid Design 1 is composed of glass fibre layers and carbon fibre layers, which possesses a stacking sequence of $[(0_C)_2/(\pm45_C)_2/(\pm45_G)_2/(\pm45_C)]_s$. The description of the fatigue test and the result of the test are presented in the section. Moreover, the S-N curve and L-N curve were built in order to study the fatigue behaviour and loading capacity of Hybrid Design 1" (Han 2013).

"4.3.1 Fatigue Test 2 - Hybrid Design 1" (Han 2013)

"In order to study the fatigue behaviour of Hybrid Design 1, a series fatigue tests were performed on the Dartec HC10 under the three point bending rig. Three 100 cycles test, three 1,000 cycles test, and three 10,000 cycles test were required to be accomplished in the Fatigue Test 2. The applied loads of 100, 1000, 10000 cycle fatigue tests were calculated respectively from 90%, 80%, and 70% of the failure stress of Hybrid Design 1 with the same method as Fatigue Test 1, which are shown in Appendix J.

All the fatigue tests were performed at a loading ratio R=10 with a 2 Hz test frequency, and performed under the applied loads listed in the Table D.2 (shown in Appendix J). After the specimen was placed properly on the support rollers, a pre-load (about 10% of the applied load) was added on the specimen to make sure the loading nose was touching the specimen. The actual applied load was the sum of the collected applied load value and the pre-load value, due to the offset was set after the pre-load was added. The test was stopped while the specimen failure occurred, and the number of cycles to the failure was read from the computer.

As the applied load was kept dropping during the test if the specimen was performed under displacement control due to the deformation of the specimen, which would cause the problem that the specimen did not fail at when it expected. Therefore, most 100 cycles tests were performed under displacement control, while 1,000 cycles and 10,000 cycles tests were performed under load control. The same as Fatigue Test 1, short specimens were used to perform 100 and 1,000 cycles tests, and long specimens were selected to perform 10,000 cycles tests." (Han 2013).

“4.3.2Results of Fatigue Test 2” (Han 2013)

“As the same as All Carbon Design, the required data of Hybrid Design 1 were calculated with the same equation in the previous chapter and then listed in Table 4.3 and Table 4.4 respectively. The S-N curve and L-N curve of Hybrid Design 1 were created based on the two tables by the same method as All Carbon Design, as presented in Figure 4.5 and Figure 4.6respectively.” (Han 2013).

”

Table 4.3. Failure stress and peak load per unit width of Static Test 2 specimens

Specimen	Failure Load (N)	Cycle	Peak Load per Unit Width (N/mm)
1	2552	1	369.86
2	2577	1	374.56
3	2535	1	366.33
9	2588	1	373.45
10	2506	1	361.10
3L	2718	1	373.87
4L	2436	1	369.65

Table 4.4. Failure stress and peak load per unit width of Fatigue Test 2 specimen

Specimen	Percentage of Stress	Control Type	Applied Load (N)	Cycle	Peak Load per Unit Width (N/mm)
4	90%	Displacement	2170	99	312.68
6	90%	Displacement	2240	130	327.96
11	90%	Load	2000	73	288.60
15	80%	Load	2000	1700	288.60
16	80%	Load	2000	1050	290.70
5L	80%	Load	1900	537	292.31
1L	70%	Load	1600	19820	242.06
2L	70%	Load	1950	13722	265.31
6L	70%	Load	1900	6788	258.50

“(Han 2013)

APPENDIX H

TITLE **Ji Han's MSc thesis (Han 2013)**
Specifications and Experimental Setup

"Specifications and Experimental Setup" (Han 2013)

"A.1 Specifications of Specimens" (Han 2013)

"There are three designs of specimens which were tested in the project, one carbon fibre reinforced composite laminate and two carbon fibre and glass fibre reinforced composite laminates. The WHMS 417 Type 3 carbon fibre prepreg and WHMS 405 glass fibre prepreg were utilised in the project for manufacturing the specimens. **As the project is a joint project, Jony (Author of this thesis) who is from Agusta-Westland designed these specimens and provided the theoretical specifications of the designs" (Han 2013) (Hybrid Design 1 and Hybrid Design 2)**."

"A.1.1 Specifications of the Three Designs" (Han 2013)

" All Carbon Design is a 24 plies composite laminates, which all the lamina are reinforced by carbon fibre. The design thickness of Design1 is 3.00 mm, for the thickness of each carbon ply is 0.125 mm. Moreover, the design width is 5.96 mm and the design length is 16 (the calculation of design width and length will be illustrated in the following section). The layupof this 24 plies symmetric composite laminate is $[(0/45/90/-45)_3]_s$, as shown in Table A.1 (of this Appendix).

Table A.1. Layup of All Carbon Design

Ply	Angle	Material
1	0	Carbon
2	45	Carbon
3	90	Carbon
4	-45	Carbon
5	0	Carbon
6	45	Carbon
7	90	Carbon
8	-45	Carbon
9	0	Carbon
10	45	Carbon
11	90	Carbon
12	-45	Carbon

" (Han 2013)

"Hybrid Design 1 is a 24 plies composite laminates as well, which is composed of 16 plies of carbon fibre reinforced laminae and 8 plies of glass fibre reinforced lamina.

The design thickness of Hybrid Design 1 is 3.136 mm, for the thickness of each carbon ply is 0.125 mm while the thickness of each glass ply is 0.142 mm. Moreover, the design width and length are the same as All Carbon Design, which are 5.96 mm and 16 mm respectively. The stacking sequence of this 24 plies symmetric composite laminate is $[(0_C)_2/(\pm45_C)_2/(\pm45_G)_2/(\pm45_C)_2]_s$, as shown in Table A.2 (of this Appendix).

Table A.2. Layup of Hybrid Design 1

Ply	Angle	Material
1	0	Carbon
2	0	Carbon
3	45	Carbon
4	-45	Carbon
5	45	Carbon
6	-45	Carbon
7	45	Glass
8	-45	Glass
9	45	Glass
10	-45	Glass
11	45	Carbon
12	-45	Carbon

Hybrid Design 2 is a 24 plies composite laminates composed of 16 plies of carbon fibre reinforced laminae and 8 plies of glass fibre reinforced lamina same as Hybrid Design 1. The design thickness of Hybrid Design 2 is 3.136 mm, which is the same as Hybrid Design 1. Moreover, the design width and length are the same as All Carbon Design and Hybrid Design 1, which are 5.96 mm and 16 mm respectively. The stacking sequence of this 24 plies symmetric composite laminate is $[(0_C)_2/(\pm45_G)/(90_C)_4/(\pm45_G)/(90_C)_2]_s$, as shown in Table A.3 (of this Appendix).

Table A.3. Layup of Hybrid Design 2

Ply	Angle	Material
1	0	Carbon
2	0	Carbon
3	45	Glass
4	-45	Glass
5	90	Carbon
6	90	Carbon
7	90	Carbon
8	90	Carbon
9	45	Glass
10	-45	Glass
11	90	Carbon
12	90	Carbon

" (Han 2013)

"A.1.2 Calculation of Width and Length" (Han 2013)

"The calculation of the width and length of the specimens are based on D 2344/2344M standard test method for short-beam strength of polymer matrix composite materials and their laminates issued by ASTM International in 2006.

In the D 2344/2344M standard, the width of the specimen is recommended as 2 times of its thickness (specimen width, b = thickness × 2.0)."(Han 2013)

"Thus, the equation of calculating the width of the specimens in this project is presented:

Specimen Width, b = thickness × 1.9

In order to compare the three different designs, the width of the specimens should be equal. The thickness here is chosen as 3.136 mm, for the thickness of Hybrid Design 1 and Hybrid Design 2 are bigger than All Carbon Design. Therefore, the width of the specimens are calculated as 5.96 mm, as shown below:

Specimen Width, b = 3.136 mm × 1.9 = 5.96 mm

In the D 2344/2344M standard, the span length between the supports rollers is recommended as 4 times of thickness of the specimen. Furthermore, the specimen should be overhung at least 2 mm at each side on the side supports. Therefore, the equation of calculating the length of the specimen inthis project is shown:

Specimen Length,L ≥ thickness × 4.0 + 4 mm

In order to compare the three different designs, the length of the specimens should be equal as well. The thickness here is selected as 3.136 mm for the same reason as illustrated above. Thus, the length of the specimens shouldbe at least 16.54 mm, as shown below:

Specimen Length, L ≥ 3.136 mm × 4.0 + 4 mm = 16.54 mm "(Han 2013)

"A.2 Manufacturing of Composite Laminates" (Han 2013)

"Preparing specimens is significant in the 'Fatigue testing of thick composite laminates' project, for the manufacturing process is highly related to the quality of the specimens and it may affect the results of the static test and fatigue test. Generally, there are three steps in manufacturing a composite laminate, which are preparing constituent plies, laying-up, and curing (Jones 1999).

In the project, carbon fibre prepreg tape and glass fibre prepreg tape were utilised as the constituent materials. Firstly, the prepreg tapes were cut into designated angles and required dimensions, as shown in Figure A.1 (of this Appendix). The accomplished prepreg plies are presented in Figure A.2 (of this Appendix), which the black ones are carbon fibre prepreg plies and the red ones are glass fibre prepreg plies. Then, they were laid-up by hand according to the requirements of the three designs of composite laminates, as shown in Figure A.3 (of this Appendix). Each time, after laying-up a group of four layers, the laminates would be putted into a vacuum bag with two valves to be vacuumed and then standing for about 10 minutes, as shown in Figure A.4 and Figure A.5 (of this Appendix) respectively (the gas-pressure meter in the figure was utilised to check whether there is leaking or not). Kinawy (2011) pointed out in his PH.D. thesis that the vacuum process was established to ensure a homogenous thickness of the prepreg, and release the air voids in the composite laminates. Moreover, the two vacuum valves was utilised to ensure the vacuum pressure is distributed uniform over the composite laminates. After all the layers were laid-up, some cork tapes were placed around the laminates to prevent excess resin from flowing sidewise. After that, the laminates were putted into the bag and then vacuumed. At last, the composite laminates in the vacuum bag were putted into the autoclave for the curing process. After accomplished these steps, the required composite laminates of the three designs were manufactured.

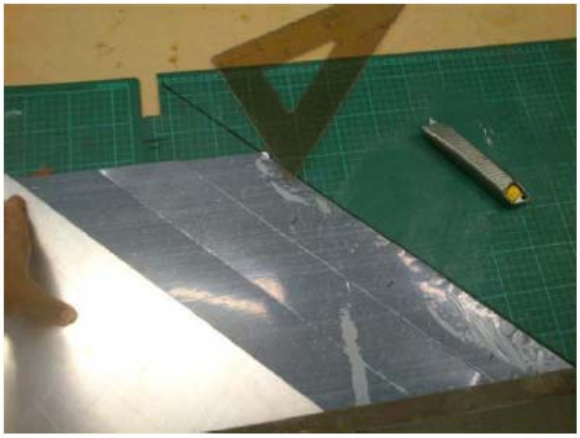

Figure A.1. Cutting prepreg tape

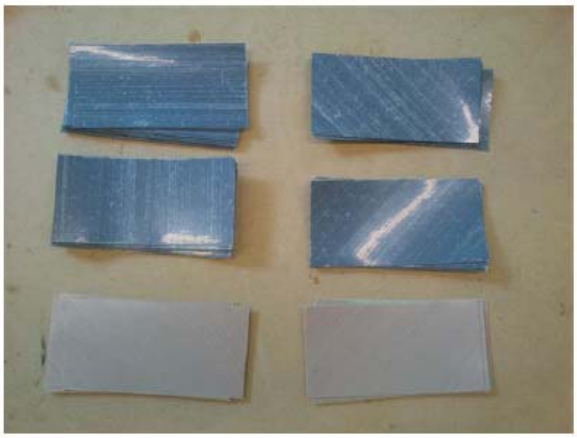

Figure A.2. The accomplished prepreg plies "

(Han 2013)

"

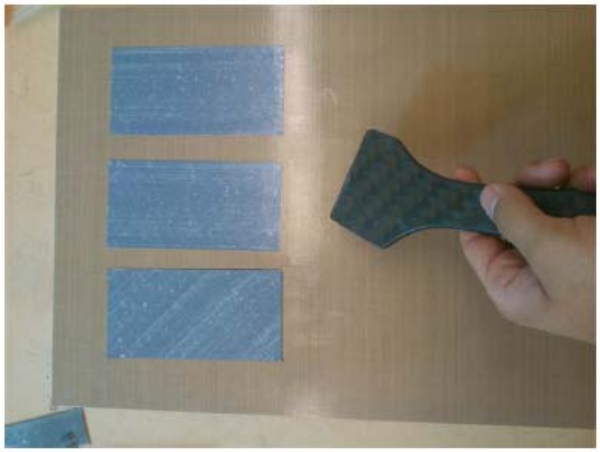

Figure A.3. Laying-up prepreg plies

Figure A.4. Vacuum the laminates

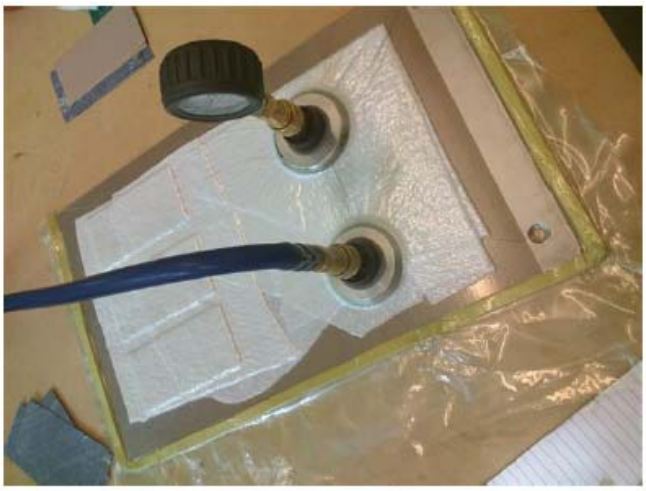

Figure A.5. Standing for 10 minutes

" (Han 2013)

"As the required laminates were manufactured, it came to the machining process which the plates were cut into specimens with required dimension. Cutting specimens from plates should avoid notches, undercuts, rough surface, and delaminations, which will affect the quality of the specimens and even affect the results of static test and fatigue test (D 2344/2344M 2006). The plates were cut into rectangular shape specimens according to the designed specifications illustrated in the previous section. As shown in Figure A.6, from top to bottom are All Carbon Design, Hybrid Design 1, and Hybrid Design 2. Then the specimens were labeled in roman numerals with white paint pen, as presented in Figure A.7 (of this Appendix).

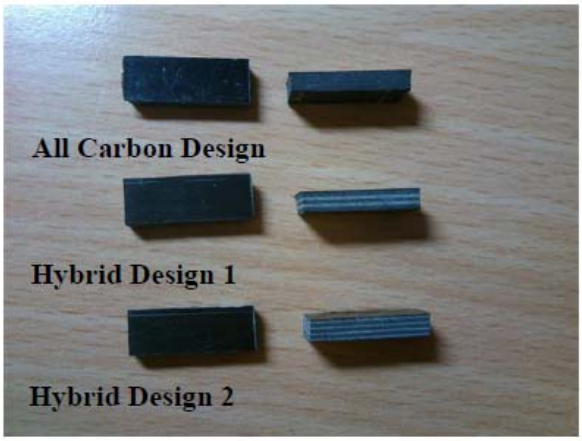

Figure A.6. Specimens of the three designs

Figure A.7. Labeled specimens

After labeling, the width and length of the specimens were measured with slide caliper and the thickness of the specimens were measured with micrometer, as shown in Figure A.8 and Figure A.9 respectively. The data of these measurements were collected and made into spreadsheets for later utilisation. The measurement data spreadsheets of All Carbon Design, Hybrid Design 1,

and Hybrid Design 2 are presented in Appendix B. As shown in the spreadsheets, the width, thickness, and length of the experimental designs are all a bit larger than the theoretical designs.

Figure A.8. Measure width and length with slide caliper

Figure A.9. Measure the thickness with micrometer

Moreover, some longer specimens of All Carbon Design and Hybrid Design 1 were manufactured as well, in order to investigate whether there is a difference of static failure behaviour between short specimens (about 18 mm long) and long specimens (about 25 mm long). And these long specimens were used to perform 10,000 cycles fatigue test. The dimensions of these specimens were measured with slide caliper and micrometer, and the data were collected and made into spreadsheets, as shown in Appendix I. **“** (Han 2013)

“A.3 Test Machines and Test Rig” (Han 2013)

“In the ‘Fatigue testing of thick composite laminates’ project, two types of experimental tests(static test and fatigue test)had to be conducted. Static test was established to measure the failure load of the specimens and study the static failure behaviour of the composite laminates, while fatigue test was established to study the fatigue behaviour of the laminates and estimate the fatigue lifetime of the laminated composites. Instron 3369 (Instron 2013) and Dartec HC10, shown in Figure A.10 and Figure A.11 (of this Appendix) respectively, were utilised in the project to perform static test and fatigue test respectively.

Figure A.10. Instron 3369

Figure A.11. Dartec HC10

The test rig for performing the static test and fatigue test was a three point bending rig with one cylinder loading nose and two cylinder supports, as shown in Figure A.12 (of this Appendix). The diameter of the loading nose and the two supports were the same, which was 6 mm. The centre distance between the two cylinder supports were 14 mm, for the span length between the supports rollers was recommended as 4 times of the thickness of the specimen which is approximately about 14 mm. Moreover, some relevant fittings were manufactured as well, in order to fit the testing rig into the Instron 3369 and the Dartec respectively.**"** (Han 2013)

“

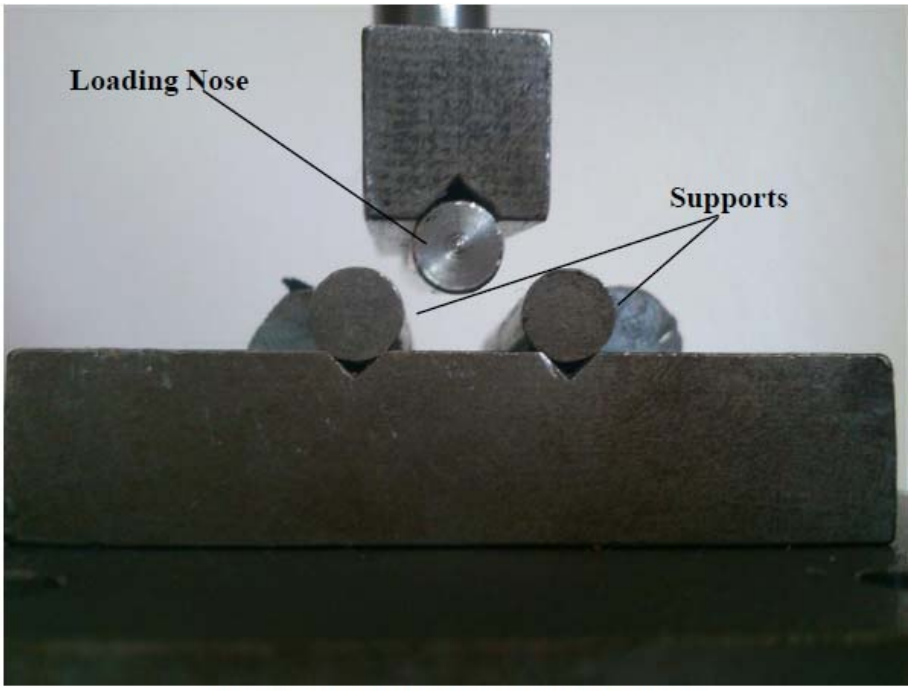

Figure A.12. The three point bending rig

” (Han 2013)

“A.4 Summary” (Han 2013)

”The chapter mainly illustrates the methodology of the ‘Fatigue testing of thick composite laminates’ and briefly demonstrates the testing machines. In the first section, the specifications, for instance the lay-up, the angle of each plies, and the dimension, of the three designed laminated composites are presented and calculated. The following section is mainly about the manufacturing of the laminates, which illustrates the manufacturing processes of the laminates. Moreover, the dimensions of the manufactured specimens are measured,and three measured dimension spreadsheets of the All Carbon Design, the Hybrid Design 1, and the Hybrid Design 2 are presented in the Appendix I. The last section shows the main features of the machines (Instron 3369 and DartecHC 10) which are utilised in the project, as well as the three point bending testing rig that is utilised to perform the static test and fatigue test. The chapter presents the essential requirements of the project, which are regarded as the preparations of the experimental test phase.” (Han 2013)

APPENDIX I

TITLE **Ji Han's MSc thesis (Han 2013)**
Measured Dimension Data of the Designs

Measured Dimension Data of the Designs (Han 2013)

Average values of loads and gemetric dimentions of the laminate that has been tested:

”

Table 3.4. Specifications and applied loads of the experimental designs

Design	Width b (mm)	Total thickness t_{total} (mm)	Carbon Ply Thickness t_{carbon} (mm)	Glass Ply Thickness t_{glass} (mm)	Applied Load P (N)
All Carbon Design	7.06	3.330	0.139		2507
Hybrid Design 1	6.92	3.367	0.139	0.143	2559
Hybrid Design 2	6.91	3.449	0.139	0.153	1939

„ (Han 2013)

All Carbon Design:

“ Measured Dimension Data of All Carbon Design (Short Specimen)

Table B.1. Measured dimension data of All Carbon Design

Design 1							
Specimen	Thickness (mm)		Average T (mm)	Width (mm)		Average W (mm)	Length (mm)
	Side 1	Side 2		Side 1	Side 2		
1	3.34	3.38	3.36	6.94	6.91	6.93	18.82
2	3.40	3.34	3.37	6.84	6.90	6.87	18.58
3	3.30	3.29	3.29	7.26	7.17	7.22	18.61
9	3.41	3.37	3.39	6.90	6.82	6.86	18.62
10	3.33	3.33	3.33	6.88	6.85	6.87	19.08
13	3.37	3.38	3.37	6.88	6.93	6.91	18.09
17	3.38	3.38	3.38	6.84	6.82	6.83	18.64
18	3.36	3.34	3.35	7.32	7.32	7.32	18.40
20	3.34	3.29	3.32	6.86	6.76	6.81	18.74
24	3.31	3.38	3.34	6.81	6.82	6.82	18.29

Measured Dimension Data of All Carbon Design L (Long Specimen)

Table B.4. Measured dimension data of All Carbon DesignL

Design 1L							
Specimen	Thickness (mm)		Average T (mm)	Width (mm)		Average W (mm)	Length (mm)
	Side 1	Side 2		Side 1	Side 2		
1	3.33	3.32	3.33	7.38	7.30	7.34	26.54
2	3.33	3.33	3.33	7.40	7.38	7.39	26.50
3	3.30	3.27	3.29	7.37	7.35	7.36	26.74
4	3.29	3.29	3.29	7.30	7.33	7.32	26.94
6	3.33	3.34	3.34	7.17	7.17	7.17	25.81

„

(Han 2013)

HYBRID DESIGN 1:

" Measured Dimension Data of Hybrid Design1 (Short Specimen)

Table B.2. Measured dimension data of Hybrid Design 1

Design 2							
Specimen	Thickness (mm)		Average T (mm)	Width (mm)		Average W (mm)	Length (mm)
	Side 1	Side 2		Side 1	Side 2		
1	3.39	3.38	3.38	6.89	6.91	6.90	18.60
2	3.37	3.41	3.39	6.87	6.88	6.88	18.81
3	3.27	3.35	3.31	6.94	6.90	6.92	18.62
4	3.39	3.39	3.39	6.93	6.94	6.94	17.71
6	3.39	3.42	3.40	6.86	6.80	6.83	17.99
9	3.40	3.40	3.40	6.94	6.92	6.93	18.37
10	3.41	3.39	3.40	6.95	6.93	6.94	17.97
11	3.27	3.29	3.28	6.90	6.96	6.93	18.41
15	3.36	3.35	3.36	6.95	6.91	6.93	18.27
16	3.34	3.39	3.37	6.86	6.90	6.88	18.26

Measured Dimension Data of Hybrid Design 1L (Long Specimen)

Table B.5. Measured dimension data of Hybrid Design 1L

Design 2L							
Specimen	Thickness (mm)		Average T (mm)	Width (mm)		Average W (mm)	Length (mm)
	Side 1	Side 2		Side 1	Side 2		
1	3.30	3.32	3.31	6.62	6.59	6.61	24.41
2	3.47	3.44	3.46	7.36	7.34	7.35	25.14
3	3.29	3.39	3.34	7.27	7.26	7.27	25.26
4	3.33	3.36	3.35	6.58	6.59	6.59	24.97
5	3.34	3.38	3.36	6.50	6.49	6.50	25.39
6	3.40	3.42	3.41	7.35	7.34	7.35	24.91

HYBRID DESIGN 2:

Measured Dimension Data of Hybrid Design 2

Table B.3. Measured dimension data of Hybrid Design 2

Design 3							
Specimen	Thickness (mm)		Average T (mm)	Width (mm)		Average W (mm)	Length (mm)
	Side 1	Side 2		Side 1	Side 2		
1	3.44	3.46	3.45	6.91	6.86	6.89	19.02
2	3.44	3.43	3.43	6.96	6.95	6.96	18.22
3	3.38	3.38	3.38	7.01	6.95	6.98	18.68
6	3.50	3.45	3.47	6.86	6.89	6.88	18.54
7	3.47	3.50	3.48	6.82	6.82	6.82	17.96
9	3.48	3.47	3.48	6.93	6.82	6.88	18.28
10	3.36	3.33	3.34	6.97	6.94	6.96	18.67

"

(Han 2013)

APPENDIX J

TITLE **Ji Han's MSc thesis (Han 2013)**
Load that has been used in the fatigue experiments.

"Applied load of **All Carbon Design"** (Han 2013) – Used to proceed with the fatigue experiments

"

Table D.1. Applied load of All Carbon Design

Design 1								
Specimen	Width b (mm)	Thickness d (mm)	span (mm)	σ (MPA)	F (N)	90%F (N)	80%F (N)	70%F (N)
13	6.91	3.37	14.00	670.63	2506.12	2255.51	2004.89	1754.28
17	6.83	3.38	14.00	670.63	2491.83	2242.64	1993.46	1744.28
18	7.32	3.35	14.00	670.63	2623.40	2361.06	2098.72	1836.38
20	6.81	3.32	14.00	670.63	2397.10	2157.39	1917.68	1677.97
24	6.82	3.34	14.00	670.63	2429.63	2186.67	1943.71	1700.74
1L	7.34	3.33	14.00	670.63	2599.25	2339.33	2079.40	1819.48
2L	7.39	3.33	14.00	670.63	2616.96	2355.26	2093.57	1831.87
5L	7.34	3.35	14.00	670.63	2630.57	2367.51	2104.45	1841.40
6L	7.17	3.34	14.00	670.63	2554.32	2298.89	2043.46	1788.03

Applied loads of **Hybrid Design 1**

Table D.2. Applied loads of Hybrid Design 1

Design2								
Specimen	Width b (mm)	Thickness d (mm)	L (mm)	σ (MPA)	F (N)	90%F (N)	80%F (N)	70%F (N)
4	6.94	3.39	14.00	679.11	2579.17	2321.25	2063.33	1805.42
6	6.83	3.40	14.00	679.11	2553.29	2297.96	2042.63	1787.30
11	6.93	3.28	14.00	679.11	2411.03	2169.92	1928.82	1687.72
15	6.93	3.36	14.00	679.11	2530.07	2277.06	2024.06	1771.05
16	6.88	3.37	14.00	679.11	2526.79	2274.11	2021.43	1768.75
1L	6.61	3.31	14.00	679.11	2341.95	2107.76	1873.56	1639.37
2L	7.35	3.46	14.00	679.11	2845.51	2560.96	2276.41	1991.86
5L	6.50	3.36	14.00	679.11	2373.08	2135.77	1898.47	1661.16
6L	7.35	3.41	14.00	679.11	2763.87	2487.48	2211.09	1934.71

"

(Han 2013)

APPENDIX K

TITLE **Ji Han's MSc thesis (Han 2013)**
Plot and results of the Specimen number 2 for the *All Carbon Design*

Specimen number 2 – All Carbon Design.

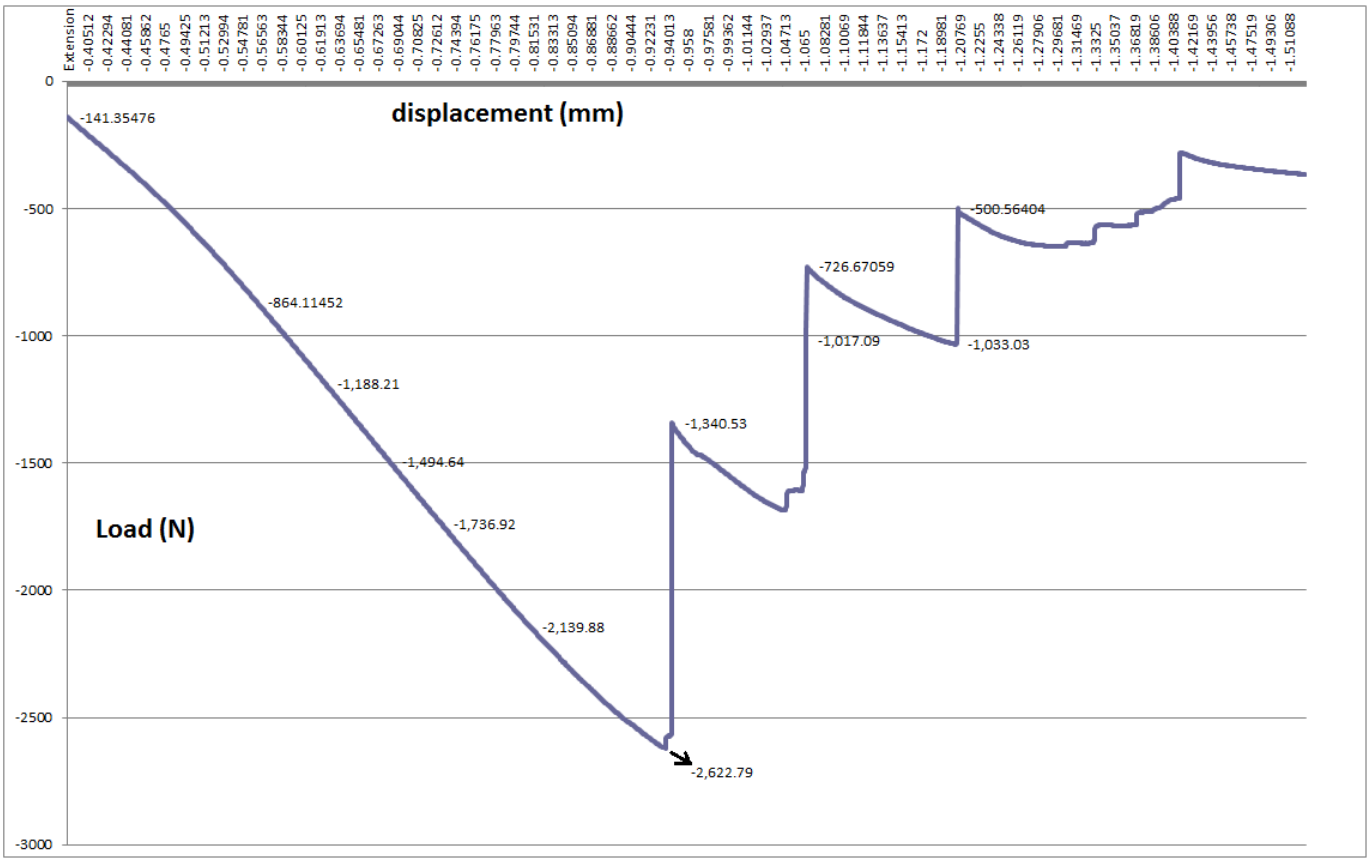

Figure 92 – Load Vs displacement plot for the All Carbon Design, Specimen number 2

APPENDIX L

TITLE **Ji Han's MSc thesis (Han 2013)**
CT scan image – Hybrid Design 1

(Han 2013)

Fatigue Test Results

"CT-Scan Images" (Han 2013)

"CT-Scan images (Figure 4.8 and Figure 69 presented in the Chapter 5, section 5.3, sub-section iv) of the specimens that performed the fatigue tests could assist observing the crack initiation of the specimens that did not show externally and understanding the fatigue behaviour of the designs better. The fatigue tests on All Carbon Design specimen 2L and Hybrid Design 1 specimen 1L were stopped while a sound of crack were heard. Specimen 2L and specimen 1L were used to perform the 10,000 cycles fatigue test at 70% of the static failure stress, which broke at 9500 cycles and 19,820 cycles respectively. The damages in these two specimens of different designs were assessed utilising a CT-Scan system. Slices across the width of the specimens were extracted from the CT-Scan model, in order to illustrate the crack initiations in the specimens of the two designs." (Han 2013)

Figure 4.8. CT-Scan image of Hybrid Design 1 specimen 1L

APPENDIX M

TITLE **Material properties**

Materials

Table 20 lists the material properties that have been used in this work.
It should be noted that the values stated in Table 20 have been derived using composite laminates made of orthotropic UD plies.

Table 20 – List of materials properties - Part 1

	MATERIAL DESIGNATION		
MATERIAL PROPERTY	**Fibredux913C HTA-G (12k)** (used in the carbon plies)	**Fibredux 913G-E-5-30%** (used in the glass plies)	**Fibredux 913** Resin (matrix) (at 70°C)
$E_{1\,Tensile}$ (MPa)	137 000	41 900	3390
$E_{2\,Tensile}$ (MPa)	12 190	11 000	-
$\nu_{12\,Tensile}$	0.294	0.31	-
$\nu_{21\,Tensile}$	0.02616	0.08	-
G_{12} (MPa) **[From CIBA-GEICY (1983)] ****	5 290	4 010	-
ν_{xy} Tensile at 45 degrees to axis 1	0.767	0.62	-
E_X Tensile at 45 degrees to axis 1 (MPa)	20 600	12 980	-
E_Y Tensile at 45 degrees to axis 1 (MPa)	20 600	12 980	-
$E_{11\,Compressive}$ (MPa)	128 250	42 550	-
$E_{22\,Compressive}$ (MPa)	18 520	15 880	-
σ Tensile strength for 0 Degrees (MPa)	1909	991.08	-
σ Tensile strength for 45 Degrees (MPa)	274.29	255.17	-
σ Tensile strength for 90 Degrees (MPa)	59.15	58.27	-
σ Flexural strength for 0 Degrees (MPa)	1836.9	1417.97	-
σ Flexural strength for 90 Degrees (MPa)	83	-	-
σ Compressive strength for 0 Degrees (MPa)	1341	1202.71	-
σ Compressive strength for 45 Degrees (MPa)	250.2	187.59	-
σ Compressive strength for 90 Degrees (MPa)	272	220.89	-

** The value for the Shear Modulus, G_{12}, obtained through the application of the Huber's equation (39) (Craig & Summerscales 1988) on the UD orthotropic carbon ply has presented a difference almost 10% higher than the value of G_{12} given by CIBA-GEICY (1983), which is presented in Table 20. The value obtained through the application of the equation (39) in the UD orthotropic glass ply has presented a difference of near 0.1% lower than the value given by CIBA-GEICY (1983) which is shown in Table 20. The differences between these values could be due to the direct application of the values shown on the Table 20 ($E_{X\ \text{Tensile at 45 degrees to axis 1}}$ and $\nu_{xy\ \text{Tensile at 45 degrees to axis 1}}$) into the equation (39). The values presented in Table 20 are average results over numerous experiments performed to achieve credible material property values.

NOTE: In this thesis, the value for the Shear Modulus G_{12} that has been used was the one given by CIBA-GEICY (1983) (shown in Table 20).

Table 21– List of materials properties - Part 2

	MATERIAL DESIGNATION		
MATERIAL PROPERTY	**Fibredux913C HTA-G (12k)** (used in the carbon plies)	**Fibredux 913G-E-5-30%** (used in the glass plies)	**Fibredux913** Resin (matrix)
ILSS = τ_{zx} for 0 Degrees (MPa)	94.89	90.18	-
ILSS = τ_{zx} for 45 Degrees (MPa)	94.8	-	-
τ_{xy} 45 Degrees (MPa)	137	127.59	-
ε_{eff} (Tensile) for 0 Degrees	0.013934	0.023653	-
ε_{eff} (Tensile) for 90 Degrees	0.004852	0.005297	-
ε_{eff} (Compressive) for 0 Degrees	0.010456	0.028266	-
ε_{eff} (Compressive) for 90 Degrees	0.014687	0.013910	-

All the material properties shown on the Table 20 and Table 21 were taken from CIBA-GEICY (1983), and the coordinate axis x, y, z, 1, 2 and 3 are in regards to the composite laminate as shown in Figure 23.

Table 22 - List of materials properties - Part 3

	MATERIAL DESIGNATION		
MATERIAL PROPERTY	**Fibredux913C XAS** (used in the failure criterion)	**Fibredux 913G-E-5-30%** (used in the glass plies)	**Fibredux913** Resin (matrix)
G_{IC} (N/mm) (Fracture toughness in the longitudinal direction. Mode I, for plies laid up in UD)	0.3150	0.3580	-
G_{IIC} (N/mm) * (Fracture toughness in the longitudinal direction. Mode II, for plies laid up in UD)	0.5833	0.6629	-
σ Tensile Strength (MPa) at 90^oC	-	-	63.0
σ Tensile Strength (MPa) at 70^oC	-	-	65.5
σ Tensile Strength (MPa) at 25^oC (A linear extrapolation has been done to get this value. It was used the tensile strength for 70^oC and 90^oC)	-	-	71.13

FIBRES WITHOUT THE RESIN SURROUNDING IT		
MATERIAL PROPERTY	**TENAX HTA-12K** (Carbon fibre)	**E-GLASS** (Carbon fibre)
$E_{1_{Tensile}}$ (MPa)	238 000	76 000

* Fracture toughness G_{IIC} of UD carbon fibre was obtained by approximation. Since the fracture toughness for the UD glass fibre has the same resin (Fibredux 913) as the carbon fibre, the ratio was taken between $G_{IC\,Glass}$ and $G_{IIC\,Glass}$, and applied on the carbon fibre in order to get an approximation for the $G_{IIC\ carbon}$.

The equation that has been used was: $G_{IIC\ carbon} = \frac{G_{IIC\,Glass}}{G_{IC\,Glass}} \times G_{IC\,carbon}$

The fracture toughness G_{IC} of the UD carbon was taken from Beng et al. (2001), and it is for both 16 and 24 plies laid up in the UD direction, while the fracture toughness G_{IC} and G_{IIC} of the UD glass was taken from Harris (2003, p.2, table 7.2 and p.206, table 7.5), for 16 plies laid up in the UD direction.

APPENDIX N

TITLE **General equations for a laminate under SBS test conditions**

General equations for a laminate under SBS test conditions

The following demonstrates how the principal stresses on each ply of the laminate were derived:

- Stress equations for the plane x-z of the 3-D element shown on Figure 54. Equations restricted to the plane stress as shown on Figure 54:

According to Budynas (1998, p.97), the stress state for the 3-D element shown in Figure 54, and for the reference system axis that has been used in this thesis (Figure 22 and Figure 23) will be:

$$\sigma_{x\prime} = \sigma_x n_{x\prime x}^2 + \sigma_z n_{x\prime z}^2 + \sigma_y n_{x\prime y}^2 + 2\,\tau_{xz}\, n_{x\prime x}\; n_{x\prime z} + 2\,\tau_{zy}\, n_{x\prime z}\, n_{x\prime y} + 2\,\tau_{yx}\, n_{x\prime y}\; n_{x\prime x} \tag{107}$$

$$\tau_{x\prime z\prime} = \sigma_x\, n_{x\prime x}\, n_{z\prime x} + \sigma_z\, n_{x\prime z}\, n_{z\prime z} + \sigma_y\, n_{x\prime y}\, n_{z\prime y} + \tau_{xz}\left(n_{x\prime x}\; n_{z\prime z} + n_{x\prime z}\; n_{z\prime x}\right) + \tau_{zy}\left(n_{x\prime z}\; n_{z\prime y} + n_{x\prime y}\; n_{z\prime z}\right) + \tau_{yx}\left(n_{x\prime x}\; n_{z\prime y} + n_{x\prime y}\; n_{z\prime x}\right) \tag{108}$$

Note: the x'; y' and z' system axis are in accordance with the shown in Figure 93, with the exception that the z' system axis is not coincident with the z axis system axis (this exception is to be considered for equations (107) up to (124)).

By applying the assumptions given in Chapter 2, section 2.6, in which for a 2-D assessment in the through-thickness direction:

$$\sigma_z = \sigma_y = \tau_{yx} = \tau_{zy} = 0$$

then, the equations (107) and (108) become:

$$\sigma_{x\prime} = \sigma_x n_{x\prime x}^2 + 2\,\tau_{xz}\, n_{x\prime x}\; n_{x\prime z} \tag{109}$$

$$\tau_{x\prime z\prime} = \sigma_x\, n_{x\prime x}\, n_{z\prime x} + \tau_{xz}\left(n_{x\prime x}\; n_{z\prime z} + n_{x\prime z}\; n_{z\prime x}\right) \tag{110}$$

- Stress equations for the normal stress, $\sigma_{z\prime}$ and the shear stress, $\tau_{y\prime x\prime}$.

According to Budynas (1998, p.97), the stress state for the 3-D element shown in Figure 54, and for the reference system axis that has been used in this thesis (Figure 22 and Figure 23) will be:

$$\sigma_{z\prime} = \sigma_x n_{z\prime x}^2 + \sigma_z n_{z\prime z}^2 + \sigma_y n_{z\prime y}^2 + 2\,\tau_{xz}\, n_{z\prime x}\; n_{z\prime z} + 2\,\tau_{zy}\, n_{z\prime z}\, n_{z\prime y} + 2\,\tau_{yx}\, n_{z\prime y}\; n_{z\prime x} \tag{111}$$

$$\tau_{y\prime x\prime} = \sigma_x\, n_{x\prime x}\, n_{y\prime x} + \sigma_z\, n_{x\prime z}\, n_{y\prime z} + \sigma_y\, n_{x\prime y}\, n_{y\prime y} + \tau_{xz}\left(n_{x\prime x}\; n_{y\prime z} + n_{x\prime z}\; n_{y\prime x}\right) + \tau_{zy}\left(n_{x\prime z}\; n_{y\prime y} + n_{x\prime y}\; n_{y\prime z}\right) + \tau_{yx}\left(n_{x\prime x}\; n_{y\prime y} + n_{x\prime y}\; n_{y\prime x}\right) \tag{112}$$

For a 2-D assessment in the through thickness direction:

$$\sigma_z = \sigma_y = \tau_{yx} = \tau_{zy} = 0$$

then, the equations (107) and (108) become:

$$\begin{cases} \sigma_{z\prime} = \sigma_x n_{z\prime x}^2 + 2\,\tau_{xz}\, n_{z\prime x}\; n_{z\prime z} & (113) \\ \tau_{y\prime x\prime} = \sigma_x\, n_{x\prime x}\, n_{y\prime x} + \tau_{xz}\left(n_{x\prime x}\; n_{y\prime z} + n_{x\prime z}\; n_{y\prime x}\right) & (114) \end{cases}$$

- Stress equations for the plane y-z of the 3-D element shown in Figure 54. Equations restricted to the plane stress as shown in Figure 54:

According to Budynas (1998, p.97), the stress state for the 3-D element shown in Figure 54, and for the reference system axis that has been used in this thesis (Figure 22 and Figure 23) will be:

$$\begin{cases} \sigma_{y\prime} = \sigma_x n_{y\prime x}^2 + \sigma_z n_{y\prime z}^2 + \sigma_y n_{y\prime y}^2 + 2\,\tau_{xz}\, n_{y\prime x}\; n_{y\prime z} + 2\,\tau_{zy}\, n_{y\prime z}\, n_{y\prime y} + 2\,\tau_{yx}\, n_{y\prime y}\; n_{y\prime x} & (115) \\ \tau_{z\prime y\prime} = \sigma_x\, n_{z\prime x}\, n_{y\prime x} + \sigma_z\, n_{z\prime z}\, n_{y\prime z} + \sigma_y\, n_{z\prime y}\, n_{y\prime y} + \tau_{xz}\left(n_{z\prime x}\; n_{y\prime z} + n_{z\prime z}\; n_{y\prime x}\right) & (116) \\ \qquad + \tau_{zy}\left(n_{z\prime z}\; n_{y\prime y} + n_{z\prime y}\; n_{y\prime z}\right) + \tau_{yx}\left(n_{z\prime x}\; n_{y\prime y} + n_{z\prime y}\; n_{y\prime x}\right) \end{cases}$$

For a 2-D assessment in the through thickness direction:

$$\sigma_z = \sigma_y = \tau_{yx} = \tau_{zy} = 0$$

then, the equations (107) and (108) become:

$$\begin{cases} \sigma_{y\prime} = \sigma_x n_{y\prime x}^2 + 2\,\tau_{xz}\, n_{y\prime x}\; n_{y\prime z} & (117) \\ \tau_{z\prime y\prime} = \sigma_x\, n_{z\prime x}\, n_{y\prime x} + \tau_{xz}\left(n_{z\prime x}\; n_{y\prime z} + n_{z\prime z}\; n_{y\prime x}\right) & (118) \end{cases}$$

The general equations for a composite laminate submitted to a SBS test as shown in Figure 54 will be:

For a 2-D stress state, in which each ply is subjected to the stresses: $\sigma_{(x,z)}$; τ_{xz} and τ_{zx} , as shown in Figure 54, and applying the derivation given previously, the general equations to obtain the stress values for any rotation in space of the 3-D stress element shown in Figure 54 will be:

$$\begin{cases} \sigma_{x\prime} = \sigma_x n_{x\prime x}^2 + 2\,\tau_{xz}\, n_{x\prime x}\; n_{x\prime z} & (119) \\ \sigma_{y\prime} = \sigma_x n_{y\prime x}^2 + 2\,\tau_{xz}\, n_{y\prime x}\; n_{y\prime z} & (120) \\ \sigma_{z\prime} = \sigma_x n_{z\prime x}^2 + 2\,\tau_{xz}\, n_{z\prime x}\; n_{z\prime z} & (121) \\ \tau_{y\prime x\prime} = \sigma_x\, n_{x\prime x}\, n_{y\prime x} + \tau_{xz}\left(\, n_{x\prime x}\; n_{y\prime z} + \; n_{x\prime z}\; n_{y\prime x}\right) & (122) \\ \tau_{z\prime y\prime} = \sigma_x\, n_{z\prime x}\, n_{y\prime x} + \tau_{xz}\left(\, n_{z\prime x}\; n_{y\prime z} + \; n_{z\prime z}\; n_{y\prime x}\right) & (123) \\ \tau_{x\prime z\prime} = \sigma_x\, n_{x\prime x}\, n_{z\prime x} + \tau_{xz}\left(\, n_{x\prime x}\; n_{z\prime z} + \; n_{x\prime z}\; n_{z\prime x}\right) & (124) \end{cases}$$

Where the directional cosines, for a rotation in space of the 3-D stress element will be given as:

$$\begin{bmatrix} \mathrm{x}' \\ \mathrm{y}' \\ \mathrm{z}' \end{bmatrix} = \begin{bmatrix} n_{x\prime x} & n_{x\prime y} & n_{x\prime z} \\ n_{y\prime x} & n_{y\prime y} & n_{y\prime z} \\ n_{z\prime x} & n_{z\prime y} & n_{z\prime z} \end{bmatrix} \begin{bmatrix} \mathrm{x} \\ \mathrm{y} \\ \mathrm{z} \end{bmatrix}$$

NOTE: In the equations given in this section, σ_x is equal to $\sigma_{x\ (\mathrm{x},\mathrm{z})}$

.

General equations for the stresses along, and perpendicular to the fibre direction for each of the plies in the through thickness direction

By considering equations (119) up to (124) and applying a rotation around the *z* axis of the ply system axis of the 3-D stress element shown in Figure 54, it will be possible to obtain the equations of the stresses along and perpendicular to the fibre direction.

A simple image is shown in Figure 93 which shows the procedure to be implemented by using equations (119) up to (124) :

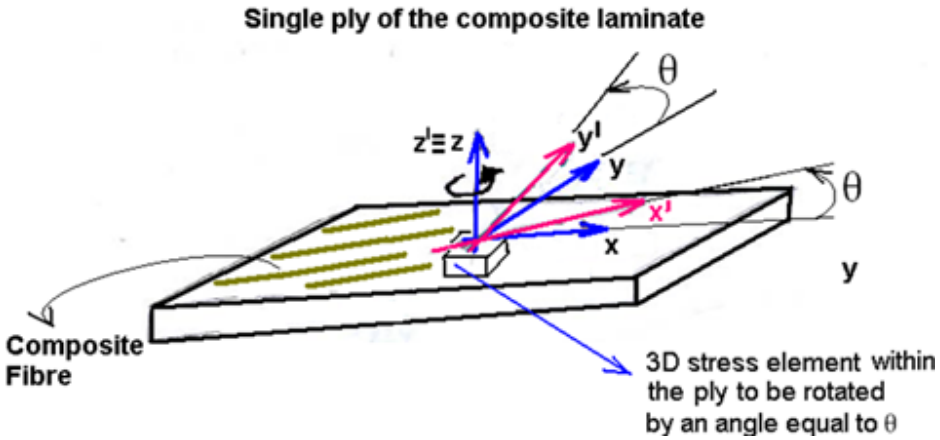

Figure 93 - Rotation to be performed on the 3D stress element within the ply

For a rotation around the *z* axis of an angle equal to θ in order to align the 3-D stress element with the fibre direction as shown in Figure 93, the equations (119) up to (124) become:

$$\sigma_{x\prime} = \sigma_x n_{x\prime x}^2 \quad (125)$$

$$\sigma_{y\prime} = \sigma_x n_{y\prime x}^2 \quad (126)$$

$$\sigma_{z\prime} = 0 \quad (127)$$

$$\tau_{y\prime x\prime} = \sigma_x \, n_{x\prime x} \, n_{y\prime x} \quad (128)$$

$$\tau_{z\prime y\prime} = \tau_{xz} \, n_{z\prime z} \, n_{y\prime x} \quad (129)$$

$$\tau_{x\prime z\prime} = \tau_{xz} \, n_{x\prime x} \, n_{z\prime z} \quad (130)$$

in which:

$$n_{x\prime x} = \cos\theta \quad (131)$$

$$n_{x\prime y} = \sin\theta \quad (132)$$

$$n_{y\prime x} = -\sin\theta \quad (133)$$

$$n_{y'y} = \cos\theta \tag{134}$$

$$n_{z'z} = 1 \tag{135}$$

$$n_{x'z} = 0 \tag{136}$$

$$n_{y'z} = 0 \tag{137}$$

$$n_{z'x} = 0 \tag{138}$$

$$n_{z'y} = 0 \tag{139}$$

General equation for the principal stresses acting on a stress element

The principal stress is the value given when no shear stresses act on a 3-D stress element. In order to obtain such stress a rotation in space of the 3-D stress element (for instance the 3-D stress element shown in Figure 54) is required. This rotation will be performed as shown in Figure 94.

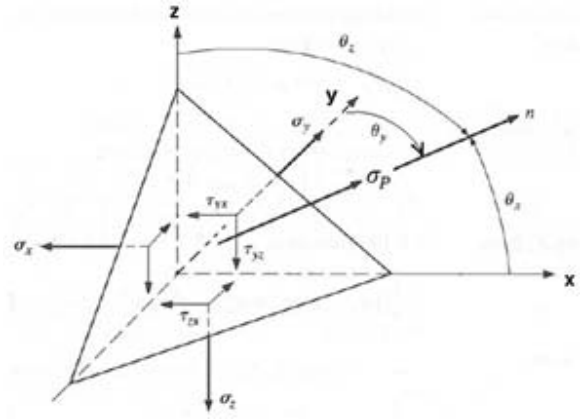

Figure 94 - Cut made on a 3-D stress element (represented by the triangle). Principal stress (σ_P) for a stress element, where no shear forces act over the surface of the 3-D stress element after a rotation in space (θ_x, θ_y and θ_z).

According to Budynas (1998), and for the system axis that has been used during this thesis, the general equation for the principal stresses will be:

$$\sigma_P^3 - (\sigma_x + \sigma_y + \sigma_z)\,\sigma_P^2 + (\sigma_x\,\sigma_z + \sigma_z\,\sigma_y + \sigma_y\,\sigma_x - \tau_{zy}^2 - \tau_{yx}^2 - \tau_{xz}^2)\,\sigma_P - (\sigma_x\,\sigma_y\,\sigma_z + 2\,\tau_{zy}\,\tau_{yx}\,\tau_{xz} - \sigma_x\tau_{zy}^2 - \sigma_z\tau_{yx}^2 - \sigma_y\tau_{xz}^2) = 0 \quad (140)$$

In order to find the orientation of the principal stresses θ_{σ_P} as shown in Figure 94, the following general equations will be used:

$$(\sigma_x - \sigma_P)\,n_x + \tau_{xz}\,n_z + \tau_{yx}\,n_y = 0 \quad (141)$$

$$\tau_{xz}\,n_x + (\sigma_z - \sigma_P)\,n_z + \tau_{zy}\,n_y = 0 \quad (142)$$

$$\tau_{yx}\,n_x + \tau_{zy}\,n_z + (\sigma_y - \sigma_P)\,n_y = 0 \quad (143)$$

$$n_x^2 + n_y^2 + n_z^2 = 1 \quad (144)$$

Where:

$$n_x = \cos\theta_x \quad (145)$$

$$n_y = \cos\theta_y \quad (146)$$

$$n_z = \cos\theta_z \quad (147)$$

Note: The directional cosines that are linked to the 3-D stress element shown in Figure 54 are shown in the Figure 94.

Principal stresses in the x-z plane for a single ply of the composite laminate shown in Figure 54

In order to obtain the principal stresses (σ_{P_1} and σ_{P_3}) for each of the plies within a composite laminate, the 3-D stress element must be rotated.

Figure 95 shows the rotation to be performed in order to find the principal stresses.

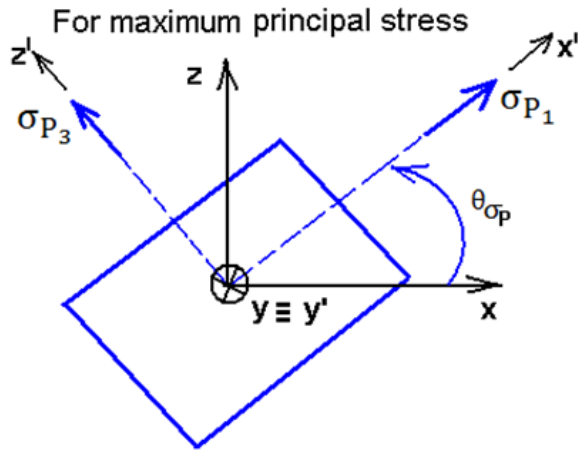

Figure 95 - Rotation of the 3-D element shown in Figure 54. Principal stress.

Applying the general equation (140) for a rotation as described in the image above, the general equation of the principal stress becomes:

Since:

$$\sigma_z = \sigma_y = \tau_{yx} = \tau_{zy} = 0 \tag{148}$$

then the general equation of the principal stress becomes:

$$\sigma_P^3 - \sigma_x \ \sigma_P^2 - \tau_{xz}^2 \ \sigma_P = 0 \tag{149}$$

$$\sigma_{P_2} = 0$$

$$\sigma_P^2 - \sigma_x \ \sigma_P - \tau_{xz}^2 = 0$$

Note: Since the analysis is performed for a stress state in the through thickness direction, the principal stress in the direction y' will be equal to zero $(\sigma_{P_2} = 0)$.

From the equation (149), the principal stresses will be given as follows:

$$\sigma_{P_2} = 0 \tag{150}$$

$$\sigma_{P_1} = \frac{\sigma_x + \sqrt{\sigma_x^2 + 4\,\tau_{xz}^2}}{2} \tag{151}$$

$$\sigma_{P_3} = \frac{\sigma_x - \sqrt{\sigma_x^2 + 4\,\tau_{xz}^2}}{2} \tag{152}$$

and

$$n_x = \cos\theta_x \tag{153}$$

$$n_y = \cos\theta_y \tag{154}$$

$$n_z = \cos\theta_z \tag{155}$$

where, $n_{x'x}$; $n_{x'z}$ and $n_{x'y}$ are the directional cosines (Budynas 1998) that define the rotation of the 3-D element shown in Figure 54.

Maximum shear stress ($\tau_{max_{z'x'}}$ and $\tau_{max_{x'z'}}$) acting on the x-z plane of a single ply:

The maximum shear stress on the plane x-z of the 3-D element shown in Figure 54 is obtained when the stresses $\sigma_{x'}$ and $\sigma_{z'}$ are equal to each other as shown in Figure 96.

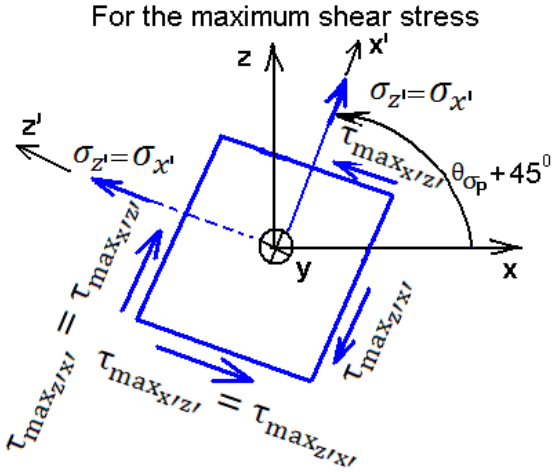

Figure 96 - Representation of the maximum shear stress of the stress element shown in Figure 54

In order to obtain the maximum shear stress acting on the 3-D stress element of a single ply the concepts in Mohr's circle were used. This is explained in Figure 97.

According to Budynas (1998, p.73), the stress equations for a 3-D stress element that has been rotated in space could be obtained from the Mohr's circle which is shown below:

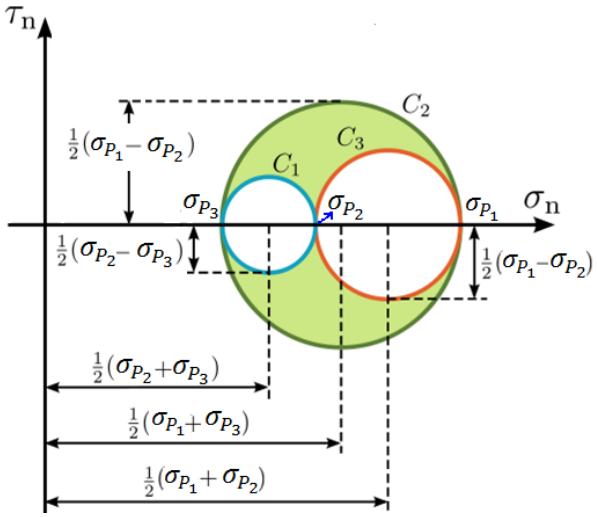

Figure 97 - Mohr circle for a 3-D stress state over a stress element.

From Figure 97, the variables C_1, C_2 and C_3 are the identification used for each of the circles. Each point on the colored area defined within circle C_2 represents a single stress state of the 3-D stress element on the plane y-z. Each single point on the perimeter defined by each of the circles C_1, C_2 and C_3 represents a single stress state of the stress element on the planes z-y; x-z and y-x respectively.

Since this thesis is based on the stress state given by the area within circle C_2 ; plane x-z, then the following equations for circle C_2 are given:

R = radius of the circle $C_2 = \sqrt{\left(\frac{1}{2}(\sigma_x - \sigma_z)\right)^2 + \tau_{xz}^2}$ (156)

$$\sigma_{AVG} = \frac{1}{2}(\sigma_x - \sigma_z) \quad (157)$$

$$\sigma_{P_1} = \sigma_{AVG} + \mathrm{R} \quad (158)$$

$$\sigma_{P_2} = \sigma_{AVG} - \mathrm{R} \quad (159)$$

$$\sigma_{P_3} = \sigma_{AVG} - \mathrm{R} \quad (160)$$

And finally the maximum shear stress will be given as:

$$\tau_{max\ x'z'} = \mathrm{R} \quad (161)$$

As shown above, Mohr's circle could be used as alternative method to equations (150), (151) and (152) to find the principal stresses.

Orientation angle of the principal stress in accordance with Figure 95 (θ_{σ_P})

Through Mohr's circle (Figure 97), the orientation angle for the principal stress will be given as:

$$\tan\left(2\,\theta_{\sigma_P}\right) = \frac{2\,\tau_{xz}}{\sigma_x - \sigma_z} \quad (162)$$

APPENDIX O

TITLE **Stresses along and perpendicular to the fibre direction for each of the plies in the through-thickness direction of the composite laminate**

By using equations (125) up to (130) from Appendix N the Table 23 is given.

All Carbon Design

$$[(0/45/90/-45)_3]_s$$

Since the stresses given in Table 23 are for a plane stress state, then $\sigma_z = 0$.

Table 23 – Specimen n. 10. Stress along and perpendicular to the fibre direction, for each ply and on the x-z plane of the *All Carbon Design* Laminate. Values presented are for a bending moment value taken at the position where the crack has occurred which is at the coordinate x= 11 mm (see Figure 49 and Figure 42).

For the Specimen 10 shown on the Table 1 - (According to Figure 93)							
TOP OF THE LAMINATE							
Ply Number	**Angle (Degrees)**	**Material**	$\sigma_{x'}$ **(MPa)**	$\sigma_{y'}$ **(MPa)**	$\tau_{y'x'}$ **(MPa)**	$\tau_{z'y'}$ **(MPa)**	$\tau_{x'z'}$ **(MPa)**
1	**0**	Carbon	- 535.58	0	0	0	0
2	**45**	Carbon	- 79.45	- 79.45	79.45	-17.55	17.55
3	**90**	Carbon	0	- 39.71	0	-32.18	0
4	**- 45**	Carbon	- 65.00	- 65.00	- 65.00	24.05	24.05
5	**0**	Carbon	- 357.06	0	0	0	40.04
6	**45**	Carbon	- 50.56	- 50.56	50.56	-40.01	40.01
7	**90**	Carbon	0	- 23.83	0	-61.27	0
8	**- 45**	Carbon	- 36.11	- 36.11	- 36.11	44.10	44.10
9	**0**	Carbon	- 178.53	0	0	0	65.72
10	**45**	Carbon	- 21.67	- 21.67	21.67	-52.32	52.32
11	**90**	Carbon	0	- 7.94	0	-76.00	0
12	**- 45**	Carbon	- 7.22	- 7.22	- 7.22	54.00	54.00
MIDDLE OF THE SYMMETRIC LAMINATE		Resin (Matrix)	0	0	0	54.47	54.47
13	**- 45**	Carbon	7.22	7.22	7.22	54.00	54.00
14	**90**	Carbon	0	7.94	0	-76.00	0
15	**45**	Carbon	21.67	21.67	- 21.67	-52.32	52.32
16	**0**	Carbon	178.53	0	0	0	65.72
17	**- 45**	Carbon	36.11	36.11	36.11	44.10	44.10
18	**90**	Carbon	0	23.83	0	-61.27	0
19	**45**	Carbon	50.56	50.56	- 50.56	-40.01	40.01
20	**0**	Carbon	357.06	0	0	0	40.04
21	**- 45**	Carbon	65.00	65.00	65.00	24.05	24.05
22	**90**	Carbon	0	39.71	0	-32.18	0
23	**45**	Carbon	79.45	79.45	- 79.45	-17.55	17.55
24	**0**	Carbon	535.58	0	0	0	0
BOTTOM OF THE LAMINATE							

Hybrid Design 1

$$\left[(0_C)_2/(\pm 45_C)_2/(\pm 45_g)_2/(\pm 45_C)\right]_s$$

Since the stresses given in Table 24 are for a plane stress state, then $\sigma_z = 0$.

Table 24 – Specimen n. 9. Stress along and perpendicular to the fibre direction, for each ply and on the x-z plane of the *Hybrid Design 1*. Values presented are for a bending moment value taken at the span centre x= 7 mm (see Figure 42).

For the Specimen 9 shown on the Table 2 - (According to Figure 93)							
TOP OF THE LAMINATE							
Ply Number	Angle (Degrees)	Material	$\sigma_{x'}$ (MPa)	$\sigma_{y'}$ (MPa)	$\tau_{y'x'}$ (MPa)	$\tau_{z'y'}$ (MPa)	$\tau_{x'z'}$ (MPa)
1	0	Carbon	- 1184.73	0	0	0	0
2	0	Carbon	- 1086.94	0	0	0	23.53
3	45	Carbon	- 160.06	- 160.06	160.06	- 31.90	31.90
4	- 45	Carbon	- 144.24	- 144.24	- 144.24	36.39	36.39
5	45	Carbon	- 128.42	- 128.42	128.42	- 40.44	40.44
6	- 45	Carbon	- 112.59	- 112.59	- 112.59	44.05	44.05
7	45	Glass	- 41.85	- 41.85	41.85	- 47.21	47.21
8	- 45	Glass	- 34.81	- 34.81	- 34.81	48.42	48.42
9	45	Glass	- 27.77	- 27.77	27.77	- 49.43	49.43
10	- 45	Glass	- 20.73	- 20.73	- 20.73	50.23	50.23
11	45	Carbon	- 31.65	- 31.65	31.65	- 50.83	50.83
12	- 45	Carbon	- 15.82	- 15.82	- 15.82	51.72	51.72
MIDDLE OF THE SYMMETRIC LAMINATE		Resin (Matrix)	0	0	0	52.16	52.16
13	- 45	Carbon	15.82	15.82	15.82	51.72	51.72
14	45	Carbon	31.65	31.65	- 31.65	- 50.83	50.83
15	- 45	Glass	20.73	20.73	20.73	50.23	5023
16	45	Glass	27.77	27.77	- 27.77	- 49.43	49.43
17	- 45	Glass	34.81	34.81	34.81	48.42	48.42
18	45	Glass	41.85	41.85	- 41.85	- 47.21	47.21
19	- 45	Carbon	112.59	112.59	112.59	44.05	44.05
20	45	Carbon	128.42	128.42	- 128.42	- 40.44	40.44
21	- 45	Carbon	144.24	144.24	144.24	36.39	36.39
22	45	Carbon	160.06	160.06	- 160.06	- 31.90	31.90
23	0	Carbon	1086.94	0	0	0	23.53
24	0	Carbon	1184.73	0	0	0	0
BOTTOM OF THE LAMINATE							

Hybrid Design 2

$$\left[\left(0_c\right)_2/\left(\pm45_g\right)/\left(90_C\right)_4/\left(\pm45_g\right)/\left(90_C\right)_2\right]_s$$

Since the stresses given in Table 25 are for a plane stress state, then $\sigma_z = 0$ **.**

Table 25 – Specimen n. 10. Stress along and perpendicular to the fibre direction, for each ply and on the x-z plane of the *Hybrid Design 2*. Values presented are for a bending moment value taken at the position where the crack has occurred which is at the coordinate x= 9 mm (see Figure 42 and Figure 47).

For the Specimen 10 shown on the Table 11 - (according to Figure 93)							
TOP OF THE LAMINATE							
Ply Number	Angle (Degrees)	Material	$\sigma_{x'}$ (MPa)	$\sigma_{y'}$ (MPa)	$\tau_{y'x'}$ (MPa)	$\tau_{z'y'}$ (MPa)	$\tau_{x'z'}$ (MPa)
1	0	Carbon	- 872.43	0	0	0	0
2	0	Carbon	- 802.09	0	0	0	24.25
3	45	Glass	- 51.22	- 51.22	51.22	-32.92	32.92
4	- 45	Glass	- 45.80	- 45.80	- 45.80	35.13	35.13
5	90	Carbon	0	- 51.33	0	-52.49	0
6	90	Carbon	0	- 45.07	0	-53.92	0
7	90	Carbon	0	- 38.81	0	-55.17	0
8	90	Carbon	0	- 32.55	0	-56.25	0
9	45	Glass	- 20.68	- 20.68	20.68	-40.41	40.41
10	- 45	Glass	- 15.27	- 15.27	- 15.27	41.31	41.31
11	90	Carbon	0	- 12.52	0	-59.35	0
12	90	Carbon	0	- 6.26	0	-59.70	0
MIDDLE OF THE SYMMETRIC LAMINATE		Resin (Matrix)	0	0	0	- 59.87	0
13	90	Carbon	0	6.26	0	-59.70	0
14	90	Carbon	0	12.52	0	-59.35	0
15	- 45	Glass	15.27	15.27	15.27	41.31	41.31
16	45	Glass	20.68	20.68	- 20.68	-40.41	40.41
17	90	Carbon	0	32.55	0	-56.25	0
18	90	Carbon	0	38.81	0	-55.17	0
19	90	Carbon	0	45.07	0	-53.92	0
20	90	Carbon	0	51.33	0	-52.49	0
21	- 45	Glass	45.80	45.80	45.80	35.13	35.13
22	45	Glass	51.22	51.22	- 51.22	-32.92	32.92
23	0	Carbon	802.09	0	0	0	24.25
24	0	Carbon	872.43	0	0	0	0
BOTTOM OF THE LAMINATE							

APPENDIX P

TITLE **Maximum Bending Stress Equation**

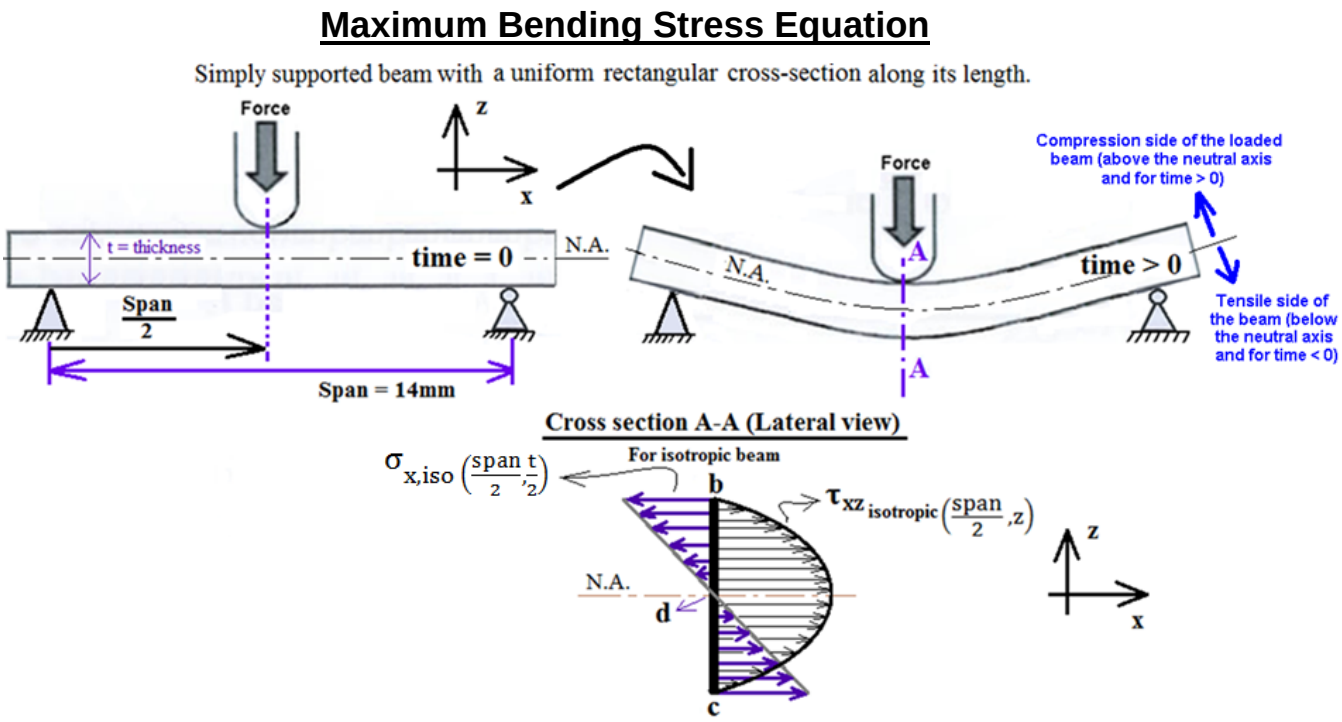

Figure 98 – Simply supported beam subjected to a deflection caused by an external transverse force.

In Chapter 2, the *Classical Laminated Plate theory* Reddy (2004) has been used to derive two different bending stress equations, the composite bending stress equation according to Reddy (2004), equations (73), (78) and (80), and 2-D composite bending stress equation (91) and the ILSS equation (99), which is the equation that has been used in the analytical assessment made in chapter 4.

The fatigue experiments were performed by Han (2013) after the static tests were concluded on the specimens shown in Table 1 (All Carbon Design) and Table 2 (Hybrid Design 1). Since the highest and low failure loads have fallen within the widest and narrowest samples respectively (as it is shown in the Table 2), a simple method was required to average the ultimate load (Force = P_z) as a function of the mid-span cross section of the specimen (cross-section A-A of Figure 98).

By considering an isotropic beam, simply supported with the stress distribution on the mid-span cross section as shown in Figure 98. Is possible to find an equation which can be utilized as simple method to average the ultimate load required to setup the fatigue rig.

As can be seen from points *b* and *c*, shown in Figure 98, the bending stress $\sigma_{x,iso}\left(\frac{span}{2},\frac{t}{2}\right)$ has its maximum value when the shear stress τ_{xz} is equal to zero. In contrast, point *d* shown in

Figure 98 shows that the bending stress, $\sigma_{x,iso\left(\frac{span}{2},\frac{t}{2}\right)}$ is equal to zero when the shear stress τ_{xz} is a maximum.

Thus, the resultant stress of the beam acting on points *b* and *c* of the mid-span cross section A-A (Figure 98) is given by:

$$\hat{\sigma}_{x,iso\left(\frac{span}{2},\frac{t}{2}\right)} = \frac{M_{x\ around\ y\ axis\left(\frac{span}{2}\right)} \times z_{max}}{I_{yy}} \quad (163)$$

In which, $z_{max} = \frac{beam\ thickness}{2}$, $\tau_{xz\ on\ point\ b\ and\ c} = 0$ and I_{yy} is the cross section moment of inertia in regards to the *y* axis which for the rectangular cross-section A-A (Figure 98) will be equal to: $I_{yy} = \frac{b \times t^2}{12}$, in which *b* is the width of the component and *t* is the thickness.

According to Young & Budynas (2002, section 8.17, table 8.1, case 1c) (for a beam simply supported at both ends), the bending moment on an SBS test will be: $M_{x\ around\ y\ axis\left(\frac{span}{2}\right)} = \frac{P_z}{2} \times \frac{span}{2}$; in which, P_z is the ultimate load applied at centre span (Figure 98), and the *span* is the distance between the centre of each of the support roller's cross-section in accordance with the Standard D2344/2344M (2006, figure 6).

By substituting $M_{x\ around\ y\ axis\left(\frac{span}{2}\right)}$; z_{max} and I_{yy} given above into equation (163), the maximum bending stress equation becomes:

$$\hat{\sigma}_{x,iso\left(\frac{span}{2},\frac{t}{2}\right)} = \frac{3 \times P_z \times span}{2 \times b \times t^2} \quad (164)$$

Before commencing the fatigue experiments, Han (2013) has calculated the resultant stress at the point *b* of a cross-section A-A, as shown in Figure 98 by taking the average values given in table 3.4 of Appendix I and substituting them into equation (164) in order to obtain the maximum resultant stress (equal to $\hat{\sigma}_{x,iso\left(\frac{span}{2},\frac{t}{2}\right)}$) for each design, the *All carbon Design* and the *Hybrid Design 1*.

The average value of $\hat{\sigma}_{x,iso\left(\frac{span}{2},\frac{t}{2}\right)}$ (named as σ by Han (2013)) is shown in table D.1 and D.2 which are given in Appendix J.

Once the average value of $\widehat{\sigma}_{x,iso\left(\frac{span}{2},\frac{t}{2}\right)}$ has been obtained for each of the designs subjected to a fatigue test (*All Carbon Design* and *Hybrid Design 1*), Han (2013) has calculated the apparent static ultimate load (*F*) for each of the specimens.

The apparent static ultimate load, *F* has been obtained from equation (164) and is given as follows:

$$F = P_{z\,for\,fatigue} = \frac{2 \times t_{average}{}^{2} \times b_{average} \times \widehat{\sigma}_{x,iso\left(\frac{span}{2},\frac{t}{2}\right)average}}{3 \times span} \tag{165}$$

in which, the values for $\widehat{\sigma}_{x,iso\left(\frac{span}{2},\frac{t}{2}\right)average}$ (named as σ by Han (2013)), $t_{average}$ (named as *d* by Han (2013)) and $b_{average}$ (named as *b* by Han (2013)) are given in table D.1 and D.2 of the Appendix J.

In order to ensure that the fatigue test rig is set up with a load below the apparent static ultimate load (*F*) for each individual specimen tested, Han (2013) has calculated different load values by using the equation (165) in which the stress $\widehat{\sigma}_{x,iso\left(\frac{span}{2},\frac{t}{2}\right)average}$ has been multiplied by 90%, 80% and 70% giving the load values as shown in the table D.1 and D.2 of the Appendix J, and which were entitled by Han (2013) respectively as: *90%F*; *80%F* and *70%F*.

From the load values that have been calculated for each of the specimens (*90%F*; *80%F* and *70%F*), just one has been selected to setup the fatigue rig to proceed with the fatigue test.

APPENDIX Q

TITLE **Transverse displacement according to Timoshenko (1948, p.173)**

Transverse Displacement

The laminate constitutive equations (given in section 2.4) which are used by the software LAP (for instance), were based on the Kirchhoff Hypothesis (Reddy 2004). In this Thesis each ply was considered to have a small thickness (approximately 0.139 mm for the carbon ply and 0.153 for the glass ply) when compared to the in-plane dimensions (x-y plane). This allows the assumption that straight lines perpendicular to the midsurface before deformation occurs remain straight after the deformation occurs (since the assessment has been made on the z-x plane, the in-plane (x-y plane) dimensions should be limited to the *x* axis which refers to the length of each specimen (approximately 21 mm)). The analytical assessment, presented in chapter 4, which derives from the laminate constitutive equations (section 2.4) has shown a good correlation when compared to the analytical results with the FE-Models and the static tests (see for the All Carbon Design: Figure 43, Figure 49, Table 6 and Table 7; for the Hybrid Design 1: Figure 45, Figure 55 and Table 10; and for the Hybrid Design 2: Figure 47, Figure 59, Table 13 and Table 14).

For the case of the calculation of the transverse deflection, where the thick beam composite laminate is considered as a whole single component loaded under an SBS test condition, the effect on the transverse displacement of the bending stress should be considered together with the effect on the transverse displacement of the shear stress. In this situation the Timoshenko's equation (Timoshenko 1948) for isotropic beams gives an approximation of the real deflection of the thick composite beam under a SBS test loading condition.

According to Timoshenko (1948, p.173) the total deflection of an isotropic beam considering the sum of both the curvature caused by the shear stress and the curvature caused by the bending moment is given by equation (166).

According to Timoshenko (1948, p.172 and p.173), for a central load, *P* (applied to the middle of the span of the beam) and for a simply supported beam, the transverse displacement equation will be given by equation (166).

$$w_0 = \frac{P \times span^3}{48 \times E_x \times I_y} \times \left(1 + \frac{12 \times \alpha \times {k_y}^2}{span^2} \times \frac{E_x}{G_{xy}}\right) \qquad (166)$$

in which, k_y is the radius of gyration of the cross section with respect to the *y* axis and which is given by equation (167).

$$k_y = \sqrt{\frac{I_y}{cross - section\ area\ of\ the\ beam}} \qquad (167)$$

and α is a factor used in Timoshenko's equation (166). For rectangular cross-section beams α = 3/2 .

For a rectangular cross-section of thickness equal to *t* , the radius of gyration becomes equal to $k_y = \frac{1}{12} \times t^2$.

Since the factor $\frac{E_x}{G_{xy}} = 2 \times (1 + v_{xy}) = 2.6$, then equation (166) becomes,
(Timoshenko 1948, p.173)

$$w_0 = \frac{P \times span^3}{48 \times E_x \times I_y} \times \left(1 + 3.90 \times \frac{t^2}{span^2}\right) \quad (168)$$

Ghugal & Sharma (2011) have derived the transverse deflection by considering the curvature caused by the shear stress with the curvature caused by the bending moment. The equation proposed by Ghugal & Sharma (2011) for an isotropic simply supported beam with a central transversal load applied to it is given by:

$$w_0 = \frac{P \times span^3}{48 \times E_x \times I_y} \times \left(1 + 2 \times (1 + v_{xy}) \times \frac{t^2}{span^2}\right) \quad (169)$$

As can be seen, equations (168) and (169) are similar with the unique difference in the assumption of the factor $2 \times (1 + v_{xy})$, Timoshenko (1948) considers this factor equal to 2.6.

Note that, equations (168) and (169) are derived for isotropic beams, which give an approximation of the transverse displacement on a composite beam (considering that an error will be generated by the use of equations (168) and (169) in composite beams).

In this thesis, the transverse displacement was not assessed because, it was not considered relevant to assess and conclude the objectives of the research work given in section 1.8. However, as reference for future works that could require an assessment in terms of transverse displacement of composite beams.

APPENDIX R

TITLE **S-N Curve derivation**

S-N Curve Equation

The S-N curve presented in the Chapter 5, was built through the application of the four parameter Weibull's equation (170) (Freudenthal et al. 1963, p.76), and was used in order to capture the probability of failure after a given number of cycles of a certain stress acting on a composite laminate.

$$S = (S_u - S_e) \times \left(\frac{N}{B} + 1\right)^{-A'} + S_e \quad (170)$$

In which, according to Freudenthal et al. (1963, p.76):

- A' is the shape parameter.

- *N* is the number of cycles.

- *B* is the scale parameter of time which has the dimension of the cycle life *N* and is the rational unit of fatigue life.

- *S* is the Interlaminar shear stress.

- S_e is the median shear stress at infinite number of cycles (Endurance).

- S_u is the median of the static strength.

According to Freudenthal et al. (1963) there are three methods to determine the four parameters, S_u, A', S_e and B, these methods are: best fit of the observed data points (experimental static test data), by graphical analysis, or by analytical evaluation.

In this thesis will use the observed data points method together with the graphical method to obtain the parameters, S_u, A', S_e and B. The graphical method should be based on a semi-logarithmic plot which presents the median data points and the average S-N curve equation (170) (four parameter Weibull's equation) which should be fitted by eye (according to Freudenthal et al. (1963, p.77)), "thereby determining the values of S_u and S_e". Here the median data points refer to the points (values) of the Interlaminar shear stress, $\tau_{xz\ j=\text{total number of plies}/2}$ as a function of the number of cycles to failure that were obtained from fatigue test specimen.

According to Freudenthal et al. (1963, p.77), the maximum slope of the *S-N* curve which is located at the point of inflection (S_i, N_i) shown in Figure 99 is given by the equation (171).

$$\frac{ds}{d\log N} = -2.3026 \times \left(\frac{A'}{1 + A'}\right)^{(1+A')} \times (S_u - S_e) \quad (171)$$

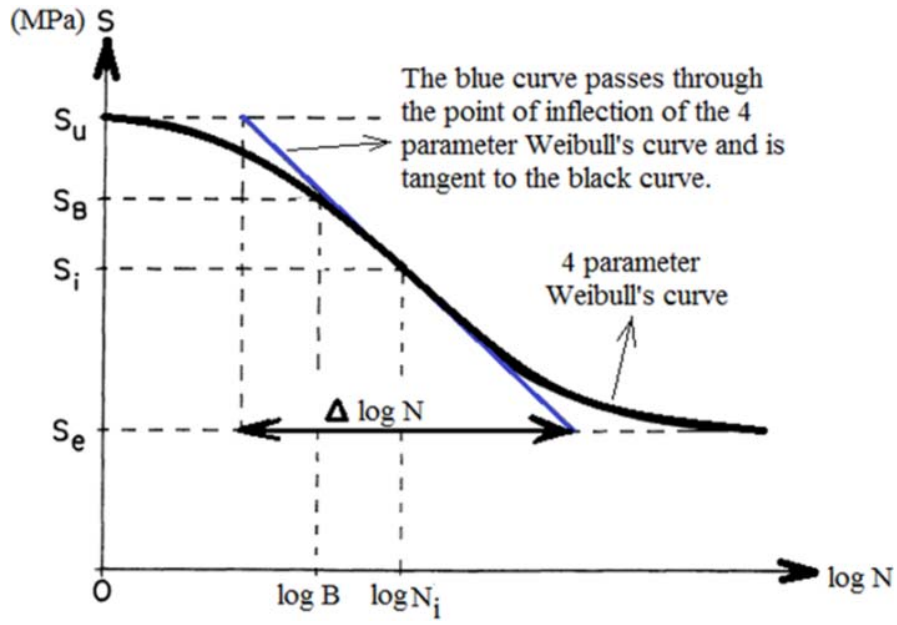

Figure 99 – Graphical estimation of the parameters of an S-N curve to Freudenthal et al. (1963, p.77)

Considering the variables shown in Figure 99, equation (171) is reduced to equation (167).

$$\frac{ds}{d\log N} \approx \frac{-(S_u - S_e)}{\Delta \log N} = -2.3026 \times \left(\frac{A'}{1+A'}\right)^{(1+A')} \times (S_u - S_e) \Leftrightarrow \tag{172}$$

$$\Leftrightarrow \Delta \log_{10} N = 0.43429 \times \left(\frac{1+A'}{A'}\right)^{1+A'} \tag{173}$$

In which,

$$\frac{S_B - S_e}{S_u - S_e} = 2^{-A'} \tag{174}$$

$$\frac{S_i - S_e}{S_u - S_e} = \left(\frac{A'}{1+A'}\right)^{A'} \tag{175}$$

In this thesis the four parameter Weibull's equation (170) will be transformed into equation (176).

$$S = S_e + C \times (N + B)^{-A'} \tag{176}$$

In which,

$$C = (S_u - S_e) \times \left(\frac{1}{B}\right)^{-A'} \tag{177}$$

The Least square method has been used to graphically fit the curve given by equation (176) in between the data points given by the fatigue experiments that were performed on the composite laminates (for instance the Interlaminar shear stress ($\tau_{xz\ j=total\ number\ of\ plies/2}$) ; and the number of cycles N_i) :

Rearranging equation (176) in a logarithmic form, equation (178) will become.

$$\log_{10}(S - S_e) = -A' \times \log_{10}(N + B) + \log_{10}(C) \tag{178}$$

Since the linear curve equation is given by (179)

$$y = m \times x + b \tag{179}$$

thus, the parameters shown in equation (178) assume the equality given in equation (180).

$$\begin{cases} y = \log_{10}(S - S_e) \\ m = -A' \\ x = \log_{10}(N + B) \\ b = \log_{10}(C) \end{cases} \tag{180}$$

According to (Freudenthal et al. 1963, p.79) "more accurate values of the four parameters (A',B and C which is function of A', B, S_e and S_u) can be obtained by applying the method of *Least Squares* to this evaluation problem".

Note: Although the parameter S_u could be used as an unknown value to be determined through the Least square method, in order to reduce graphical errors with the curve fitting, in this thesis the parameter S_u of the *All Carbon Design* S-N curve has been fixed with the Interlaminar Shear Stress value, $\tau_{xz\ j=total\ number\ of\ plies/2}$ given in the static experiment that has been performed on specimen number 10 ($S_u = \tau_{xz\ j=total\ number\ of\ plies/2} = 77.04\ \text{Mpa}$) , while the *Hybrid Design 1* S-N curve has been fixed with the interlaminar Shear Stress value, $\tau_{xz\ j=total\ number\ of\ plies/2}$ obtained from the static experiment that has been performed on specimen 9 ($S_u = \tau_{xz\ j=total\ number\ of\ plies/2} = 73.77\ \text{Mpa}$).

The *Least Squares* method is used by adjusting the parameters of the S-N curve to best fit the data set (Interlaminar shear stress ($\tau_{xz\ j=total\ number\ of\ plies/2}$) values; and the number of cycles $\mathrm{N_i}$) given by the fatigue experiments that have been performed on each of the specimens.

The Least Squares method is base of the equation (181) that gives the value of the *variance* of the S-N curve. Considering equation (180), the variance will be given as follows:

$$variance = \sum_{i=1}^{\substack{total\ number\ of \\ fatigue \\ experiments}} (y - m \times x + b)^2 \tag{181}$$

To work with equation (181), the following should be considered:

- $\mathrm{S_u}$ should be fixed by considering the Ultimate Static strength of the material or this could be a variable to be obtained through the Least Square method.

- The parameters A', B and $\mathrm{S_e}$ should be manually varied in order to achieve the best fit SN curve shape for the data found during fatigue tests.

- Typically, $0 \leq A' \leq 2$; $B\ and\ C \geq 300$ (should have values around 3000 or more) and $\mathrm{S_e} \ll \mathrm{S_u}$.

- The use of equation (181), and the process of attributing arbitrary values to the parameters A', B and $\mathrm{S_e}$ could be performed using an excel sheet in which logarithmic S-N plot with the fatigue experiment data points plotted on it should be presented (the number of cycles run by each fatigue experiment with the respective interlaminar shear stress ($\tau_{xz\ j=total\ number\ of\ plies/2}$)).

The best fit in the least-squares sense is based on the minimization of the sum of squared residuals, which means that the variance given by equation (181) should tend to zero. A variance equal to zero means that all the data points are coincident with the S-N curve given by the equation (170) (which is unlikely to happen in reality) or that all data points are equally close to the S-N curve given by the equation (170).

Thus, having the data points from the experimental fatigue tests and considering the equations (170) and (181). Is possible to build an S-N curve in a logarithmic scale by considering that the *variance* (equation (181)) should be a minimum.

APPENDIX S

TITLE **Matlab input instructions and commands to be used in the *command window* of Matlab in order to visualize the output results.**

Inputs to be given by the user

In order to give an overview of the procedures performed by the software, this section will present images of the input process when the Matlab algorithm is run.
Every time that the user inputs the values and clicks the *ok* button, the software will shows another window asking for more inputs.

i. Angle limit definition

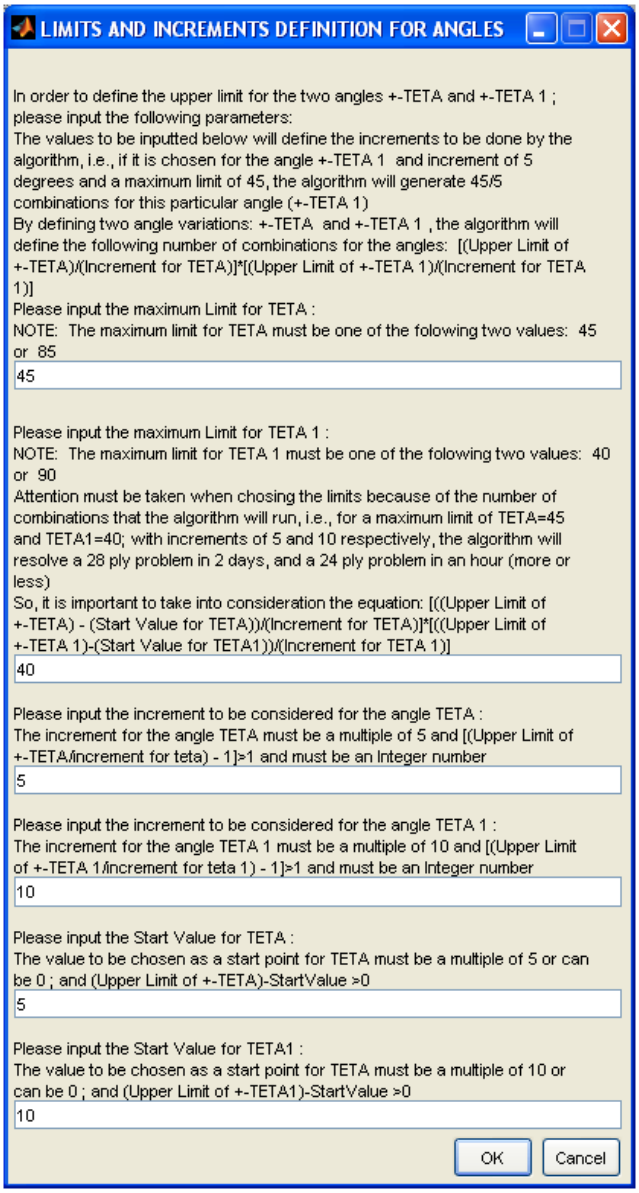

Figure 100 - First window shown by Matlab when the algorithm is executed

In this first menu the user is asked to insert the values to define the limits shown in Figure 117. By default, the software will give the values shown in Figure 100, which could be changed by the user as described.

Since the angle θ_j shown on Figure 117 could be equal to θ or θ', each of the angles θ and θ' should have defined maximum and minimum limit. Then, according to Figure 100, the maximum and minimum limit defined in the 1st and 5th rows of the table shown in Figure 100 are the maximum and minimum limits respectively, for the angle θ, while the values to be input in the 2nd and 6th rows, are to define the maximum and minimum limits respectively for the angle θ' in accordance with Figure 117.

The 3rd and 4th rows show the increment angle to be given to the angles θ and θ' respectively in order to rotate the fibre shown in Figure 100 from the minimum angle limit (limit θ_{min}) up to the maximum limit angle (limit θ_{max_1}).

ii. Definition of the number of solutions to be given by the algorithm after the input of the user

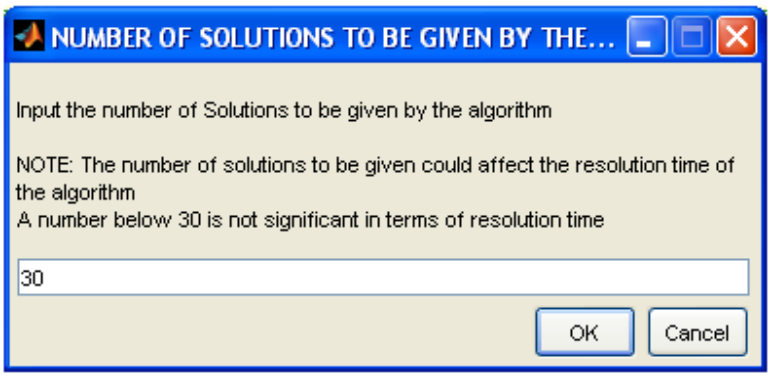

Figure 101 - Second window shown by Matlab when the algorithm is executed

In this case, the software will ask the user to input the number of the first best stacking sequences found to minimize the damage in the middle of a composite laminate.

For instance, if the user wants to find not just the best stacking sequence, but the best five stacking sequences to minimize the damage in the middle of the laminate, then, in the window shown in Figure 101, the default value should be substituted for the number *5*.

iii. Definition of the number of solutions to be given by the algorithm after the input of the user

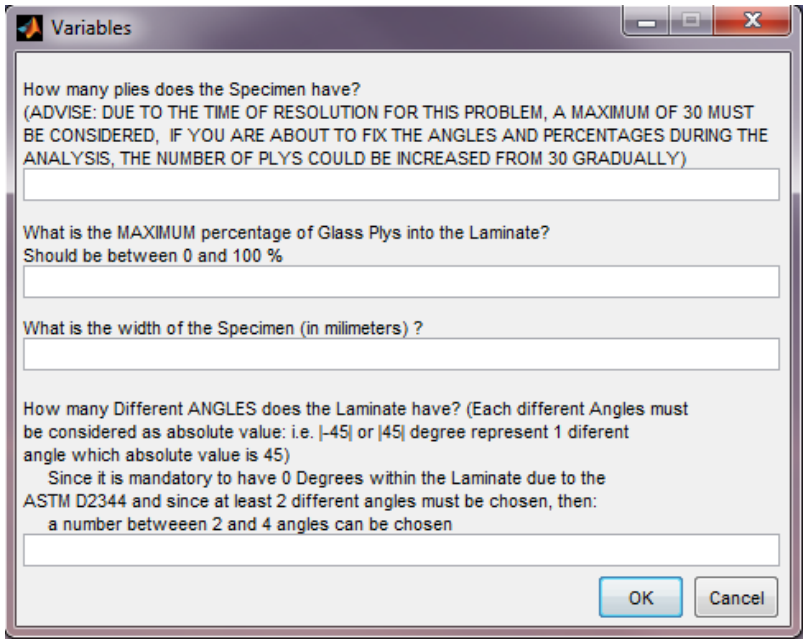

Figure 102 - Third window shown by Matlab when the algorithm is executed

In this window (Figure 102) the user will define how many plies the composite laminate has (to be input in the first row), then, in the second row will be asked for the maximum percentage of glass plies that the user wants to define in the composite laminate that will be built, then, in the third row of the window shown above will be required to input the width of the specimen, and finally, in order to determine how many angles the user wants to be varied in the composite laminate, as shown in Figure 40, is required to input in the last row, on an integer value which should be between 2 and 4.

According to Figure 40, and following the explanation given underneath of that figure, for an input in the 4th row equal to:

- $2 \rightarrow$ The angles will be 0° and one of either θ or 90° .
- $3 \rightarrow$ The angles will be 0° ; θ and one of either θ' or 90° .
- $4 \rightarrow$ The angles will be 0° ; θ ; θ' and 90° .

After this input, a series of questions will be asked to the user in order to determine the user requirements.

iv. User requirements to define each of the angles chosen in the previous step

In order to explain the procedure taken by the software in this step, an example will be given (Figure 103) of an input equal to 4 in the last row of Figure 102, then, after the filling of the remaining rows and after clicking *ok*, will appear questions shown on the image below.

Note: In the image below, a fixed angle means that the software will fix the angle θ_j shown on Figure 117 in the position that the user wants without proceeding with any variation of that angle. If the user does not want to fix any of the angles then the software will vary angle θ_j between its minimum limit (limit θ_{min}) up to the maximum limit angle (limit θ_{max_1}).

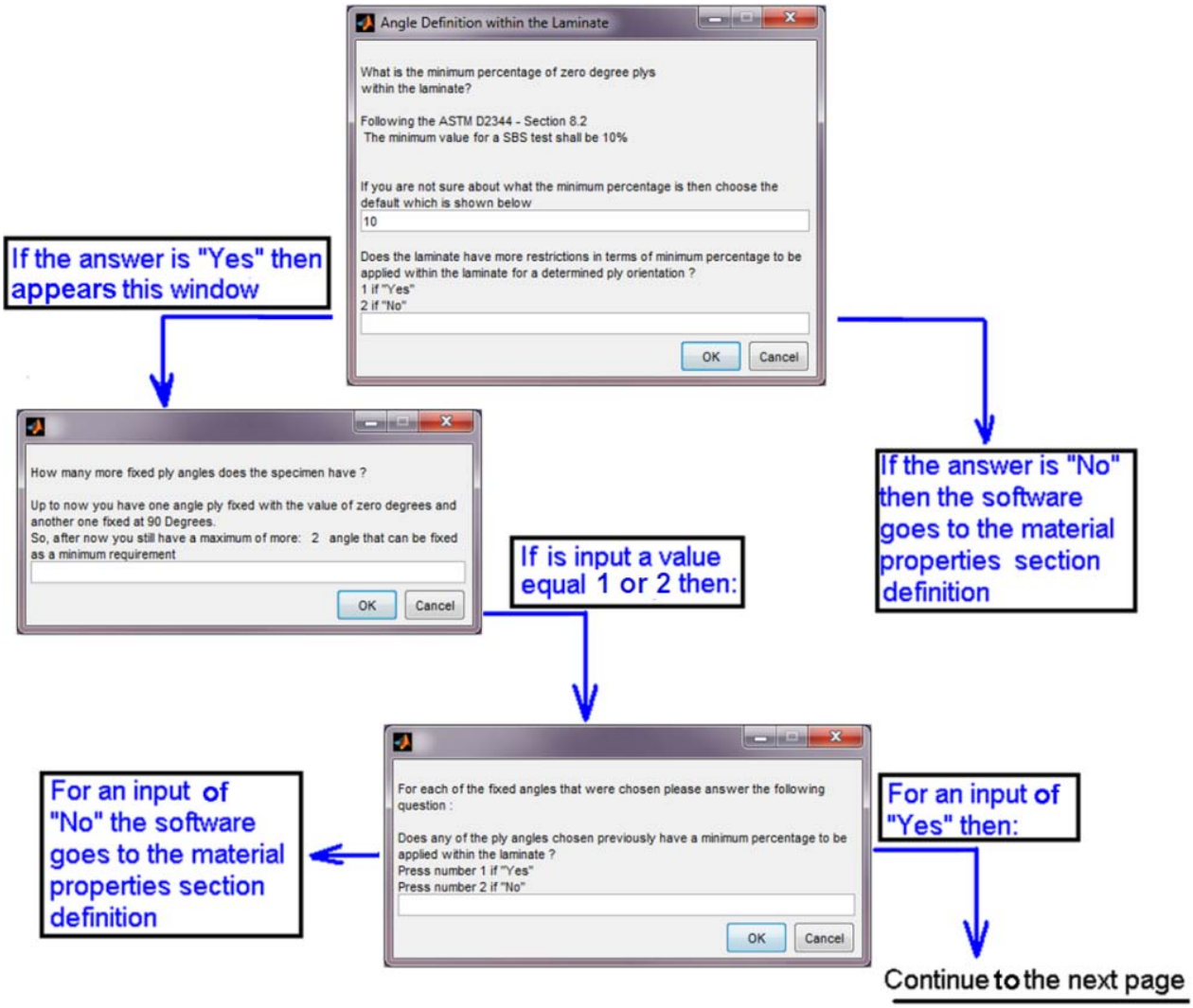

Figure 103 - Series of Matlab windows required to define the user requirements for each of the angles that were chosen on the previous section

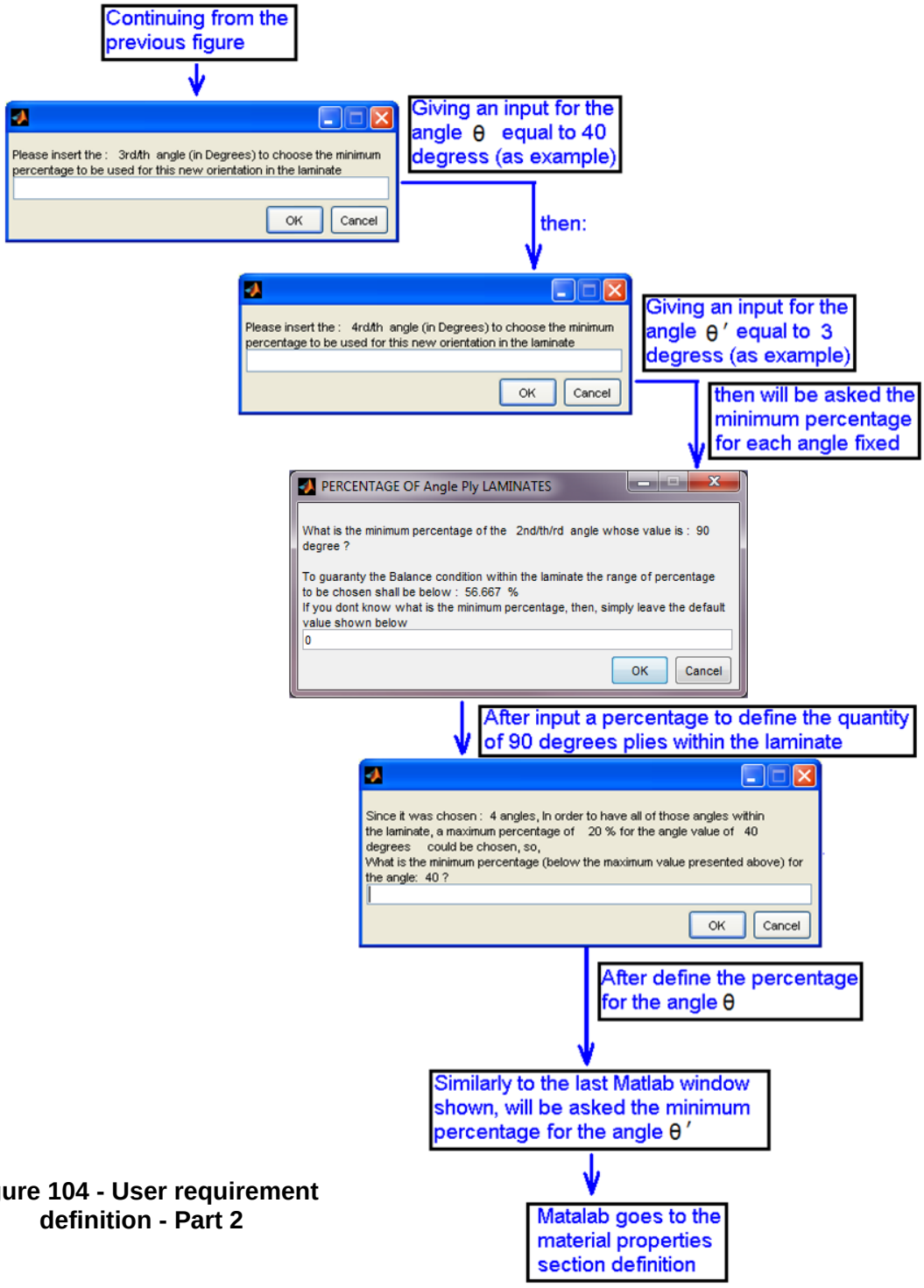

Figure 104 - User requirement definition - Part 2

Note: According to the Figure 104, 4 was chosen as the number of angles in Figure 102, then the software will give to the first angle a value equal to zero degrees, the second angle will be equal to 90^0, and the remaining angles will be identified as the third (θ) and fourth (θ') angles.

v. Material properties definition and line load

After defining the user requirements for the angles, the software will ask for the input of the material properties in accordance with Figure 105.

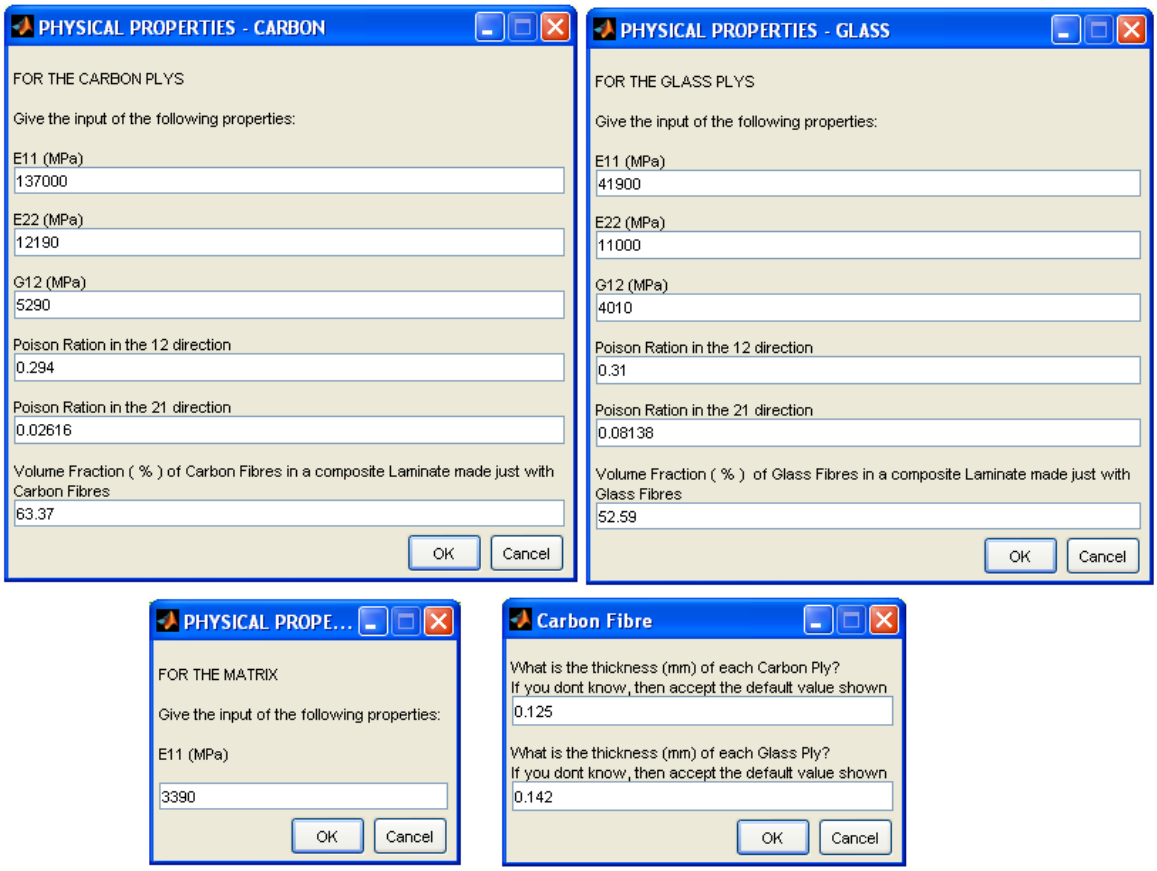

Figure 105 - Material properties input to be given by the user

Note: Each of the windows shown on the Figure 105 will appear one at a time.

The values shown on the Figure 105 are default material property values given by the software, in which the carbon material default values are related to the material specifications for Fibredux 913C HTA, and the glass material default values are related to the material specifications for Fibredux 913 XAS.
The ply thicknesses are average dimensions values.

After the user has defined the material properties, Matlab will show another window (Figure 106) in which the user needs to input the line load that the composite laminate will be subjected to when under SBS test conditions.

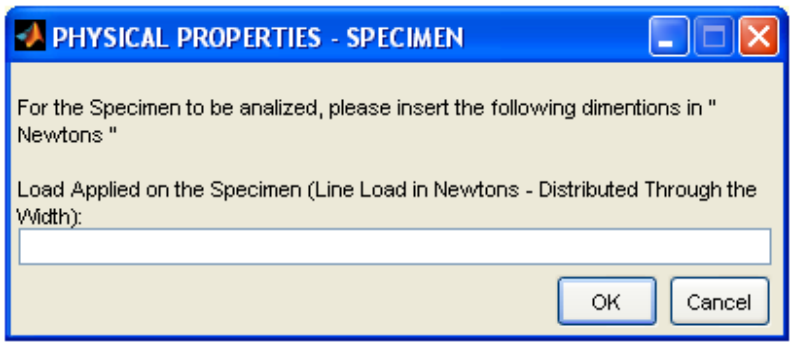

Figure 106 - Line load input requested by Matlab

vi. Confirmation of the input values

The final step to be confirmed by the user consists of a cross-check of all the values entered during the input process. If the user finds that something is wrong then *No* (number *2*) should be selected in the input box in the screen below (Figure 107). This will allow the user to go back to previous screens and correct the input.

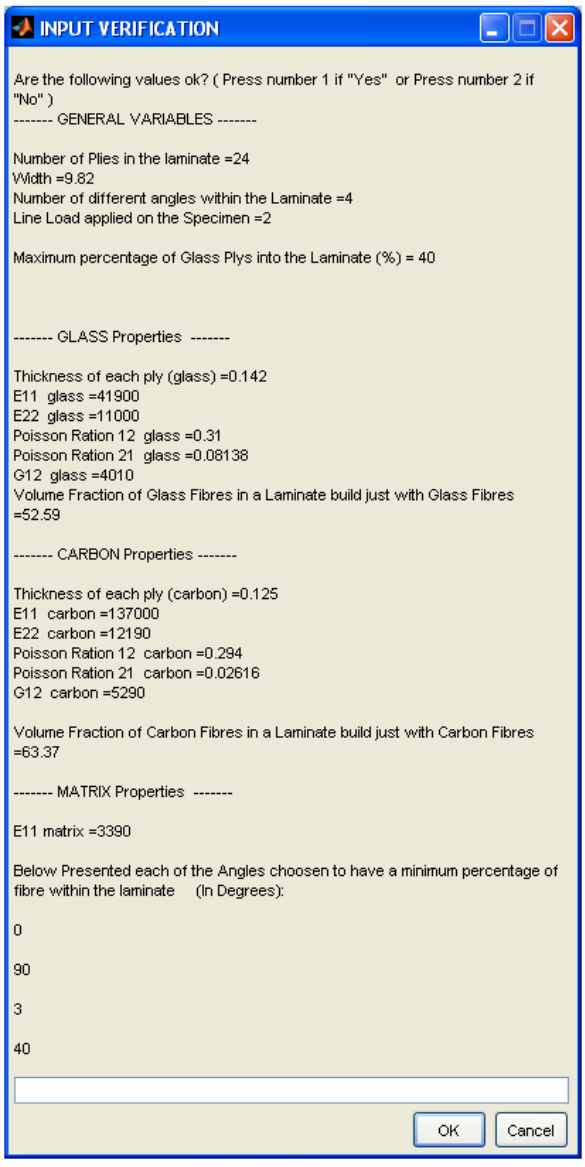

Figure 107 - Confirmation process

vii. Algorithm procedure after the inputs

After the user has given the requested inputs, the algorithm will generate all the valid combinations of materials and angles to be given to the composite laminate shown in Figure 40, and will perform an assessment on every increment made during the rotation of the fibres as shown in Figure 117.

Each of the combinations will use the following equations:

(23); (24); (25); (26); (27); (32); (55); (57); (58); (60); (82); (83) and (97).

Finally, after the ILSS has been determined for a given combination the software will save this into a bulk file, before running the remaining iterations. At any point while the software is running if the resulting ILSS is better than that of the preceding iteration in terms of minimizing the ILSS (τ_{xz} and τ_{zx}) on the central ply of the composite laminate, the current result will overwrite the previous one in the bulk file. Thus, the final result for ILSS in the bulk file once the software run has completed, will be the best for the input parameters given by the user.

Note: Instructions for accessing the Matlab results via the *command window* are given in Appendix S.

Matlab Output Commands

Each of the commands that will be described below will present a number of columns equal to the number of best solutions that was input by the user in the Figure 101, each of those columns represents a single composite laminate, and the first column will be the best result found to minimize the damage in the middle of the composite laminate, while the last column will be the worse value in between the columns shown. the columns of the Figure 108 up to Figure 111 will be organized in a crescent order, from the best ILSS up to the worse ILSS that minimize the damage in accordance with what has been told.

When is required to visualize more than one command, since the columns are in a crescent order, whichever is the command, the 1st column will represents the best solution in regards to the ISS, and the last column will represents the worse solution in regards to the ISS.

Commands to be used in the command window of Matlab

All the commands required to access the results are shown below. Each one should be typed in the Matlab Command Window in order to visualise the output.

- Command to access of all the possible material combinations generated by the algorithm:

Type into the Matlab command window: **materialcomb**

- Get access to total number of valid angle combinations in a base number :

numbercombinations

- Get access to values obtained for the interlaminar shear stress:

taufinal

- Get access to material combinations generated for the best results of ISS:

materialchosen

- Get access to values obtained for the plies orientations generated for the best results of ISS:

anglechosen

- Get access to laminate stiffness in the direction 1, in accordance with the Rule of Mixtures for the best results of ISS:

xxmodulus

- Get access to thickness of each ply, that was chosen for the best results of ISS:
  eachthickchosen

- Get access to total thickness that was chosen for the best results of ISS:
  totalthickchosen

- Get access to variable z_i , which was chosen for the best results of ISS:
  ydistancechosen

Example of an Output Given by the Software

This example has been used to obtain the best stacking sequence for a 24 ply laminate, in which the geometrical characteristics are the average of the static experiments performed on the Hybrid Design 1 (Han 2013).

For an input equal to (Just the main variables are shown):

$[\theta_{1_{\min}}; \theta_{1_{\max}}] = [5^{\circ}; 45^{\circ}];$

$[\theta_{2_{\min}}; \theta_{2_{\max}}] = [10^{\circ}; 40^{\circ}];$

$\theta_{\text{increment\_1}} = 5^{\circ};$

$\theta_{\text{increment\_2}} = 10^{\circ};$

$N_{\text{solution}} = 10;$

$\text{Plies}_{\text{\_n}} = 24;$

$\text{Glass}_{\text{ply \%}} = 40\%;$

width=6.92 mm;

$\text{angles}_{\text{\_n}} = 3$;

Without any 90^0 plies, and without fixing angles $\boldsymbol{\theta_1}$ and $\boldsymbol{\theta_2}$;

Accepting all the default materials except the ply thicknesses which are:
t_{glass}= 0.143 mm and t_{carbon}= 0.139 mm ;

Load=2559 N;

- COMPUTING TIME REQUIRED TO RUN THE SOFTWARE UNDER THE CONDITIONS GIVEN DURING THE INPUT PROCESS

56 min

(for a computer with an i7 processor and with two core at 2.20 GHz each one and 8GB memory)

- TOTAL NUMBER OF MAIN COMBINATIONS GENERATED

(Valid Angle Combinations × All the Material Combinations)

6 930 432 Combinations

- TOTAL NUMBER OF VALID ANGLE COMBINATIONS GENERATED

1 692 Valid Combinations

- INTERLAMINAR SHEAR STRENGTH RESULTS (MPa)

(Called ILSS because the Ultimate Load was applied)

The bottom of the laminate is represented by the first row of values and
The middle plane of the laminate is represented by the last row of values.

taufinal =

0	0	0	0	0	0	0	0	0	0
23.295	22.37	23.267	23.217	24.373	22.344	22.298	20.498	23.189	23.28
44.668	42.894	44.613	44.518	46.734	42.843	42.755	39.304	44.463	44.638
50.963	50.54	50.9	50.791	53.319	50.481	50.377	49.685	50.729	50.929
56.635	57.431	56.566	56.444	59.254	57.363	57.245	59.04	56.376	56.598
61.685	62.28	61.61	61.478	61.605	62.207	62.079	63.484	61.403	61.644
66.113	66.532	66.032	65.89	63.658	66.454	66.317	67.38	65.81	66.069
67.806	68.158	67.723	67.839	65.413	68.078	68.188	68.87	67.756	67.761
69.215	69.511	69.13	69.46	66.87	69.429	69.745	70.109	69.375	69.169
70.338	70.589	70.426	70.58	69.475	70.673	70.82	71.098	70.666	70.292
71.177	71.395	71.393	71.415	71.428	71.602	71.623	71.836	71.63	71.13
72.422	72.59	72.636	72.656	72.73	72.796	72.814	72.931	72.869	72.703
73.044	73.188	73.257	73.276	73.381	73.393	73.41	73.478	73.489	73.49

Figure 108 – Final result obtained from the software for the ILSS (τ_{xz} and τ_{zx}) in the middle of a composite laminate (central ply of the laminate).

- MATERIAL COMBINATION CHOSEN

```
materialchosen =

  ' C '    ' C '    ' C '    ' C '    ' C '    ' C '    ' C '    ' C '    ' C '    ' C '
  ' C '    ' C '    ' C '    ' C '    ' C '    ' C '    ' C '    ' C '    ' C '    ' C '
  ' C '    ' C '    ' C '    ' C '    ' C '    ' C '    ' C '    ' C '    ' C '    ' C '
  ' C '    ' C '    ' C '    ' C '    ' C '    ' C '    ' C '    ' C '    ' C '    ' C '
  ' C '    ' C '    ' C '    ' C '    ' G '    ' C '    ' C '    ' C '    ' C '    ' C '
  ' C '    ' C '    ' C '    ' C '    ' G '    ' C '    ' C '    ' C '    ' C '    ' C '
  ' G '    ' G '    ' G '    ' G '    ' G '    ' G '    ' G '    ' G '    ' G '    ' G '
  ' G '    ' G '    ' G '    ' G '    ' G '    ' G '    ' G '    ' G '    ' G '    ' G '
  ' G '    ' G '    ' G '    ' G '    ' C '    ' G '    ' G '    ' G '    ' G '    ' G '
  ' G '    ' G '    ' G '    ' G '    ' C '    ' G '    ' G '    ' G '    ' G '    ' G '
  ' C '    ' C '    ' C '    ' C '    ' C '    ' C '    ' C '    ' C '    ' C '    ' C '
  ' C '    ' C '    ' C '    ' C '    ' C '    ' C '    ' C '    ' C '    ' C '    ' C '
```

Figure 109 – Combination of materials for ten different composite laminates.

- PLIES ORIENTATION CHOSEN (Degrees)

```
anglechosen =

     0     0     0     0     0     0     0     0     0     0
     0     0     0     0     0     0     0     0     0     0
    45    40    45    45    45    40    40    30    45    45
   -45   -40   -45   -45   -45   -40   -40   -30   -45   -45
    45    45    45    45    45    45    45    45    45    45
   -45   -45   -45   -45   -45   -45   -45   -45   -45   -45
    45    45    45    40    45    45    40    45    40    45
   -45   -45   -45   -40   -45   -45   -40   -45   -40   -45
    45    45    40    45    45    40    45    45    40    45
   -45   -45   -40   -45   -45   -40   -45   -45   -40   -45
    45    45    45    45    45    45    45    45    45    40
   -45   -45   -45   -45   -45   -45   -45   -45   -45   -40
```

Figure 110 – Plies orientation angles for ten different composite laminates.

- YOUNG MODULUS IN THE DIRECTION *x* OF THE LAMINATE, IN ACCORDANCE WITH THE RULE OF MIXTURES (MPa) :

```
xxmodulus =

   48639   51005   49286   49286   48639   51651   51651   56473   49932   51005
```

Figure 111 – Young modulus in the *x* direction of the laminate (for 10 different composite laminates)

- PLOT SHOWING THE BEST 10 SOLUTIONS PROVIDED BY THE ALGORITHM:

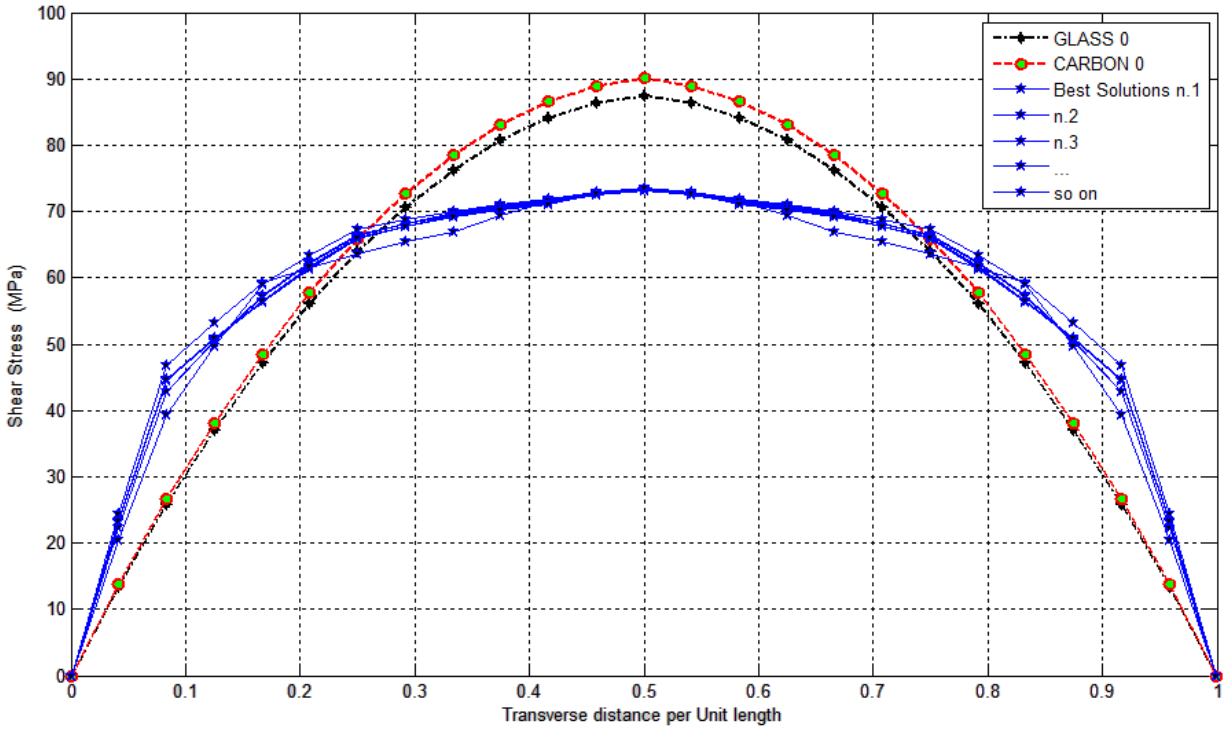

Figure 112 - Plot for the best 10 solutions in terms of ILSS for 24 plies (For a Matlab input in which $[\theta_{min}; \theta_{max}] = [5^{\circ}; 45^{\circ}]$)

- PLOT SHOWING THE BEST SOLUTION PROVIDED BY THE ALGORITHM:

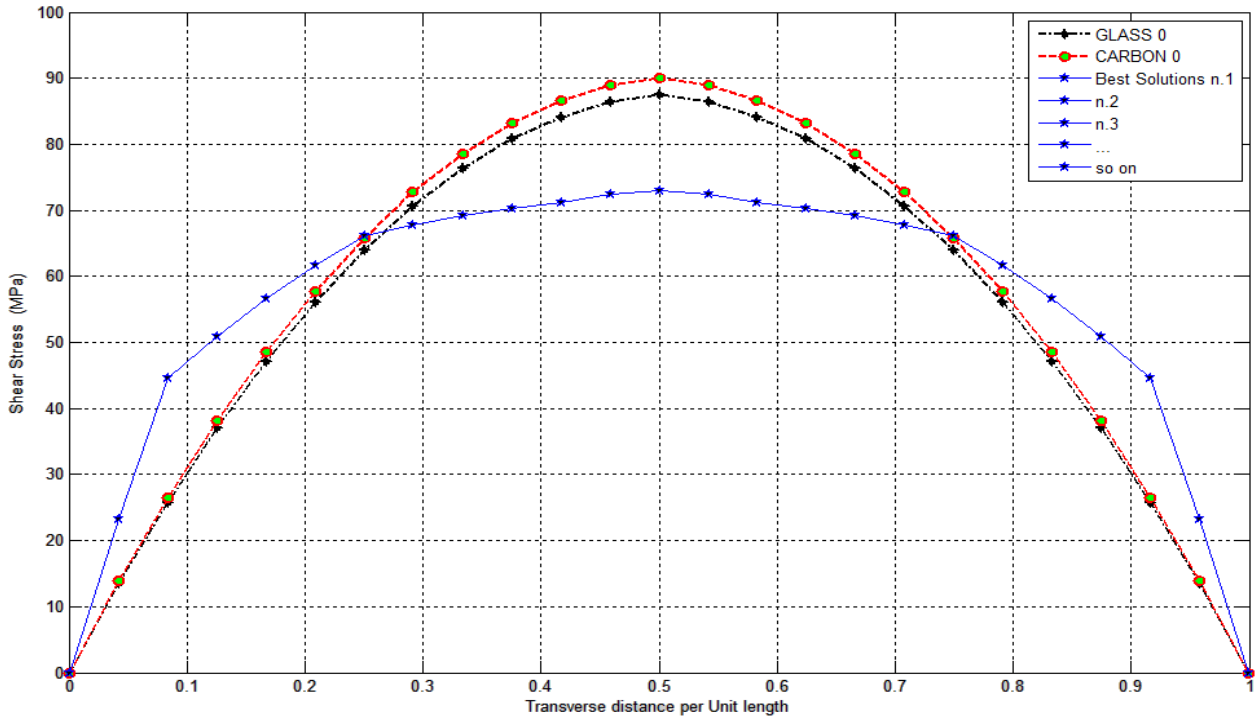

Figure 113 - Plot for the best solution in terms of ILSS to reduce the damage in the middle of the laminate (For a Matlab input in which $[\,\boldsymbol{\theta_{min}}\,;\boldsymbol{\theta_{max}}] = [\mathbf{5}^{\circ}\,;\,\mathbf{45}^{\circ}]$).

Note that the First curve shown in the Figure 112 and Figure 113 is for zero degree (UD) carbon Plies, the second curve (in black color) is for UD glass plies, then, the last curve (in blue color) represents the best result found in terms of ILSS, for a maximum limit of 45^{0}.

To complement these results, more outputs for different algorithm inputs are shown in Appendix A and B.

Notes: The Young modulus, given by the Matlab software, will have a different value in regards to the LAP software, which in accordance with the literature is expected, because LAP software uses the constitutive laminate equations to achieve the Young modulus in the direction *x* (Harris 1999), while the Rule of Mixtures and the Reuss Estimative consider the microscopic level of the laminate. Due to the simplicity in the application of both the Rule of Mixtures and the Reuss Estimative, these theories where chosen to calculate the Young modulus.

APPENDIX T

TITLE **ILSS (τ_{xz}) for each ply of the All Carbon Design found by the FE model**

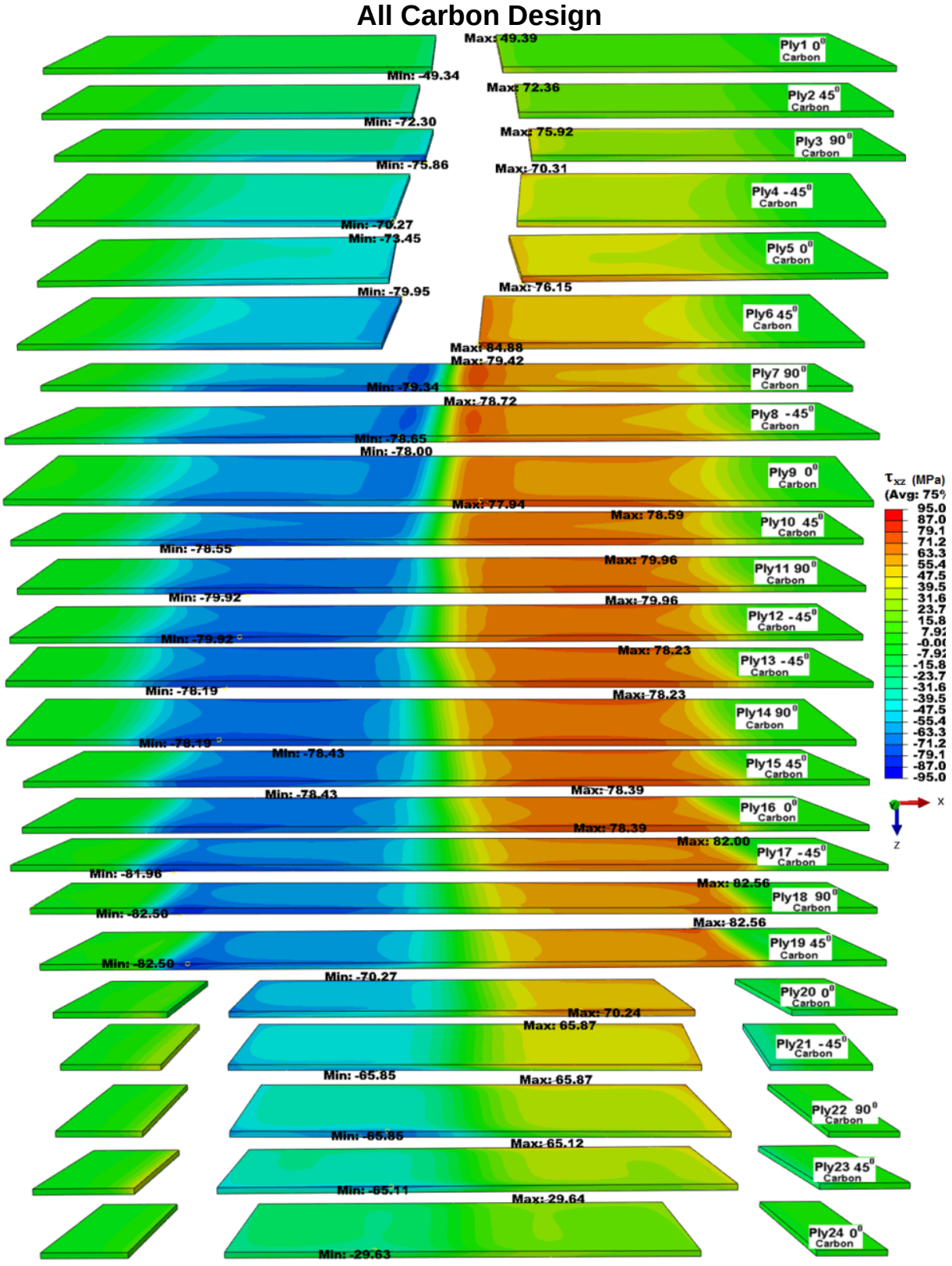

Figure 114 - ILSS (MPa) for a 24 plies carbon laminate (Specimen 10).

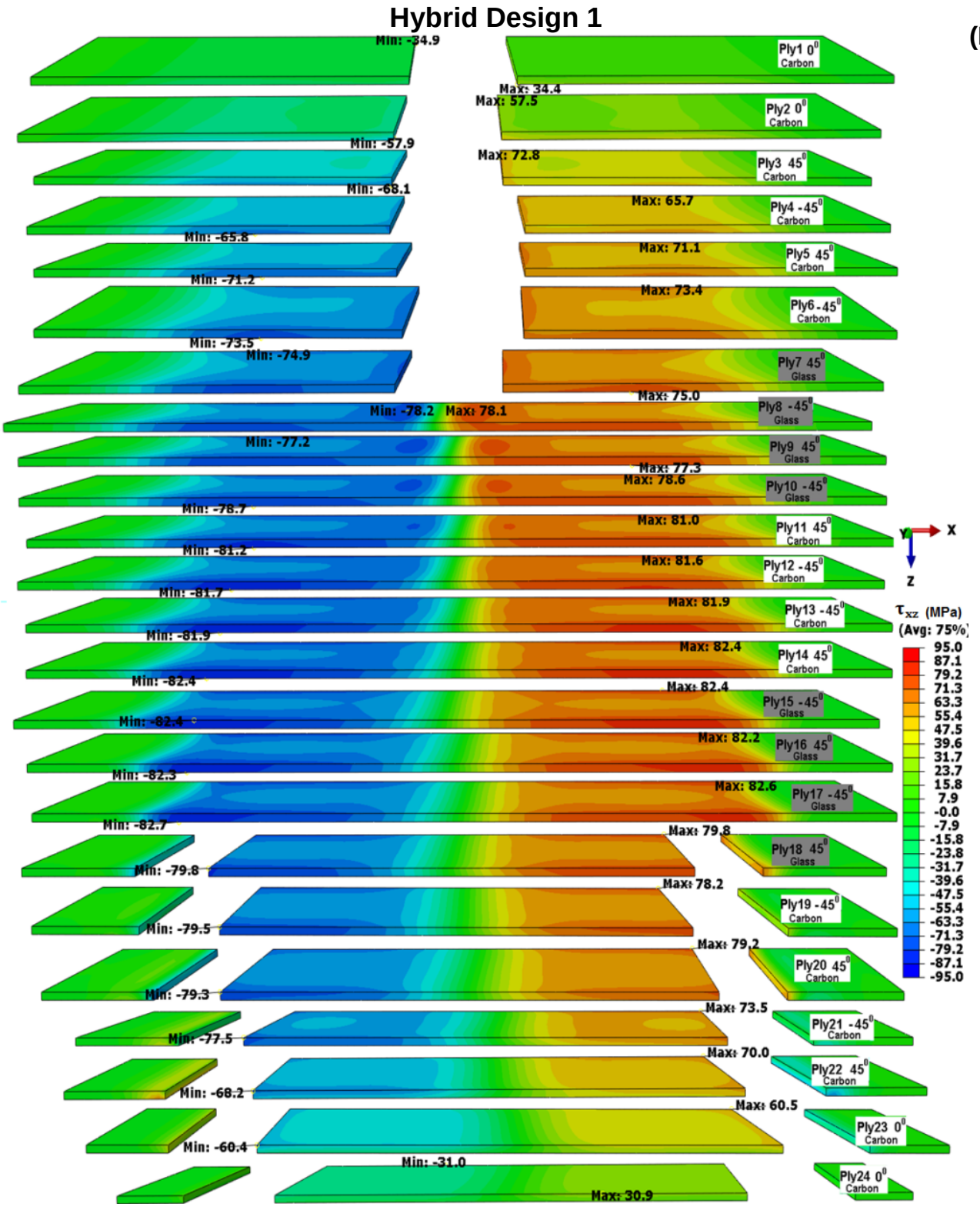

Figure 115 - ILSS (MPa) for a 24 plies *Hybrid Design 1* laminate.

Stacking Sequence :

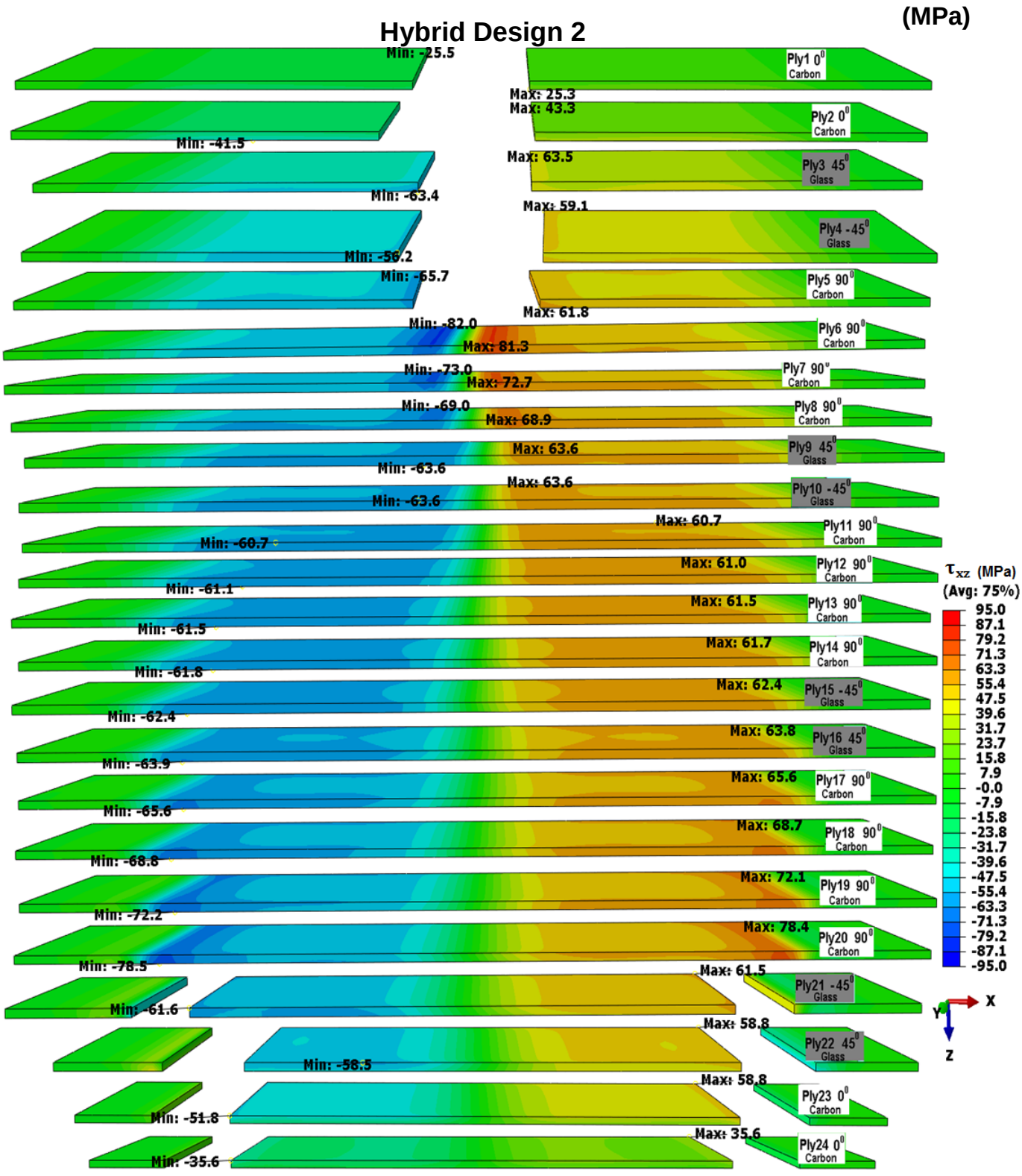

Figure 116 - ILSS (MPa) for a 24 plies *Hybrid Design 2* laminate. **Stacking Sequence :**

APPENDIX U

TITLE Algorithm: Additional information

Algorithm: Additional information

Figure 40 and Figure 117 show the main methodology used by the software. Through a determined number of angles, the software will attribute one angle to each ply. If the angle is not zero or 90^0, then the procedure will be involved as shown on the Figure 117.

From Figure 40, the digits 0,1 and 2 that define an angle equal to θ_j are numbers of base three which are used as an identification number according to the following:

- Digit *0* = 0^0
- Digit *1* = θ_j or 90^0
- Digit *2* = 90^0

Continuing with the explanation of Figure 40, the digits 0 and 1 are binary numbers used as an identification method to give the exact material properties for a given ply. Each of the digits will represent the following:

- Digit *0* = Carbon material properties
- Digit *1* = Glass material properties

When the algorithm generates a combination in which one of the plies has an angle equal to θ_j and not equal to zero or 90^0, it will proceed in accordance with the Figure 117.

For an angle θ not equal to 0 or 90 degrees:

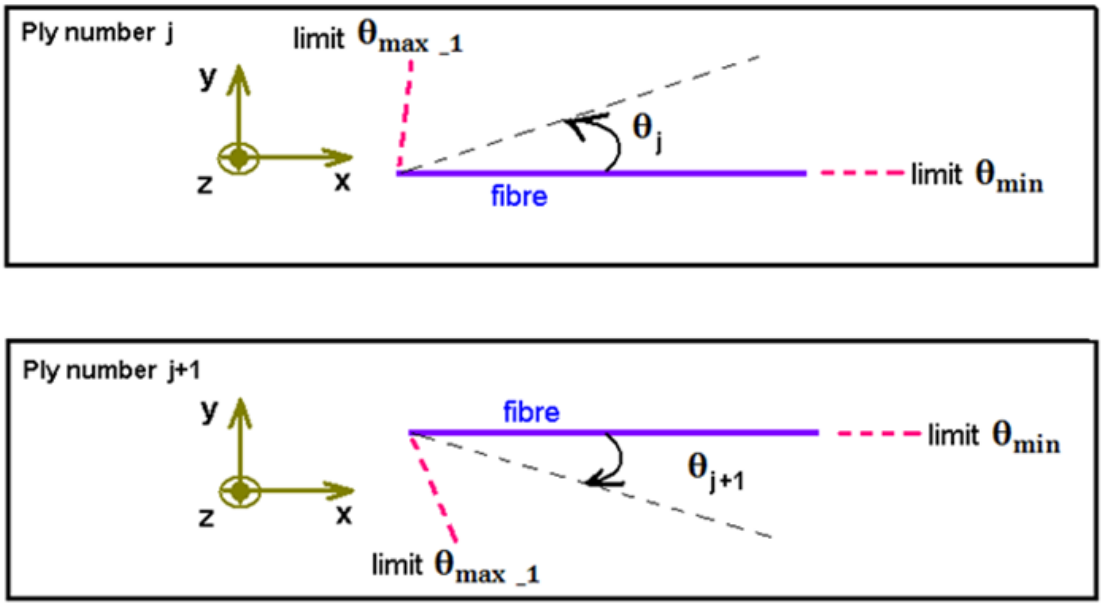

Figure 117 - Top view of a ply. Two plies are shown above. Definition of the angle θ. When the angle θ is different than 0 or 90 degrees the algorithm attributes simultaneously the values: $\theta_j = +\theta$ and $\theta_{j+1} = -\theta$.

General rules

Since the algorithm runs all possible combinations generated by the mixture of materials and angles for each of the plies that are within a composite laminate, then, a reduction of the total amount of combinations is required through the use of some rules, which are:

- Assessment done in order to minimize the damage in the middle of a composite laminate (see Figure 118).
- A minimum of 10% of zero degree plies must be within the laminate in accordance with reference (BS14130:1998, 2004).
- The laminate should be balanced and symmetric.
- A maximum of four different ply angles could be chosen by the user.
- A maximum of two different ply materials could be chosen by the user.
- In order to reduce thermal cracking and splitting along the fibre direction, no more than 4 plies of the same orientation are joined together.
- No free edge stresses exist.
- The algorithm is based on the theory for an infinite laminate in terms of length and width (according to Chapter 2, section 2.6).

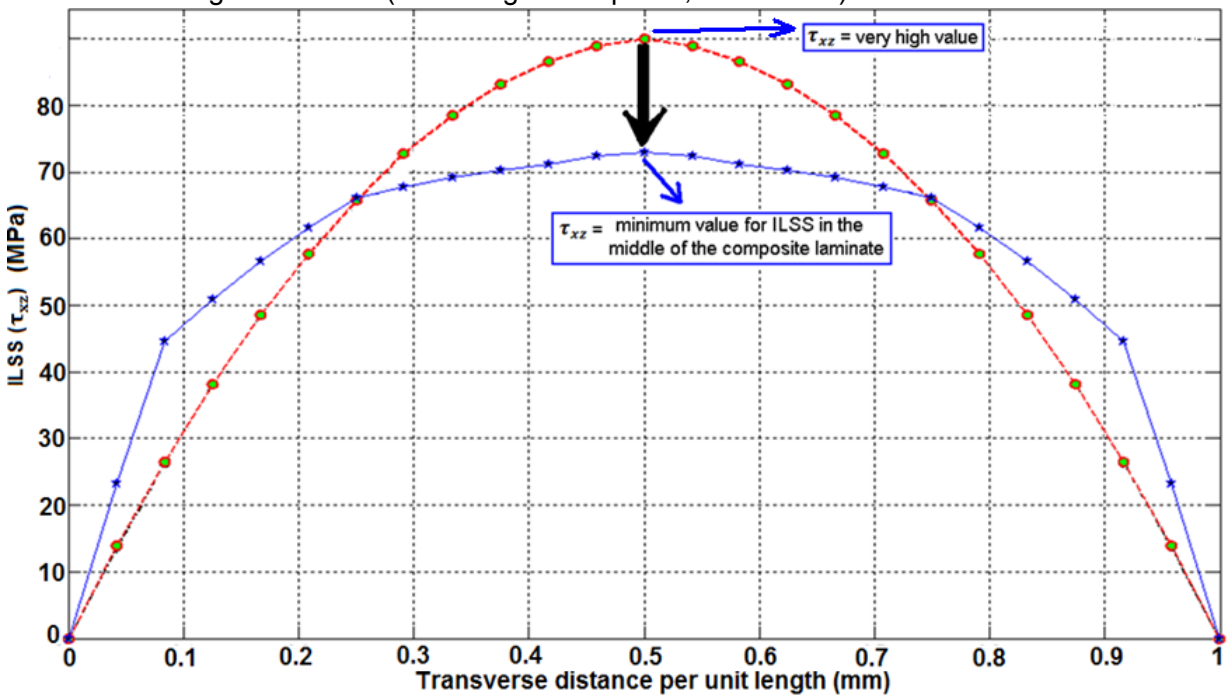

Figure 118 – Image showing the method implemented by the software to minimize the ILSS (τ_{xz}) in the middle of the laminate for a given shear force. The black arrow on this figure shows the yellow point taken by the software to determine the minimum value for the ILSS. The algorithm starts from a very high value of τ_{xz} (more than three times τ_{xz} in the middle of a 24 ply UD composite laminate). Through the assessment of each combination of materials an angles generated by the software will decrease until the minimum possible value of τ_{xz}.